



Evaluate of the Groundwater Suitability for Irrigation in Jassan Area, Wasit, Iraq

Sattar Obaid Maiws Al-Mayyahi*

Department of Biology, College of Science, University of Wasit, Wasit, Iraq.

Received: 20 June 2018

Revised: 23 July 2018

Accepted: 27 Aug 2018

*Address for Correspondence

Sattar Obaid Maiws Al-Mayyahi

Department of Biology,

College of Science,

University of Wasit, Wasit, Iraq.

E mail: sattar.mayyahi@gmail.com



This is an Open Access Journal / article distributed under the terms of the **Creative Commons Attribution License** (CC BY-NC-ND 3.0) which permits unrestricted use, distribution, and reproduction in any medium, provided the original work is properly cited. All rights reserved.

ABSTRACT

Seventeen water sample from groundwater were collected from the Jassan area, East of Wasit governorate, Iraq, during March 2017. The samples were analyzed for Total dissolved solids (TDS), pH, electrical conductivity (EC), major ions Ca^{2+} , Mg^{2+} , Na^+ , K^+ , Cl^- , HCO_3^- and SO_4^{2-} , to evaluate the suitability of analyzing water for irrigation, Sodium adsorption ratio (SAR), residual sodium carbonate (RSC), sodium percent (Na%) and electric conductivity were applied. The irrigation water classification based on electrical conductivity indicated that the water samples are of class (C3, EC= 750-2250) in Wells (W.1, W.2, W.8, W.10, W.11, and W.13), this result refers to acceptable water for irrigation, while water samples are of class (C4, EC \geq 2250) in Wells (W.3, W.4, W.5, W.6, W.7, W.9, W.12, W.14, W.15, W.16 and W.17, these results refer to unacceptable water for irrigation, except for very salt-tolerant plants. According to SAR values, all of the groundwater samples belong to (S1) excellent water class with no harmful effects of sodium, in which SAR <10.0 , except W.17 is good water belong to (S2) in which SAR 11-18 which is generally satisfactory for irrigation. While based on RSC, all the water samples showed (RSC) values less than zero; therefore, all the samples are suitable for irrigation uses regarding to this parameter. According to Na% value, the sodium percentages in groundwater samples indicate Permissible water. Applying the water-sediment relationship experiments with respect to dry and wet periods show that about 2.4% – 4.7% of the TDS were liberated after the drying condition which is believed to be of the water-soluble salts that exist within the sediment column.

Keywords: Groundwater, Irrigation suitability, Water-sediment relationship.



**Sattar Obaid Maiws Al-Mayyahi****INTRODUCTION**

About half of the Iraqi land is affected by salts, especially in agricultural lands, most of them lies in the middle and south of Iraq due to the water deficit dam construction in the neighboring countries (Turkey, Syria, and Iran) (FAO, 2003). This problem increased in Iraq, due to a low efficiency of drainage system and declining freshwater resources, in addition to the aridity condition in the study area. The washing lands are the main process for reclaiming saline lands with an efficient system of drainage. Geology and climate may affect regional differences in irrigation water characteristics (Ayers and Westcot, 1985; Rowe and Magid, 1995; and Shirazi *et al.*, 2011). Recently the groundwater has become important natural resources as a result of increasing water demand and decreasing rainfall amount and surface water supplies. The Jassan area – East of Wasit Governorate - Central Iraq is one of an important agricultural area in Iraq. The agriculture in this area depends on the ground water during water deficit periods. The Jassan area is located between latitudes (32° 39' 28" – 33° 06' 01") N and longitude (45° 49' 26" – 46° 10' 28") E. It is occupied 1893 Km² (Tab. 1) and (Fig. 1). It is a part of the low relief plain known as the Mesopotamian Plain, which has a sandy silty clay surface. It is used heavily for agricultural purposes. The farms in these areas are randomly distributed utilize groundwater for irrigation, although it has a high salinity range from 3534 ppm to 4010 ppm, (Al-Shammary, 2008). A variety of soil properties such as soil acidity, organic contents, clay and EC have been identified as affecting the behavior of TDS in soil in different parts of the world, although, the drying and wetting processes play an important role in transferring TDS between sediment and water (Al-Dabbas, 2002 and 2005; Al-Shihmani, 2015). This study aims to evaluate the groundwater quality in the Jassan area for irrigation and to investigate the water-sediment interrelation, taking into account the rainfall and utilized groundwater

MATERIALS AND METHODS

Seventeen groundwater samples were collected during March 2017 from the Jassan area (Fig. 1). The measurements were done using the procedure of APHA (2005) at the service laboratory in the College of Science – University of Wasit. All samples were analyzed for major ions (Ca²⁺, Mg²⁺, Na⁺, K⁺, Cl⁻, HCO₃⁻ and SO₄³⁻), (Table 2). Sodium and potassium were analyzed using flame photometer (APHA, 2005). Calcium, magnesium was analyzed using titration with EDTA (Ethylene Diamine Tetracetic Acid), chloride was analyzed using a Technicon autoanalyzer instrument (APHA, 2005). Carbonate and bicarbonate were determined by titrimetric method. Sulfate was determined using of spectrophotometer (U.V.). The hydrogen number (pH), electrical conductivity (EC), TDS was measured directly in the field. Some of the high values of TDS water samples were measured by drying at 105 °C at the service laboratory in the College of Science – University of Baghdad (Boyd, 2000). The analytical accuracy was calculated according to Stoodley *et al.* (1980); and Hem (1985), accordingly the accuracy of the results is accepted.

The sediments of the Jassan area are composed of sand, silt and clay. They are characterized from the topsoil to 1.5 m depth by sandy, silty clay. The mineral composition of the Jassan area sediments show that the main components of the studied samples are quartz, gypsum, calcite, feldspar and clay minerals, which represented by chlorite, montmorillonite, kaolinite, illit, mixed layer and to less extent palygorskite (Al-Shammary, 2008 and Al-Mayyahi, 2016). In an attempt to construct a suitable model for the water-sediment interaction that represents the natural conditions of the recycles water for irrigation as an additional recharge which leads to salinity increase. The proposed method was applied in this research. This method is dealing with the extracted water from the sediment samples after washing with distilled water and well water water. This method is used by continuous immersion and washing of the sediment column by many liters of water during the required time period. The infiltrates were analyzed for the total dissolved salts (TDS), as well as measuring the electrical conductivity (EC). Groundwater sampling from wells has been carried out from 17 wells to investigate TDS variability in space during March 2017. In the present work experiments were carried out to investigate the "TDS cyclicity between groundwater and soils, taking into consideration the soil type, dry and wet periods and the environmental conditions in terms of rainfall and human impact. A sample of average condition was selected in silty clay sediments of the studied two sites locations. The





Sattar Obaid Maiws Al-Mayyahi

proposed method was applied for the sediment – water interrelation. The electrical conductivity (EC) and TDS measurements for the infiltrate were considered for this purpose. Two sites were selected for washing soil experiment (Test 1) and (Test 2), (Fig. 1). The sampling was done by using the hand auger for the top soil, which is essential for planting at depth (0 – 150 cm) to show the effect of the leaching effect in the soil section (Al-Shihmani, 2015). The soil section is situated in plastic tube with perforated end (designed by the searcher), (Fig. 2). The distilled water was used (to represent rainfall) for the purpose of washing the soil and then dried for two weeks and re-wash with distilled water again, and then dried two weeks to represent the dry and wet period effect. Then the soil section in the tube was re-washed with Well water (represent irrigated by high salinity water). This method is described by continuous immersion of the sediment column by distilled water. The EC is measured for each liter of infiltrating at different time of immersion (Al-Dabbas, 2002 and 2005; Al-Hamdani, 2009; and Al-Shihmani, 2015). In fact, the time consuming for infiltration depends on the lithology of the selected sediment samples, where for, site one (A) (Test 1), needed about 10.5 hours for 10 liters poured water while for, site two (B) (Test 2), took 8.5 hours for 10 liters poured water infiltration. The EC measurements for each experiment show decrease with time, i.e. further reduction of EC at the last liter, which is obvious due to the continuous washing of the sediment sample. The infiltrated liters of distilled water that used to wash the two sites were taken separately and analyzed for their TDS and EC (Tab. 3 and 4). The results reflect that most of the major anions and cations will be washed out from the sediment sample by using the first five liters and their concentrations decrease to the minimum at the last liter.

RESULTS AND DISCUSSION

Assessment Parameters of Irrigation Water

There are four most popular criteria to assess water quality for irrigation: TDS or EC, sodium adsorption ratio (SAR), soluble sodium percentage (Na%), chemical concentration of elements like Na⁺, Cl⁻ and residual sodium carbonate (RSC) (Ayers and Westcot, 1985; Michael, 1992; and Qannam, 2003).

Salinity Hazard

To assess the quantity of salts in solution the irrigation water was classified according to the total concentrations of soluble salts into low (C1), medium (C2), high (C3) and very high (C4) salinity zones based on the EC values (Glover, 1996; and Turgeon, 2000) Table 2. Based on this classification, the groundwater samples of Jassan area are of class (C4) for the groundwater samples, that reflect unacceptable for irrigation, except for very salt-tolerant plants with excellent drainage, frequent leaching, and intensive management (Tab. 2 and 3).

Sodium Adsorption Ratio (SAR)

The sodium adsorption ratio (SAR) is calculated according to the following equation (Hem, 1985; and Todd, 1980 and 2007):

$$SAR = rNa^+ / (rCa^{2+} + rMg^{2+} / 2)^{0.5}$$

Where: SAR = sodium adsorption ratio.

rNa⁺, rCa²⁺ and rMg²⁺: Concentration of ions by (epm) units. Turgeon (2000) classified irrigation water according to SAR values (Tab. 4). According to SAR values, all of the groundwater samples belong to (S1) excellent water class with no harmful effects of sodium, in which SAR <10.0, except W.17 is good water belong to (S2) in which SAR 11-18 which is generally satisfactory for irrigation. (Tab. 4 and 5).





Sattar Obaid Maiws Al-Mayyahi

Residual Sodium Carbonate (RSC)

RSC was calculated using the following equation: $RSC = (CO_3^{2-} + HCO_3^-) - (Ca^{2+} + Mg^{2+})$

Where, the ionic concentrations in meq/l units. (Turgeon, 2000), (Tab. 6). Accordingly, all the samples showed (RSC) values less than zero; therefore, all the samples are suitable for irrigation uses regarding RSC, (Tab. 5 and 6).

Soluble Sodium Percentage (Na%)

The sodium in irrigation waters is usually denoted as percent sodium and can be determined using the following formula:

$$Na \% = \frac{(Na + K)}{(Ca + Mg + Na + K)} \times 100$$

Where: rNa^+ , rCa^{2+} , rMg^{2+} , and rK^+ : Concentration of ions by (epm) units. Don (1995) classified the quality of irrigation water according to Na% values (Tables 6 and 4). Accordingly, the sodium percentages in groundwater samples indicate permissible water. (Tab. 5 and 7).

The Water-sediment Relationship

According to, Al-Hamdani, 2017, the Geo-chemical behavior of TDS is mainly affected by the environmental conditions prevailing during its migration between sediment and water at wet and dry periods. In this research an attempt was made to verify this situation during wet and dry periods where the experiment was carried out with a design to simulate these environmental conditions (Van Hoorn, 1970). Two sites of sediment columns were selected and tested under dry and wet conditions using simulated rainwater and Well salty water of 11800 and 13100 ppm TDS concentration for washing the sediment column (Fig. 2). Ten liters of distilled water for continuous immersion of sediment column were used in both locations (Test 1 and Test 2).

All of these liters were collected from the perforated end of the plastic tube that designed for TDS measurements. The TDS results of the collected distilled water are shown in Tables 8A and 9A. The sediment columns were left to dry at room temperature for two weeks, then the same experiment repeated again by six liters of distilled water, the results were shown in (Tab. 8B and 9B). The TDS of water extract for the first liter was very high (23100 ppm) in Test 1, compared with last washing liter that was (3300 ppm) (Tab. 8). Comparing the extracted salt percentages of the sediment column by the first liter distilled water is (34.2%) to that of the last liter (85.5%) in Test 1, indicated that within each liter more salt removed from the soil to reach 85.5%. The extracted salt percentages in Test 2 of the sediment column by the first liter distilled water (TDS is 21900 ppm represent 36.9% of removable salt from the soil) to that of the last liter (TDS is 2750 ppm represent 87.4% of removable salt from the soil) in Test 2, indicated that within each liter more salt removed from the soil to reach 87.4% (Tab. 9). More salts were liberated from the sediment column after drying and washing with distilled water (Tab. 8A and B in Test 1; Tab. 9A and B in Test 2).

The sediment columns were dry again for two weeks at room temperature. Then sediment column was washed by using high salinity water (TDS 13100 ppm in Test 1), and (TDS 11800 ppm in Test 2) representing the Well water (W.5 and W.17) that may be used in irrigated by the farmers during the water deficit periods (summer months), and the seven liters were collected from the perforated end for TDS measurements (Table 8C, and 9C). The TDS of water extract for the first liter was TDS (2720 ppm) that indicate about 79.2% of the salt amount within the used water was staying in the sediment column compared with last washing liter that was (10000 ppm) that indicate about 23.6% of the salt content of the used water was staying in soil for Test 1. This experiment indicted salt accumulation in the sediment column section that within each liter more salt is stay in the sediment column (Table 8C). While for Test 2, the TDS of water extract for the first liter was TDS (2250 ppm) that indicate about 80.9% of the salt amount within the



**Sattar Obaid Maiws Al-Mayyahi**

used water was staying in the sediment column compared with last washing liter that was (9000 ppm) that indicate about 23.7% of the salt content of the used water was staying in the sediment column for Test 2. This experiment indicated that the salts accumulate in the sediment column section (Tab. 9C). The increasing of the salts from the sediment after drying, which is about 4.7% for the first test (Tab. 8) and about 2.4% for the second test (Tab. 9). Such results are in concordance with (Al-Hamdani, 2017) findings.

CONCLUSIONS**Groundwater Assessment**

The irrigation water classification based on electrical conductivity indicated that the water samples are of class (C3, EC= 750-2250) in Wells (W.1, W.2, W.8, W.10, W.11, and W.13, this results refer to acceptable water for irrigation, while water sample are of class (C4, EC \geq 2250) in Wells (W.3, W.4, W.5, W.6, W.7, W.9, W.12, W.14, W.15, W.16 and W.17. Such results refer to unacceptable water for irrigation, except for very salt-tolerant plants.

According to SAR values, all of the groundwater samples belong to (S1) excellent water class with no harmful effects of sodium, in which SAR <10.0 , except W.17 is good water belong to (S2) in which SAR 11-18 which is generally satisfactory for irrigation. While based on RSC, all the water samples showed (RSC) values less than zero; therefore, all the samples are suitable for irrigation uses regarding to this parameter. According to Na% value, the sodium percentages in groundwater samples indicate Permissible water.

The Water-sediment Relationship

There is a continuous decrease of available salt content within the sediment column by washing the sediment column with a distil water, and increase of salt in the sediment column by using the high salinity water. The increase of the TDS concentration in the water extracted either by using distilled water or drained water after drying the sediment samples for two weeks may give an indication of the significance of the wetting and drying processes in TDS release from the soil. If this is indeed the case, then there will be always available TDS in the soils of the Jassan area at the end of the irrigation period (May – June) prepared to be filtrate again by the first percolated rainfall (effective rainfall).

REFERENCES

1. Al-Dabbas, M.A., 2002. Sediment water interchanges of Boron during dry and wet conditions in the upper Dibdiba formation, Karbala- Najaf area, M. Iraq, Karbala University.
2. Al-Dabbas, M.A., 2005. High concentrations of Boron in groundwater at the Safwan – Zubair and Karbala – Najaf areas, S., and M. Iraq, IGJ, Vol.34, p.166 – 179.
3. Al-Hamdani, j.A., 2009. The efficiency of three different methods of washing in the washing severe soil salinity in central Iraq. Proceedings of the Eighth Scientific Conference of the Agricultural Engineers Association research. Baghdad, Iraq. Volume II 405 – 385.
4. Al-Hamdani, J.A., 2017. Urban environmental geochemistry in Kirkuk, Iraq, Unpub. Ph.D. Thesis, College of Science, University of Baghdad.
5. Al-Mayyahi, S.O.M., 2016. Assessment of Dujaila River Water and its relationship with the agricultural soils of Dujaila project – Wasit Governorate – Central Iraq, Unpub. M. Sc. Thesis, College of Science, University of Baghdad.
6. Al-Shammary, S.,H., E., 2008, Hydrogeology of Galal Basin- Wasit- East Iraq, unpublished Ph.D. Thesis, University of Baghdad, 172 p.





Sattar Obaid Maiws Al-Mayyahi

7. Al-Shihmani, L.S.S., 2015. Leaching of saline soil (Sabakh) by using some qualities of water and its impact on some chemical and physical properties of the soil, M, SC In Agriculture/ Soil Sciences and Water Resources. College of Agriculture At the University of Al-Qasim Green, unpublished.
8. APHA, 2005. Standard method for the examination of water and wastewater, 21st Ed. American public health Association, Washington, D.C.
9. Ayers, R.S., and Westcot, D.W., 1985. Water quality for agriculture. Irrigation and drainage. Paper No. 29. Food and Agriculture Organization of the United Nations, Rome, Italy, p. 1 – 117.
10. Boyd, C.E., 2000. Water quality an introduction, Kluwer Academic publisher, USA. 330pp.
11. Don, C.M., 1995. A grows guide to water quality, University college station, Texas.
12. FAO., 2003. Water quality for agriculture, Irrigation and Drainage. Paper No.29, Rev. 1 FAO. Rome – Italy.
13. Glover C.R., 1996. Irrigation Water Classification Systems, Guide A-116, New Mexico State University. NMSU and the U.S. Department of Agriculture.
14. Hem, J.D., 1985. Study and interpretation of the chemical characteristics of natural water. 3rd edit. U.S.G.S. Water supply paper. 2254.
15. Michael, A.M., 1992. Irrigation theory and practices. Vikash Publishing House Pvt. Ltd., New Delhi, India. p. 686 – 740.
16. Qannam, Z., 2003. A hydrogeological, hydrochemical and environmental study in Wadi ALArroub drainage basin, South, West Bank, Palestine, 9, 211pp.
17. Rowe, D.R., and Magid, I.M.A., 1995. Handbook of wastewater reclamation and reuse. CRC Press Inc., Florida, U.S.A., 550pp.
18. Shirazi, S.M., Ismail, Z., Akib, S., Sholichin, M., and Islam, M.N., 2011. Climatic parameters and net irrigation requirement of crops. *International Journal of Physical Sciences*. 6, p. 15 – 26.
19. Stoodly, K.D., Lewis, T., and Staintun, C.L., 1980. Applied statistical technique, John Willey and Sons, London, 215pp.
20. Todd, D.K., 1980. Groundwater hydrology second edition, John Wiley and Sons, Inc. New York. 535pp.
21. Todd, D.K., 2007. Groundwater hydrology, John Wiley and Sons, Third Reprint. Inc. India. 535pp.
22. Turgeon, A. J., 2000. Irrigation Water Quality, College of Agricultural sciences the Pennsylvania State University, USA, <http://turfgrass.cas.psu.edu/Education/Turgeon/Case Study/Old Ranch/IrrWat Qual.html>.
23. Van Hoorn, J.W., 1970. Quality of irrigation water, limits of use and predication of long term effects, Salinity Seminar Baghdad, Irrigation and Drainage paper No.7, FAO, p. 117 – 135.

Table 1: Location of all stations, samples and test in study area.

Wells	Longitude	Latitude
W1	45°45'13"E	32°51'55"N
W2	45°35'28"E	32°51'03"N
W3	45°34'27"E	32°56'57"N
W4	45°33'21"E	33°02'59"N
W5	45°40'17"E	33°00'07"N
W6	45°39'11"E	33°04'28"N
W7	45°45'09"E	33°03'53"N
W8	45°47'11"E	32°58'11"N
W9	45°51'02"E	33°01'29"N
W10	45°54'57"E	32°59'05"N
W11	45°52'34"E	32°52'11"N
W12	45°57'28 "E	32°46'21"N





Sattar Obaid Maiws Al-Mayyahi

W13	45°59'24"E	32°52'20"N
W14	46°03'31"E	32°54'09"N
W15	46°06'27"E	32°51'25"N
W16	46°02'25"E	32°47'02"N
W17	46°05'03"E	32°43'31"N
Test 1	45°40'17"E	33°00'07"N
Test 2	46°05'03"E	32°43'31"N

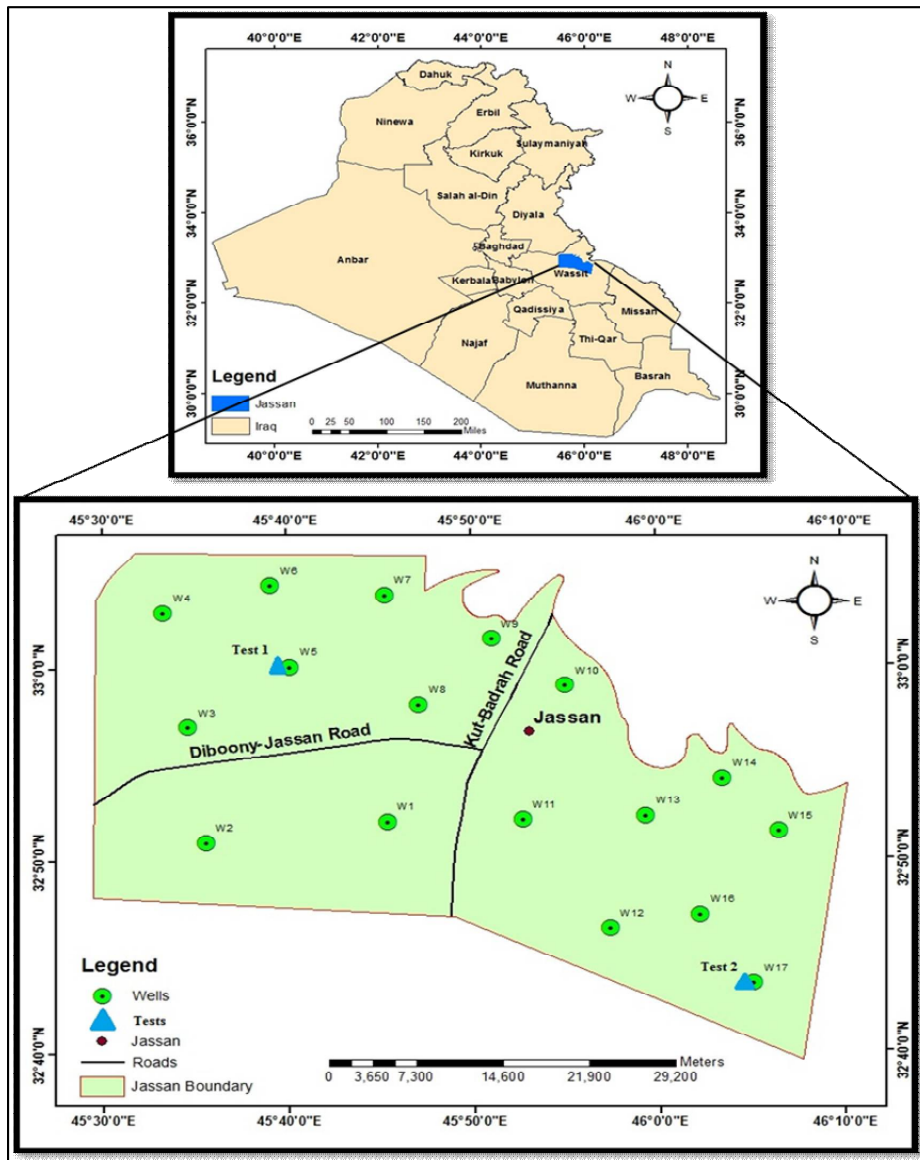


Fig. 1: Locations of groundwater samples and the sediment-water interrelation tests in the study area.





Sattar Obaid Maiws Al-Mayyahi

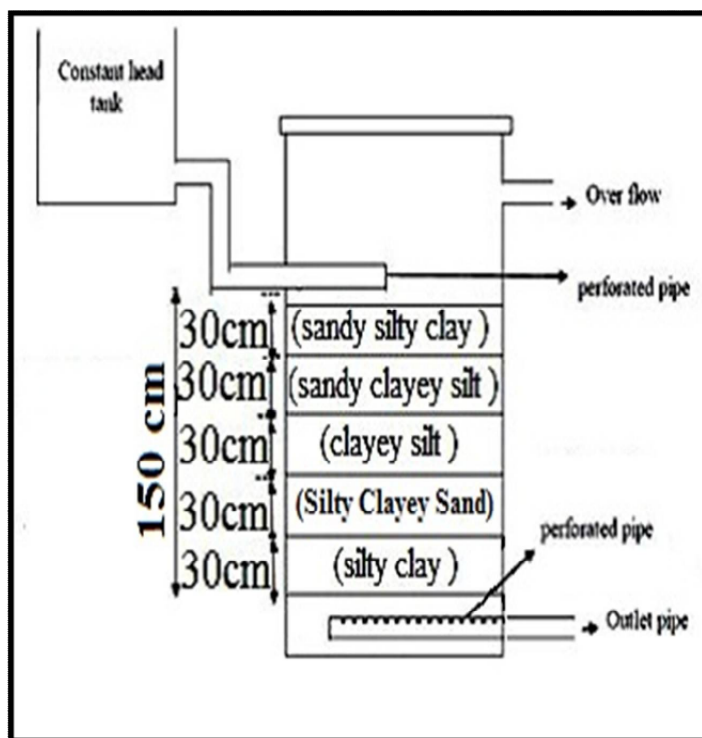


Fig. 2: The laboratory setup of the filtration process.

Table 2: Chemical properties of water samples during March 2017.

Sample No.	K ⁺	Na ⁺	Ca ²⁺	Mg ²⁺	Cl ⁻	SO ₄ ²⁻	HCO ₃ ⁻	Accu.	TDS Mg/L	pH	EC (µs/cm)
	Mg/L										
W.1	7.2	246	138	70	264	470	300		1510	7.2	2195
epm	0.18	10.7	6.9	5.8	7.4	9.8	4.9	97			
W.2	9.3	248	141	69	266	472	310		1525	7.2	2200
epm	0.23	10.7	7.0	5.7	7.5	9.8	5.0	97.2			
W.3	6.5	340	220	80	212	700	560		2370	7.2	3400
epm	0.16	14.7	11	6.6	5.9	14.5	9.2	95.3			
W.4	7.4	853	655	118	890	1580	890		5090	7.3	7400
epm	0.18	37.1	32.7	9.8	25.1	32.9	14.6	95.3			
W.5	12.3	1760	966	260	1880	2620	1550		9000	7.4	13100
epm	0.31	76.5	48.3	21.6	52.9	54.5	25.4	95			
W.6	6.7	350	240	88	235	770	700		2550	7.3	3690
epm	0.17	15.2	12	7.3	6.6	16	11.4	99.1			
W.7	7.5	647	595	124	390	1810	1150		4875	7.5	7075
epm	0.19	28.1	29.7	10.3	10.9	37.7	18.8	99.3			
W.8	7.1	172	97	49	184	300	270		1150	7.4	1660
epm	0.18	7.4	4.8	4.0	5.1	6.2	4.4	97.5			





Sattar Obaid Maiws Al-Mayyahi

W.9	6.9	247	160	71	285	486	310		1640	7.5	2375
epm	0.17	10.7	8	5.9	8	10.1	5	96.6			
W.10	7.2	240	130	63	255	455	280		1510	7.2	2195
epm	0.18	10.4	6.5	5.2	7.1	9.4	4.6	98.1			
W.11	7.1	245	125	55	234	460	290		1490	7.2	2150
epm	0.18	10.6	6.2	4.5	6.6	9.5	4.7	99			
W.12	11.8	1030	860	230	1520	1950	1400		7100	7.5	10200
epm	0.30	44.7	43	19.1	42.8	40.6	22.9	99.6			
W.13	7.0	213	133	62	215	455	280		1430	7.5	2070
epm	0.17	9.2	6.6	5.1	6	9.4	4.5	97.3			
W.14	7.1	230	150	65	275	480	305		1600	7.5	2315
epm	0.18	10	7.5	5.4	7.7	10	5	99.3			
W.15	6.7	340	230	80	225	750	650		2350	7.3	3400
epm	0.17	14.7	11.5	6.6	6.3	15.6	10.6	99.4			
W.16	7.5	872	597	129	842	1530	930		5154	7.4	7450
epm	0.19	37.9	29.8	10.7	23.7	31.8	15.2	94.7			
W.17	12.7	1410	1150	255	1830	2415	1100		8150	7.3	11800
epm	0.32	61.3	57.5	12.7	51.5	50	18	95.1			

W = groundwater samples

Table 3: Classification of irrigation water based on salinity EC values (Turgeon, 2000).

Level	EC (µs/cm)	Hazard and limitations
C1	≤ 250	Low Hazard; no detrimental effects on plants, and no salt buildup expected.
C2	250 – 750	Sensitive plants may show stress; moderate leaching prevents salt accumulation in soil.
C3	750 – 2250	Salinity will adversely affect most plants; requires selection of salt tolerant plants, careful irrigation, good drainage, and leaching.
C4	≥ 2250	Generally unacceptable for irrigation, except for very salt-tolerant plants, excellent drainage, frequent leaching, and intensive management.

Table 4: Classification of irrigation water based on SAR values (Turgeon, 2000).

Level	SAR	Hazard
S1	≤ 10	No harmful effects of sodium
S2	11 – 18	An appreciable sodium hazard in fine – textured soil of high CEC but could be used on sandy soils with good permeability.
S3	18 – 26	Harmful effects could be anticipated in most soils and amendments such as gypsum would be necessary to exchange sodium ions.
S4	≥ 26	Generally unsatisfactory for irrigation





Sattar Obaid Maiws Al-Mayyahi

Table 5: SAR, Na% and RSC values of groundwater samples, March 2017.

Samples No.	March 2016		
	SAR	Na%	RSC
W.1	3.4	46.1	-7.8
W.2	3	46.2	-7.7
W.3	3.5	45.4	-8.4
W.4	5.7	46.7	-27.9
W.5	10	52.3	-44.5
W.6	4.9	44	-7.9
W.7	6.3	41.4	-21.2
W.8	3.7	46.2	-4
W.9	4.1	43.8	-8.9
W.10	4.3	47.4	-7.5
W.11	4.6	50.2	-6
W.12	8.1	42	-39.2
W.13	3.8	44.4	-7.2
W.14	4	44.2	-7.9
W.15	4.9	45.1	-10.6
W.16	8.4	48.4	-25.3
W.17	10.3	46.7	-52.2

Table 6: Classification of irrigation water based on RSC values, according to Turgeon (2000).

RSC	Hazard
< 0	None
0 – 1.25	Low, with some removal of calcium and magnesium from irrigation water
1.25 – 2.50	Medium, with appreciable removal of calcium and magnesium from irrigation water
> 2.50	High, with more calcium and magnesium removed, leaving sodium to accumulate

Table 7: Classification of irrigation water based on Na% values (Don, 1995).

Water quality	Excellent	Good	Permissible	Doubtful	Unsuitable
Na%	20	20 – 40	40 – 60	60 – 80	> 80





Sattar Obaid Maiws Al-Mayyahi

Table 8: The TDS and TDS% of the washing sediment column by distil and Well water to site (Test 1).

Extract Liter. No.	Extract LiterTDS ppm	Extracted Salt % from the soil by distilled water	
Wash with distilled water			
A	1	23100	34.2
	2	15200	53.3
	3	10700	68.8
	4	7200	74.4
	5	5900	77.9
	6	5100	80.9
	7	4400	83.1
	8	3900	85.5
	9	3300	85.5
	10	3300	85.5
After drying two weeks, Wash with distilled water			
B	1	3465	3.8
	2	3330	10.5
	3	3100	19.2
	4	2800	23.5
	5	2650	23.5
	6	2650	23.5
Extract Liter. No.	TDS is resulting from soil washing by Well water used in irrigation	% of difference between the Well water and the extracted water	
After drying two weeks, Wash with Well water TDS= 13100 ppm from well No.5			
C	1	2720	79.2
	2	3210	75.4
	3	4800	63.3
	4	6100	53.4
	5	8400	35.8
	6	9200	29.7
	7	10000	23.6





Sattar Obaid Maiws Al-Mayyahi

Table 9: The TDS and TDS% of the washing soil by distil water and Well water to site (Test. 2).

Extract Liter. No.	Extract LiterTDS ppm	Extracted Salt % from the soil by distilled water	
Wash with distilled water			
A	1	21900	36.9
	2	13800	65.2
	3	7600	76.2
	4	5200	80.3
	5	4300	84
	6	3500	85.8
	7	3100	87.2
	8	2800	87.4
	9	2750	87.4
	10	2750	87.4
After drying two weeks, Wash with distilled water			
B	1	2820	5.3
	2	2670	10.2
	3	2530	14.8
	4	2400	21.9
	5	2200	21.9
	6	2200	21.9
Extract Liter. No.	TDS is resulting from soil washing by Well water used in irrigation	% of difference between the Well water and the extracted water	
After drying two weeks, Wash with Well water TDS= 11800ppm from Well No.17			
C	1	2250	80.9
	2	2600	77.9
	3	3900	66.9
	4	5000	57.6
	5	6100	48.3
	6	7500	36.4
	7	9000	23.7





Histological, Histomorphometrical and Histochemical Study of Stomach Development in Guinea Pigs (*Cavia porcellus*)

Iman M. Khaleel^{1*} and Alaa N.Salih²

¹Assist. Professor, Department of Anatomy and Histology, College of Veterinary Medicine, University of Baghdad, Iraq.

²Assist. Lecturer, Department of Biology, College of Education, University of Wasit, Iraq.

Received: 17 June 2018

Revised: 20 July 2018

Accepted: 27 Aug 2018

*Address for Correspondence

Iman M. Khaleel

Assist. Professor

Department of Anatomy and Histology,

College of Veterinary Medicine,

University of Baghdad, Iraq.



This is an Open Access Journal / article distributed under the terms of the **Creative Commons Attribution License** (CC BY-NC-ND 3.0) which permits unrestricted use, distribution, and reproduction in any medium, provided the original work is properly cited. All rights reserved.

ABSTRACT

The aim of this study was to determine the histological, histomorphometrical and histochemical properties of the stomach in the neonatal guinea pigs. For this purpose, thirteen healthy neonatal male guinea pigs *Cavia porcellus* were used. This study was carried out on different ages of guinea pigs, from 1 day, 7 to 10 days of age. This study showed that the wall of stomach in five age groups was consist of four tunicae. The tunica mucosa in all age groups was covered by simple columnar cells that extend in the gastric pits where the gastric glands were opened, also showed an increased in the thickness of all tunicae of the stomach wall with the advancing of age. The numbers of glands in the three stomach regions was increased with the age and the type of gastric glands in studied groups showed as a short branched tubular and coiled glands in both cardiac and pyloric glands regions, whereas in the fundic glands regions they showed as simple branched tubular long straight over most of their length which coiled at the basal part. The prominent cells in the cardiac glands region were the mucous secreting cells and a few numbers of parietal cells which do not increase obviously in its numbers with the age, while in the fundic glands, different types of cells were present but the two main cells were the parietal and chief cells which slightly increased in its numbers with the age, Whereas in the pyloric glands the prominent cells were the mucous secreting cells with few numbers of parietal cells which do not increased obviously in its numbers with the age. The surface lining cells of stomach, gastric pits and the gastric glands in both cardiac and pyloric glands regions react positively with PAS stain whereas in the fundic glands region only the surface lining epithelium and the gastric pits showed a positive reaction with the PAS stain. The Masson Trichrome stain was used to detect the connective tissue fibers in the stomach wall. The silver



**Iman M. Khaleel and Alaa N.Salih**

nitrate stain showed presence argentaffine cells, type of endocrine cells in the base of pyloric glands of the stomach in five studied groups.

Keywords: histomorphometrical, *Cavia porcellus*, endocrine cells,

INTRODUCTION

The Guinea pig or as called the cavy is belong to: Order; Rodentia, Family: Caviidae, Genus; *Cavia*, Species: *porcellus* [1]. In South America the guinea pig still raised as a source of meat. The body of guinea pig is compact, stocky short legs and no tail. Guinea pigs weighing 700 to 1200 (gr.) , its measuring 20 to 25 cm in length and live to 4 - 5 years, or may live to 8 years [2]. Males reach sexual maturity at 3 to 5 weeks whereas females as early as four weeks [3]. The biological characteristics of guinea pig make the animal valuable animal model for human medical conditions, for research in the fields of biology, medicine, physiology and immunology [4] and for studying developmental biology and the pathogenesis of many diseases [5]. The stomach is a component of the gastrointestinal tract. Generally, the stomach in vertebrate is serving a number of important functions such as its direct role in digestion by acid and enzyme secretion [6], storage of food, milling and mixing of food with gastric juice, the strongly acidic gastric secretion serves to diminish a numbers of microorganisms which invade the body through the mouth and one component of the gastric juice is the intrinsic factor which promotes vitamin B12 absorption [7].

This study is aimed to determine the histological features, histomorphometrical and histochemical properties of stomach in neonatal guinea pigs *Cavia porcellus* to understand any stomach pathological changes due to different diseases and to understand its physiology.

MATERIALS AND METHODS

Thirteen healthy neonatal male guinea pigs *Cavia porcellus* were used in this investigation, obtained from AI-kindly Company for vaccines product. These animals were divided into five age groups include this ages (1, 7, 14, 21, 28) day. Specimens were obtained along the greater curvature from Cardiac, Fundic and pyloric glands regions of the stomach [8], were fixed in the 10% formalin at room temperature for 48 h, dehydrated in a series of alcohol at increasing concentrations (70, 80, 90-100%) for 2 hour of each and embedded in paraffin wax. Histologic serial sections of 6 μ m of thickness were stained routinely with haematoxylin and eosin and with the special periodic acid-Schiff (PAS), Masson Trichrome and the silver nitrate stain [9]. The morphometric data were expressed as Mean \pm SE. The statistical analysis of data was performed using analysis of ANOVA test and L.S.D and significant differences limited on $p < 0.05$ of probability [10] and the figures were documented under light microscope with a different power of light microscope (Olympus) using a digital camera (Winjoe).

RESULT AND DISCUSSION

Histological study

In all studied groups of male guinea pigs, the stomach was lined by a mucous membrane which divided into three regions according to the type of glands in each region, cardiac, fundic and pyloric glands regions as found in some mammalian stomach [11]. In all studied ages the wall of stomach has the same four tunicae; mucosa, submucosa, muscularis and serosa (Fig.1), as observed in some laboratory animals by [12]. The mucosa was covered by simple columnar epithelium that extend to line the gastric pits (Fig. 2), as found in human fetuses, the surface epithelium appeared at 21th week [13]. The mucosa and submucosa in fundic region in empty stomach showed longitudinal





Iman M. Khaleel and Alaa N.Salih

folds more than in the pyloric region, this finding was compatible with that observed in rat stomach at first week of birth [12], these folds increase the stomach surface area and enable it to occupy more amount of food [14].

Cardiac glands region

Epithelial heights, tunicae thickness and feature of gastric glands

In all studied groups the tunica mucosa covered by simple columnar epithelium that extend to lined the gastric pits which continuous with the opening of cardiac glands in the lamina propria (Fig. 3), similar finding was observed in dog and cats [15]. The mean epithelial height was showed increase in values with the advancing age and no significant differences between them as showed in (Table2), this result may be due to the function of the surface lining epithelium is the same in all age groups and these epithelial cells are critical for protective and resisting attack by gastric acid and enzymes, these cells secret amucopolysaccharide that acts as buffer system protection against acidic materials [16].

The lamina propria appear as large amount of connective tissue contains cardiac glands and extend from underlying epithelium to muscularis mucosa (Fig.1,3). The mean lamina propria height was increased from the 1st to 5th group (Table2). This finding may be due to thickness increment in the stomach wall with age and the increment in lamina propria thickness which companied by elongation of the cardiac glands into the lamina propria [17]. The cardiac glands in the lamina propria in all age groups appears as branched tubular coiled, short glands and long pits (Fig.1,3), this is similar to that found in rabbit stomach by [18].

The muscularis mucosa showed as longitudinal and circular smooth muscle layers, small bundles of fibers were extended between the cardiac glands (Fig. 4), there was an increase in the muscularis mucosa thickness with the age (Table2). This result may explain the same function of muscularis mucosa in all studied groups in its contractile activity to release the gastric glands contents, this observation confirms the previously found in rat [12]. In all studied ages the tunica submucosa was composed of loose connective tissue, blood and lymph vessels and nerve plexuses (Fig. 1,3). The mean thickness of tunica submucosa was a minimum in the 1st age and increased with the age to reach a maximum value in the 5th age (Table2). These results may be due to that the submucosa houses the blood vessels that increase in its diameter with the growing stomach. Tunica muscularis in all studied ages showed an inner circular and an outer longitudinal layers of smooth muscle fibers, Auerbachs plexus was observed between the two layers (Fig. 5). The mean thickness of tunica muscularis recorded lowest value in the first group and slightly increased in the second group then highly increased in the third, fourth and fifth group to reach respectively (Table2). This result mean that there was a growth of tunica muscularis and increase in its thickness with the growth and the development of animal, in the 1st and 2nd groups, the main source of diet was milk and a few amount of solid foods but with the advancing of age the quality and quantity of food intake which is a plant origin was increased and changed which lead to increment in the tunica muscularis thickness with the stomach and animal growing and may be due to the need of animal to more quantity of plant food origin which play a key role in the wall developing especially the muscular layer that permite elastic stomach distension and for subsequent peristaltic movement required for the mechanical food mixing and secrete products [19]. The tunica serosa noticed as a loose connective tissue covered by mesothelium, in all studied groups, as found in feline by [20]. The mean serosa thickness was a minimum in the 1st stage and a maximum value at the 5th (Table2), the increment may be due to the increases in the stomach layers thickness with the age.

Fundic glands Region

Epithelial heights, tunicae thickness and feature of gastric glands

The mucosa and submucosa in all studied groups were thrown into longitudinal large rugae which protruded into the gastric lumen (Fig. 6), as previously observed in the neonatal rats by [12]. The surface lining epithelium were simple columnar epithelium which continuous to lined the shallow gastric pit, as observed in the stomach of mice,



**Iman M. Khaleel and Alaa N.Salih**

they explains that the presence of abundance epithelial cells is an evidence protective function to the mucosa from the erosive effect of HCl which released by parietal cells[21]. The mean epithelial height was a minimum in the 1st group and slightly increases to 2nd, 3rd, 4th groups in the 5th group respectively (Table3), this findings mean that the lining epithelium has a mucous secreting cells which acts as a protection against acidic material [22]. Very difficult to distinguish connective tissue of lamina propria between the long, crowded fundic glands which opened in the gastric pits bases (Fig. 7). The fundic glands in the different studied ages shows as simple branched tubular, long and penetrate its whole thickness, perpendicularly to the mucosal surfaced densely arranged. Each gland display narrow lumen with blind coiled end (Fig.7), this finding previously observed in monkey by [23] and in Malayan pangolin by [24]. The mean thickness of lamina propria showed in (Table 3), this result was compatible with the previously found in rat by [12]. Tokeoka and Kataoka (1986) stated that with the age there were elongation of gastric glands in the lamina propria. The muscularis mucosa appeared as layers of smooth muscle fibers oriented in an outer longitudinal and an inner circular layers. The mean thickness of muscularis mucosa was increased with the age (Table 3), as previously found in rabbit by [18].

The tunica submucosa appeared as a loose connective tissue contain lymphocyte, blood and lymph vessels, the submucosa form the core of the mucosa folds of (Fig. 8), Similar organization observed in some laboratory animals by [25]. The mean thickness of tunica submucosa was showed in (Table3), this result may be due to growth of stomach wall with the growth of animal which was the main source of diet was milk and a few amount of dry food in the first days which changes to dry feed eater with the age, this finding confirmed the previously observed in goat by [26]. The tunica muscularis in all studied groups showed as a thin outer longitudinal and a thick inner circular layers of smooth muscle fibers and between these layers; Auerbach's plexus was present (Fig. 9). Similar organization was display in hamster by [25]. The mean thickness of tunica muscularis was increase with the age, there were no significant differences between the 1st and 2nd groups and between the 3rd and 4th groups at $P < 0.05$ (Table3), this finding may be due to the need of animal to more plant origin food with the advancing age, this changing in the quality and quantity of food intake plays an a crucial role in the wall developing especially the muscular layer that permits the elastic stomach distension and for subsequent peristaltic movement required for food mechanical mixing [19]. The outer most layer was the tunica serosa which appears as a loose connective tissue covered by mesothelium (Fig. 9), same result was observed in rat at early fetal and neonatal stages by [12]. The mean thickness of tunica serosa showed in (Table3), there were no significant differences $p < 0.05$ between the 1st four groups and between the 4th and the 5th groups, these findings mean that there was a gradual increment in the thickness of tunica serosa with the age.

Pyloric glands region

Epithelial heights, tunicae thickness and feature of gastric glands

The histological organization of the pyloric glands region in all studied ages was similar to that in cardiac gland region but the histomorphometrical measurements was differ. The surface epithelial lining cells and gastric pits was simple columnar cells (Fig. 10), the pits in this region showed deeper than those found in the fundic and cardiac gland regions, as previously observed in simple stomach of domestic animals by [27]. The mean height of surface epithelial cells were showed in (Table4), there were no significant difference between all studied groups at $p < 0.05$, this result may be due to that the surface lining cells have the same function in all studied groups which was mucus secreting that plays critical role in the defense mechanism against the corrosive effect of hydrochloric acid and pepsin of the gastric juice [28]. Underneath the epithelium was vascularized lamina propria more than in fundic glands region which appears as a distinguish connective tissue occupied by the pyloric glands (Fig. 11). The pyloric glands appear as simple branched, short tubular, coiled in its end and open into the base of deep gastric pits in all studied ages (Fig. 11), as observed in rabbit by [18].

The mean thickness of lamina propria showed an increment in the lamina propria with the age which may be due to the increment in the stomach wall thickness with the growing of animal. The muscularis mucosa represents a layer of smooth muscle fibers oriented in longitudinal and circular layers underneath the mucosa (Fig. 11, 12). The histological composition of muscularis mucosa was same to that observed in the simple stomach by [29].



**Iman M. Khaleel and Alaa N.Salih**

The mean thickness of muscularis mucosa was showed in (Table4), No significant importance between all studied ages at $P < 0.05$, this investigation showed there was a gradual increment in the thickness of muscularis mucosa with the advancing age, this finding may be due to the requirement of the contractile activity of muscularis mucosa to empty the contents of the gastric glands. The tunica submucosa appeared as a loose connective tissue houses blood and lymphatic vessels, the appearance and composition of tunica submucosa were same to that observed in the rabbit, hamster, gerbil by [25]. The mean thickness of tunica submucosa in the 1st group was showed in (Table4), There was a significant difference between the 1st and 5th group at $p < 0.05$, this result mean that the thickness of this layer was a minimum at the 1st group and a maximum at the 5th group.

The tunica muscularis in all studied groups showed two layers arranged in a thick inner circular and thin outer longitudinal layers of smooth muscle fibers. The mean thickness of tunica muscularis appeared as higher than those recorded in cardiac and fundic gland regions, this result was compatible with that observed in Malayan pangolin [24] and in rabbit stomach [18]. The mean thickness of tunica muscularis was showed (Table4), there were a significant difference between the 1st and the 2nd with the other groups at $p < 0.05$, as observed in the cardiac and fundic regions, there was an increase in the thickness of tunica muscularis with the age, this finding may be due to the growing of the animal tissues with the advancing of age and to requirement of muscular activity to deflation contents of the stomach into the duodenum. The tunica serosa was the outer most layer of stomach wall which appears in all studied ages as a loose connective tissue covered by simple squamous epithelium.

The mean thickness of tunica serosa recorded a minimum value at the 1st group and increased gradually to reach the 5th group (Table 4), there was no significant difference between the studied groups at $p < 0.05$. The previous study have reported same histological structure of tunica serosa in mammalian stomach by [19].

Cardiac glands region: Numbers of glands, parietal and chief cells

The present study showed that the numbers of cardiac glands were a minimum in the 1st group and increase with the age (Table5), there were a significant differences between the 1st and 2nd groups with the other groups at $P < 0.05$, this result may be due to the growth of the stomach wall including the mucosa which accompanied by elongation of gastric pits and gastric glands [17], this finding was confirm the previous study in the local rabbit [18].

The present finding revealed that the principal cell type in all aged groups of the cardiac glands were the mucous secreting cells and few numbers of parietal cells are present. No chief cells are present in the cardiac glands (Fig. 13). Similar observations were observed in goat, rabbit and mouse in gastric mucosa by [30, 18, 21]. The dominance or abundance of mucous cells in the cardiac region of the gastric mucosa is an indication that large quantities of mucous are produce in this region to neutralized the damaging and corrosive effect of hydrochloric acid which produce by the parietal cells in the fundic region. Mucous cells does not produce digestive enzymes but mucous. This is evidence that digestion of food does not occur in this part of the stomach [21]. The presence of few parietal cells in this region indicates that little quantity of acid is produced here [31] and it may be due to that the acid produced in the body region is not enough to carry out complete conversion of pepsinogen to pepsin [32].

The present study was incompatible with [33] who reported that the cardiac region composed of only mucous cells and no parietal and chief cells are present [27] explain that this differences may be due to that passing from fundic glands region to the cardiac glands region, the number of parietal cells become fewer and more proximally the parietal cells are very scant and most proximal portion of cardiac glands area contain only mucous secreting cells. The mucous cells appeared as a pyramidal cell or cuboidal with round and oval nuclei and basally located (Fig. 13). The scattered parietal cells appeared as large, rounded or pyramidal cells with central spherical nucleus and eosinophilic cytoplasm (Fig. 14).



**Iman M. Khaleel and Alaa N.Salih**

The number of parietal cells per glands was showed in (Table6), there was no significant importance between all groups at $P < 0.05$, as observed previously, all types of gastric glandular cells become to be present and mature at birth [34].

Fundic glands region: Numbers of glands, parietal and chief cells and the diameters of parietal cells

The number of fundic glands were showed in (Table5), there were no significant differences between the 2nd, 3rd, 4th and 5th groups at $P < 0.05$, this result confirms that previously found in goat by [26]. The fundic glands contains a mixed cells population, but the principle cells were parietal and chief cells, the parietal cells were scattered along the length of the gland but they were found mainly in the upper half of the glands (Fig. 15), they appeared as a large round cells with an eosinophilic cytoplasm, centrally located nucleus (Fig. 15, 16), this finding agree with that previously observed in rat by [35].

The numbers of parietal cells in the 1st, 2nd, 3rd, 4th and 5th groups showed in (Table5), there was no significant differences between the studied ages at $P < 0.05$. This study showed that the parietal cells were most numerous in fundic glands region. This observation compatible with that previously investigated [23], the abundance of parietal cells signifies that the largest volume of hydrochloric acid is produced in this region, the hydrochloric acid converts the pepsinogen to pepsin to digest the protein [21].

The chief cells were the other principle type cells of the fundic glands found mainly in the bases of the glands (Fig. 15), they appeared as pyramidal or cuboidal cells with basally located nuclei, basophilic cytoplasm and more smaller than the parietal cells (Fig. 16), this findings confirms the previous observation in rat and mice [21], these cells are responsible for digestive enzymes secretion in the stomach, the presence of parietal cells and zymogenic cells suggests that the main digestive portion in the stomach was the fundic glands region. The number of chief cells per gland was 6.81 ± 0.33 , 6.89 ± 0.26 , 7.32 ± 0.53 , 7.34 ± 0.17 , 7.55 ± 0.24 in the first, second, third, fourth and fifth groups (Table5). There was no significant differences at $P < 0.05$ between the studied age groups, this result may be due to that all types of gastric glands cells become to be present and mature at birth [34].

The numbers of parietal and chief cells in the fundic glands in different aged groups might showed a significant importance of these cells in the digestive process occurs in the stomach and may be explains the reason of ability of the neonatal guinea pigs to consume the diet immediately after the birth. The diameter of parietal cells showed in (Table5), there were no significant differences between the studied ages at $P < 0.05$, this result means that the function of parietal cells is the secretion of the hydrochloric acid that convert the pepsinogen to pepsin to digest the protein [21]. The parietal cells constitute enormous percentage of the complete population of cells in the fundic region while in the pyloric and cardiac regions were lower than that in the fundic indicates that a few acid is produced in these regions [31], this may be due to that the amount of acid which produced in the fundic glands regions is not enough to convert the pepsinogen to pepsin [32].

Pyloric glands region. Numbers of glands, parietal and chief cells

The numbers of pyloric glands were a minimum in the 1st age group and increased with the age (Table 5), there were a significant differences between the 1st and 5th another groups at $P < 0.05$, this observation due to that during the development of stomach wall that accompanied by elongation of gastric pit and gastric glands [17] and since the glands were branched and coiled and that appear as an oblique and in cross section and may be these sections were increased with the elongation of glands. These finding in agreement with that found in goat [26]. Currently the predominant cell types in the pyloric glands were mucous secreting cells with a few parietal cells but no chief cells (Fig. 17), the mucous secreting cells appeared as cuboidal or pyramidal cells with basally located spherical or oval nucleus and basophilic cytoplasm (Fig. 18).



**Iman M. Khaleel and Alaa N.Salih**

The number of parietal cells were showed in (Table5), there were no significant differences between the studied groups, as in the fundic glands region the parietal cells have the same function. The chief cells were not observed in the pyloric glands region (Table5), this result was compatible with that reported in mice [36], this result may be due to that the parietal cells are decrease in its number from the fundic glands region toward the pylorus. The abundance of mucous secreting cells to protect the gastric mucosa of the cardiac and pyloric glands region and to neutralize the effect of the acid secreted and help to lubrication of foods for the enzyme to act upon [21].

Special stains

Periodic acid-Schiff stain (PAS)

The PAS stain has been used to highlight the mucus secreting cells of the gastric mucosa. This study revealed that the surface lining cells of the entire gastric mucosa including the gastric pits in all studied groups were mucous secreting cells. The surface lining cells, gastric pits and cardiac glands were revealed a positive reaction for PAS and showed pink color, therefore they were considered as mucous secreting cells (Fig. 3), many cardiac glands composed of mucous secreting cells entirely and others contains few parietal cells that gave a negative reaction for PAS (Fig. 3), this result was compatible with the previously found in rabbits [18]. The mucous is a positive for PAS due to its a polysaccharide which represent as buffer system protection against acidic substance and from auto digestion and also acts as a lubricant for mucosa [22].

In the fundic glands region, the positive reaction for PAS was limited to the surface lining cells and gastric pits that showed pink in color in all studied group whereas the fundic glands gave a negative reaction (Fig. 9), this result was confirms the finding in mouse and hamster [37]. The current study confirm that the surface lining cells and gastric pits were mucous secreting cells, while the fundic glands consisted of parietal cells which acts as acid secreting cells [38] and chief cells which responsible for the digestive enzyme secretion [39]. As in cardiac glands region, same pattern of staining was noticed in the pyloric glands region that revealed a positive reaction for PAS in the surface lining epithelial cells, gastric pits and pyloric glands which appeared as pink color in all studied age groups (Fig. 11, 17, 18), similar finding in rabbit by [18]. Many pyloric glands composed of the predominant mucous secreting cells and others contains a few numbers of parietal cells which gave PAS negative reaction.

Silver nitrate stain (Fontana stain)

This stain was used for detection of argentaffin granules in endocrine cells of the gastric mucosa. In his study the argentaffin cells were observed in the pyloric glands of all age groups which gave a positive reaction with silver nitrate stain and appears as dark pyramidal cells, oval or flattened cells rest on the basement membrane. Argentaffin cells scattered among the parietal and mucous cells of the pyloric glands (Fig. 19, 52). Some of them extended from the basement membrane to the glands lumen while others do not have luminal contact (Fig. 19, 20), as found in Gerbil by [40].

REFERENCES

1. Weir, B.J. (1974) : "Notes on the Origin of the Domestic Guinea-Pig". In Rowlands, I. W.; Weir, Barbara J.. The Biology of Hystricomorph Rodents. Academic Press. pp: 437– 446.
2. Cohn, D.W.; Tokumaru, R.S and Ades, C. (2004): Breeding and reproduction of Male Guinea Pigs. Braz. J. Med. and Biol. R. 37 (6): 847–851.
3. Aitken, M.L. Villaon, M. Pier, M. (1993). Characterization of a marker of differentiation for tracheal ciliated Respiration. Cell Mol. Biol. 9:26-32. Pub med: 8338674.





Iman M. Khaleel and Alaa N.Salih

4. Abidu- figueiredo, M., Xavier-silva, B., Cardinot, M., Babinski, M. and Chagas, M. (2008). Celiac artery in New Zealand Rabbit: anatomical study of its origin and arrangement for experimental research and surgical practice. *Pesq. Vet. Bars.* Vol. 28, No.5.
5. Mess A. (2007). The guinea pig placenta model of placental growth dynamic placenta.28:812.815 [Pub med: 17382996].
6. Walker, W. F. and Liem, K. F. (1994). *Functional anatomy of the vertebrates. An evolutionary perspective.* 2nd ed. Saunders College Publishing. Philadelphia. Pp. 602-617.
7. Saldain, Kenneth S (2004). *Anatomy and physiology-The unity of form and function* ,international 3rded. TheMcgraw-Hill companies pp.950.
8. Samuelson, D. A. *Textbook of veterinary histology.* ISBN- 31: 978- 0-7216-8174-0. Printed in China. (2007).
9. Bancroft, J. D. and A. Stevens, (1990). *Theory and Practice of Histological Techniques.* 3rd Ed., Churchill Livingstone, London, UK 10.
10. Al-Mohammed, N. T., Al-Rawi, K. M., Younis, M. A. and AlMorani, W. K. *Principle of statistics.* J. Al Mousl University. (1986).
11. Ownby, C. L. (2002). *Histology of parts index. Digestive system-1.* Htm
12. Ceredig R. and Toh B. H. (2012). Ontogeny of actin and microsomal antigens in gastric parietal cells. *Journal of clinical pathology*, 31, 578-584.
13. Chimmalgi M. and Sant S.M. (2005). Study of fetal stomach under light microscope. *J. Anat. Soc. India* (2)1-9.
14. Dyce, K. M., Sack, W. O. and Wensing, C. J. G. (2010). *Veterinary Anatomy.* 4thedn, Pp. 680-684. ISBN 978-1-4160-6607-1.
15. Aughey, E. and Fray, F. L. (2010). *Comparative veterinary histology with clinical correlates.* Manson publishing/The Veterinary Press, Pp.107-113.
16. King, D. (2010). Gastric surface mucous cell. <http://www.siumed.edu/dking2/erg/gicells.htm>. Ghoshal, N. G. and Bal, H. S. (1989). *Comparative morphology of the stomach of some laboratory mammals laboratory animals.* Vol 23. Pp. 21-29.
17. Takeoka, Y and Kataoka, K. (1986). Histogenesis of the mouse pyloric mucosa with special reference to the development of surface mucous cells and pylorocytes, and the formation of the generative zone. *Arch. Histol. Jpn.* (5):519-34.
18. AL-Shamery, H.D. (2011). *Anatomical and histological study of stomach in adult local rabbits Oryctolagus cuniculus.* Ms.c. thesis Baghdad University. Coll. Vet. Med.
19. Smith, D. M., Grasty, R. C., Theodosiou, N. A., Tabin, C. J. and Nasconer-Yoder, N. M. (2000). Evolutionary relationships between the amphibian, Ovipar and mammalian stomachs. *Evolution and Development* . 2. (6):348-359.
20. AL-Tikriti, M., Al-Baghdadi, F. K., Henry, R. W., Hoskins, H. and Titkemeyer, C. (1987). Correlative Light and Scanning Electron-Microscopic Study of Feline Gastric Mucosa: The Cardiac Region (*Pars cardiac*). *Acta anat.* 128:281-285.
21. Dare, W. N, Charles, A. O. and Al-Hassan, M I. (2012). Study of the Structure of the Gastric Mucosa in the Mouse Cell Population, *J. Life Sci. Biomed.* 2(5): 182-186.
22. Ahmed, YA., El-Hafez, A.A.E and Zayed, A.E. (2009). Histological and histochemical studies on the esophagus, stomach and small intestines of *Varanus niloticus*. *J. Vet. Anat.* Vol 2 No1, pp35-48.
23. Fayed, M. H.; Elnasharty, M. & Shoab, M. (2010). Localization of sugar residues in the stomach of three species of monkeys (*Tupaia daealis*, *Nycticebus cocang* and *Callithrix jacchus*) by lectin histochemistry. *Int. J. Morphol.*, 28(1):111-120.
24. Nisa. C., N. Kitamura, M. Sasaki, S. Agungprijono, C. Choliq, *Nomina Anatomica Veterinaria* (1992) .IV, ed Vergiliu, Bucharest.
25. Ghoshal, N. G. and Bal, H. S. *Comparative morphology of the stomach of some laboratory mammals laboratory animals.* Vol 23. Pp 21-29. (1989).
26. AL-Neamy, E. M. K. (2007). *Anatomical, histological and ultrastructural study of Abomasum and its glands development in Iraqi male goat,* PH. D thesis Baghdad university Coll. Vet. Med.





Iman M. Khaleel and Alaa N.Salih

27. Grossman, and Marks, (1960).Official publication of the American gastroenterological association.Gastroenterology.Vol. 38.No. 1. pp. 1-6.
28. Ferri, D. & Liquori, G. E. (1992).Characterization of secretory cell.glycoconjugatesin alimentary tract of ruin lizard (Podarcissicula-campestrisdebetta) by means of lectin histochemistry. Acta.Histochem., 93(1):341-49.
29. Bacha, W. and Bacha, L.M.S.(2000).color Atlas of Veterinary Histology. Second edition.
30. Hill K.J. (1985).The glands of the mucous membrane of the goat abomasum.Journal of Anatomy,Vol 85, pp.215-219.
31. Richter JE. (2007).The many manifestations of gastroesophageal reflux disease: presentation, evaluation, and treatment. GastroenterolClin North Am.36:577–59.
32. Schubert ML.(2008). Control of Gastric Acid Secretion in Health and Disease, Gastroenterology 134: 7, 1842-1860.
33. Johannes, A. G. and Rhodin, M. D. (1974).Histology A text and Atlas.Oxford University Press. New York. London. Toronto.J. Anat. 149, pp. 21-39.
34. Asari, M., Fukaya, K, and Kano, Y.(1984).Fine structure of developing gastric parietal cells in the bovine abomasum.Res.Vet.Sci.36(1):127-8.
35. EL-Shall. M. Laila.(2010). Age related changes in the fundic mucosa of stomach of male albino rats (Histological and immunohistochemical study).Egypt. J. Histol. Vol.33, No.1, March, 32-44. Embryol. 175: 7-14.
36. Treuting, P.M and Ddintzis. S .M(2012).Comparative anatomy and histology a mouse and human atlas 1st ed. UK: Elsevier Saunders. pp23-167.
37. Sheahan, D. G. and Jervis, H. R. (1976).Comparative histochemistry of gastrointestinal mucosubstances. Am. J. Anat. 146.103-132.
38. Young, B. and Health, J. W. (2000).Functional histology.Atext and color atlas. 3rd ed. Pp. 249-259.
39. Kurabayashi, Y., Yamada, J., Andren, A. and Kitamura, N. (1991).Cellular and subcellular localization of progastricsin in calf fundic mucosa colocalization with pepsinogen and prochymosin.Acta.Anat 140(1): 75-84.
40. Kapur,S.P.(1982). An ultra-structural cytochemical study of entero-endocrine cells of the pyloric antrum in the gerbil *Merionesunguiculatus*. Acta.Anat.112:220-232.

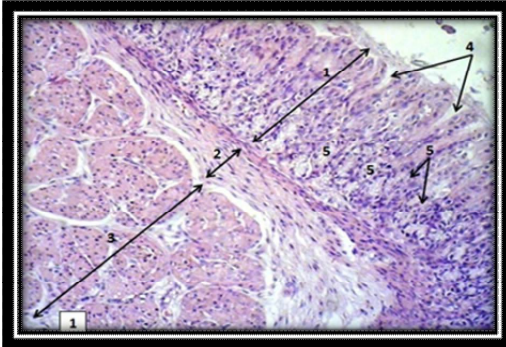


Fig. (1): Shows the cardiac glands region in the stomach in male guinea pig 1 day age: 1-Tunica mucosa 2-Tunica submucosa 3-Tunica muscularis 4-Gastric pit 5-Cardiac glands 6- lamina propria H&E X40



Fig.(2) Shows the tunica mucosa of fundic glands region in the stomach of 1 day male guinea pig: 1- Simple columnar epithelium 2-Gastric pits H&E X400





Iman M. Khaleel and Alaa N.Salih

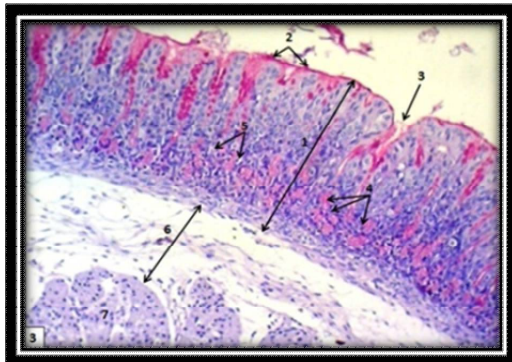


Fig .(3)Shows the tunica mucosa of cardiac glands region in 7 day age of male guinea pig: 1-Tunica mucosa 2-surface lining cells 3-gastric pits 4-cardiac glands 5-Lamina propria 6-Tunica submucosa 7-Tunica muscularis PAS X40

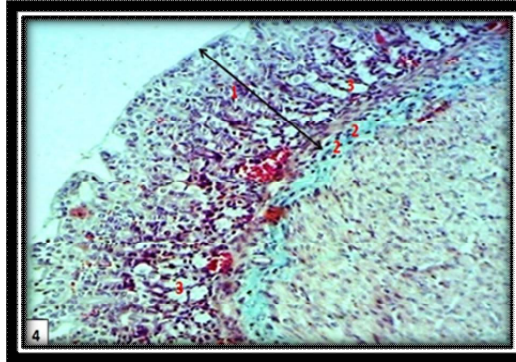


Fig (4): Shows the tunica mucosa in cardiac glands region of stomach in 21 day age of male guinea pig: 1- Tunica mucosa 2-muscularis mucosa 3-cardiac glands Masson Trichrom stain X40.

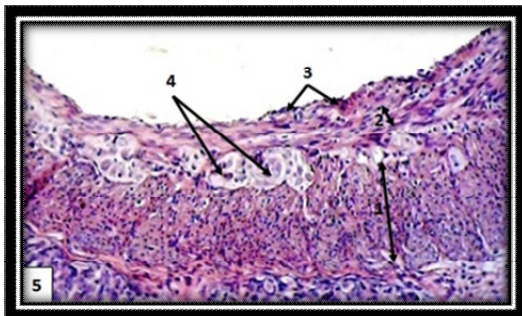


Fig. (5): Shows the tunica muscularis in cardiac glands region in the stomach in 1 day age of male guinea pig: 1- Inner layer 2- Outer layer 3- Tunica serosa 4- Auerbach's plexus H&E X 10.

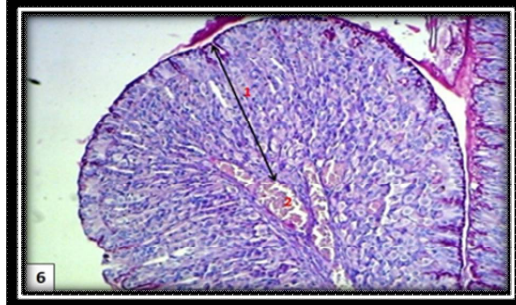


Fig. (6): Shows the rugae of fundus glands region in contracted the stomach in 14 day age of male guinea pig: 1-Tunica mucosa 2-Tunica submucosa PAS X 100.

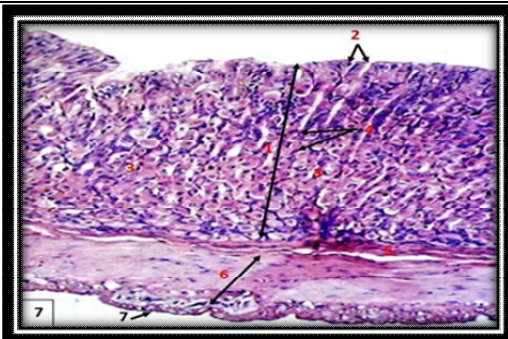


Fig. (7) Shows tunics of the fundic glands region of the stomach in 21 day age of male guinea pig: 1-Tunica mucosa 2- Gastric pit 3-Fundic glands 4-Lamina propria 5-Tunica submucosa 6-Tunica serosa 7-Tunica serosa H&E X100.

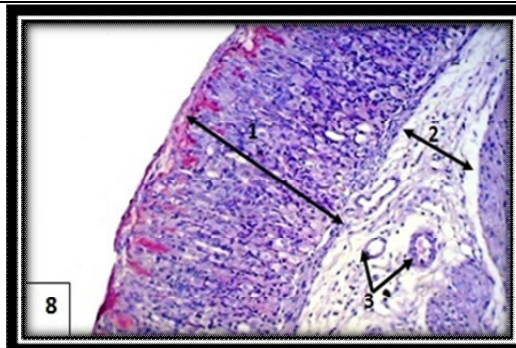


Fig. (8): Shows the tunics of the fundic glands region of the stomach in 7 day age of male guinea pig: 1-Tunica mucosa 2-Tunica submucosa 3- Blood vessels 4-Tunica muscularis PAS stain X100





Iman M. Khaleel and Alaa N.Salih

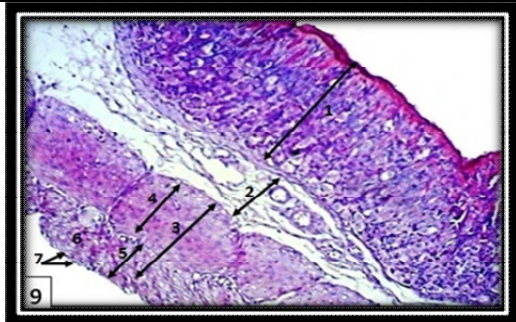


Fig.(9):Shows the tunics fundic glands region of stomach in 21 dayage of male guinea pig: 1-Tunica mucosa 2-Tunica submucosa 3-Tuinca muscularis 4- inner layer 5-Outer layer 6-Tunica serosa 7- mesotheliumPAS stainX100



Fig. (10):Shows the surface lining cells of pyloricmucosa of the stomach in 14day age of male guinea pig: 1-Simple columnar epithelium 2- Gastric pit 3-Parietal cell PAS x400.

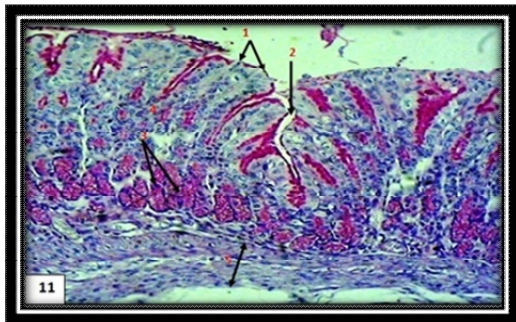


Fig (11):Shows the tunica mucosa of the pyloric glands region of the stomach in 21 day age of male guinea pig:1-Simple columnar epithelium2-Gastric pit 3- Pyloric glands 4-Lamina propria5-muscularis mucosaPAS stain X100.

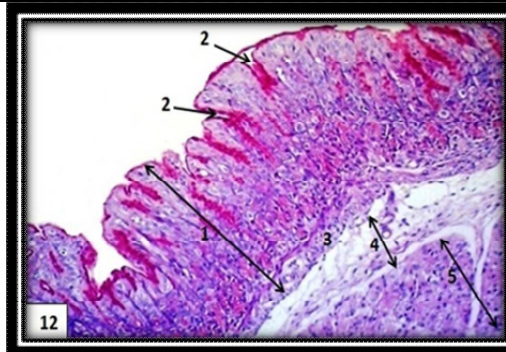


Fig. (12): Shows the tunics of pyloric glandsregion of the stomach in 7dayage of male guinea pig: 1-Tunica mucosa2-Gastric pit3- muscularismucosa4 - Tunica submucosa5-Tunica muscularis PAS X100.

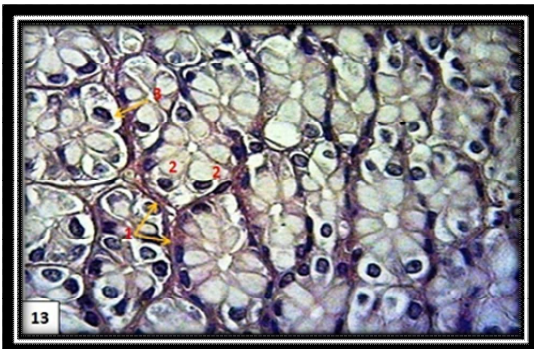


Fig.(13):Shows the cardiac glands of stomach in 21dayage of male guinea pig:1-Cardiac glands 2- Mucous cells 3-Parietal cell H &EX400.

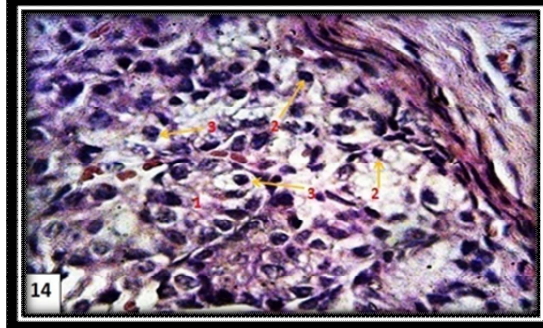


Fig. (14):Shows the cardiac glands of the stomach in 14dayage of male guinea pig:1-Cardiac glands 2- Mucous cells 3-Parietal cellMassonTrichrom stain X400.





Iman M. Khaleel and Alaa N.Salih

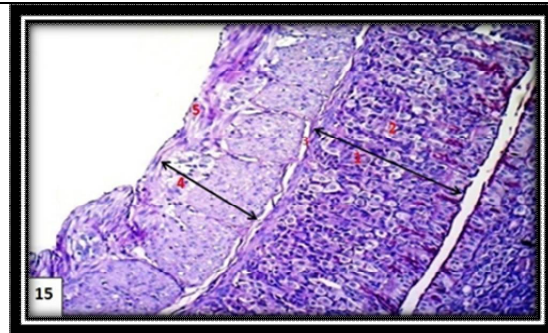


Fig. (15):Shows the fundic glands in 14 day age of male guinea pig: 1-Tunica mucosa 2-fundic glands 3-Tunica submucosa 4-Tunica muscularis 5-Tunica serosa PAS stain X100.

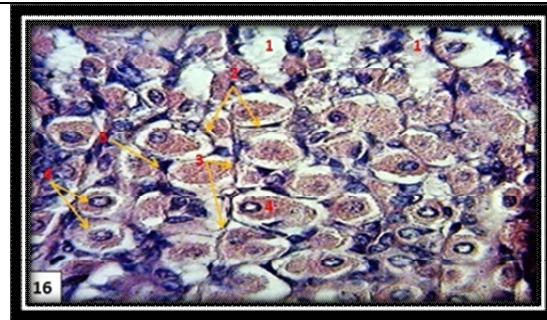


Fig. (16): Shows the fundic glands in fundic region of the stomach in 28 day age of male guinea pig: 1-gastric pits 2-gastric glands 3-lamina propria 4-parietal cells 5-chief cells H&E X400.

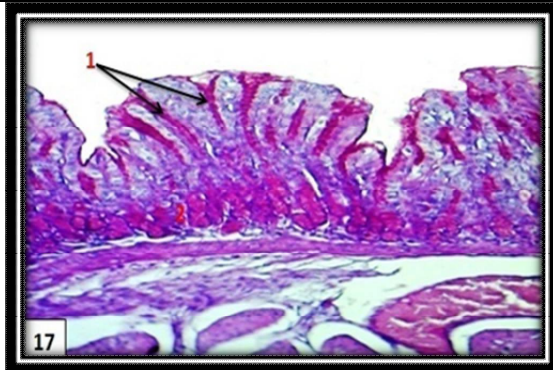


Fig. (17):Shows the pyloric glands of the stomach in 21 day age of male guinea pig: 1-gastric pits 2-Pyloric glands X100.



Fig. (18):Shows the pyloric glands of the pyloric mucosa of stomach in 14 day age of male guinea pig : 1-Pyloric glands 2-mucous cells 3-Parietal cells PAS X400

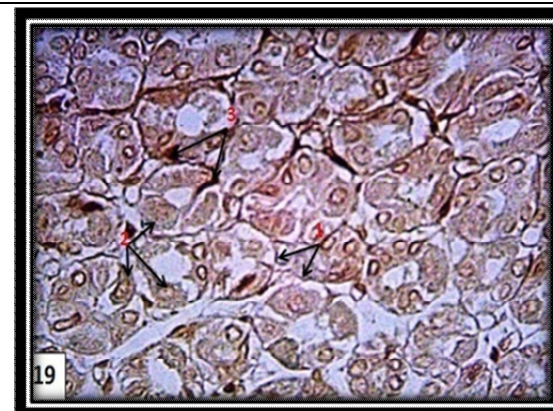


Fig. (19):shows the enteroendocrine cells in pyloric glands in stomach in 28 day age of male guinea pig- 1-pyloric glands 2-mucous cells 3-enteroendocrine cell silver nitrate stain X400.



Fig. (20): Shows the enteroendocrine cells in the pyloric glands region of the stomach in 28 day age of male guinea pig. Silver nitrate stain (Masson Fontana) X400





Iman M. Khaleel and Alaa N.Salih

Table 1. Shows the thickness of tunicae in the cardiac glands region of stomach in different ages of male guinea pig (Micrometer).

Age	Tunica mucosa			Tunica Submucosa M±SE L.s.d=37.57	Tunica muscularis M±SE L.s.d=75.30	Tunica serosa M±SE L.s.d=12.89
	Height of epithelium M±SE L.s.d=4.09	Lamina propria M±SE	Muscularis mucosa M±SE			
1day	a 15.42±0.64	a 315.00±29.4	a 34.96±5.46	a 35.70±2.52	a 200.53±19.2	a 18.23±2.52
7days	a 17.82±0.62	a 336.00±18.37	a 36.53±2.33	ab 56.83±2.41	a 202.12±11.55	ab 25.23±4.09
14 days	a 18.36±1.32	a 343.35±14.32	a 38.14±0.72	ab 67.22±10.05	b 398.12±25.41	ab 27.82±4.2
21 days	a 18.38±0.54	b 358.15±12.80	a 38.89±1.20	ab 71.4±10.03	bc 449.40±6.09	ab 29.44±3.09
28 days	a 19.45±1.35	b 360.15±22.89	a 39.97±0.51	b 83.32±5.3	c 474.60±9.03	b 32.40±2.25

Table 2. Shows the thickness of tunics in the fundic glands region of stomach in different ages of male guinea pig (Micrometer).

Age	Tunica mucosa			Tunica submucosa M±SE L.s.d=43.01	Tunica muscularis M±SE L.s.d=47.91	Tunica serosa M±SE L.s.d=13.73
	Height of epithelium M±SE L.s.d=1.21	Lamina propria M±SE	muscularis mucosa M±SE			
1day	a 17.16±0.64	a 367.50±18.16	a 42.00±5.98	a 37.81±2.52	a 155.44±22.36	a 14.50±3.71
7days	a 17.28±0.44	ab 420.00±30.24	a 45.46±2.35	b 94.50±14.38	a 201.60±6.09	a 18.9±2.1
14 days	a 17.82±1.32	bc 437.53±9.24	a 48.46±3.46	bc 119.73±20.05	b 320.89±11.97	a 28.87±2.62
21 days	a 17.88±2.37	cd 500.53±15.22	a 52.5±5.98	c 136.52±16.59	bc 365.90±12.6	ab 30.52±3.42
28 days	a 18.36±1.35	d 504.00±26.35	a 55.96±9.24	b 184.05±4.93	c 410.98±2.31	b 34.13±7.35

The similar letters represent no significant differences between groups at P<0.05.

The different letters represent significant differences between groups.





Iman M. Khaleel and Alaa N.Salih

Table 3. shows the thickness of tunics in the pyloric glands region of stomach in different ages of male guinea pig (Micrometer).

Age	Tunica mucosa			Tunica submucosa M±SE L.s.d=37.80	Tunica muscularis M±SE L.s.d=55.85	Tunica serosa M±SE L.s.d=12.15
	Height of epithelium M±SE L.s.d=4.62	Lamina propria M±SE	Muscularis mucosa M±SE			
1day	a 15.96±0.99	a 304.50±5.98	a 36.96±6.93	a 69.33±15.25	a 197.40±20.79	a 15.75±3.03
7days	a 18.09±1.35	b 318.15±22.89	a 41.37±3.99	ab 88.24±2.28	a 228.91±6.09	ab 26.25±3.10
14 days	a 18.36±1.00	ab 332.85±51.55	a 42.00±5.98	ab 98.72±6.34	b 432.68±25.72	b 30.76±5.02
21 days	a 18.98±1.08	bc 374.85±24.46	a 44.10±2.30	ab 100.84±3.61	bc 459.37±14.38	b 32.84±3.12
28 days	a 20.26±1.89	c 416.85±9.24	a 45.46±6.19	b 108.37±2.50	c 495.6±10.08	b 32.95±5.03

The similar letters represent no significant differences between groups at $P < 0.05$

The different letters represent significant differences between groups.





Study of Thermal Conductivity and Thermal Analysis (DSC, TGA, and DTGA) of (EPOXY –ZrO₂) Nanocomposites

Ruaa. H. Hassani*, Najwa. J.Jubier and Mohammed and J.Resen

Department of Physics, College of Science, University of Waist, Iraq

Received: 15 June 2018

Revised: 19 July 2018

Accepted: 27 Aug 2018

Address for Correspondence

Ruaa. H. Hassani

Department of Physics,

College of Science,

University of Waist, Iraq

E mail: ruaahilal83@gmail.com, najwajassim24@yahoo.com, mohamedjresen@gmail.com



This is an Open Access Journal / article distributed under the terms of the **Creative Commons Attribution License** (CC BY-NC-ND 3.0) which permits unrestricted use, distribution, and reproduction in any medium, provided the original work is properly cited. All rights reserved.

ABSTRACT

The aim of this work is to study the thermal conductivity and thermal analysis of prepared specimens from a thermosetting Epoxy resin mixing with different weight fraction (2, 4, 6, 8, and 10%) of Yattrastableazid zirconia nanoparticle (ZrO₂) using hand lay-up method, by using (Leesdisk) for Thermal conductivity evaluation, and thermal analysis has been investigated using differential scanning calorimetry (DSC), thermogravimetric analysis (TGA). The samples were heated from room temperature to 600 °C at a constant heating rate of 10 C/min under oxidative atmosphere using air. the glass temperature transitional (T_g) were determined From DSC curves for all the samples, while the activation energy were obtained from TGA curves and by using the Coats-Redfern Method. and other Kinetic parameters (Enthalpy, Entropy and Free energy) were determined for all specimens.

Keywords: Polymer nanocomposite, Epoxy, Yattrastableazid zirconia nanoparticle (ZrO₂), Thermal conductivity, Thermal analysis.

INTRODUCTION

Epoxy resin systems are class of polymers and mostly used as matrices in nanocomposite materials for a wide range of applications [1], on the other hand the development of composites and nanocomposites polymer filler can produce new materials with unique properties. The filler or reinforcing materials have micro or nano scale and are dispersed into the polymeric matrix, having as main function to improve the mechanical properties, gas barrier properties, thermal stability, fire retardancy, and other areas [2]. The improvement of these properties in polymeric nanocomposites is mainly due to the interaction between the filler particles and polymer matrix as a result of the higher surface area when compared to the traditional composites, however the interaction depends on the nature and





Ruaa. H. Hassani et al.

the structure of filler being used [3]. Zirconium Oxide (ZrO₂) Nanoparticles that composed of particles of zirconium oxide, known as zirconia; this material is used in various fields for applications ranging from polishing semiconductors to producing artificial jewelry. In addition, the zirconium oxide particle is known as yttria-stabilized zirconium oxide, and also as yttria-stabilized zirconia or zirconia-yttria. This material is produced when some of the zirconium ions in zirconia are replaced with yttrium, stabilizing the cubic phase of the material [4]. Thermal conductivity of nanocomposite is an important thermal property for both nanocomposite applications and processing. Most nanocomposite typically has intrinsic thermal conductivity much lower than those for metals or ceramic materials, and therefore are good thermal insulators [5]. The thermal analysis can provide important information on the temperature dependent properties of materials and of thermally induced processes (phase transition, decomposition, etc.). The thermal analysis gives a general view of the thermal behavior of a material under various conditions [6]. There are several researchers who have investigated the effect of reinforcement materials on polymer properties such that in (2012) A. Pegoretti and A. Dorigato noticed from DSC test that the glass transition temperature of Epoxy/ZrO₂ was noticeably improved by the addition of nanoparticles with a maximum value for an optimal filler concentration [7]. In (2015) S. Halder et al. show that the thermal stability and activation energy of the thermal decomposition of Ep/ZrO₂ enhanced significantly at the low nanoparticle content of [8]. and in (2017) H. Hong et al. show that nanoscale ceramic fillers are considered ideal candidates due to their thermal conductivity, and low thermal expansion coefficient and enhancing the thermal conductivity of a randomly dispersed ceramic-polymer composite is limited by its discontinuous filler contact and thermal expansion coefficient mismatch [9].

Thermal conductivity

Thermal conductivity means the quantity of heat flow in unit time through a unit area of a substance caused by a unit thermal gradient. The heat transfer process depends upon several factors, such as a type of material, state of the thermal substance and temperature. Mainly there are two mechanisms for heat transfer through a solid substance.

- 1- In solid conductors the free electrons and lattice vibration are the dominant mechanisms of heat transfer.
- 2- The phonons are the unique mechanism in solid insulator substances [10].

In the present work, Lee's disc was employed which was made by (Griffin and George) England, Available in Applied Sciences Laboratory, Department of Applied Sciences, and University of Technology. The value of thermal conductivity is determined by using the following equations:

$$K \left(\frac{T_B - T_A}{d_s} \right) = e \left[T_A - \frac{2}{r} \left(d_A - \frac{1}{4} d_s \right) T_A + \frac{1}{2r} d_s T_B \right] \dots (1)$$

Where:

K : The thermal conductivity coefficient (W/m.°C).

T_A , T_B , & T_C : Temperature of the metal discs A, B, C respectively (°C).

d_A , d_B & d_C : Thickness of the discs A, B & C respectively (mm).

d_s : Sample's thickness (mm).

r : disc's radius (mm).

e : The quantity of heat flowing through the cross sectional area of the specimen per unit time (W/m².°C) is calculated from the following equation:

$$I \cdot V = \pi r^2 e (T_A + T_B) + 2\pi r e \left[d_A T_A + d_s \frac{1}{2} (T_A + T_B) + d_B T_B + d_C T_C \right] \dots (2)$$

Where:

I = Current through the heater (Ampere)

V = Applied voltage (Volt) [11]





Ruaa. H. Hassani et al.

Thermal Analysis (TA)

The advantages of thermal analysis can be summarized as[12]:

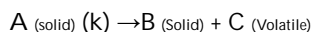
- The sample can be studied in a wide temperature range.
- Almost any physical form of sample (solid, liquid or gel) can be used.
- A small amount of sample (0.1 µg-10 mg) is required.
- The atmosphere in the vicinity of the sample can be standardized.
- The time required to complete one experiment ranges from minutes to hours

Thermal characterization of all nanocomposites has been used to study the thermal and thermo-oxidative degradation [13]. In DSC, the heat flow to and from a sample and a reference material is measured as a function of temperature as the sample is heated, cooled or held at constant temperature. In TGA measures the weight and hence the mass of a sample as a function of temperature. In DTA the temperature difference between the sample and an inert reference substance is measured as a function of temperature[14].

Kinetic theory

There are many methods to analyzing non-isothermal solid-state kinetic data from TGA. These methods can be divided into two types: (model-fitting) and (model-free), both presented in Table (1),[15].

The application of dynamic thermal analysis methods is very useful to understand the mechanisms of physical and chemical processes that occur during solids' degradation. In this paper, Coats-Redfern method has been used to analyze the non-isothermal kinetics of (EP-ZrO₂)nanocomposites. The pyrolysis process may be represented by the following reaction [16].



Where k is defined as the rate constant of reaction whose temperature dependence is expressed by the Arrhenius equation:

$$K = A e^{-E_a/RT} \dots\dots (3)$$

Where E_a is the activation energy, T is the absolute temperature, R is the universal gas constant (8.31), A : is the pre-exponential factor.

The rate of transformation from solid-state to volatile product is described by the following expression:

$$\frac{d\alpha}{dt} = K(T)f(\alpha) \dots\dots (4)$$

Where α is the conversion degree of the process, $k(T)$ is the time of process, $f(\alpha)$ is the rate constant and the reaction model.[17]

Conversion (α) represents the normalized form of weight loss data of decomposed sample and is defined as follows:

$$\alpha = (m_i - m_a) / (m_i - m_f) \dots\dots (5)$$

Where m_i is the initial mass of the sample, m_a is the actual mass; m_f is the mass after combustion. From above we found the fundamental expression of analytical methods to calculate kinetic parameters, based on TG results, as follows:

$$\frac{d\alpha}{dt} = Ax f(\alpha) x e^{-E_a/RT} \dots\dots (6)$$

The function $f(\alpha)$ and its derivative $f(\alpha)$ are used for describing solid-state reaction:

$$f(\alpha) = (1 - \alpha)^n \dots\dots (7)$$

Where n is the reaction order.

The Coats-Redfern method is also an integral method, and it involves the thermal degradation mechanism [16], as illustrate in equation (8).





Ruaa. H. Hassani et al.

$$\ln\left[\frac{-\ln(1-\alpha)}{T^2}\right] = \ln\left(\frac{A_0 R}{\beta E_a}\right) \left\{1 - \left(\frac{2RT}{E_a}\right)\right\} - \left(\frac{E_a}{RT}\right) \dots\dots (8)$$

By plotting $\ln\left[\frac{-\ln(1-\alpha)}{T^2}\right]$ against $1/T$ for each heating rate gives a family of straight lines of slope $-E/R$. Frequency factor directly determined from Y axis's intercept by substituting values of activation energies as in equation (9)

$$\text{intercept} = \ln\left(\frac{A_0 R}{\beta E_a}\right) \left\{1 - \left(2R \frac{T}{E_a}\right)\right\} \dots\dots (9)$$

The thermodynamic properties were determined by the following equation[18].

$$\Delta H = E - RT_{peak} \dots\dots (10)$$

$$\Delta S = R \left[\ln \left(\frac{h A_0}{K_b T_{peak}} \right) - 1 \right] \dots\dots (11)$$

$$\Delta G = \Delta H - T_{peak} \Delta S \dots\dots (12)$$

Where

ΔH : is activation enthalpy, ΔS : is activation entropy, ΔG : is activation free energy, T_{peak} : is maximum peak temperature, h : is Plank constant and K_b : is Boltzmann constant.

EXPERMANTAL WORK

A- Raw materials used in this work are listed below

Matrix Materials

Epoxy (Euxit 50 KI) as a matrix is a liquid resin with low viscosity as compared with other thermosets polymer, which was manufactured by (Egyptian Swiss Chemical Industries Company). The properties of the epoxy resin used in this work are given in (Table 2) according to the properties of a product company. The molecular formula for the epoxy resin is shown in Fig. (1). This epoxy (Euxit 50 KI) is converted to a solid state by adding with mixing of hardener of (Euxit 50 KII) at the ratio of (1:3), the molecular formula for epoxy hardener is shown in Fig. (2).

Filer Materials

Table (3) shows some properties of zirconium oxide particle used as reinforcement to epoxy resin. Atomic force microscopy (AFM) was used (CSPM scanning probe microscope) to measure the average nanoparticles size of ZrO_2 , however the particles size distribution is shown in Fig. (3).

B-Preparation method

In this work, the specimens were prepared by hand lay-up technique and mixing process that can be summarized by the following steps:

1-preparation the neat epoxy

The specimens of neat epoxy were prepared by hand mixing, The weight ratio of the epoxy resin to the hardener was 3: 1, mixing together for 30 minutes in a clean mold were used for casting, the casting was cured at room temperature for 24 hours, then specimens were placed in an oven for 1hour with temperature 50°C, wait 72 hours to test the specimens.





Ruaa. H. Hassani et al.

2-Preparation of epoxy-ZrO₂ nanocomposites

Nanocomposite with different weight fraction (2,4,6,8 and 10%) of zirconia nanoparticle(ZrO₂) was prepared by mixing together epoxy resin and ZrO₂ nanoparticles approximately for 10 minute at room temperature continuously and slowly to avoid bubbles formed through the mixing to reaches a homogeneous case after that the hardener was added to the mixture and mixed by hand for (10 minutes), and cast it in to the mold, then placed in an oven for 1 hour with (50°C), wait 72 hours to test the specimens.

RESULTS AND DISCUSSION

Thermal conductivity:thermal conductivity values obtained in this work were illustrated in Table (4): For epoxy, when the molecules heated, a vibration will occur in chains and phonon. So, the energy will transfer from the hot region to the cold region. When adding ZrO₂ nanoparticle to the epoxy,the particles will distribute one by one and the energy will transfer through these particles.The result shows that the thermal conductivity coefficient has a random behavior, the higher value was obtained at a weight fraction 2% as shown in Fig. (4A), in another side the thermal expansion coefficient increases with increasing the ZrO₂ weight fraction, this behavior was noticed at the rate (6, 8, 10) % and have values higher than for neat epoxy as shown in the Table (4) and Fig. (4B).

2-Thermal analysis:The thermal behaviors of epoxy and the EP-ZrO₂ nanocomposite were characterized by DSC and TGA in the atmosphere at a heating rate (10°C/min). Fig. (5) Is the DSC curves of the nanocomposites around the glass transition temperature (T_g)on the first heating scan.From DSC curvesFig. (5), it was noticed that the pure epoxy has T_g value of 74°C and when the ZrO₂ nanoparticles are introduced, the T_gs of the EP-ZrO₂ nanocomposites increased with increasing ZrO₂, it increase from 80.57°C at 2% to 94.528°C at 10% as shown in Table(5)and Fig.(6), this due to intermolecular interactions between the epoxy resin and (ZrO₂) nanoparticle. These interactions reduce the free volume and mobility of the epoxy chains and the free volume occupied by the end of the polymer chains; therefore T_g values increases [18].

In order to determine the kinetic, and thermodynamic parameters of thermal degradation of epoxy and its nanocomposites,(TGA) profiles have been recorded the mass loss for these samples as shown in Table(6), Thermal stability is an important property for applications of nanocomposite, Thermogravimetric analysis, The pure epoxy resin and other samples content of the material is determined from the mass loss due to decomposition up to about 600 °C by oxidize the carbon black formed during the pyrolysis reaction.It is obviously seen thatTGA curvesFig.(7) of pure epoxy and its nanocomposites that the curve for epoxy and epoxy with 2 % of ZrO₂ are very similar and have only two-steps decomposition, in other words, the interaction of 2% from ZrO₂ did not change degradation mechanism of the epoxy matrix. Whileincreasing ratio of(ZrO₂) up to 2%in epoxy resin will increased steps of decomposition in to three-steps, therefore, it will be concluded that the epoxy resin composites thermal stability was improved due to addition of ZrO₂.The Coats - Redfern method was applied to calculate the kinetic parameters. This method can determine the decomposition activation energy with specific the heating rate.Figure (8) shows Coats-Redfern plot of EP-ZrO₂ of different weight fraction at constant heating ratesby taking the slope of straight line and substitute in equation (9).The results of the non-isothermal kinetic analysis for Ep-ZrO₂ nanocomposites are shown inTable (7).

It was noticed that the activation energy increased when zirconium oxidenanoparticles were added to theepoxy, it increase from 59.323 KJ/mol for pure epoxy to 161.93 KJ/molat10% weight fractions of ZrO₂nanoparticles. The increasing in the value of activation energy is due to the increase in the decomposition temperature of all examined samplesand in turn thermal stability will increases.





Ruaa. H. Hassani et al.

Table (8) shows the thermodynamics parameters of pure Epoxy and Epoxy-ZrO₂ nanocomposites such as activation enthalpy, activation entropy, and activation free energy that were calculated from equations (10, 11, and 12) respectively by taking T_{max} from DTG curve as in Fig.(11). From the results obtained it was noticed that the values of enthalpy and entropy increased with the increases of activation energy, the positive value of ΔG shows that the reaction not spontaneous in the decomposition of ZrO₂ nanocomposites, and there is a linear dependence between the activation entropy ΔS and the activation energy E_a as shown in Fig (12).

CONCLUSION

Adding the ZrO₂ nanoparticle as a filler to the Epoxy resin shows enhancement in the thermal conductivity and in the thermal stability of nanocomposites, the T_g will increased. When increased the weight fraction of ZrO₂ nanoparticles and the activation energy, activation entropy show the linear relationship between them that's mean The nanocomposites Ep-ZrO₂ has a high thermal stability.

REFERENCES

- [1] F. Bondioli, V. Cannillo, E. Fabbri, and M. Messori, "Preparation and characterization of epoxy resins filled with submicron spherical zirconia particles," *Polimery*, vol. 51, 2006.
- [2] N. J. Jubier, K. J. Majeed, and E. A. Ajaj, "Effect of UV irradiation on fatigue behavior of epoxy/SiO₂ nanocomposites reinforced with E glass fiber," *Int J Appl Innov Eng Manag*, vol. 3, pp. 31-40, 2014.
- [3] E. Kicko-Walczak, "Studies on the mechanism of thermal decomposition of unsaturated polyester resins with reduced flammability," *Polymers and Polymer Composites*, vol. 12, pp. 127-134, 2004.
- [4] R. Jossen, R. Mueller, S. E. Pratsinis, M. Watson, and M. K. Akhtar, "Morphology and composition of spray-flame-made yttria-stabilized zirconia nanoparticles," *Nanotechnology*, vol. 16, p. S609, 2005.
- [5] H. Ebadi-Dehaghani and M. Nazempour, "Thermal conductivity of nanoparticles filled polymers," in *Smart nanoparticles technology*, ed: InTech, 2012.
- [6] W. S. Lopes, C. R. da Silva Morais, and A. de Souza, "Synthesis and Determination of the Kinetic Parameters for Non-Isothermal Decomposition of Complexes Ln (thd) 3phen," in *Materials science forum*, 2006, pp. 506-512.
- [7] A. Pegoretti and A. Dorigato, "Epoxy Nanocomposite Adhesives," *European Conferneec on Composite Materials*, 2012.
- [8] S. Halder, M. Goyat, and P. Ghosh, "Morphological, structural, and thermophysical properties of zirconium dioxide-epoxy nanocomposites," *High Performance Polymers*, vol. 28, pp. 697-708, 2016.
- [9] H. Hong, J. U. Kim, and T.-i. Kim, "Effective assembly of nano-ceramic materials for high and anisotropic thermal conductivity in a polymer composite," *Polymers*, vol. 9, p. 413, 2017.
- [10] A.-A. Ekram, H. Jafeer, and A. Shawky, "The Effect of metals as Additives on Thermal conductivity of Epoxy Resin," *Iraqi Journal of Physics*, vol. 8, pp. 74-79, 2010.
- [11] R. Sengupta, M. Bhattacharya, S. Bandyopadhyay, and A. K. Bhowmick, "A review on the mechanical and electrical properties of graphite and modified graphite reinforced polymer composites," *Progress in polymer science*, vol. 36, pp. 638-670, 2011.
- [12] T. Hatakeyama and F. Quinn, *Thermal analysis: fundamentals and applications to polymer science*: [sl], 1999.
- [13] N. Navrátilová, P. Dermek, M. Drienovský, R. Čička, and A. Náplava, "THE USAGE OF DIFFERENTIAL SCANNING CALORIMETRY AND THERMOGRAVIMETRIC ANALYSIS FOR OPTIMIZATION OF PLASTICS PROCESSING," *Technical Gazette*, vol. 21, pp. 1235-1238, 2014.
- [14] P. J. Haines, *Thermal methods of analysis: principles, applications and problems*: Springer Science & Business Media, 2012.
- [15] K. Słowiecka, P. Bartocci, and F. Fantozzi, "Thermogravimetric analysis and kinetic study of poplar wood pyrolysis," *Applied Energy*, vol. 97, pp. 491-497, 2012.





Ruaa. H. Hassani et al.

- [16] A. Aboulkas and K. El Harfi, "Study of the Kinetics and Mechanisms of Thermal Decomposition of Moroccan Tarfaya Oil Shale and Its Kerogen," *Oil Shale*, vol. 25, 2008.
- [17] C. C. Bueno, A. A. Maia, L. C. d. Morais, and A. H. Rosa, "Investigation on Prospective Energy Power from Corn cob Husk Biomass and its Biochars by Kinetic Parameters and Isoconversional Models," *Journal of the Brazilian Chemical Society*, vol. 28, pp. 2202-2210, 2017.
- [18] S. A. Al-Bayaty and A. J. Farhan, "Thermal decomposition kinetics unsaturated polyester and unsaturated polyester reinforcement by toner carbon nano powder (TCNP) composites," *Int. J. Appl. Innovation Eng. Manag.*, vol. 4, pp. 139-146, 2015.

Table 1 : shows the methods of analyzing non-isothermal solid-state kinetic data from TGA.

Model -fitting		Model-free	
isothermal	Non-isothermal	isothermal	Non-isothermal
Conventional	-Differential -Freeman-Carrol -Coats-Redfern	-Standard -Friedman -AIC	-Kissinger -Flynn-Wall-Ozawa -Vyazovkin-AIC -Kissinger-Akahiara-Sonuse

Table 2 : The epoxy resin properties

Density(gm/cm ³)	1.05
Viscosity (pois) at 35 □	1
Tensile strength (Mpa)	72
Module of elasticity(Mpa)	2800

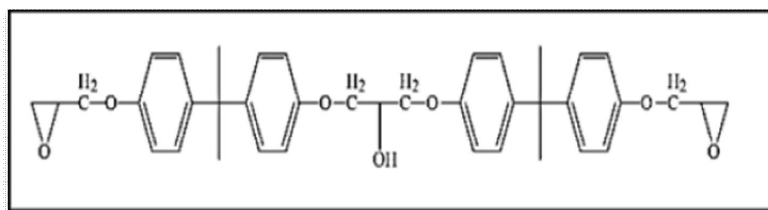


Fig. 1: The molecular formula for epoxy resin [6].

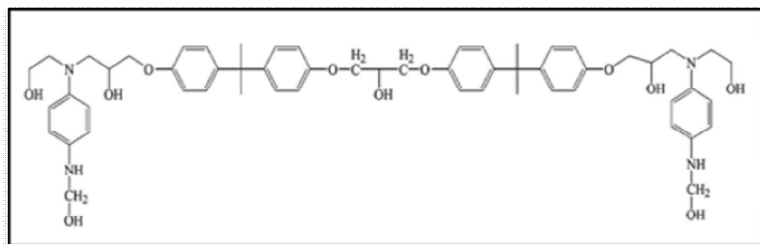


Fig. 2: The molecular formula for epoxy hardener [6].





Ruaa. H. Hassani et al.

Table 3 :The Zirconium oxide properties

Particular material	Nano Zro ₂
Density (gm/cm ³) at 20 c	5.89
Form	Off-white powder
Particle size	52.65nm
Purity	99.9

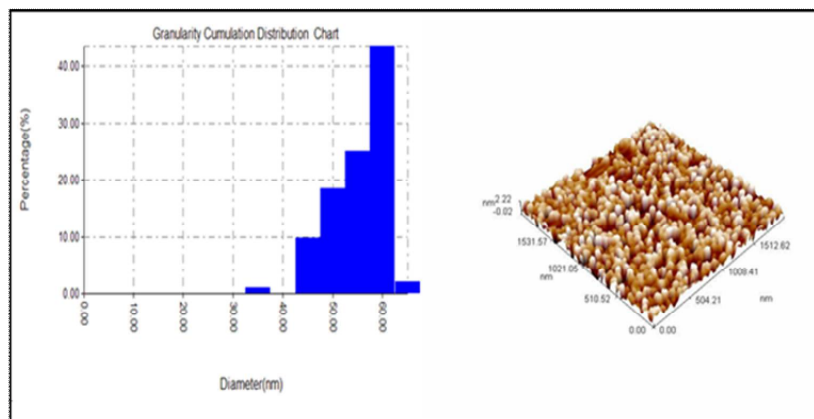


Fig. 3: AFM of nanoparticles ZrO₂

Table 4: shows the values of thermal conductivity and thermal expansion for Epoxy, and Ep-ZrO₂ nanocomposites.

Samples	e(watt/m ² .c)	K(watt/m.c)
Ep	5.930	0.1945
Ep+2%ZrO ₂	5.430	0.2222
Ep+4%ZrO ₂	5.813	0.1966
Ep+6%ZrO ₂	5.982	0.2207
Ep+8%ZrO ₂	6.106	0.1941
Ep+10%ZrO ₂	6.123	0.1414

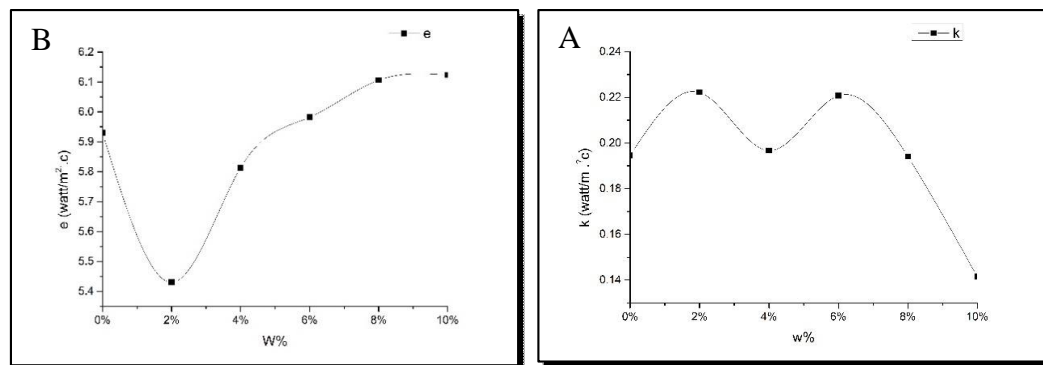


Fig. 4: A- thermal conductivity B-thermal expansion for Epoxy and Ep-ZrO₂ nanocomposites.



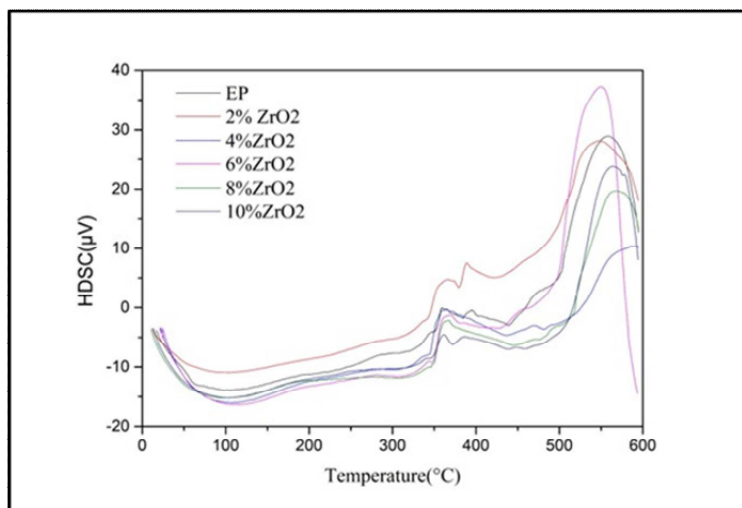


Fig. (5): The DSC curves for Epoxy and Ep-ZrO₂ nanocomposites.

Table (5): T_g values for Epoxy and Ep -ZrO₂ nanocomposites

Samples	T _g (°C)
Epoxy	74
Ep+2%Zro2	80.57
Ep+4%Zro2	87
Ep+6%Zro2	87.14
Ep+8%Zro2	89.97
Ep+10%Zro2	94.53

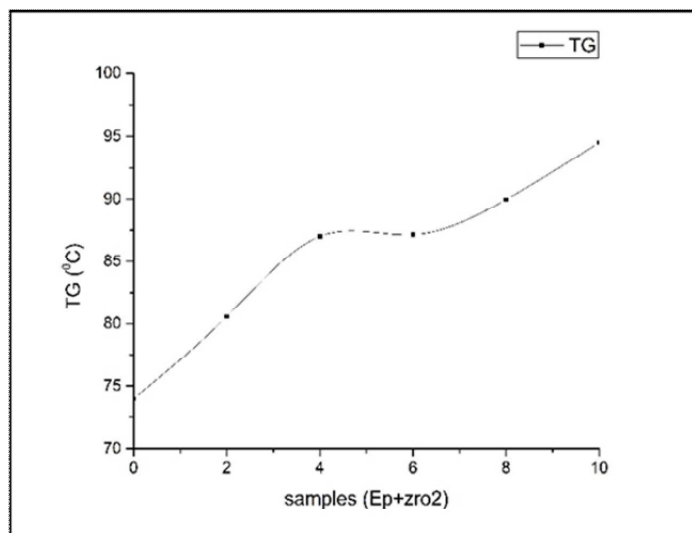


Fig.6: The relation between the T_g and the weight fraction of ZrO₂ nanoparticles for Ep -ZrO₂ nanocomposites.





Ruaa. H. Hassani et al.

Table 6: the mass loss values of Epoxy and Ep-ZrO₂ nanocomposites

Samples	Mass loss1 %	Mass loss2 %	Mass loss(3) %	Total mass loss %
Pure Epoxy	448.56 °c -71.268%	594.573 °c -21.206%	-----	-92.49
EP+2%ZrO ₂	400.4 °c -63.4123%	594.579 °c -30.8763%	-----	-94.28
Ep+4%ZrO ₂	332.98 °c -14.851%	448.322 °c -52.474%	593.671 °c -14.638%	-81.95
Ep+6%ZrO ₂	325.014 °c -14.789%	441.717 °c -50.741%	593.584 °c -25.175%	-90.69
Ep+8%ZrO ₂	324.844 °c -14.285%	455.456 °c -50.193%	594.611 % -18.299%	-82.76
Ep+10%ZrO ₂	332.175 °c -15.051%	451.411 °c -47.887%	594.39 °c 23.759%	-86.68

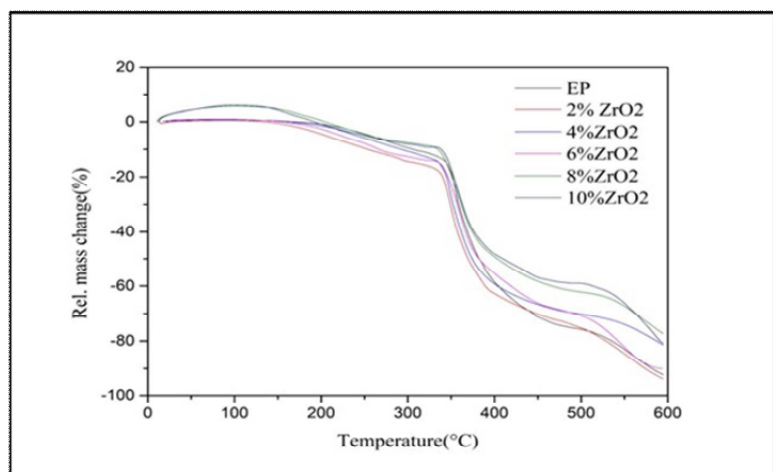


Fig. 7: The TGA curves for Epoxy and Ep-ZrO₂ nanocomposites

Table 7: The results of the non-isothermal kinetic analysis for Ep-ZrO₂ nanocomposites using Coast-Redfen method

Samples	Peak temperature ,K	Activation Energy, E (KJ/mol)	Reaction rate constant ,A ₀ (S ⁻¹)	R ²
Pure Epoxy	359	59.361	422492.6688	0.999
EP+2%ZrO ₂	349.1	66.26	2149774.582	0.997
Ep+4%ZrO ₂	349.3	118.41	64585034401	0.999
Ep+6%ZrO ₂	358.6	127.34	3.13106E+11	0.999
Ep+8%ZrO ₂	359.1	131.21	5.5367E+11	0.999
Ep+10%ZrO ₂	360.5	161.93	2.23E+14	0.998





Ruaa. H. Hassani et al.

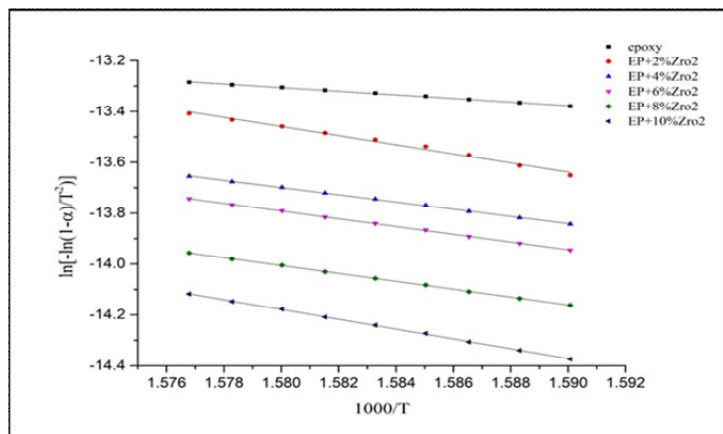


Fig.10. Coats-Redfern plot for thermal degradation of Epoxy and EP-ZrO₂ nanocomposites at constant heating rate 10 °C/min

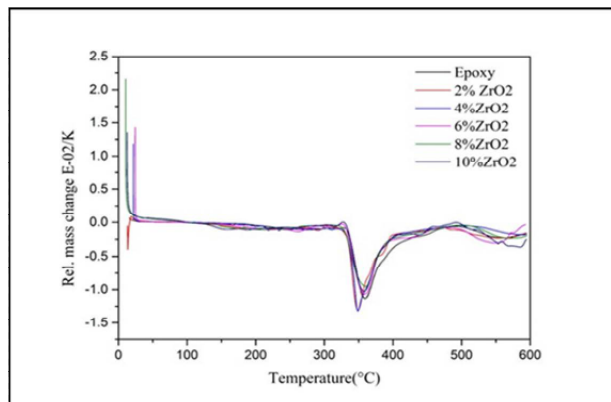


Fig .11. The DTGA for epoxy resin and Ep/ZrO₂ nanocomposites

Table .8: Thermodynamics parameter values for pure epoxy and Ep/ZrO₂ nanocomposites.

EP/ZrO ₂ , Wt. %	Activation Energy, E (KJ/mol)	Reaction rate constant ,A ₀ (S ⁻¹)	ΔH, KJ/mol	-ΔS,J/mol	ΔG,KJ/mol
0%	59.323	422492.6688	54.10300274	-147.0778046	93.06478295
2%	66.26	2149774.582	61.0052537	-133.3181005	84.31804479
4%	118.41	64585034401	113.237567	-47.59753824	29.7236661
6%	127.34	3.13106E+11	122.1659041	-34.69112094	21.71045047
8%	131.21	5.5367E+11	125.9585795	-29.96323392	19.05073712
10%	161.93	2.23E+14	156.6744222	19.87760554	-12.40796004





Ruaa. H. Hassani et al.

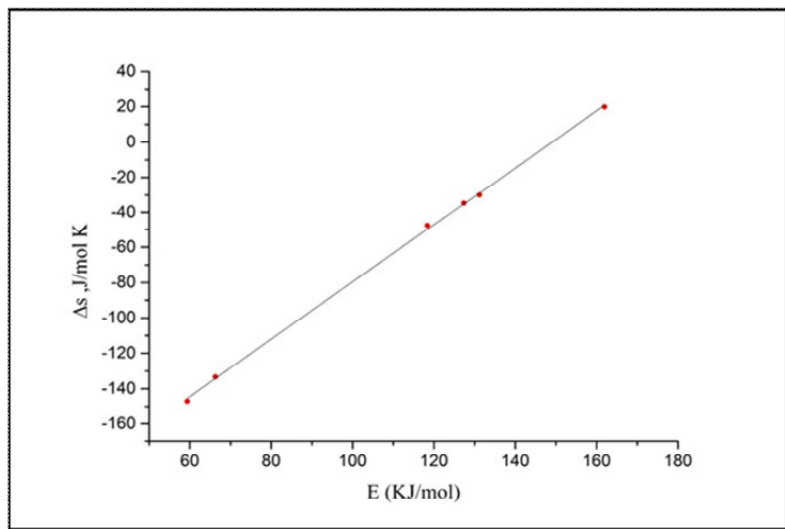


Fig. 12. The activation energy versus activation Entropy for Epoxy-ZrO₂ nanocomposites.





RESEARCH ARTICLE

Histomorphological and Histochemical Postnatal Developmental Study of the Uteruses of the Local Rabbits (*Oryctolagus cuniculus*)

F. J. Al-Saffar* and Masarat S. Almayahi

Department of Anatomy, College of Veterinary Medicine, University of Baghdad, Baghdad, Iraq

Received: 20 June 2018

Revised: 22 July 2018

Accepted: 28 Aug 2018

Address for Correspondence

F. J. Al-Saffar

Prof., Head & Senior of Histology

Department of Anatomy,

College of Veterinary Medicine,

University of Baghdad, Baghdad, Iraq

E mail: assaffar1955@yahoo.com or fayak1955@gmail.com/ Co author: masaratswadi44@gmail.com



This is an Open Access Journal / article distributed under the terms of the **Creative Commons Attribution License** (CC BY-NC-ND 3.0) which permits unrestricted use, distribution, and reproduction in any medium, provided the original work is properly cited. All rights reserved.

ABSTRACT

This project was carried out to find out the structural histomorphological changes that take place in the uteruses of the female local rabbits at three different postnatal periods of their life that were kitten, immature and mature does. To conduct such project, 24 female rabbits were collected (8 for each age) from the local breeders. Rabbits were euthanized, dissected and subsequently uteruses were collected and fixed with 10% neutral buffered formalin then subjected to routine processing such as dehydration, clearing, embedding and block preparation. Finally, sections of 6 µm were prepared and stained with hematoxylin-eosin and Masson's trichrome stains. Gross findings revealed duplex uterus, having two separate uterine horns ended by two united cervixes suspended by mesometrium in the abdominal cavity. Caudally, cervixes were projected into the vaginal cavity forming rosette-like end called portio vaginalis uteri. Microscopic findings revealed abrupt changes in the wall of the isthmus-uterine horn junction. Prominent structural changes in the uteruses of immature does compared to those of kittens and mature does indicated that immature does after the period of weaning face great developmental growth and changes. The changes were recorded characteristically in their endometrium such as the growth of endometrial glands and the thicknesses of their myometrium.

Keyword: Uterus, Uterine horn, Cervix, Rabbit, Endometrium, Myometrium

INTRODUCTION

In the past decade, rabbits were considered good experimental animal model in conducting various researches in both human and animals. They have been used as experimental model in inducing many diseases and subsequent



**F. J. Al-Saffar and Masarat S. Almayahi**

studies focused on many aspects such as toxicology, pharmacology and surgery at different universities [1]. Accordingly, microscopic structure of different organs of this animal is required depth description and exploration and out of which those of the uterus of the female reproductive system. Previously, four main types of uteri have been reported in different mammalian orders based principally on the differences in their two parts, the body and the two horns. These types were bipartite (in cows), bicornuate, (in pigs), simplex (one pear-shaped found in humans and horses), duplex (in rabbits, guinea pigs, mice and rats) [2]. In the female Wistar rats, the histological features of the uterus indicated endometrium made up of a single layer of columnar epithelium with subepithelial lamina propria which was connected to the myometrium, a compactly arranged smooth muscle layer. The myometrium was surrounded by the serosa and deep to it a rich network of blood vessels [3]. In the young female albino rats of 4 months, the wall of the uterus showed well differentiated layers of serosa, muscularis. The endometrium was constructed of a single layer of columnar epithelial cells with numerous well developed subepithelial glands and heavily cellular stroma. In the myometrium, the established lamina propria was connected with the densely arranged smooth muscle layer, surrounded by the serosa, its deep part possessed rich network of blood vessels [4].

Aim of the study

Up to date there are no available researches in the previous and the current literatures investigated the developmental changes in the uterus of the female reproductive system in the local rabbit (*Oryctolagus Cuniculus*). Based on such reason and the importance of this animal species as an experimental model, the plan was performed to study the structural developmental changes of the uterine horns and cervixes of the local rabbits at different postnatal developmental periods that were kitten, immature and mature stages.

MATERIALS AND METHODS**Animals and study design**

Twenty four female local rabbits (*Oryctolagus cuniculus*) of three different ages were selected to perform the current investigation. Apparent healthy rabbits were purchased directly from local rabbit's breeders. The collected rabbits were one week newly born female kittens, 8 to 10 weeks aged immature does and mature does of 5 months (virgin). Animals were left three days under supervision to insure their good healthy condition during such period before their euthanasia and subsequent dissection.

Dissection of animals

Each selected rabbit was weighed with a sensitive weighing balance and euthanized by intramuscular injection of sodium pentobarbitone. The rabbit was placed on dorsal recumbency to view the ventral aspect, thereafter; a mid-line abdominal incision was made to expose the structures in the peritoneal cavity. The reproductive organ exposed and both uterine horns and cervixes were observed and photographed in situ and later dissected out. The organs were temporarily kept in glass container to keep them moist in physiological saline solution. Then after each tube was transfer to filter paper to dry before weighing. After their extirpation on board, the length and weight were measured using ruler and thread, weighing balance with a sensitivity of 0.0001 g, and vernier callipers, respectively. The data obtained expressed as mean \pm standard error of the mean (mean \pm SEM). Values of $p < 0.05$ were considered significant. All measurements were listed in table.

Preparation of histological specimens

The uterus as a whole were dissected and their different regions such as horns and cervixes were cut out and washed with normal saline and then by 10% neutral buffered formalin and eventually immersed in 10% neutral buffered formalin for 72 hrs. For future staining with histochemical stains, some specimens were fixed by Bouin's



**F. J. Al-Saffar and Masarat S. Almayahi**

solution. Next to fixation, specimens were dehydrated through ascending series of ethyl alcohol (70%, 80%, 90% and 100%) each for 2 hrs, then cleared with xylene for ½ hr. Specimens were infiltrated with paraffin wax (58 – 60 °C) then embedded with paraffin wax to obtain blocks of paraffin. Paraffin sections of six microns were obtained by using rotary microtome. General and special stains were used to stain the tissue sections such as hematoxyline-eosin (H&E), Masson Trichrome (MTC), Gomori Trichrome, Alcine blue (AB) (pH 2.5), Periodic acid schiff (PAS) [5].

Micromorphometric measurements

Thickness of tunica mucosa and muscularis in uterine horns and cervixes were measured using the colour USB 2.0 digital image system (Scope Image 9.0) which is provided with image processing software. All above parameters were set in table to achieve comparison among different postnatal ages. Tissues sections of 6 mm thick were stained by Gomori Trichrome stain because this stain facilitates the identification of the different tissues when carrying out micromorphometric measurements [6].

Statistical analysis

All data of both macromorphometric and micromorphometric measurements were analyzed by ANOVA and student *t* - test using SPSS software (version 14).

RESULTS

Gross examination of the present study revealed duplex uterus in the local rabbits, having two separate uterine horns ended by two united cervixes. The latter were fused together forming a septum. Uterine horns were tortuous and having larger diameters than those of corresponding uterine tubes. They were held distinctly by the mesometrium to the dorsal abdominal wall through which passed the supplying blood vessels. It seemed that these ligaments connected or continuous with those of uterine tubes (mesosalpinx) on both right and left sides of the abdominal cavity. Both of uterine horns and large parts of united cervixes were situated in the abdominal cavity, whereas the small remaining parts were inside the pelvic cavity together with the vagina. The cranial ends of uterine horns were wide and rounded which were traversed by the thinner uterine tubes forming distinct utero-tubal junction. Caudally, cervixes were projected into the vaginal cavity forming rosette-like end called portio vaginalis uteri. These were not united but were so close and surrounded by space called the fornix. The cervixes were more solid in texture and they were distinctly whitish in color (Fig. 1).

Macromorphometric measurements of the uterine horns and cervixes such as lengths and weights were listed in table 1. The means of lengths and weights of the uterine horns of one week kittens were 1.40 ± 0.25 cm and 0.01 ± 0.40 g, respectively. These measurements were changed into 4 ± 0.20 cm and 0.07 ± 0.01 g in immature does. Similarly, these measurements were increased up to 7 ± 0.01 cm and 0.34 ± 0.10 g in mature does. The means of lengths and weights of the cervixes of one week kittens were 0.20 ± 0.01 cm and 0.04 ± 0.13 g, respectively. These measurements were changed into 0.6 ± 0.01 cm and 0.10 ± 0.03 g in immature does. Similarly, these measurements were jumped into 0.8 ± 0.04 cm and 0.12 ± 0.01 g in mature does. Microscopic examination revealed abrupt changes in the wall of the isthmus-uterine horn junction. The distance of this junction was very short. Prominently, the lining epithelium of junction loses the mucosal folds that were present in isthmus. In the female kittens, immature does and mature does the uterine horns and cervixes were showed three distinct tunicae that were from inward to outward endometrium, myometrium and perimetrium.

Uterus of female kittens

In the female kittens, the endometrium of uterine horns showed simple low columnar epithelium supported by lamina propria of loose connective tissue infiltrated with lymphocytes and filled obviously with numerous blood



**F. J. Al-Saffar and Masarat S. Almayahi**

vessels. The endometrium was devoid of endometrial glands. The myometrium was made of two muscular layers of smooth muscle fibers that were inner longitudinal and outer circular in direction. These two layers were separated distinctly by vascular layer of large and numerous blood vessels. The perimetrium was a thin layer of loose connective tissue covered by simple squamous mesothelium on both uterine horns at their free borders, whereas, covered by adventitial connective tissue at their attached borders to the broad ligament (Fig. 2). In the cervixes, the endometrial epithelium remains simple low columnar in nature rested on wider lamina propria than that in the uterine horns. The endometrium thrown into 6 to 7 cervical folds caused smaller cervical lumen than that observed in the uterine horns. Tunica muscularis in cervixes was thinner than that measured at the horns with lesser obvious vascular layers. Right and left cervixes were united together with connective tissue septum filled with blood vessels. The free ends of the cervixes which were projected into the vaginal lumen as portio vaginalis were characterized by widest lamina propria of loose connective tissue and thinner muscularis not well differentiated into two muscular layers as in the wall of cervixes and the horns.

Uterus of immature does

In the immature does, the endometrium of uterine horns showed simple low columnar epithelium with the presence of few small invaginations extended into the underlying lamina propria forming uterine glands distributed within the underlying loose connective tissue. These superficial glands were lined by simple low columnar epithelial cells. Similarly to the uterine horns of kittens, the myometrium was made of inner longitudinal and outer circular bundles of smooth muscle fibers but with small blood vessels intervening between them instead of the recorded vascular layer in the previous studied age. The thickness of myometrium was relatively thicker than that measured in kittens. The perimetrium was as same as observed in the uterus of female kittens but few bundles of smooth muscle fibers were present in the suspensory broad ligament (Fig. 3). In the cervixes, similar histological structures were found to those structured in the kittens but with the presence of few small cervical glands located superficially under the lining epithelium. In addition to that the adventitia surrounding the cervixes and associated septum between them showed loose connective tissue with few fasciculi of smooth muscle fibers. Thickness of cervical adventitia was thicker than that recorded to the uteruses of kittens (Fig. 4). Portio vaginalis was characterized by widest lamina propria of loose connective tissue and thinner muscularis or even sparse thin bundles of smooth muscle fibers (Fig. 5).

Uterus of mature does

In the mature does, the simple columnar epithelial lining of the endometrium in the uterine horns was invaginated into the underlying lamina propria forming uterine glands some of them goes deeply and distributed within the loose connective tissue adjacent to the inner layer of myometrium. Lamina propria was shorter than that of kittens but similar to that in immature does. It was filled with numerous blood capillaries surrounding the initiated up uterine glands. Similarly to the uterine horns of the immature does, the myometrium was made of two layers of smooth muscle fibers but the inner longitudinal muscle layer was prominently thicker than the outer circular one. The diameter of uterine horns of mature does was largest than those of the kittens and immature does (Fig. 6, 7).

In the cervixes, similar histological structures were found to those structured in the immature does with the presence of many small cervical glands distributed in the lamina propria surrounded by blood capillaries. Cervical folds were longer prominently compared to the previous ages and going deep into the lumen of the cervical canal. The septum between right and left cervixes was thicker than the previous ages with the presence of many dispersed fasciculi of smooth muscle fibers. Portio vaginalis was characterized by widest lamina propria of loose connective tissue and thinner muscularis or even sparse thin bundles of smooth muscle fibers (Fig. 7).





F. J. Al-Saffar and Masarat S. Almayahi

Histochemical staining findings

Histochemical staining techniques that were conducted by the staining with either Mason Trichrome or Gomori Trichrome stains for the connective tissues on the uteruses of female kittens, immature does and mature does showed that the walls of their uterine horns were constructed of inner endometrium, middle myometrium and outer perimetrium. The stains were successfully stained the loose connective tissues constituted the lamina propria of endometrium, loose connective tissue intervening between muscular bundles of myometrium and the loose connective tissue of the perimetrium which was thin at the free borders of the uterine horns and wide and thick at their attached borders to the related mesometrium. Most of the fibers were collagenous that were stained green or blue when the compositions of the above stains included light green or aniline blue, respectively. The stains showed numerous blood capillaries and lymphocytes infiltrated in the lamina propria. The myometrium appeared clearly of inner circular and outer longitudinal muscular bundles with presence of many blood capillaries inside and between these muscular layers of smooth muscle fibers (Fig. 6 & 7).

In the cervixes, similar results to those of uterine horns were obtained, but it showed wider lamina propria in the endometrium and thinner myometrium compared to those recorded in their related uterine horns (Fig. 4 & 8). In the portio vaginalis uteri, the myometrium subsided into sparse bundles of smooth muscle fibers, whereas, the lamina propria appeared wider compared to the wall of the cervixes (Fig. 5).

Lining epithelium in the endometrium of the uteruses of female kittens, immature does and mature does was simple low columnar cells negatively stained with PAS, AB (pH 2.5) staining procedures. These results indicated absence of any secretory granules in their cytoplasm. Also, the newly formed superficially situated endometrial glands and the deeply extended endometrial glands in immature and mature does uteruses, respectively showed negative responses toward the above staining procedures. These findings indicated absence of secretory function of these glands at these studied ages of the local rabbits.

Micromorphometric data of the uteruses

Morphometrical data in Table 2 revealed that the thicknesses of the wall, lamina propria, muscularis interna and muscularis externa were 145.08 ± 0.91 SE, 67.87 ± 0.77 SE, 40.56 ± 0.65 SE and 37.44 ± 0.72 SE in the uterine horns of kittens, whereas in their cervixes the same measurements were in order 171.01 ± 0.03 SE, 92.04 ± 0.44 SE, 27.14 ± 0.31 SE and 19.26 ± 0.07 SE. In immature does similarly the thicknesses of the wall, lamina propria, muscularis interna and muscularis externa of uterine horns were 193.72 ± 0.00 SE, 52.06 ± 0.00 SE, 85.13 ± 0.00 SE and 93.46 ± 0.00 SE. Same measurements for their cervixes were in order 207.39 ± 0.05 SE, 83.61 ± 0.21 SE, 88.93 ± 0.33 SE and 44.15 ± 0.80 SE. Similar measurements for mature does, the thicknesses of the wall, lamina propria, muscularis interna and muscularis externa of uterine horns were 206.52 ± 0.02 SE, 58.08 ± 0.40 SE, 96.60 ± 0.22 SE and 47.45 ± 0.10 SE. The measurements for their cervixes were in order 495.40 ± 0.60 SE, 226.08 ± 0.05 SE, 220.27 ± 0.21 SE and 67.63 ± 0.40 SE. Thicknesses of the wall and lamina propria of the cervixes were higher than those of the uterine horns in all studied ages, specifically in mature does. The muscularis in cervixes were thinner than those in uterine horns in case of kittens, but in contrary it inversed in immature and mature does as the muscularis became thicker in cervixes compared to those of uterine horns. In addition to that, the thickness of muscularis interna was approximately equal to muscularis externa in both uterine horns and cervixes of kittens but the case changed in both immature and mature dose where the muscularis interna was thicker than that of the externa.





F. J. Al-Saffar and Masarat S. Almayahi

DISCUSSION

Current gross findings indicated that the type of uterus in the local rabbits was duplex which was similar to other small laboratory species such as guinea pigs, mice and rats but was different than others documented types that were bipartite (in cows), bicornuate (in pigs) and the simplex type (one pear-shaped found in humans and horses) [2].

Gross examination of the present study revealed duplex uterus in the local rabbits, having two separate uterine horns ended by two united cervixes that were projected into the vagina as portio vaginalis uteri. Both of uterine horns and large parts of united cervixes were situated in the abdominal cavity. Similarly in African giant rat, the uterus was described as *uterus duplex* in which the two uteri were suspended by the mesometrium which is originated from the dorsolateral pelvic wall and the lumbar region [7, 8]. Such observations were also described in the female genitalia of other species such as laboratory rat [9], the Mongolian gerbil [10] and female agouti [11]. But in the mouse, the uterus was described differently because it composed of a cranial part contained two cavities separated by a median septum and undivided caudal portion named the cervix [12].

Uterine horns in female agouti were continuing as uterine body caudally. The paired horns were found flattened dorso-ventrally and were converged together to form the uterine body giving rise to a Y-shape organ [11]. Similarly to the local rabbits, recent records of [13] and [14] showed two uterine horns in the uterus of the rat and hamster, respectively leading to the cervix, which in turn leads to the vagina and the vulva but in these species, the cervix composed of upper dual cervix part leading to the two uterine horns and a lower cervix part composed of a single canal that leads to the upper vagina different from those recorded in the local rabbits.

Current measurements showed that the of mean of lengths of the uterine horns were 1.40 ± 0.25 cm, 4 ± 0.20 cm and 7 ± 0.01 cm in female kittens, immature and mature does, respectively which appeared longer than those recorded in the female agouti (10.4 ± 5.5 mm) by [11]. Previously, it was recorded that the mean length of the uterus in the rat was 3.9 cm [9] and recently in African giant rat was 4.877 ± 0.011 cm [11] and both were shorter than the length in mature local rabbits. One decade before other measurements conducted on rabbits to estimate the length of their uteruses reported 7.0 cm by [15] which were approximately similar to those recorded in mature local rabbits. But 8.07 ± 0.409 cm recorded in the mixed breed rabbits) by [16] which were longer than the local rabbits.

Microscopic data showed histological developmental changes that were takes place in the wall of uterine horns and their related cervixes in the kittens, immature and mature does. The changes were recorded characteristically in their endometrium and myometrium. Distinctly in female rabbits, the wall of the utero-tubal junction was gradually changed from the isthmus to the cranial end of the uterine horn in which the junction appeared very short canal without folds or crypts that were noted in both joined organs. The wall of the uterine horns in the female kittens showed well developed vascular layer intervening between the internal and external muscular layers of the myometrium. In addition, numerous capillaries were detected in the lamina propria of the endometrium. It can be proposed the role of such rich blood supply in the growth of the uterine horns. The newly born female kittens of one week could be underwent the hormonal effect of their dam during pregnancy.

In immature does, the wall appeared well developed characterized by many features reflected important changes advanced toward the maturity. These features were newly formed uterine glands. The endometrium showed invaginations into underlying lamina propria. The myometrium was thickened with the diminishing of the vascular layer into numerous blood vessels with the presence of nerve plexuses intervening between its internal and external layers. These changes were more advanced subsequently in the mature does showing many uterine glands grew deeply in the endometrium. The myometrium was thickened specially its tunica externa. The lining simple columnar epithelium remain not secretory because this layer and the other structures of the wall of the uterus are usually affected by the ovarian hormones which in the studied does were not functionally enough to did such effect. These



**F. J. Al-Saffar and Masarat S. Almayahi**

ovarian hormones in the does are related and associated with gonadotrophic hormones which in turn associated with the events of the coitus [17]. The does in the current study were virgin and were not allowed for mating with males. Other mammalian species have estrous cycle in which these gonadotrophic hormones and subsequent release of ovarian hormones will control the changes in the wall of the reproductive tract one of them is the uterus [18].

Present postulation comes parallel and agreement with recent knowledge that estrogens and progesterone are contributed in the structural integrity maintenance of the oviduct, uterine and vaginal tissues by regulating activities of the epithelial cells existed in the reproductive tract such as growth, proliferation and secretion. Accordingly, the changes in their concentrations during the oestrus cycle will induce hemodynamic changes in the vascular tissue which caused an increment in the permeability of the blood vessels and humid weight of the uterus [19 & 20]. The important hormone estrogen is usually manufactured by the granulosa cells of the ovarian follicles which convert androgens synthesized by the theca interna in response to blood levels of the anterior pituitary hormones [21].

In fact results and hypothesis of the present study regarding the hormonal effects on the wall structures of the uterus were highly agreed and confirmed the recent findings and postulations of [22]. The researcher induced pseudo-pregnancy by intramuscular injection of HCG in the female New Zealand rabbits to investigate the hormones effects on the histological and immunohistochemical changes in their uteruses. His records revealed that the uterine epithelium and endometrial glands epithelium were columnar with oval basal nuclei, few and small endometrial glands, six longitudinal folds and the uterine epithelium form crypts which were similar to those recorded in the studied local rabbits. But post hormone injection, he found dramatic changes in the uterine architecture such as increased epithelial proliferation, crypt formation, increased the complexity of luminal folding, increase in length, size and abundance of the uterine endometrial glands, increase in the uterine micro vascular development and finally the appearance of tunica vascularis between the inner circular and outer longitudinal smooth muscle fibers of the myometrium. He identified cell-specific of progesterone receptors alpha in the endometrial epithelial cells, endometrial glands and in the smooth muscles fibers of the myometrium.

CONCLUSIONS

This current study recorded differences in both macroscopic and microscopic as well as morphometric aspects of the uteruses of the local rabbits compared to other animal species, specifically the species belong to rodent's family. The study findings were in agreement and confirmed previous records and postulations of [23, 24, 25, 26 & 27] that rabbits were different from rodents in their organs anatomically, histologically and histochemically. The earlier reference documented different type of pancreas and pancreatic duct organization whereas, the latter reference found different structural components of the wall of the small and large intestine. Such differences were in the distribution of Brunner glands, stem cells, paneth cells, nerve plexus and sympathetic ganglia.

Conflict of Interests

The authors have not declared any conflict of interests.

ACKNOWLEDGEMENTS

The authors strongly acknowledge the council of the Veterinary Medicine College / Baghdad University to support this research project





F. J. Al-Saffar and Masarat S. Almayahi

REFERENCES

1. Abidu-Figueiredo, Xavier-Silva M, Cardinot B, Babinski TM, M.A, Chagas, MA. Celiac artery in New Zealand rabbit: Anatomical study of its origin and arrangement for experimental research and surgical practice. *Pesq.Vet. Bras*; 2009; 28(5): 237-240
2. Hafez ESE. Reproduction and breeding techniques for laboratory animals. Philadelphia, USA, Lea & Febiger 1979.
3. Akpantah AO, Ekong MB, Uruakpa KC, Akpaso MK, Eluwa MA, Ekanem TB. Gonadal histo-morphologies and serum hormonal milieu in female rats treated with *azadirachta indica* leaf extract. *Iranian J. Rep. Med.* 2010;8(4): 185-190.
4. Lalithamma A, Naik, AG, Changamma C. Cytoarchitectural variations in selected rat tissues following the administration of estradiol valerate in aged female rats. *Asian Pacific J. Reprod.* 2016;5(1): 36–41
5. Culling CFA, Allison RT, Barr WT. Cellular Pathology Technique. 4th edn. 1985.
6. Butterworth, Wellington Wei S, Bai J, Gong Z, Ma W, Wei M. GnRH agonist active immunization influences ovarian development and GnRH receptor mRNA expression levels of pituitary in Japanese white rabbits (*Oryctolagus cuniculus*). *Livest. Sci.* 2011;139(3): 222-229
7. Ali MN, Onyeanusi BI, Ojo SA, Ayo JO, Maidawa SM, Imam J. Biometric and morphologic studies of the female reproductive organs of the African giant rat (*Cricetomys gambianus*: Waterhouse). *Folia Morphol.* 2010;69(4): 213–215
8. Akinloye AK, Oke AB. Characterization of the Uterus and Mammary Glands of the Female African Giant Rats (*Cricetomys gambianus*, Waterhouse) in Nigeria. *Int. J. Morphol.* 2010;28(1): 93-96
9. Hebel R, Stromberg MW. Anatomy of laboratory rats. Williams and Wilkins Company, Baltimore, pp. 76–80, 1976.
10. Camila, C. D., Patricia, F. F. P., Tania, M. S., Carls, M. M., Francisco, E. M. (2001). Estrous cycle anatomy and histology of the uterine tube of the Mongolian gerbil (*Meriones unguiculatus*). *Revista Chilena De Anatomia*, 19: 191–196
11. Singh MD, Adogwa AO, Mollineau WM, Garcia GW. Gross and microscopic anatomy of the reproductive tract of the female agouti (*Dasyprocta leporina*): A neotropical rodent with potential for food production. *Trop. Agric. (Trinidad)*, 2014;91(1): 38-46
12. Claudio JC, Irma BG, Fernando B, Anita FW, Mariano AC. Atlas of laboratory mouse histology. Accessed on March 2009 at <http://www.ctrgenpath.org/static/alas/mousehistology/windows/femaleu/diagrams.html>.
13. Hamid HY, Zakaria MZ, AB. Reproductive characteristics of the female laboratory rat. *Afr. J. Biotech.* 2013;12(19): 2510-2514
14. Chanut FJ, A, Williams AM. The syrian golden hamster estrous cycle: unique characteristics, visual guide to staging, and comparison with the rat. *Toxicologic Pathology*, 2016;44(1): 43-50
15. Praag VE. Reproductive tract of the female rabbit. Accessed on March 11, 2008 at www.medirabbit.com//EN//uro-gen-diseases?generalities/female-organ.pdf
16. Bitto II, Arubi JA, Gumel, AA. Reproductive tract morphometry and some haematological characteristics of female rabbits fed pawpaw peel meal based diets. *Afr. J. Biomed. Res.* 2006;9: 199–204
17. Dufy-Barbe L, Franchimont P, Faure JMA. Time-courses of LH and FSH release after mating in the female rabbit. *Endocrinology*. 1973;92: 1318-21
18. Gu W, Janssens P, Holland M, Seamark R, Kerr P. Lymphocytes and MHC class II positive cells in the female rabbit reproductive tract before and after Ovulation. *Immunol. Cell Biol.* 2005;83: 596–606
19. Kim NN, Min K, Pessina MA, Munarriz, R, Goldstein I, Traish AM. Effects of ovariectomy and steroid hormones on vaginal smooth muscle contractility. *Int. J. Impot. Res.* 2004;16(1): 43-50
20. Vinci A, Bacci B, Benazzi C, Caldin M, Sarli G. Progesterone receptor expression and proliferative activity in uterine tumours of pet rabbits. *J. Comp. Path.* 2010;142(4): 323-7
21. Young JM, McNeilly AS. Theca: the forgotten cell of the ovarian follicle. *Reproduction*, 140: 489–504, 2010.
22. Abd-Elkareem MD. Morphological, histological and immunohistochemical study of the rabbit uterus during pseudopregnancy. *J. Cytol. Histol.* 2017;8(1):1-7





F. J. Al-Saffar and Masarat S. Almayahi

23. Al-Saffar FJ, Al-Hasnawy AHA. Histomorphological developmental study of advanced postnatal of the pancreas of local rabbit. J. Biol. Sci. 2014;14: 387-402
24. Al-Saffar F J, Al-Haik AG. Histomorphological relationship of paneth cells with stem cells in the small intestine of indigenous rabbit at different postnatal ages. Singapore J. Chem. Biol, 2016a;5(1): 11-19
25. Al-Saffar FJ, Al-Haik AG. Histochemical study of carbohydrates foundation in the gut of indigenous rabbits at different postnatal ages. Inter. J. Curr. Res. 2016b;8(8): 37223-37230
26. Al-Saffar FJ, Al-Haik AG. Histomorphological and Immunohistochemical postnatal developmental changes in the small intestine and colon of the indigenous rabbits (*Oryctolagus cuniculus*). PhD thesis, Dept. of Anatomy, Histology & Embryology / College of Veterinary Medicine/Baghdad University, 2017a.
27. Al-Saffar FJ, Al-Haik AG. Gross and microscopic developmental study of the local rabbit's spinal cord. Journal of Entomology and Zoology Studies, 2017b;5(6): 2555-2562.

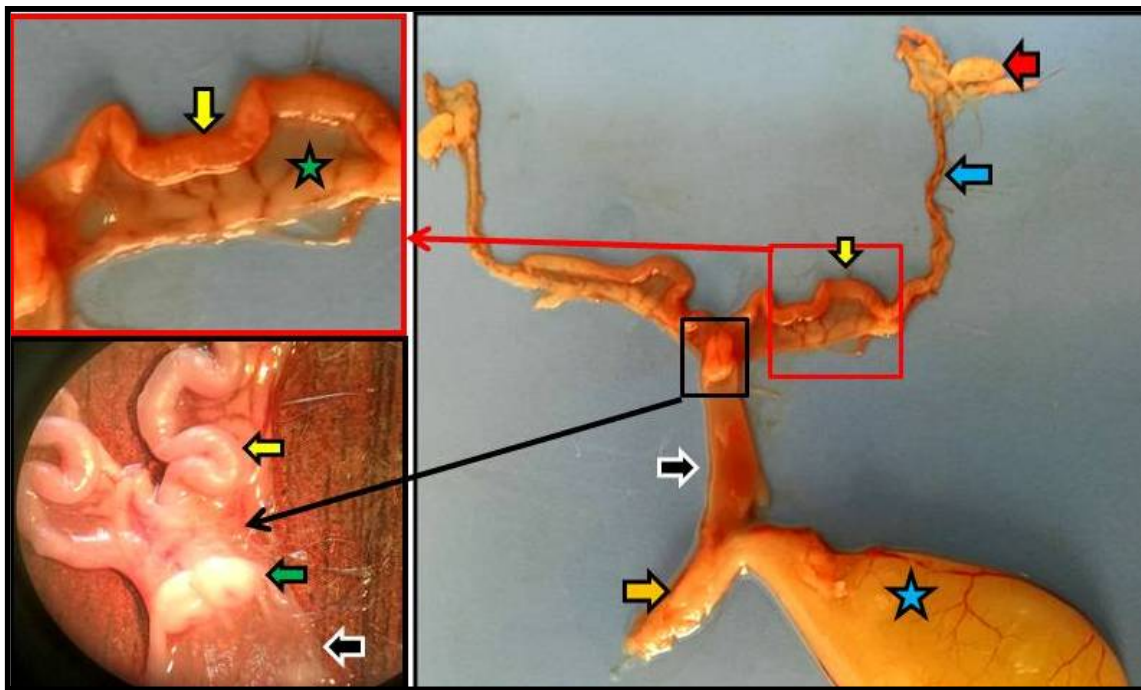


Fig.1.Reproductive system of immature does showed uterine horns (yellow arrows), broad ligament (green star), cervix (black thin arrow), portio vaginalis (green arrow), vagina (black thick arrows), vestibule (orange arrow), urinary bladder (blue star), ovary (red arrow), uterine tube (blue arrow),

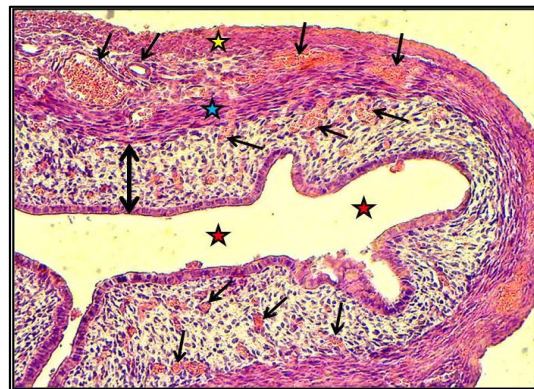


Fig.2.Uterine horn of kitten showed endometrium (double heads black arrow) highly vascularized with absence of uterine glands and lined by simple low columnar, muscularis interna (blue star), muscularis externa (yellow star), lumen (red stars), blood vessels in the vascular layer (black arrows). X20, H&E





F. J. Al-Saffar and Masarat S. Almayahi

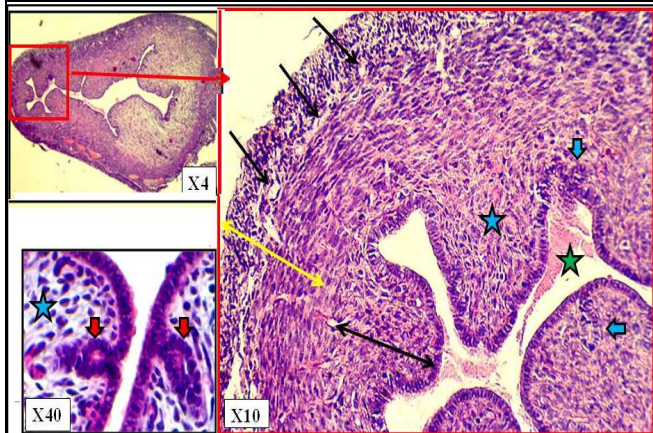


Fig.3.Uterine horn of immature doe showed endometrium (blue arrow), myometrium (double heads black arrow), uterine lumen (green star), uterine glands formation (blue arrows), connective tissue lamina propria (blue stars), blood vessels (black arrows). X4, X40, X10, H&E



Fig.4.Immature cervix showed endometrium (blue arrow), myometrium (yellow arrow), smooth muscle fibers in the broad ligament (red arrow), cervical canal (green stars), cervical folds (yellow stars), last part of uterine horn (orange arrow), cervical glands (black arrows), septum (green arrow). X4, MTC

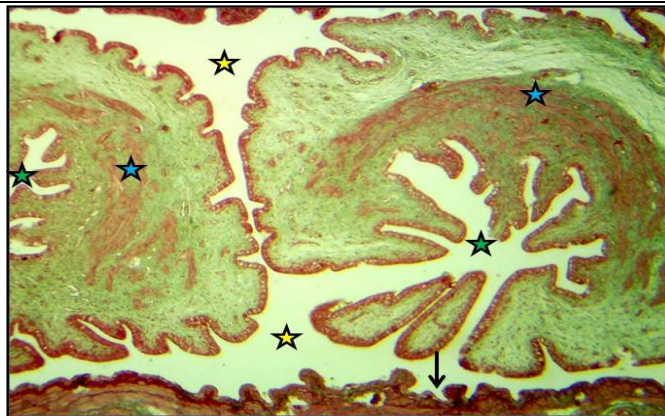


Fig. 5. Portio vaginalis of immature doe cervixes showed cervical canals (green stars), fornix (yellow stars), circular smooth muscle fibers (blue stars), vagina (black arrow). X4, Gomori.

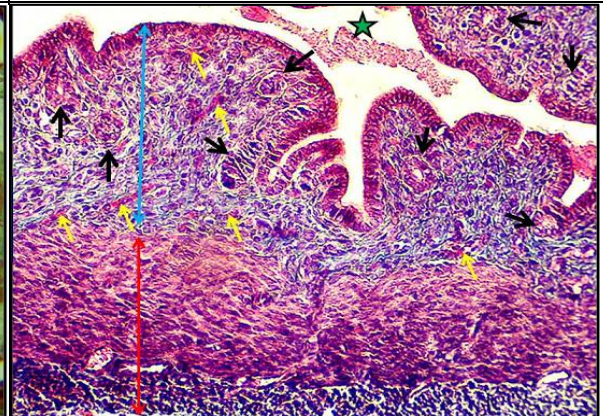


Fig.6.Uterine horn of mature doe showed endometrium (blue arrow), myometrium (red arrow), uterine glands (black arrows), uterine lumen (green star), and blood vessels (yellow arrows). X10, X20, MTC.





F. J. Al-Saffar and Masarat S. Almayahi

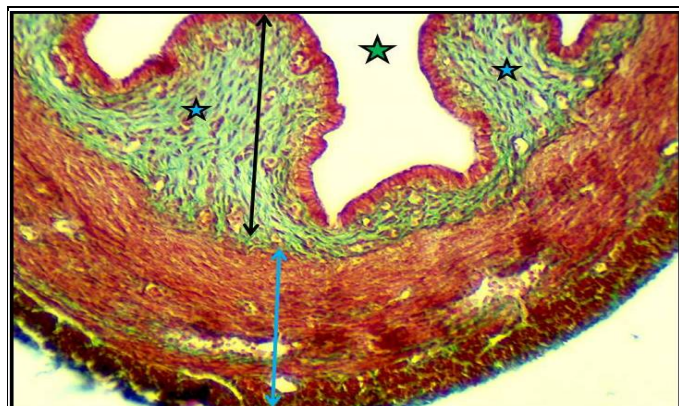


Fig.7.Uterine horn of mature does showed endometrium (double heads black arrow), myometrium (double heads blue arrow), lamina propria showed uterine glands and blood vessels (blue stars), lumen (green star). X20, Gomori Trichrome

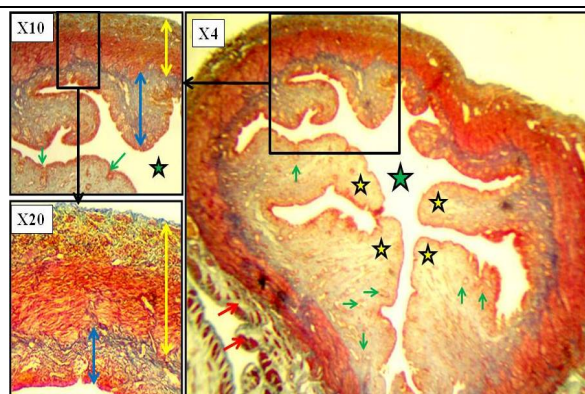


Fig. 8. Mature cervix showed endometrium (blue arrow), myometrium (yellow arrow), smooth muscle fasciculi in the septum (red arrows), cervical canal (green star), cervical folds (yellow stars), and cervical glands (green arrows). X4, X10, X20, MTC

Table 1. Gross measurements of uteruses of the local rabbits at different ages

Organs	Different ages of rabbits	Measurements	
		Length (mm)	Weight (mg)
Uterine horn	Kittens	14.0 ± 0.25	10.0 ± 0.40
	Immature does	40.0 ± 0.20	70.0 ± 0.01
	Mature does	70.0 ± 0.01	340.0 ± 0.10
Cervix	Kittens	20.0 ± 0.01	40.0 ± 0.13
	Immature does	60.0 ± 0.01	100.0 ± 0.03
	Mature does	80.0 ± 0.04	120.0 ± 0.01

Table 2. Micromorphometric measurements of the wall of the uterine horns and cervices in the female kittens, immature and mature does

Organs	Measurements	Different ages of female rabbits			
		Kittens	Immature does	Mature does	
Uterine horn	Thickness (µm)	Wall	145.08 ± 0.91 SE	193.72 ± 0.00 SE	206.52 ± 0.02 SE
		Lamina propria	67.87 ± 0.77 SE	52.06 ± 0.00 SE	58.08 ± 0.40 SE
		Muscularis interna	40.56 ± 0.65 SE	85.13 ± 0.00 SE	96.60 ± 0.22 SE
		Muscularis externa	37.44 ± 0.72 SE	93.46 ± 0.00 SE	47.45 ± 0.10 SE





F. J. Al-Saffar and Masarat S. Almayahi

Cervix	Thickness (μm)	Wall	171.01 \pm 0.03 SE	207.39 \pm 0.05 SE	495.40 \pm 0.60 SE
		Lamina propria	92.04 \pm 0.44 SE	83.61 \pm 0.21 SE	226.08 \pm 0.05 SE
		Muscularis interna	27.14 \pm 0.31 SE	88.93 \pm 0.33 SE	220.27 \pm 0.21 SE
		Muscularis externa	19.26 \pm 0.07 SE	44.15 \pm 0.80 SE	67.63 \pm 0.40 SE

Notes:

- Serosa or adventitia was excluded.
- Thicknesses of the wall and lamina propria of the cervixes were higher than those of the uterine horns in all ages, specifically in mature does.
- Muscularis in cervixes were thinner than those in uterine horns in case of kittens, but in contrary it inversed in immature and mature does as the muscularis became thicker in cervixes compared to those of uterine horns.
- Thickness of muscularis interna was approximately equal to muscularis externa in both uterine horns and cervixes of kittens but the case changed in both immature and mature dose as the muscularis interna was thicker than the externa





Analytical Studies For Coronal Mass Ejections, Solar Flare and Radio Solar Emission During the Solar Cycle 24

Zena F. K.*

Department of Astronomy and Space, College of Science, University of Baghdad, Baghdad, Iraq

Received: 06 Aug 2018

Revised: 08 Sep 2018

Accepted: 12 Oct 2018

*Address for Correspondence

Zena F. K.

Department of Astronomy and Space,
University of Baghdad,
College of Science, Baghdad,
Baghdad, Iraq.



This is an Open Access Journal / article distributed under the terms of the **Creative Commons Attribution License** (CC BY-NC-ND 3.0) which permits unrestricted use, distribution, and reproduction in any medium, provided the original work is properly cited. All rights reserved.

ABSTRACT

The Coronal Mass Ejection (CMEs) which are related to the Sun radio radiation is very important for obtaining and information about their origin and relation with the Sun flares. The aim of this research is to make a statistical study of the solar storms number type II, type III and the number of coronal mass ejection (CMEs) associated to the solar flares during the period from 2008 to 2017 through the solar cycle 24. The data for type II and type III burst are taken from Radio Jove Archive, while the CMEs and the flares are recorded from SOHO. It found that there are 15,893 numbers of CMEs and 823 flares event also calculated 133 total number of solar storm type II and type III burst. Under certain temporal condition, the calculation for the associated radio emission type II, type III with the flares and CMEs at the same day revealed that there are a good relation between the number of CMEs and flares. Furthermore it found that the distribution of the selected events depending on their flare class, also the number of flares and its class related to the solar cycle.

Key words: Sun: flares, coronal mass ejections (CMEs) , Sun: radio radiation, type III storm, type II radio burst.

INTRODUCTION

The study and analyses of the Coronal Mass Ejection (CMEs) which is one of the main solar phenomena [1] related to the sun radio radiation type III and type II burst is very important for obtaining and information about their origin and relation with sun flares [2]. While the CME causes the geomagnetic storms so that the direction to the earth is very important [3]. Many researchers examined the relation between CMEs and other sun phenomena such as (e.g.,



**Zena F. K.**

Munro et al., 1979 and Kahler, 1992) which were helped us to understanding and measurements the speed of CMEs [4]. (Wild et al. 1963) observed the metric type II burst and calculate its speed and explain the associated with a flare [5]. By sky lab space station and OSO-7 satellite the white-light coronagraph are observed and produce away for measuring the CMEs speed (Brueckner, 1974; Mac Queen et al., 1974. At (1983 Mac Queen and Fisher resolved six flare-related CMEs and six non-flares with eruption observed by the MK3 coronagraph, and they pay attention that the former ones were faster, animated at nearly fixed velocities while as the latter were more slowly showing great accelerations. Then the concept of two separate classes of CMEs; the CME-Flare related ones and the non-Flare CME [6].

(H.V. Cane & W.C. Erickson & N.P. Prestage, 2002) made correlative study between >20 MeV solar proton events flare, (CMEs) and radio burst it is found that all proton events are preceded by groups of type III bursts and all are submit by CMEs this bursts observed in the low frequency from space [7]. At (2003 Moon et al) explain that the CME are exceedingly related to flare. and them expect that there also intimate CMEs, i.e. a pair of sequential CMEs produce from different strong regions and physically linked with each other. Then as a implied by statistical conclusion of waiting-time division and the angular variance division the number of well-disposed CMEs is much considerably smaller than that of separate CMEs [8]. At the same period (Can and Reames 1990) establish that type III burst happen at the beginning of flare and it is related with short-duration flare [9] Andrews and Howard [2001] offered the height-time plots of sundry well-observed limb events, upholding the two CME classes idea. In (2002)

Yashiro et al) made a recently a comprehensive CME catalog include acceleration and speeds of 3271 CMEs which observed from 1996 to 2000 by SOHO [10]. While Nat Gopalswamy (2007) explain how CMEs is effect of space weather where he improve the ability of CME for producing geomagnetic storms and how it is effect on solar energetic particles [11]. In (2009), E.A. Kasatkina and other discuss the relation of solar flare and CME and solar energetic charged particle and it is effect about atmospheric electric field anomalies and they research the effect on three events and how it is take a similar distribution at the same time. Finally at (2012) M. Youssef made a statistically researched about the relation between the CME and solar flare by using a great sample of solar flare and CME events for a period of time from 1996- 2010. At (2004 Vrsnak et al) explain that the interval of the CME acceleration rely on the solar flares phases [12-15]. In this research is to made a statistical study of the solar storms number type II, type III and the number of coronal mass ejection (CMEs) associated to the solar flares during the period from 2008 to 2017 through the solar cycle 24.

MATERIALS AND METHODS

Data Selection

In this research the data obtained from radio JOVE archive (this project began in 1998), which is observed by radio JOVE project hands-on inquiry-based educational project that allows students, teachers and the general public to learn about radio astronomy by building their own radio telescope from an inexpensive kit and or JOVE using remote radio telescopes through the internet. Participants are also collaborate with each other through interactions and sharing of data on the network. Since then, more than 1100 teams of students and interested individuals have purchased our non-profit radio telescope kits and are learning radio astronomy by building and operating a radio telescope. This self-supporting program continues to thrive and inspire new groups of students as well as individuals. The Radio project has developed a low cost radio telescope kit which is used to receive radio signals from the Sun, the planet Jupiter, and the Galaxy. The signals are recorded, displayed, analyzed and archived using free Radio Jove software. An internet connection will allow students to view and share data with other observers around the globe. Solar and Jupiter radio bursts can be viewed on a desktop or laptop computer running the Radio-SkyPipe software package. This program generates a strip-chart representation of the data and allows us to view other observer's records via the Internet, share our records in real-time over the internet, and chat with other Jove





Zena F. K.

observers and professional radio astronomers. Individual solar bursts usually last for about half a minute. Often there is a rapid onset in signal strength followed by a slow decay. The resulting record on Sky Pipe looks like a shark fin. The Jove archive contains many Sky Pipe records of solar bursts. In this research 133 storms record of solar burst through the solar cycle 24 from years (2008-2017)

Also the data of CMEs record by catalog during the period from 2008 to 2010, this catalog contains all CMEs manually identified since 1996 from the Large Angle and Spectrometric Coronagraph (LASCO) on board the Solar and Heliospheric Observatory (SOHO) mission. LASCO has three telescopes C1, C2 and C3. However, only C2 and C3 data are used for uniformity because C1 was disabled in June 1998. In the absence of a perfect automatic CME detector program, the manual identification is still the best way to identify CMEs, in this research 15,893 events recorded. While the X-ray flares data which are measured and provided by Geostationary Operational Environmental Satellite (GEOS), during the same interval (2008- 2017) records 823 flare events. The temporal condition is used to select the associated events of CM- Flare data which are required the detection day of the CMEs (when the CMEs ejected from the solar surface) must be simultaneous to the same day of the associated flares.

The flare data which we record used from solar soft which is a set of integrated software libraries, data bases and system utilities which provide a common programming and data analysis environment for solar physics. The solar software (SSW) system is built from Yohkoh, SOHO, SDAC and Astronomy libraries and draws upon contributions from many members of those projects. It is primarily an IDL based system, although some instrument teams integrate executables written in other languages. The SSW environment provides a consistent look and feel at widely distributed co-investigator institutions to facilitate data exchange and to stimulate coordinated analysis. Commonalities and overlap in solar data analysis goals are exploited to permit application of fundamental utilities to the data from many different solar instruments. The use of common libraries, utilities techniques and interfaces minimizes the learning curve for investigators who are analyzing new solar data sets, correlating results from multiple experiments or performing research away from their home institution.

RESULTS AND DISCUSSION

In this study we made a statistical analysis to number of solar burst type III storm; type II radio burst associated with flares and CMEs For the 24rd solar cycle during the period | (2008–2017) from results it is found that the total number of burst are (133) burst where it is divided to (124) burst type III and (9) burst type II . Where according to flare in the same period the total number of it is (823) flare, the coronal mass ejection [CME] are found approach at each day in the each month for the above period with total number equal to (15,893). as shown in figure (1).

We can list our results as follows:

1. At first, in the beginning of the period at 2008 the total number of bursts are (4) type III. the total number of flare is (14) ,and the total number of CME is (855),as shown in figure (2-a) .
2. According to 2009 we found that the total number of burst are (3) type III and the total number of flare are (26) and the total number of CME is (747), as shown in figure (2-b) .
3. In the 2010 the total number of bursts (45) type III and (1) burst type II with number of flare were (30) once and the total number of CME are (1100), as shown in figure (2-c) .
4. At 2011 the total number of burst were (22) type III with a total flare were (116) and the total CME are (1955), as shown in figure (2-d) .
5. In 2012 we can obtain (2) burst type III as a boundary of our radio JOVE archive with total number of flare equaled to (103) and the total CME are (2176), as shown in figure (2-e) .
6. In 2013 (3) burst type III where found with (119) flare with total CME are (2423), as shown in figure (2-f) .





Zena F. K.

7. At 2014 there are (12) burst type III and (4) type II while the total number of flare are (122) with total CME (2463), as shown in figure (2-g) .
8. In 2015 there are (140) flare and (3) burst type III and the total CME is (2072), as shown in figure (2-h) .
9. At 2016 the total number of burst are (18) type III and (4) type II and the total flare (139) and total CME (1390), as shown in figure (2-i) .
10. Finally at 2017 the total number of burst are (12) type III and (3) type II with total flare is (140) with total CME is (712), as shown in figure (2-k) .

Also we are found a correlation between sun storm and CME, flare according to our result collection which can be explain below. At 2008 there is only one burst corresponding with a flare type B at April (26-4-2008). The speeds of coronal mass ejection at this day are between (230-703Km/Sec). At 2009 At May exactly at (8-5-2009) there is one burst type III corresponding with flare type B and the speed of coronal mass ejection at the same day is (260Km/Sec) .

At 2010 in January, exactly at (18-1-2010) there is burst type III corresponding with flare type C and the speed of coronal mass ejection at this day are alternating between (76-444Km/Sec).and also there is another burst type III at the same month but another day were corresponding with a flare type M and the speed of CME where alternating between (101-740 Km/Sec). At February 2010 we found fifteen burst type III some of this burst where corresponding with flare, for example at (6-2-2010) there is a burst corresponding with flare type C and the speed of coronal mass ejection at this day was equal (240Km/Sec). And the other one was at (7-2-2010) with a flare type M with speed of CME alternating between (232-421 Km/Sec). and at (12-2-2010) there is another burst with a flare type M to the same while the speed of CME at this day was between (183-1180 Km/Sec),finally at (15-2-2010) there is another burst corresponding with flare type C and the speed of coronal mass ejection at this day are alternating between (177-774Km/Sec).

At 2011 some of this storm where corresponding with a flare for example in February there are four burst type III but two of this burst where happened with a flare at the same day which is at (13-2-2011)where the storm was type III and the flare was type M with a speed of CME between (267-438 Km/Sec)and at (15-2-2011)where burst type III happened with a flare type X with a speed of CME (326-669Km/Sec).and at March there are ten burst type III but one of this burst happened at the same day with a flare type M in (25/3/2011) with a speed of CME are between (45-320 Km/Sec).the other burst type III was happened at the same day with a flare type C was at September in (20-9-2011)with a speed of CME (221-661Km/Sec).finally at October in (12-10-2011) there is three burst of type III in this month one of them where corresponding with a flare type C with a speed of CME between (319-476Km/Sec).

In 2013 where we found that at June ,exactly at (10-6-2013)there are one burst type III happened with a flare type C and the speed of CME were between (208-577 Km/Sec).and the other burst type III corresponding with a flare type X happened at November in (5-11-2013) with a speed of CME between (225-850Km/Sec).

At 2014 the corresponding burst and flare where at January where we found one burst type II happened at the same day with a flare type X at (7-1-2014)with speed of CME (18-360Km/Sec).and at February in (12-2-2014) we found one burst type III at the same day with a flare type M with CME speed between (344-1830Km/Sec).at March we found burst type III at the same date in [29/3/2014] with a flare type X so the speed of CME are between (103-544Km/Sec).at April we found burst type II corresponding with a flare type M at (2-4-2014)with CME speed between (110-1471Km/Sec).and at the same month there is another storm but here it is type III happened at the same day in(2-4-2014)with a flare type C with speed between (164-618 Km/Sec).while we found at May 2014 there is a storm type III in (10-5-2014)and also a flare type C at the same day where the speed of CME is (303-1086Km/Sec).while at July there are three burst type III and one type II , one of burst type III corresponding with a flare type M at (8-7-2014) and the storm type II happen also at the same day with a speed of CME between (173-773Km/Sec).finally in 2014 at September we found two burst type III corresponding with a flare the first one at (10-9-2014)with a flare type X with a speed of CME (305-1267Km/Sec)and the other one is at (18-9-2014)with a flare type M and the speed of CME is





Zena F. K.

(108-307Km/Sec). At 2015 at March we found that is burst type III corresponding with a flare type M in (12-3-2015) with a speed of CME between (204-529Km/Sec). And at Jun we found there is burst type III corresponding with a flare type C in (29-6-2015) with a speed of CME between (187-483Km/Sec). and at July there is burst type III corresponding with a flare type C in (14-7-2015) with a speed of CME between (158-552Km/Sec). In 2016 at July we found that is burst type III corresponding with a flare type M in (23-7-2016) with a speed of CME between (270-835Km/Sec) and at August 2016 we found type III corresponding with a flare type C in [9-8-2016] with a speed of CME between (128-380Km/Sec), and at September there is burst type III happened with a flare type C in (22-9-2016) with CME speed is (322-425Km/Sec).

In 2017 at April for the same year found that is burst type III corresponding with a flare type C in (14-8-2017) with a speed of CME between (303-926Km/Sec).

CONCLUSION

We have discussion the relation between solar flares and coronal mass ejection (CME) with sun radio radiation type III and type II burst during the 24rd solar cycle. We found that the number of coronal mass ejection and solar flare are corresponding where we found from our temporal condition that the number of (CME) and solar flare at beginning (2008 and 2009) are small as comparable with there number at peak in (2012,2013 and 2014) where we found there are reach to its maximum value. then it is return to its minimum value at (2017). And we found that the maximum number of burst we found was corresponding with coronal mass ejection and solar burst is type III more than type II. Also we found at 2012 with the maximum event of the 24rd solar cycle there are no type of burst are corresponding with flare and coronal mass ejection at the same day. Where there are some effects that make the number of storm not collate to CME, flare behavior during the study period year (2008-2017) these effect can be list as below:

1. In the research the collection storm number data depend on Radio JOVE archive which is one of many archives that gives the storm number but the frequency band of this archive is about (20-30 MHz) where this band represent a small band from actual storm radio emission which is (300KHz -3GHz).
2. The earth ionosphere layers effect which is effect on the number of storm that reach to earth ,because of absorption of the storm during ionosphere but the CME, flare detection is carried out by space satellite such as SOHO, wind which are outside of earth.

Also we found that the type of flare class are relate to the number of flare where we found at (2008 and 2009) the large ratio of flare class are type B and at the following year with increasing number of flare we notice that the maximum type of flare are type C and at tope in (2014) the type of flare class are M and its return to type C and at the end of solar cycle where the number of flare are reach to its minimum value the maximum value of flare class are type B also.

REFERENCES

1. Cane, H.V., Sheely Jr., N.R., Howard, R.A., " Energetic interplanetary shocks, radio emission, and coronal mass ejections". Journal of Geophysical Research 92, 9869, 1987.
2. Gosling, J.T., Abridge, J.R., Bame, S.J., Feldman, W.C., " Solar wind speed variations – 1962–1974". Journal of Geophysical Research 81, 5061–5070, ERDA-NASA-sponsored research, 1976.
3. Mac Queen, R.M., Fisher, R.R., " The kinematics of solar inner coronal transients". Solar Physics 89, 89–102, 1983





Zena F. K.

4. H. V. Cane W. C. Erickson N. P. Prestage, " Solar flares, type III radio bursts, coronal mass ejections, and energetic particles". Journal of Geophysical research, vol. 107, NO. 0, 10.1029, 2002.
5. Zhang, J., Wang, T., Zhang, C., Liu, Y., Nitta, N., Slater, G.L., Wang,J.," Flare-CME events associated with a super active region, recent insights into the physics of the sun and heliosphere: highlights from SOHO and other space missions. In: Pa° I Brekke (Ed.), Proceedings of IAU Symposium 203, 2001.
6. Yashiro, S., Gopalswamy, N., Michalek, G., Kaiser, M.L., Howard, R.A., Reames, D.V., Leske, R., von Roseninge, T. 2002.
7. Cane, H. V., and D. V. Reames, " The relationship between energetic particles and flare properties for hnpulsive solar flares, hstrophys. J. Suppl. Set.,73, 253, 1990.
8. Moon, Y.-J., Choe, G. S., Wang, H., & Park, Y. D., The Astrophysical Journal , 588, 1176, 2003.
9. Veronig, A. M., & Brown, J. C., The Astrophysical Journal , 603, L117, 2004.
10. Chang Liu1, and other " SUCCESSIVE SOLAR FLARES AND CORONAL MASS EJECTIONS ON 2005 SEPTEMBER 13 FROM NOAA AR 10808 " The Astrophysical Journal, 703:757-768, 2009.
11. Vrsn' ak, B., Maric' ic' , D., Stanger, A.L., Veronig, A., Coronal mass ejection of 15 May 2001: II. Coupling of the CME acceleration and the flare energy release N. Solar Physics 225 (2), 355-378, 2004.
12. T. Tsuda, R. Fujii, K. Shibata, and M. A. Geller, " Coronal mass ejections and space weather", NASA Goddard Space Flight Center, Greenbelt, Maryland, USA Climate and Weather of the Sun- Earth System(CAWSES), pp. 77-120.
13. Gopalswamy, N., S. Yashiro, and S. Akiyama, Geoeffectiveness of halo coronal mass ejections, J. Geophys. Res., 112, 2007.
14. M. Youssef "On the relation between the CMEs and the solar flares, " NRIAG journal of Astronomy and Geophysics,172- 178, 2012.
15. E. A. Kasatkina1 and other " Atmospheric electric field anomaliesassociated with solar flare/coronal mass ejection events and solar energetic charged particle Ground Level Events" Atmos. Chem. Phys. Discuss., 9, 21941-21958, 2009.

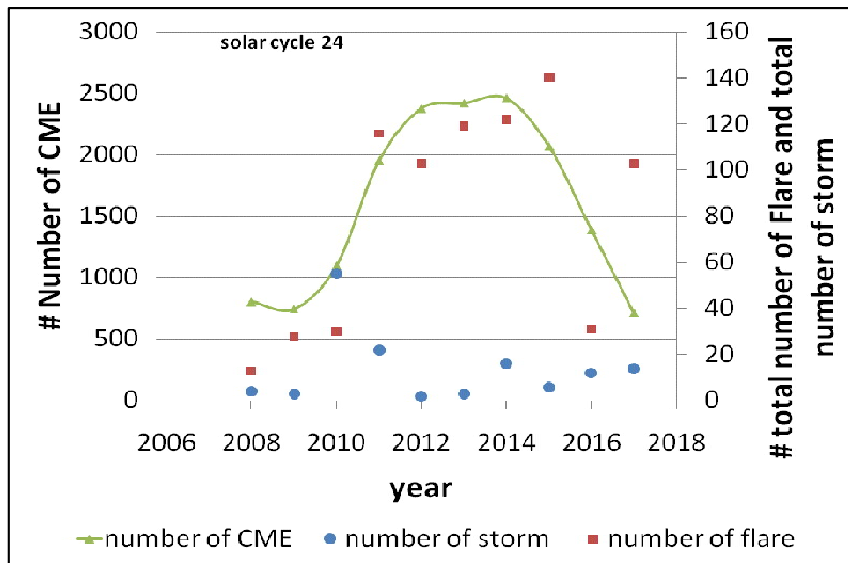


Fig.1.Monthly distribution of CME , FLARE, SOLAR STORM numbers at all year





Zena F. K.

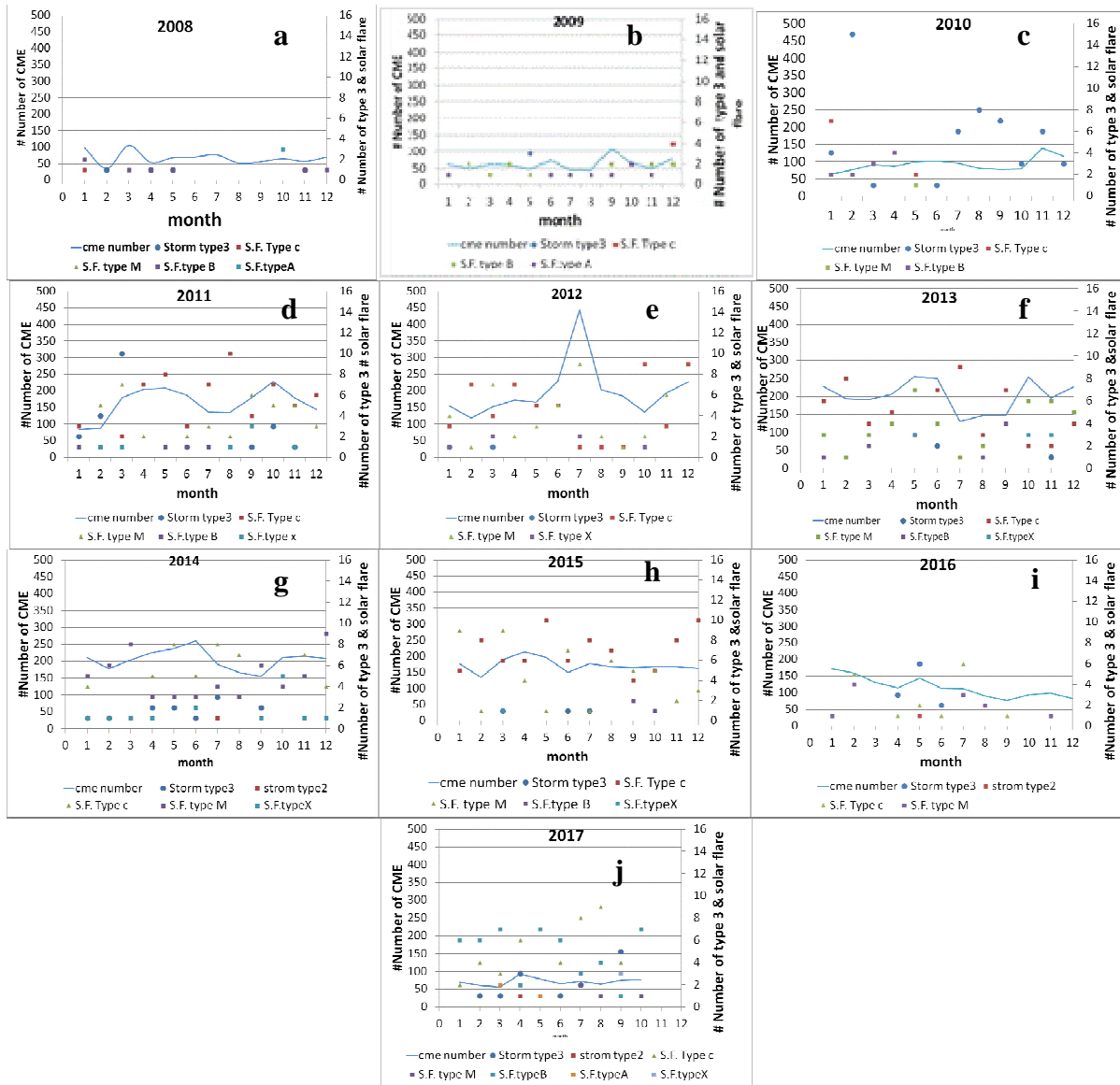


Fig.2.Monthly distribution of CME and flare and radio storm for years (2008-2017)





Connecting People with Nature

INDIAN JOURNAL OF NATURAL SCIENCES

ISSN: 0976-0997

MJL& Cited by Clarivate Analytics (Formerly Thomson Reuters) for Zoological survey

ISI Impact Factor :1.265 , NAAS Rating :3.56,IC Value: 47.65

Tamil Nadu Scientific Research Organization is working for the promotion of society by transferring science & technology since 1997. We are very keen in appreciating and recognizing the contribution of every one of you. We are publishing **Indian Journal of Natural Sciences - IJONS** from **August 2010**. The Journal is peer reviewed International Journal for publication of Original Research papers /Reviews/ Short communications/Book reviews/Reports on conferences/Seminar, Important events, News of interest, Special articles, General Articles etc.

Call for Papers: Investigations related to science in all branches

Highlights

- International Quality
- Published Bi-Monthly
- Fast acceptance and Quick Publication
- Low price
- High Rank Editorial Board
- Online manuscript submission
- Publish original Research Works and Reviews



Subscription Rate/Annum
Institution - Rs.1000/-
Individual - Rs.750/-

Published by Dr.Vijayarani on behalf of Tamil Nadu Scientific Research Organization, 40/31,
Srinivasapalan Road, Coimbatore-622 203, TamilNadu, India. and Printed by
Vignapriyanka, South End Street, Pudukkottai - Madurai - 626027 (Tamil Nadu)
Chief Editor - Dr.Vijayarani



Subscription Fee (Annual 6 Issues)

- For Individuals Rs.1000/-
- For students Rs.750/-
- For Institutions Rs.1200/-



Subscription Rate/Annum
Institution - Rs.1000/-
Individual - Rs.750/-

Published by Dr.Vijayarani on behalf of Tamil Nadu Scientific Research Organization, 40/31,
Srinivasapalan Road, Coimbatore-622 203, TamilNadu, India. and Printed by
Vignapriyanka, South End Street, Pudukkottai - Madurai - 626027 (Tamil Nadu)
Chief Editor - Dr.Vijayarani



Publication fee for Authors

- **Rs.3000/-** (Processing fee)
- **USD100/-** for Foreign author

Send all correspondence to

-----Chief Editor -----

Indian Journal of Natural Sciences (IJONS)

C/o TNSRO, 39 Mura Bhavan, Koodal Nagar, Rajagopalapuram Post
Pudukkottai-622003, TamilNadu, India.
Phone:04322-261088 Mobile: 99528 86637

E-mail: ijonstnsro@gmail.com, www.tnsroindia.org.in

Plant More Trees

Love Animals

Conserve our Nature





Study the Effect of B-Sitosterol on *E.coli* Diseases in Broilers

Mohammad Bashar Hazim* and Sameer Mezher Abdullah

Department of Pathology and Poultry Diseases, College of Veterinary Medicine, University of Baghdad, Iraq

Received: 15 June 2018

Revised: 20 July 2018

Accepted: 28 Aug 2018

Address for Correspondence

Mohammad Bashar Hazim

Department of Pathology and Poultry Diseases,
College of Veterinary Medicine,
University of Baghdad, Iraq
E mail: ssmmaa1977@gmail.com



This is an Open Access Journal / article distributed under the terms of the **Creative Commons Attribution License** (CC BY-NC-ND 3.0) which permits unrestricted use, distribution, and reproduction in any medium, provided the original work is properly cited. All rights reserved.

ABSTRACT

This study was carried out to investigate the effect of B-sitosterol added in the drinking water for broiler chicken, on body weight, feed conversion ratio, feed intake and measuring the Gene expression for interleukine-1 and interleukine-6 before and after challenge with avian pathogenic Esherichia coli (APEC) which isolated in Al-Emad laboratories in Baghdad also related it's effect with mortality rate and lesion score. 200 hundred chicks were used randomly divided in to four groups Each group was 50 chicks: G1:-50 chicks control, receiving E.coli at 26 day's old. G2:-50 chicks, supplied with β -sitosterol 20 mg per liter daily in drinking water at 5-30 days old then receiving the challenge E.coli with in 26 day's old. G3:-50 chicks supplied with β -sitosterol 20 mg per liter daily in drinking water at 22-26 days old then receiving the challenge E.coli at 26 days old. G4:-50 chicks receiving challenge E.coli at 26 days' old then supplied with β -sitosterol 20 mg per liter daily in drinking water at 26-30 day's old. Blood samples were collected from wing vein at 30 days old for measuring the gene expression of IL-1, IL6 by quantative real time-polymerase chain reaction. Trachea, air sac, lung, liver, heart, and parts of intestines (duodenum, jejunum, and ileum) were taken from different groups after challenge with APEC to detect histopathological changes and score lesion recorded. The result showed that the groups that were used B-sitosterol showed asinificant increase at ($P \leq 0.05$) in the final weight, and in feed conversion ratio compared with the control group. Our study find out: - Easy isolation and identification of APEC by using Polymerase chain reaction, The third group that supplued with Beta-sitoterol as prevention for APEC gave high final body weight, and recorded lowest lesion scores with less mortality rate after challenge with APEC due to the low level of IL-1 and IL-6 in comparson with other groups. Third group is best group in term of immune response before and after challenge with APEC.

Keywords: APEC, β -sitosterol, qRT-PCR





Mohammad Bashar Hazim and Sameer Mezher Abdullah

INTRODUCTION

Lately, The (herbal medicines) in popularity all over the world are increasingly [1], consumers perceive herbals as (natural), safe, harmless with no adverse side effects, therefore they are being used in both preventing and treating several diseases or health supplements, and tonics [2]. Phytosterols is a one of herbal medicines also; it is a general term for plant-derived sterols and stanols. Plant sterols and plant stanols is commonly known as phytosterols, which are plant-derived composition, that are structurally close to cholesterol. B-sitosterol is phytosterol, which **is** widely distributed in the plant kingdom and found in vegetable oil, nuts, avocados, sesame oil...etc [3]. B-Sitosterol is being studied for its ability to reduce benign prostatic hyperplasia (BPH) [4,5]. and high blood cholesterol levels [6]. High levels of β -Sitosterol concentrations in blood have been correspond with make severity of heart disease increased in men having previously suffered from heart attacks [7]. have plenty of Pharmacological activities: anti-inflammatory activity [8], Hypocholesterolemic Activity[9]Angiogenic Effect [10], Analgesic Bioassay [11] Immunomodulatory Activity [12], Anti-oxidant and larvicidal activity [13] and, have antimicrobial activity[14].

MATERIALS AND METHODS

Collection of Samples

The E.coli strain isolated from the clinically affected broiler farms with colibacillosis manifested the characteristic clinical signs of colibacillosis (respiratory signs, watery diarrhea, weakness, anorexia and weight loss etc.). Blood samples were collected from heart and jugular vein in Al-Emad Lab. then isolation confirm by culturing on selective culture media and the biochemical test were carried out to be sure that it was Avian pathogenic Escherichia coli.

Isolation of bacteria in pure culture

Nutrient broth was used to incubate the samples at 37 °C for 24 hours. the overnight bacterial broth were streaked on to MacConkey, MacConkey sorbitol and EMB, at 37°C for 24 hours incubation. One colony was further subcultured until a pure growth was obtained.

Morphological characteristic

For studying morphological characteristics of E.coli the morphology showed growing organisms on MacConkey and EMB agar was considered [15]. Microscopic properties of isolated bacteria with gram stain were also studied through examining stained slide under light microscope to establish the gram stain reaction and cellular morphology of typical E.coli the slide showed coccoid and rod red cells [16]. Colony characteristics such as shape, size, surface texture, edge and elevation color development after 24 hours of incubation at 37 °C [17].

Gram's stain

Gram's staining of the pure culture was performed according to method described by [17]. Gram's stain determines the staining characteristic of bacteria as well as the purification (Dutta et al., 2015). E.coli is gram negative bacteria and appear red color [18].





Mohammad Bashar Hazim and Sameer Mezher Abdullah

Chromogenic agar

Bacteria isolate was cultured on chromogenic agar and incubated at 37 °C for 48 hours, the development of blue color colonies indicate the positive result for E.coli.

A Confirmation Test Api-20E system

It was done according to [19]: This test (**Api-20E system BIOMÉRIEX**) was used for the diagnosis of bacterial isolates, this test has 25 strips, each strip contains 20 small tubes with upper orifice (Cupule) and lower orifice (tube) which contain dried material and represent the bio-chemical test.

Primer Design

The primers were designed specifically and the sequence of nucleotides was synthesized in IDT Company, USA). The sequences of primers (forward and reverse) were shown in Table 1.

Molecular detection of E.coli by PCR

The amplification of PCR product was prepared by using (Forward primer 10 pmole) and (Reverse primer 10 pmole), master mix containing MgCl₂. The list of primer is listed in table 2.

Sequencing preparation

FimH (509) bp PCR product was sent to the sequencing company (UNCIM, South Korea) with forward and reverse primer (5 pmole), the PCR product (50 ml) was purified in the above company and sequenced it by sanger sequencer.

Electrophoresis

The 1.2 % agarose (sigma) Gel was used for electrophoresis of PCR products (Kawasaka et al., 2009). The procedure of Gel electrophoresis is given below:

- 1- Gel casting tray was assembled with Gel comb of appropriate size and number.
- 2- The 1.2 agarose solution was prepared in (1x) TBE buffer by melting in a microwave oven for 90 seconds.
- 3- Melting agarose was poured on to the casting tray and allowed to solidify on the bench.
- 4- The solidified Gel in its tray was transferred to the electrophoresis tank containing sufficient TBE buffer to cover the Gel ≈ 1mm. The comb was gently removed.
- 5- The 7 µl of each PCR product was mixed with 2-3 µl of (6x) loading DNA buffer and the sample was loaded to the appropriate well of gel.
- 6- The 5 µl DNA size marker (AMB, Canada) was loaded in one well.
- 7- The lead of electrophoresis apparatus was connected to the power supply and the electrophoresis was run at 125 V for 60 min.
- 8- When DNA migrated sufficiently, as judged from the migration of bromophenol blue of loading buffer, the buffer supply was switched off.
- 9- The gel stained with ethidium bromide (0.5 µg/ml) for 10 minutes, in a dark place.
- 10- The gel was destained in distilled water for 10 minutes.
- 11- The destained gel was placed on the UV transilluminator in the dark chamber of the image documentation system.
- 12- The UV light of the system was switched on, the image was viewed on the monitor focused, accurate and safe if it is a USB flash drive.

Preparation of blood samples for gene expression of cytokines by Real Time-PCR



**Mohammad Bashar Hazim and Sameer Mezher Abdullah**

- 1-For each 250µl of samples added 750 µl of AccuZol™
2. Lysed cells in the sample suspension passing the suspension several times through a pipette or vortexing
- 3-Added 200 µl of chloroform per 1ml of AccuZol™ and shake vigorously for 15 seconds
- 4-Incubated the mixture on ice for 5 min.
- 5-Centrifuged at 12000 rpm for 15 minutes at 4°C
- 6-Transferred the aqueous phase to a new 1.5 ml tube and add equal volume of isopropyl alcohol
- 7-Mixed by inverting the tube 4-5 times and incubate at -20°C for 10 minutes
- 8-Centrifuged at 12000 rpm for 10 minutes at 4°C, then carefully removed the supernatant.
- 9-Added 1 ml of 80% ethanol and mix well by inverting or vortexing
- 10- Centrifuged at 12000 rpm for 10 minutes at 4°C, then carefully removed the supernatant.
- 11-Dried the pellet
- 12-Dissolved the RNA in RNase-free water or 0.5% SDS solution by passing the solution a few times through a pipette tip, and incubating for 10 minutes at 55 to 60 °C and stored the RNA at (-20 °C).

Maintenance of stock culture

Stock culture of bacteria was prepared by adding 800 ml of 100% sterilized glycerol, and 200% of pure culture of bacteria, the stock was stored at -20 °C for further use, next step by determination of LD 50 Dose.

Preparation of study place

The study was done in veterinary medicine college in Abu-Grib (animal house) post cleaning and sterilization with sodium hypochlorite, in addition, feeder and water utensils were cleaned and disinfected before being introduced into field; and brush the floor with wood shavers.

Experimental chicks

Two hundred broiler chicks (Breed: Rose 308, origin: Belgium) were brought in good condition from AL-Shuker Hatchery-Baghdad. The chicks were weighted at hatching (39 gm), and divided into 4 groups, each group contains 50 chicks.

The experimental design

200 Chicks will be divided into 4 groups:

- G1:-50 chicks control, receiving E.coli at 26 days old
- G2:-50 chicks, supplied with β-sitosterol 20 mg per liter daily in drinking water from 5- 30 days old, receiving the challenge E.coli at 26 days old and receiving β-sitosterol to 30 days old.
- G3:-50 chicks supplied with β-sitosterol 20 mg per liter daily in drinking water from 22-26 days old then receiving the challenge E.coli at 26 days old.
- G4:-50 chicks receiving challenge E.coli at 26 days old then supplied with β-sitosterol 20 mg per liter daily in drinking water at 26-30 days old.

The production parameters**Body weight**

Weight was measured weekly by weighting 10 chicks and the collective weight of all birds then divided by number to evaluate the medium weight of chicks.



**Mohammad Bashir Hazim and Sameer Mezher Abdullah****Feed conversion ratio (FCR)**

Measuring nourishes transformation of each group along the study period was done according to the following equation:

$$\text{FCR} = \frac{\text{Final feed intake (gram)}}{\text{Final body weight gain (gram)}}$$

Description of organs lesion scoring

At postmortem examination gross lesions of the liver (perihepatitis), heart (pericarditis) and air sac (airsaculitis) were scored macroscopically :the fibrinous pericarditis and perihepatitis were considered to represent systemic E.colipathology, and thoracic air sac lesions were considered to represent E.coli pathology of respirotory system, the lesion scoring was performed according to [20,21] .

Gene Expression

The Study of Gene Expression for some Genes by Quantitative Real Time- PCR (qRT-PCR) techniques. Were studied to measure the RNA level of IL-1, IL-6 compared with B-actin gene.

Estimation of RNA Concentration and Purity

Nanodrop instrument was used to estimate RNA concentration and purity. One μl of each RNA samples was applied in nanodrop to measure the optical density (O.D) at wavelength 260 nm. Purity was 100 ng/ml.

Preparation of primers

These primers (IDT DNA , USA) were provided in lyophilized form, dissolved in sterile deionized distilled water to give a final concentration of 100 picomole/ μl as recommended by provider and stored in a deep freezer until use. Concerning monoplex PCR, forward and reverse primers were specific for these genes.

Amplification reaction of B-actin gene, IL-1, IL-6 primers

(B-actin). PCR mixture final volume 25 μl was composed from 12.5 of GoTaq® Green Master Mix (2x), 5 μl template DNA, 1.5 μl primers (for each forward and reverse), and 4.5 μl nuclease free water in PCR tube. Eppendorf tubes then were briefly mixed by vortex before been placed in thermocycler polymerase chain reaction. The program used for each Uniplex PCR mixture was illustrated in this table.

Gene expression by (qRT-PCR) B-actin, interlukin 1 gene, interlukin 6 gene

Detection of gene expression by ABM's One-Step BrightGreen qRT-PCR Kit is a complete qPCR system containing all necessary reagents for both reverse transcription and PCR amplification to occur in a single qPCR reaction tube.





Mohammad Bashar Hazim and Sameer Mezher Abdullah

1. Prepare the following reaction mixture in a qPCR tube on ice.

Component	Reaction Volume	Concentration
	20 μ l	
RNA template	6 μ l	2 pg- 0.2 μ g/rxn 0.01 pg - 2 ng/rxn
BrightGreenqPCRMasterMix (one step)	10 μ l	1X
qRT-PCR Enzyme Mix (reverse transcriptse)	0.4 μ l	1X
Forward Primer	1 μ l	300 nM
Reverse Primer	1 μ l	300 nM
Nuclease-free H2O	Up to 20 μ l	-

Gently mix and ensure all the components are at the bottom of the amplification tube. Centrifuge briefly if needed.

1. Program the thermal cycler so that cDNA synthesis is followed immediately by qPCR amplification.

Step	Temperature	Duration	Cycle(s)
cDNA Synthesis	42°C	30 mins	1
Pre-Denaturation	95°C	10 mins	1
Denaturation	95°C	15 secs	40
Annealing	55°C	60 secs	
Extension	72°C for 30 sec		

Calculate the value of Δ CT using an equation $\Delta\Delta$ CT method

The equation below is used to calculate the value of Threshold Cycle (CT) (where the Reporter fluorescence) is greater than the brightness at the Threshold, which represents the amount of gene expression of isolates under study as follows:

$$\text{The fold change} = 2^{-\Delta\Delta\text{CT}}$$

$$\Delta\Delta\text{CT} = \Delta\text{CT} (\text{treated target gene - Treated R16}) - \Delta\text{CT} (\text{untreated target gene - untreated R16}).$$

Statistical analysis

The statistical analysis system –SAS (2012) program was used to effect of different factors in study parameters. least significant differences –LSD test (ANOVA) was used for significant means comparison

RESULTS

PCR assay for detection of APEC by using FimH gene and incidence of it in broiler according sample types





Mohammad Bashar Hazim and Sameer Mezher Abdullah

Depending on FimH gene which is the target of APEC, two APEC isolates were formed PCR product of 509 bp and gave positive result as APEC and product analyzed by 1% agarose gel electrophoresis as shown below.

Feed conversion ratio

The result of current study showed no significant differences at level ($P \leq 0.05$) in the feed conversion ratio among all groups so the G1, G2, G3, G4 gave 1.71, 1.75, 1.54, 1.65. The lowest mean of FCR was given by G3 which is 1.54 followed by G4, G1 which are 1.64 and 1.71 respectively as compared with highest mean were given by G2 which was 1.75 at level ($P \leq 0.05$).

Final body weight

The mean of body weight of the chicks in present study in all groups at one day old was 39 gm; the progress in weight gain has been evident in all groups show as significant differences at level ($P \leq 0.05$). The highest mean of final body weight (gm) was given by G3 which was 1774 gm followed by G4, G1 were given 1605, and 1185 gm respectively, comparing with lowest mean of weight was given by G2 which was 1075 g at level ($P \geq 0.05$), as showing in table (7).

Feed intake

The highest feed intake was G3, which was 2749.4 followed by G4 and G1, which were 2648 and 2133.1 respectively the lowest feed intake was G2 which was 1881.3

Mortality rate result

The result of present study showed the mortality rate among all groups after challenge with APEC. The lowest mean of mortality rate was G3, which was percentage 30%, followed by G4 and G1 were percentage 40% and 60% percentage respectively and the highest mortality rate was G2, which was percentage 70%.

Pathological changes of air sac, heart and liver after infection with APEC (lesion score)

The result pathological change in the current study showed the presence of significant differences at level ($p \leq 0.05$) among all groups in mean air sac lesion score at day 30, the lowest mean was recorded in G3 which was 0.62 followed by G4 and G1 which were 0.75 and 2 respectively as compare with G2 which was 2.12.

The mean heart lesion score also recorded as significant differences at level ($p \leq 0.05$) among all groups at day 30 and the lowest mean was recorded in G3 which was 0.75 followed by G4 and G2 which were 1.12 and 2 respectively as compared with G1 which was 2.5. In addition to that the result of mean liver lesion score also recorded as significant differences at level ($p \leq 0.05$) among all groups at day 30 and the lowest mean was recorded in G3 which was 0.5 followed by G4 and G1 which were 1 and 1.75 respectively as compared with G2 which was recorded 1.87.

Quantitative Real Time-Polymerase Chain Reaction

Fold change (gene expression) for IL-1.

Figure 4: Gene expression of IL-1 gene measured by Real time PCR using Syber filter. Expression of IL-1 gene compared with control (GAPDH) Each sample has been replicated triple times and the average calculated using the formula: $\Delta\Delta Ct = (\Delta Ct \text{ Test sample} - \Delta Ct \text{ Calibrator})$, relative quantification ($\Delta\Delta Ct$ method), and finally as showed The fold-change has been calculated by the formula $2^{-\Delta\Delta Ct}$.



**Mohammad Bashar Hazim and Sameer Mezher Abdullah****Fold change (gene expression) for IL-6.**

Figure 4: Gene expression of IL-6 gene measured by Real time PCR using Syber filter. Expression of IL-6 gene compared with control (GAPDH). Each sample has been replicated triple times and the average calculated using the formula: $\Delta\Delta Ct = (\Delta Ct \text{ Test sample} - \Delta Ct \text{ Calibrator})$, relative quantification ($\Delta\Delta Ct$ method), and finally as shown. The fold-change has been calculated by the formula $2^{-\Delta\Delta Ct}$ and $\Delta\Delta Ct - s$.

DISCUSSION**E.coli isolation**

The result of the current study is in agreement with Bopp (2003) who found the growth of E. coli on Eosin Methylene Blue (EMB) agar was indicated by smooth, circular, blue-black color colonies with metallic sheen. In the present study, MacConkey and Eosin Methylene blue agar was used to isolate E. coli from clinical sample in the laboratory. Colonies which are characteristics of E. coli observed on EMB and MacConkey agar [22,23] also observed similar culture and staining which was characteristic of E. coli. The identity of E. coli spp. was confirmed by sugar fermentation and biochemical tests and these tests also used for identification of E. coli [23].

Gram's stain

Our results are in agreement with Cheesbrough M (1985), who found that the Gram's staining of E. coli appears as Gram-negative, short plump rod shaped bacteria, arranged in single, paired or in short chain under the microscope examination.

Culturing on chrom agar

When E. coli isolate cultured on chrom agar showed different color colonies according to type of isolate, the result of present study showed that chrom agar aids in diagnosis of E. coli, which utilize one of chromogenic substrates which produce blue colored colonies, Tarr et al (2005) and Philips et al (2005) and Tavakoli et al (2008) recorded that the use of chromogenic agar has more advantage and can be appropriate alternative for conventional and routine procedure and Ngwa et al (2013) found that chromogenic agar is an effective supplemental medium for the isolation of possible E. coli strains.

Virulence factors of APEC

Several potential virulence factors have been identified on APEC, mainly from a positive correlation between phenotypic characteristics and virulence for chickens. The study of the involvement of these factors in virulence using experimental models of infection is just beginning. This involvement includes the adherence ability of bacteria to the respiratory tract, mediated by fimbriae, the resistance of bacteria to the immunological defences, the multiplication of bacteria in the host physiological liquids through the expression of iron siderophores, and the ability to produce cytopathic effects. More recently, genomic methods have been used, providing very interesting additional hypotheses. Evidence that the ability of E. coli to adhere to the epithelium of the respiratory tract of chickens could be a virulence factor was first provided by the observation that a virulent and fimbriated strain was less easily cleared from the trachea of turkeys than an avirulent and less fimbriated strain [28]. These results were strengthened by the demonstration that virulent E. coli strains were better colonizers of the chicken trachea than avirulent strains, and that these adhesive properties were mediated by type I fimbriae [29]. Adhesion of type I fimbriae to chicken epithelial cells of the pharynx and trachea was demonstrated both in vivo and in vitro [30]. So the figure (7) shows the presence of FimH gene in both samples. Gene expression of interleukin-1 and IL-6



**Mohammad Bashir Hazim and Sameer Mezher Abdullah**

The result of gene expression show as the G2 was the highest one as mentioned in Figure (9) and (10). The lowest one was G3 as preventive effect because the Anti-inflammation activity of plant sterols as mentioned it [31] have reviewed the possible roles of phytosterols in the etiology or preventive role of phytosterols in various diseases and conditions. The mechanisms by which plant sterols display their anti-inflammatory activity are thought to include inhibition of secretion of inflammatory mediators such as interleukin-6, and tumor necrosis factor- α by monocytes [32]. Most of the work has been conducted with animals from these provocative results. The result show as that the administration of betasitosterol for long time will increasing the secretion of IL-1 and IL-6 as in G2 [33] Chronic treatment with BS reduces its anti-inflammatory potential but the administration of betasitosterol for short course will inhibit the secretion of IL-1 and IL-6 as in G3,G4.

Mortality rate

The Table (9) showing that the G3 which supplied by B-sitosterol before challenge have lowest mortality rate compared with other groups, which can refer to the decreased in the level of IL-1 and IL-6 because B-sitosterol decrease the pro-inflammatory cytokines [34] followed by G4 while G1 have the highest mortality rate due to the increase in IL-1 and IL-6 followed by G2 due the over production of pro inflammatory cytokines leads to multiple organ damage, associated with numerous serious acute insults such as severe trauma, thermal injury, ischemia-reperfusion injury, septic shock, and systemic infections [35,36].

Growth performance

Combined feed with phytosterols and unsaturated fatty acids has been demonstrated to have not only complementary but also synergistic effects on circulating lipid levels without adverse effects [37]. The highest growth performance in the third group followed by fourth group that given beta-sitosterol before and after the challenge because the beta-sitosterol increase the body weight, and Feed conversion ration [38]

CONCLUSIONS

- The PCR is consider as more sensitive and accurate technique for decided whether pathogenic or non-pathogenic E.coli by measuring the virulent factors like FimH gene.
- The RT-PCR is consider as more sensitive and accurate technique for measuring the lymphokines levels.
- The best result of B-sitosterol on APEC by giving as preventative for 4 days before infection.
- B-sitosterol can increase the growth performance.

REFERENCES

1. Verma, S., & Singh, S. P. (2008). Current and future status of herbal medicines. *Veterinary world*, 1(11), 347-350.
2. Foster, S. (2012). *Tyler's honest herbal: a sensible guide to the use of herbs and related remedies*. Routledge.
3. Othman, R. A., & Moghadasian, M. H. (2011). Beyond cholesterol-lowering effects of plant sterols: clinical and experimental evidence of anti-inflammatory properties. *Nutrition reviews*, 69(7), 371-382.
4. Wilt, T. J. (2002). Treatment options for benign prostatic hyperplasia: Choice depends on patient's weighting of severity and bother, with risks and benefits of various options. *BMJ: British Medical Journal*, 324(7345), 1047.
5. Kim, M. Y., Kim, E. J., Kim, Y. N., Choi, C., & Lee, B. H. (2012). Comparison of the chemical compositions and nutritive values of various pumpkin (Cucurbitaceae) species and parts. *Nutrition research and practice*, 6(1), 21-27.
6. Oranje, R. P. A. (2014). Proposed mechanisms of action of serum triglyceride lowering by plant sterols and stanols (Master's thesis).




Mohammad Bashar Hazim and Sameer Mezher Abdullah

7. Baumgartner, S., P Mensink, R., & Plat, J. (2011). Plant sterols and stanols in the treatment of dyslipidemia: new insights into targets and mechanisms related to cardiovascular risk. *Current pharmaceutical design*, 17(9), 922-932.
8. Boroushaki, M. T., Mollazadeh, H., & Afshari, A. R. (2016). Pomegranate seed oil: a comprehensive review on its therapeutic effects. *International Journal of Pharmaceutical Sciences and Research*, 7(2), 430.
9. Sugano, M., Morioka, H., & Ikeda, I. (1977). A comparison of hypocholesterolemic activity of β -sitosterol and β -sitostanol in rats. *The Journal of nutrition*, 107(11), 2011-2019.
10. Moon, E. J., Lee, Y. M., Lee, O. H., Lee, M. J., Lee, S. K., Chung, M. H., ... & Kim, K. W. (1999). Ancovellangiogenic factor derived from Aloe vera gel: β -sitosterol, a plant sterol. *Angiogenesis*, 3(2), 117-123.
11. Villaseñor, I. M., Angelada, J., Canlas, A. P., & Echegoyen, D. (2002). Bioactivity studies on β -sitosterol and its glucoside. *Phytotherapy Research: An International Journal Devoted to Pharmacological and Toxicological Evaluation of Natural Product Derivatives*, 16(5), 417-421.
12. Bouic, P. J. (2001). The role of phytosterols and phytosterolins in immune modulation: a review of the past 10 years. *Current Opinion in Clinical Nutrition & Metabolic Care*, 4(6), 471-475.
13. Saednia, S., Manayi, A., Gohari, A. R., & Abdollahi, M. (2014). The story of beta-sitosterol-a review. *European Journal of Medicinal Plants*, 4(5), 590-609.
14. Yinusa, I., George, N. I., Ayo, R. G., & Rufai, Y. (2015). Evaluation of the pharmacological activities of beta sitosterol Isolated from the bark of sarcocephaluslatifolius (smith bruce). *Global Journal of Pure and Applied Chemistry and Research*, 3(3), 7-14.
15. Beutin L, D Geier, S Zimmermann, S Aleksic, HA Gille-spie and TS Whittam,(1996). Epidemiological relatedness and clonal types of natural populations of E. coli strains producing shiga toxin in separate population of cattle and sheep. *Appl Environ Microbiol*, 63: 2175-2180.
16. Jorgensen, J. H., & Pfaller, M. A. (2015). Introduction to the 11th Edition of the Manual of Clinical Microbiology. In *Manual of Clinical Microbiology, Eleventh Edition* (pp. 3-4). American Society of Microbiology.
17. Cheesbrough M (1985). Culturing of anaerobes. In: *Medical Laboratory Manual for Tropical Countries*. Butterworth Co., Kent, UK.
18. Quinn, P. K., Coffman, D. J., Bates, T. S., Welton, E. J., Covert, D. S., Miller, T. L., ... & Carrico, C. M. (2004). Aerosol optical properties measured on board the Ronald H. Brown during ACE-Asia as a function of aerosol chemical composition and source region. *Journal of Geophysical Research: Atmospheres*, 109(D19).
19. Atlas, R.M. (1995). Principles of Microbiology. 1st ed., Mosby Year Book, Inc. Baier RE (1984) Initial events in microbial film formation. In: Costlow JD, Tipper RC (eds) *Marine biodetermination: an interdisciplinary approach*. E & FN Spon, London, pp57-62.
20. Brée, A., Dho, M., & Lafont, J. P. (1989). Comparative infectivity for axenic and specific-pathogen-free chickens of O2 Escherichia coli strains with or without virulence factors. *Avian diseases*, 134-139.
21. Ginns CA, Benham ML, Adams LM, Whithear KG, Bettelheim KA, Crabb BS, et al. Colonization of the respiratory tract by a virulent strain of avian Escherichia coli requires carriage of a conjugative plasmid. *Infect Immun* 2000;68:1535-41.
22. Sharada, R., Krishnappa, G., Raghavan, R., Sreevinas, G. and Upandra, H. A. (1999). Isolation and serotyping of E. coli from different pathological conditions in poultry. *Indian Journal of Poultry Science* 34: 366-369.
23. Thomas, C. G. A. (1988). Gram-negative Bacilli. In: *Medical Microbiology*, 6th ed. Bailliere Tindall. 273-74.
24. Tarr, P. I., Gordon, C. A and Chandler, W.L (2005): Shiga-toxin-producing Escherichia coli and haemolytic-uraemic syndrome. *Lancet* 365:1073-1086.
25. Tavakoli, H; Bayat, M; Kousha, A and Panahi.P.(2008): The Application of Chromogenic Culture Media for Rapid Detection of Food and Water Borne Pathogen. *American-Eurasian J. Agric. & Environ. Sci.*, 4 (6): 693-698.
26. Phillips, B., Tyerman, K and Whiteley. S.M. (2005). Use of antibiotics in suspected haemolytic-uraemic syndrome. *Br. Med. J.* 330:409-410.
27. Ngwa, G. A; Schop, R; Weir, S; León-Velarde, C.G; Odumeru, J.A.(2013): Detection and enumeration of E. coli O157:H7 in water samples by culture and molecular methods. *J Microbiol Methods*. 15;92(2):164-72.




Mohammad Bashar Hazim and Sameer Mezher Abdullah

28. Arp, L. H., & Jensen, A. E. (1980). Piliation, hemagglutination, motility, and generation time of Escherichia coli that are virulent or avirulent for turkeys. Avian Diseases, 153-161.
29. Dho M. & Lafont J.P. (1984). Adhesive properties and iron uptake abilities in E. coli lethal and non-lethal for chicks. Avian Dis. 28:1016-1025.
30. Dho, M., and J.P. Lafont. (1982). Adhesive properties and iron uptake ability in Escherichia coli lethal and nonlethal for chicks. Avian Diseases. 28:1016-1025.
31. Bouic, P. J. (2001). The role of phytosterols and phytosterolins in immune modulation: a review of the past 10 years. Current Opinion in Clinical Nutrition & Metabolic Care, 4(6), 471-475.
32. Paul, A. T., Gohil, V. M., & Bhutani, K. K. (2006). Modulating TNF- α signaling with natural products. Drug discovery today, 11(15-16), 725-732.
33. Gomez, M. A., Saenz, M. T., Garcia, M. D., & Fernandez, M. A. (1999). Study of the topical anti-inflammatory activity of Achillea ageratum on chronic and acute inflammation models. Zeitschrift für Naturforschung C, 54(11), 937-941.
34. Nirmal, S. A., Pal, S. C., Mandal, S. C., & Patil, A. N. (2012). Analgesic and anti-inflammatory activity of β -sitosterol isolated from Nyctanthes arbor-tristis leaves. Inflammopharmacology, 20(4), 219-224.
35. Hung, Y. L., & Suzuki, K. (2017). The pattern recognition receptors and lipopolysaccharides (LPS)-induced systemic inflammation. Int. J. Res. Stud. Med. Health Sci, 2, 1-7.
36. Lim, C. L., & Suzuki, K. (2017). Systemic inflammation mediates the effects of endotoxemia in the mechanisms of heat stroke. Biology and Medicine, 9(01).
37. Demonty, I., Ras, R. T., van der Knaap, H. C., Meijer, L., Zock, P. L., Geleijnse, J. M., & Trautwein, E. A. (2013). The effect of plant sterols on serum triglyceride concentrations is dependent on baseline concentrations: a pooled analysis of 12 randomised controlled trials. European journal of nutrition, 52(1), 153-160.
38. Naji, T. A., Amadou, I., Zhao, R. Y., Tang, X., Shi, Y. H., & Le, G. W. (2014). Effects of phytosterol in feed on growth and related gene expression in muscles of broiler chickens. Tropical Journal of Pharmaceutical Research, 13(1), 9-16.

Table 1: Primer sequencing of genes that were studied in gene expression of FimH, B-actin, IL-1 and IL-6.

Primer name	Product size(bp) (5'-----3')	Product size(bp)	Reference
IL-1	F: GAG ACC TTC TAC GGC CCC TC R: GTC GCT GTC AGC AAA GTC CCT	195 bp	Current study
IL-6	F: AAATCCCTCCTCGCCAATCT R: CCTCACGGTCTTCTCCATAAAC	105 pb	Current study
B-actin	F: CACCACAGCCGAGAGAGAAAT R: TGACCATCAGGGAGTTCATAGC	135 pb	Current study
FimH	F:GTGAATGTGGGGCAAAACCTGGTC R:AGGTAATACCCCAGGTTTTGGCTT	509 bp	Current study





Mohammad Bashar Hazim and Sameer Mezher Abdullah

Table 2: PCR mixture(30 µl) was prepared as follows

Component	Reaction Volume
	30 µl
10 P mole Primer F (Forward)	2 µl
10 P mole Primer (Reverse)	2 µl
2X Kapa Robust hot start master mix	15 µl
DNA	3 µl
25mM MgCL2	1 µl
D.W.	7 µl

Table 3: PCR condition

Stage	Time	Temperature (time)
Heat inactivation	3 minutes	95°C
Denaturation	20 seconds	94°C
Annealing	30 seconds	55°C
Polymerization	30 seconds	72°C
Final extension	10 minuets	72°C

Table 4: show the scoring system used to evaluate the virulence of the wild strains in the intratracheal model study.

Organ	score	Description of organ lesions
Thoracic air sac	0	No lesion
	1	Slight opaque and \or thickened membranes± slight amount of fibrin
	2	Moderate opaque and \or thickened membranes± slight amount of fibrin
	3	severe opaque and \or thickened membranes± slight amount of fibrin
Heart and pericardium	0	No lesion
	1	Vascularization ,opacity
	2	Excessive or cloudy fluid in pericardial cavity
	3	Thickened



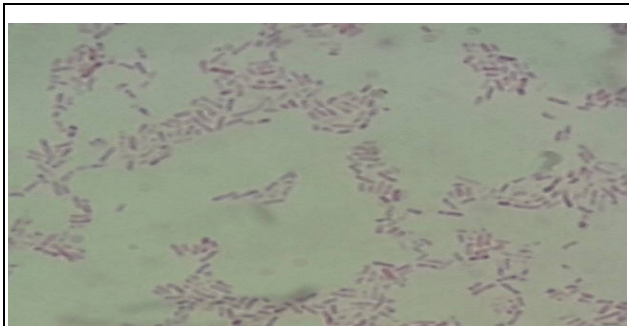


Mohammad Bashar Hazim and Sameer Mezher Abdullah

		pericardium,acutepericarditits
Liver	0	No lesion
	1	Decolourizationand\or slight amount of fibrinous exudate
	2	Marked perihepatitis with large amount of fibrinous exudate

Table 5: The program used for each Uniplex PCR mixture

Stage	Temperature (time)	
Reverse transcription	42 C for 30 minutes	
Initial denaturation	95 C for 10 min.	
Denaturation	95 C for 30 Sec.	40 cycles
Annealing	56 C for 20 sec.	
Extension	95 C for 10 min.	



Gram staining:

Figure 1.Gram under light microscop show negative result,short rod shaped bacteria.



Figure 2.colonies of E.coli on MacConkey sorbitol agar produce characteris white in color.





Mohammad Bashar Hazim and Sameer Mezher Abdullah



Figure 3.colonies of E.coli on MacConkey agar produce characteris red color.



Figure4.colonies of E.coli on EMB agar produce characteris green metallic sheen color

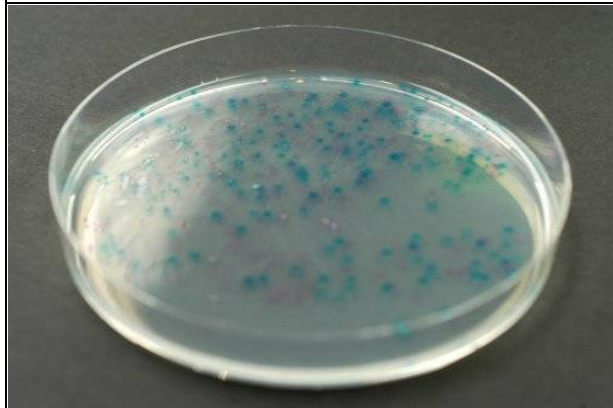


Figure 5.Result of our isolate culture on chromogenic agar produce blue color colonies.



Results of Api -20 E System:
Figure 6.Calculation the numerical profile in Api-20E system

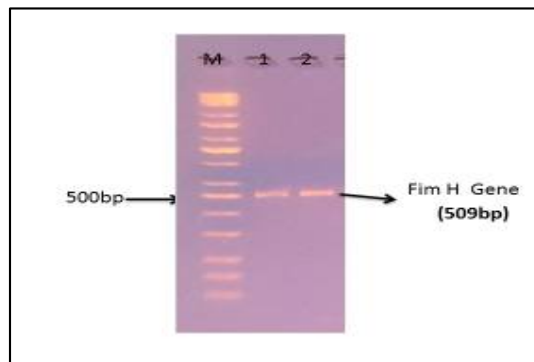


Figure 7. showing the length of our PCR product (509bp) of FimH gene in APEC with forward and reverse primers.





Mohammad Bashar Hazim and Sameer Mezher Abdullah

Escherichia coli fimberial adhesin protein (fimH) gene, complete cds					
Sequence ID: KY848624.1 Length: 903 Number of Matches: 1					
Range 1: 121 to 653 GenBank Graphics ▼ Next Match ▲ Previous Match					
Score	Expect	Identities	Gaps	Strand	
985 bits(533)	0.0	533/533(100%)	0/533(0%)	Plus/Plus	
Query 1	GTTTATGTAACCTTGGCGCCGCGGTGAATGTGGGGCAAAACCTGGTCGTGGATCTTTTCG				60
Sbjct 121	GTTTATGTAACCTTGGCGCCGCGGTGAATGTGGGGCAAAACCTGGTCGTGGATCTTTTCG				180
Query 61	ACGCAAATCTTTTGGCATAACGATTATCCGGAAACCATTACAGACTATGTCACACTGCAA				120
Sbjct 181	ACGCAAATCTTTTGGCATAACGATTATCCGGAAACCATTACAGACTATGTCACACTGCAA				240
Query 121	CGAGGCTCGGCTTATGGCGGCGTGTATCTAATTTTTCCGGGACCGTAAAAATATAGTGGC				180
Sbjct 241	CGAGGCTCGGCTTATGGCGGCGTGTATCTAATTTTTCCGGGACCGTAAAAATATAGTGGC				300
Query 181	AGTAGCTATCCATTTCTACCACCAGTGAAACGCCGCGCGTGTGTTTATAAATTCGAGAACG				240
Sbjct 301	AGTAGCTATCCATTTCTACCACCAGTGAAACGCCGCGCGTGTGTTTATAAATTCGAGAACG				360
Query 241	GATAAGCCGTGGCCGGTGGCGCTTTATTTGACGCCTGTGAGCAGTGCGGGCGGGGTGGCG				300
Sbjct 361	GATAAGCCGTGGCCGGTGGCGCTTTATTTGACGCCTGTGAGCAGTGCGGGCGGGGTGGCG				420
Query 301	ATTAAAGCTGGCTCATTAAATGCGCGTGTATTTTGGCAGACAGACCAACAACATAACAGC				360
Sbjct 421	ATTAAAGCTGGCTCATTAAATGCGCGTGTATTTTGGCAGACAGACCAACAACATAACAGC				480
Query 361	GATGATTTCCAGTTTGTGTGGAATATTTACGCCAATAATGATGTGGTGGTGCCTACTGGC				420
Sbjct 481	GATGATTTCCAGTTTGTGTGGAATATTTACGCCAATAATGATGTGGTGGTGCCTACTGGC				540
Query 421	GGCTGCGATGTTCTGCTCGTGATGTCACCGTTACTCTGCCGGACTACCCCTGGTTCAGTG				480
Sbjct 541	GGCTGCGATGTTCTGCTCGTGATGTCACCGTTACTCTGCCGGACTACCCCTGGTTCAGTG				600
Query 481	CCAATTCCTCTTACCGTTTATTGTGCGAAAAAGCCAAAAACCTGGGGTATTACCT				533
Sbjct 601	CCAATTCCTCTTACCGTTTATTGTGCGAAAAAGCCAAAAACCTGGGGTATTACCT				653

Figure 8. Alignments of sequenced PCR product with one of matched E.coliFimH gene in NCBI.

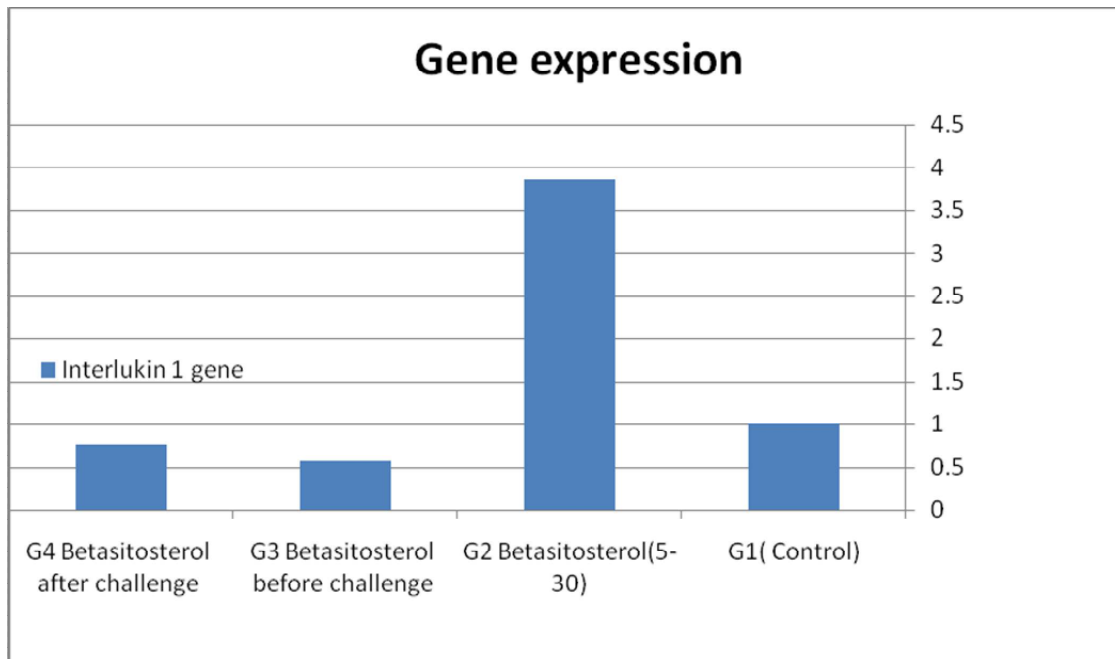


Fig. 9. Gene expression for IL-1 gene.





Mohammad Bashar Hazim and Sameer Mezher Abdullah

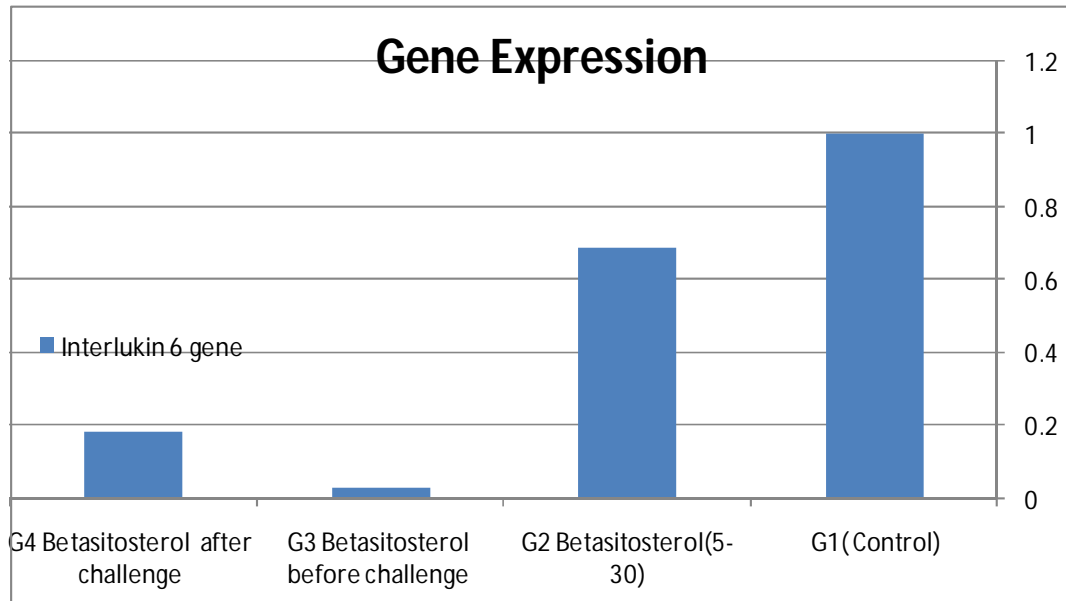


Fig.10.Gene expression for IL-6 gene.





Effect of using Different Levels of Commercial *Saccharomyces cerevisiae* in the Ration on Some Productive Traits of Awassi Lambs

Z. T. Aldoori¹ and A. S. A. Al-Obaidi²

¹Assistant Professor, Public Health, College of Veterinary Medicine, University of Tikrit, Iraq

²Animal Production, College of Agriculture, University of Diyala, Iraq

Received: 01 July 2018

Revised: 03 Aug 2018

Accepted: 05 Sep 2018

Address for Correspondence

Z. T. Aldoori

Assistant Professor,
Public Health,
College of Veterinary Medicine,
University of Tikrit Iraq.



This is an Open Access Journal / article distributed under the terms of the **Creative Commons Attribution License** (CC BY-NC-ND 3.0) which permits unrestricted use, distribution, and reproduction in any medium, provided the original work is properly cited. All rights reserved.

ABSTRACT

This study was conducted to investigate the effect of using different levels of commercial *Saccharomyces cerevisiae* in Awassi lambs ration on productive traits. Sixteen local Awassi male lambs aged 6-6.5 months with initial weight of 36 ± 0.34 kg were allocated into four treatments with four lambs each treatment as follow: treatment one T1 (control treatment), treatment two T2 (3 gmSc/head/day), treatment three T3 (5 gmSc/head/day), treatment four T4 (7 gmSc/head/day). Treatment lambs were distributed to individual cages. Each lamb was subjected to introductory period for two weeks before start the study. Wheat straw was provided *ad libitum* as a roughage diet while concentrate diet was provided for each treatment lambs by 2.5% of weekly live body weight for the whole study period which was seventy five days. At the end of the study lambs were slaughtered. During the experiment period and during the slaughter some parameters and weights have been taken. The results shows no significant differences among treatments in initial, final weight, average and total weight gain, also no significant differences within treatments in average daily, total concentrate feed intake, external and internal offal's percentage weight. Results also shows significant superiority with T3 (5 gm Sc/head/day) among the treatments in each feed conversion ratio, hot carcass weight and dressing percentage. We can conclude that Sc as a supplementation or feed additives act as a growth promoter and has a positive effect on ruminant in the experiment conditions.

Keywords: *Saccharomyces cerevisiae*, Awassi lambs, productive traits



**Z. T. Aldoori and A. S.A.Al-Obaidi**

INTRODUCTION

Saccharomyces cerevisiae (Sc) is considered one of the prominent feed additives that using with animal rations, and there are several researches have been conducted to measure or determine positives and benefits from using this kind of additives with poultry (Zhang et al.,2005) and ruminant rations (Guedes et al., 2008). Feed additives identify as it is one or more stuff that add in very small quantities to basic ration in order to enhance animal performance or replenish feed requirements (Wenk, 2000). Interest in using fungi (such as Sc) in ruminants nutrition were increased especially after feed antibiotics (Cooper and Kennedy,2007)and hormonal growth stimulators (Vdovenko et.al.,2011) get prohibited, which led to the need to evaluate using of this fungi and its effects on gastrointestinal and rumen. It has become known that there is a positive effects when using this feed additives with ruminant animals (Hassan and Saeed, 2013) which are beneficial modifications to microbial activities, fermentation and digestive functions of the rumen .This positive effects is a result of stimulating specialized groups of bacteria in the rumen possess different mechanisms depending on the type of these groups(Denev et al, 2007). Several researchers have reported that giving yeast as feed additives has improved the rumen environment and microorganisms effectiveness (Tricarico et al,2006; Chevaux and Mazzia-Fabre,2007) as well as an increase in rumen anaerobic and cellulolytic bacteria (Jouany,2001). Jurkovichet al (2007) mentioned that feed additives from yeasts in ruminant diets can act as a growth promoter, and it also works to improve and accelerate rumen maturation(McDonald, 2002) and improve rumen fermentation (Pienaar et al, 2012). Fuller (1989) also mentioned that *Saccharomyces cerevisiae* can grow quickly in the rumen and facilitate fiberdigestion. These explanations or theories proposed for the work or effect of *Saccharomyces cerevisiae* that added to ruminant diets as feed additives have not been proven yet as there are many research results were shown adverse effects or non-positive (Bayat et al, 2015; Obeidat, 2017),which may be due to differences in each added yeasts concentrations, strain characteristics (Newbold et al, 1995) and composition of the ration (Wallace, 1994). For that reasons, the aim of this research was to study the effect of adding different levels of commercial *Saccharomyces cerevisiae* as feed additives on productive traits of Awassi lambs.

MATERIALS AND METHODS

sixteen local Awassi male lambs aged 6-6.5 months with initial weight of 36 ± 0.34 kg were allocated for four treatments with four lambs each treatment which was as follow: treatment one T1 (control treatment), treatment two T2 (3 gmSc/head/day), treatment three T3 (5 gmSc/head/day), treatment four T4 (7 gmSc/head/day).

Treatment lambs were distributed to individual cages 1.75×1.25 m, each cage contain two portable plastic feeders for each concentrate and roughage feed, it also contain portable water pail and mineral salts block. Each lamb was subjected to introductory period for two weeks before start the study to accustom the lambs to the cages and feed providing style. Routinely veterinary treatments table were followed in this period for all of the lambs. At the end of this period, weight of each lamb was taken by small ruminant electronic scale. That weight was the primary weight, and then the lambs were individual to cages and treatments by the weight.

Wheat straw was provided *ad libitum* as a roughage diet for each treatment lambs for the whole study period while concentrate diet (table 1) was provided for each treatment lambs by 2.5% of weekly live body weight for the whole study period also which was seventy five days. Feed intake was taken at eight AM daily by previous feed residual quantities measurement. At the end of the study lambs final weight were taken, then the lambs were slaughtered and each hot carcasses weight, external and internal offal weights were recorded. Statistical analysis was conducted to investigate treatments effect on different measurements by statistical analysis program (SAS,2004) with completely randomized design then differences between the averages were compared by Duncan polynomial test (Duncan,1955).





Z. T. Aldoori and A. S.A.Al-Obaidi

RESULTS AND DISCUSSION

Table (2) shows the effect of different treatments on initial, final weight and average daily and total weight gain. We can notice no significant differences between the control treatment T1 and Sc treatments T2, T3 and T4 for each of final weight, average daily and total weight gain, also no significant differences can be seen among Sc treatments along with non-significant superiority of T3 (5gm Sc/head/day) in each average and total weight gain among the rest treatments.

Table (3) shows the effect of different treatments on average daily and total concentrate feed intake, feed conversion ratio, hot carcass weight and dressing percentage. We can notice no significant differences among treatments in average daily concentrate feed intake while there was a clear decline but non-significant in average total concentrate feed intake for T3 (5gm Sc/head/day) treatment comparing with the rest treatments. That decline was reflected to the rest parameters in the table which show a significant superiority of the same treatment (T3) in hot carcass weight comparing with T2 and in dressing percentage comparing with T2 and the control treatment (T1). Tables (4) and (5) show the effect of different treatments on external and internal offal percentage weight. Results revealed that there were no significant differences between control treatment T1 and treatments T2, T3, and T4, either among Sc treatments for all parameters.

These results are agreed with the results of Al-khauzai et al. (2012) who noticed no increase in daily and total weight gain of Awassi male lambs in the first period of experiment (0-4 week) and second period (4-8 week) when fed with 2gm/kg ration of Sc and 2% of black seed. Also agree with Rejab et al. (2013) in their experiment on Awassi lamb when they were noticed no significant differences between three levels of Sc (0, 4, 8gm/head/day) in daily, total of each feed intake and weight gain but disagree with them in feed conversion ratio results. Also agree with Lazim et al. (2012) who recorded significant increase in hot carcass weight and non-significant in dressing percentage when add Sc (2 kg/ton) and Iraqi probiotic (1 kg/ton) to Awassi lambs ration. Also agree with Hassan and Mohammed (2016) who noticed that there are no differences between treatments of adding Sc (0, 5 gm/head/day) to Awassi male lambs ration in each daily dry matter intake and weight gain. In this experiment we can notice that there are no significant effects of adding Sc in all of measured parameters except in feed conversion ratio, hot carcass weight and dressing percentage in T3 (5gm Sc/head/day) which considered a positive effect of this kind of feed additives. That benefits might be due to Sc supplementation which enhance the action of rumen micro-organisms, that enhancement is a result of increasing the total viable count of bacteria which is partly dependent on yeast respiratory activity which protects anaerobic rumen bacteria from damage by O₂ (Newbold et al., 1996), on the other hand that enhancement might be a result of improving activity of short chain polysaccharides degrading micro-organisms (Tripathi and karim, 2011) leading to improve feed ingredients degradation and increase TVFA (Hassan and Mohammed, 2016), amino acids and microbial protein (Oeztuerk et al., 2005) flowing into small intestine. All the above makes Sc act as a growth promoters (Jurkovich et al., 2007; Tripathi and karim, 2011).

REFERENCES

1. Al-khauzai A.L.D., Abdel-Lattif F.H., & Amer J.A. (2012). Effect of addition Saccharomyces Cerevisiae and black seed on some productive and biochemical traits of male lambs for Awassi sheeps. *Al-Furat Journal of Agricultural Sciences*. 4(2):57-68.
2. Bayat, A. R., Kairenius, P., Stefański, T., Leskinen, H., Comtet-Marre, S., Forano, E., & Shingfield, K. J. (2015). Effect of camelina oil or live yeasts (*Saccharomyces cerevisiae*) on ruminal methane production, rumen fermentation, and milk fatty acid composition in lactating cows fed grass silage diets. *Journal of dairy science*, 98(5), 3166-3181.
3. Chevaux, E., & Mazzia-Fabre, M. (2007). Probiotic yeast in small ruminants. *Feed Mix*, 15(1), 28.




Z. T. Aldoori and A. S.A.Al-Obaidi

4. Cooper, K. M., & Kennedy, D. G. (2007). Stability studies of the metabolites of nitrofurantoin antibiotics during storage and cooking. *Food additives and contaminants*, 24(9), 935-942.
5. Denev, S. A., Peeva, T.Z., Radulova, P., Stancheva, N., Staycova, G., Beev, G., Todorova, P. and Tchopanova, S. (2007). Yeast Cultures in Ruminant Nutrition. *Bulg.Journal of Agricultural Sciences*, 13: 357-374.
6. Duncan, D.D., (1955). Multiple range and multiple F-test. *Biometrics*, 11:1-42.
7. Fuller R. (1989). Probiotics in man and animals. *Journal of Applied Microbiology*, 66(5), 365-378.
8. Guedes, C. M., Goncalves, D., Rodrigues, M. A. M., & Dias-da-Silva, A. (2008). Effects of a *Saccharomyces cerevisiae* yeast on ruminal fermentation and fibre degradation of maize silages in cows. *Animal Feed Science and Technology*, 145(1), 27-40.
9. Hassan S.A., & Mohammed S.F. (2016). Effect of *Saccharomyces cerevisiae* Supplementation on Rumen Characteristics in Awassi Lamb Feed Diets With Different Roughage to Concentrate Rations. *The Iraqi Journal of Agricultural Sciences*. 47(Special Issue):1-11.
10. Hassan, S. A., & Saeed, A. A. (2013). Effect of Feeding Different Levels of Dietary Protein and Addition of Baker's Yeast (*Saccharomyces cerevisiae*) on Productive Parameters of Awassi Lambs. *Journal of Agricultural Science and Technology. A*, 3(6A), 484
11. Jouany, J. P., 2001. 20 years of research and now more relevant than ever- the coming of age of yeast cultures in ruminant diets. In: Responding to a Changing Agricultural Landscape. Alltech's European, Middle Eastern and African Lecture Tour., 44-69.
12. Jurkovich, V., Kutasi, J., Fébel, H., Brydl, E., Könyves, L., & Tirián, A. (2007). The effect of micro-capsulated yeast supplementation on rumen fermentation in sheep. In *Animal health, animal welfare and biosecurity. Proceedings of the 13th International Congress in Animal Hygiene, Tartu, Estonia, 17-21 June, 2007. Volume 2* (pp. 843-845). Estonian University of Life Sciences, Jõgeva Plant Breeding Institute, Estonian Research Institute of Agriculture.
13. Lazim J.S., Khadom B.N., & Shamran S.H.A. (2012). The Effect of Use Some Agricultural and Manufacturing Products Supplemented With Bread Yeast *Saccharomyces cerevisiae* and Iraqi Probiotic on Some Production Characteristics of Awassi Lambs Carcasses. The Second Scientific Conference of the Faculty of Agriculture, Karbala University.
14. McDonald, P. (2002). *Animal nutrition*. Pearson education.
15. Newbold, C. J., Wallace, R. J., Chen, X. B., & McIntosh, F. M. (1995). Different strains of *Saccharomyces cerevisiae* differ in their effects on ruminal bacterial numbers in vitro and in sheep. *Journal of animal science*, 73(6), 1811-1818.
16. Newbold, C. J., Wallace, R. J., & McIntosh, F. M. (1996). Mode of action of the yeast *Saccharomyces cerevisiae* as a feed additive for ruminants. *British Journal of Nutrition*, 76(2), 249-261.
17. Obeidat, B. S. (2017). The effects of feeding olive cake and *Saccharomyces cerevisiae* supplementation on performance, nutrient digestibility and blood metabolites of Awassi lambs. *Animal Feed Science and Technology*, 231, 131-137.
18. Oeztuerk, H., Schroeder, B., Beyerbach, M., & Breves, G. (2005). Influence of living and autoclaved yeasts of *Saccharomyces boulardii* on in vitro ruminal microbial metabolism. *Journal of dairy science*, 88(7), 2594-2600.
19. Pienaar, G. H., Einkamerer, O. B., Van der Merwe, H. J., Hugo, A., Scholtz, G. D. J., & Fair, M. D. (2012). The effects of an active live yeast product on the growth performance of finishing lambs. *South African Journal of Animal Science*, 42(5), 464-468.
20. Rejab A.S., Sadik H.L., & Taha A.A. (2013). Effect of Baker's Yeast (*Saccharomyces Cerevisiae*) Supplementation Diets on productive Performance and Digestibility of Sheep and Goat. *Al-Anbar Journal of Veterinary Sciences*. 6(2):68-79.
21. SAS. (2004). *Statistical Analysis System, User's Guide. Statistical. Version 7th ed.* SAS. Inst. Inc. Cary. N.C. USA.
22. Tricarico, J. M., Harrison, G. A. and Johnston, J. D. (2006). Modeling Yea-Sacc®1026 effects on ruminal function and performance in lactating dairy cattle within the framework of the CPM dairy ration analyzer. *Proceedings of the 22nd Annual Symposium. Nutritional Biotechnology in the Feed and Food Industries, USA*, 72: 23-26.
23. Tripathi, M. K., & Karim, S. A. (2011). Effect of yeast cultures supplementation on live weight change, rumen fermentation, ciliate protozoa population, microbial hydrolytic enzymes status and slaughtering performance of growing lamb. *Livestock Science*, 135(1), 17-25.





Z. T. Aldoori and A. S.A.Al-Obaidi

24. Vdovenko, M. M., Peng, C. F., Xu, C. L., Vylegzhanina, E. S., Komarov, A. A., & Sakharov, I. Y. (2011). Enzyme immunoassay for the determination of hexestrol in meat. *Applied biochemistry and microbiology*, 47(1), 77-81.
25. Wenk, C. (2000). Herbs, spices and botanicals: "Old fashioned" or the new feed additives for tomorrow's feed formulations? Concepts for their successful use. In: Lyons, T.P. and Jacques, K.A.(Eds.). *Biotechnology in the Feed Industry*. Proceedings of Alltech's 16th Annual Symposium, Nottingham Press, Nottingham ,79-95.
26. Wallace, R. J. (1994). Ruminant microbiology, biotechnology, and ruminant nutrition: progress and problems. *Journal of Animal Science*, 72(11), 2992-3003
27. Zhang, A. W., Lee, B. D., Lee, S. K., Lee, K. W., An, G. H., Song, K. B., & Lee, C. H. (2005). Effects of yeast (*Saccharomyces cerevisiae*) cell components on growth performance, meat quality, and ileal mucosa development of broiler chicks. *Poultry science*, 84(7), 1015-1021.

Table 1. Formula and chemical composition of concentrate diet

ingredient	%
Barley grain	49
Yellow corn	39
Soybean meal	10
salt	1
Min. and vit. mixture	1
Chemical composition / kg dry matter	
Dry matter	94
Organic matter	91
Total nitrogen	21.3
Crude fibers	50.8
Ether extract	34
Nitrogen free extract	700
Metabolisable energy MJ/Kg	12.7

Table 2. Effect of different treatments on initial, final weight and average weight gain in Awassi lambs (Mean±SE)

Treatments	Parameters			
	Initial weight (kg)	Final weight (kg)	Average daily weight gain (gm)	Total weight gain (kg)
T1 Control	37.75±2.14	48.75±1.64	0.15±0.01	11.00±0.54
T2 3gm Sc/head/day	34.75±1.44	46.13±2.20	0.15±0.02	11.38±1.14
T3 5gm Sc/head/day	36.50±1.55	48.75±2.39	0.16±0.01	12.25±0.853
T4 7gm Sc/head/day	36.51±1.04	46.75±1.39	0.14±0.01	10.25±1.09





Z. T. Aldoori and A. S.A.Al-Obaidi

Table 3. Effect of different treatments on average daily and total concentrate feed intake, feed conversion ratio, hot carcass weight and dressing percentage in Awassi lambs (Mean±SE)

Treatments	Parameters(%)		
	Head	Legs	Wool
T1 Control	5.26±0.06	2.41±0.09	9.86±0.27
T2 3gm Sc/head/day	5.79±0.18	2.96±0.06	10.36±0.76
T3 5gm Sc/head/day	5.51±0.19	2.69±0.11	9.41±0.2
T4 7gm Sc/head/day	6.03±0.19	2.71±0.05	9.33±0.42

Different letters within column refer to significant differences ($P \leq 0.05$) between means-

Table 4. Effect of different treatments on external offal percentage weight in Awassi lambs (Mean±SE)

Treatments	Parameters				
	Average daily concentrate feed intake (kg)	Average total concentrate feed intake (kg)	feed conversion ratio (kg feed/kg weight gain)	Hot carcass weight (kg)	Dressing percentage based on slaughtering weight (%)
T1 Control	1.32±0.06	99.25±4.90	9.02±0.06 a	23.89±0.91 ab	48.07± 0.84 b
T2 3gm Sc/head/day	1.35±0.14	101.00±10.62	8.87±0.11 a	23.32±0.69 b	49.49±1.05 b
T3 5gm Sc/head/day	1.17±0.1	87.75±7.36	7.15±0.17 b	26.22±0.91 a	52.61±0.91 a
T4 7gm Sc/head/day	1.26±0.12	94.25±9.25	9.22±0.1 a	24.23±0.69 ab	50.68±0.28 ab





Z. T. Aldoori and A. S.A.Al-Obaidi

Table 5. Effect of different treatments on internal offal percentage weight in Awassilambs (Mean±SE)

Treatments	Parameters(%)					
	Heart	Liver+lung	Kidneys	Spleen	Testes	Rumen
T1 Control	0.37±0.01	2.84±0.50	0.23±0.08	0.23±0.01	0.87±0.1	4.01±0.81
T2 3gm Sc/head/day	0.30±0.05	2.65±0.20	0.25±0.05	0.19±0.06	0.93±0.09	3.58±0.24
T3 5gm Sc/head/day	0.38±0.01	2.81±0.16	0.24±0.07	0.18±0.02	0.99±0.11	3.92±0.16
T4 7gm Sc/head/day	0.36±0.03	2.24±0.13	0.25±0.04	0.15±0.01	0.98±0.08	3.76±0.28





Preparation and Study the Physical Properties of PbI_2 by using Thermal Evaporation to use in Nuclear Detector

Zahraa razaq and Abbas Fadhel Essa

College of Science, University of Wasit, Iraq

Received: 20 June 2018

Revised: 25 July 2018

Accepted: 29 Aug 2018

*Address for Correspondence

Zahraa razaq

College of Science,
University of Wasit,
Iraq.



This is an Open Access Journal / article distributed under the terms of the **Creative Commons Attribution License** (CC BY-NC-ND 3.0) which permits unrestricted use, distribution, and reproduction in any medium, provided the original work is properly cited. All rights reserved.

ABSTRACT

Lead iodide thin films were prepared using thermal evaporation method on glass substrates for application to nuclear detection. This paper studied The influence of annealing on the structural properties and optical has been investigated at temperature (0,100,200,300)^oC for one hour in vacuum (10^{-6} torr). X- ray diffraction analysis confirmed that PbI_2 films are polycrystalline having hexagonal structure. The optical absorption data indicate an allowed direct transmission with optical energy gap varies continuously from (2.50eV to 2.51eV) .

Keywords: Lead iodide, thermal evaporation, X- ray diffraction.

INTRODUCTION

Lead iodide is an important and promising P- type semiconductor and crystallizes in an hexagonal structure and can be grown from solution, vapor and gels [1]. lead iodide PbI_2 is a wide band gap semiconductors $E_g \sim 2.3$ eV . Due to the high atomic number of its elements (ZPb=82, ZI=53), it is a material with potential use as an ionizing radiation detector (X and γ rays)[2,3,4]. atoms are located in layers of Pb and I perpendicular to caxis in the succession I-Pb-I-I-Pb-I, on account of van der Waals bonding between the iodine atoms [5]. Lead iodide (PbI_2) is a promising semi conducting material for room temperature radiation detectors [6-8]. Lead iodide is an important and promising P- type semiconductor and crystallizes in an hexagonal cadmium iodide like structure [4], The aim of this work is to prepare a thin polycrystalline lead iodide films by vacuum evaporation method, and studying the optical and structural properties of this material to present preliminary results which in this approach could be a way to develop PbI_2 nuclear imaging devices beside the electrical properties .





Zahraa razaq and Abbas Fadhel Essa

MATERIALS AND METHODS

Polycrystalline PbI_2 thin film samples were prepared on glass substrates using thermal evaporation technique at temperature (0,100,200,300) $^{\circ}C$. Take a specific weight of lead iodide powder with purity of (99.99%) and manufactured by BDH. And put it in a pod medium between the two electrodes for the purpose of vaporizing the powder later and the formation of the system of vacuum 10^{-6} torr. The powder is evaporated inside the system on the glass bases fixed above. The system is opened after a day and the glass bases are removed and kept in clean containers and the required tests are carried out. The process annealing was carried out at different temperatures on some samples using a thermal oven for one hour . the annealing samples and without annealing for one same thickness (200 nm) at temperature (0,100,200,300) $^{\circ}C$.

RESULTS AND DISCUSSION

Through studying the X-ray diffraction, one can understand the polycrystalline growth nature of PbI_2 thin films without annealing and annealing prepared by thermal evaporation technique deposition on glass substrates at (0 $^{\circ}$, 100 $^{\circ}$,200 $^{\circ}$, 300 $^{\circ}$)C. From the X-ray diffraction the planes orientation were determined, grain size of PbI_2 thin films were calculated. The XRD shows polycrystalline structure and hexagonal type [9,10,11]. Figure(1) show the X-ray diffraction of samples prepared without annealing and annealing. Peaks are observed at 2θ (12 $^{\circ}$ -52 $^{\circ}$) correspond to (001),(003) , (004), (110) planes respectively and demented peak (001),this results are in a good agreement with results achieved by authors [12]. The inter plane spacing is calculated by using diffraction Bragg equation [13]:

$$n \lambda = 2d \sin \theta \dots\dots(1)$$

Where

θ : is (Bragg's angle).

λ : is the wavelength of radiation. n :is a positive integer.

d :is the inter-planar spacing.

The average grain size is deduced by using Scherrer equation [14]:

$$G.s = 0.94 \lambda / \beta \cos \theta \dots\dots\dots(2)$$

λ : is the wavelength of radiation .

β : is the full width at half maximum (FWHM).

Table (1) summarize the obtained values of 2θ , d, average grain size and for without annealing and annealing films. as shown in Figure (1). From this table the greatest grain size are those of layers without annealing and annealing in temperature (0,100,200,300) $^{\circ}C$. Figures (3) show the variation of absorbance as a function of wavelength, at wavelength range (300-800 nm) for PbI_2 without annealing and annealing in temperature (0,100,200,300) $^{\circ}C$. It is shown that there was increasing in the absorbance with the increasing of annealing temperature while decreasing with increased wavelength, and the absorbance edge is changed with the change of annealing temperature . these values are in a good agreement with publish work [15]. Figures (3) show the variation of absorbance as a function of wavelength, at wavelength range (300-800 nm) for PbI_2 without annealing and annealing in temperature (0,100,200,300) $^{\circ}C$. It is shown that there was increasing in the absorbance with the increasing of annealing temperature while decreasing with increased wavelength, and the absorbance edge is changed with the change of annealing temperature . these values are in a good agreement with publish work [15]. To understand the optical and electrical properties of the prepared films, it is very necessary to study and estimate the mean value of the optical bandgap. This value depends on the films structure, the arrangement and distribution of atoms in the crystal lattice. The spectral absorption coefficient curves indicate the direct transitions. The optical band gaps were determined from





Zahraa razaq and Abbas Fadhel Essa

the plots of $(\alpha h\nu)^2$ versus $(h\nu)$ where the extrapolation of the straight line region gives the optical band gap. show in Figure(4) samples PbI_2 without annealing and annealing in temperature (0,100,200,300)^o C is the band gap values of samples are increase with increasing annealing temperature and these values are in a good agreement with publish work [16].Table(1)Values of band gap forr PbI_2 without annealing and annealing in temperature(0,100,200,300)^oC

CONCLUSION

The XRD shows polycrystalline structure and hexagonal type, with four main peaks: (001), (003), (004), and (110).the demented peak (001). Transmittance of all PbI_2 thin films increase with wavelength while absorbance decreasing with increased wavelength. the value of band gap varying (2.50 -2.51) eV also it was found that the energy gap for PbI_2 thin films are increase with increasing annealing temperature. The process annealing reason for the increase in the energy gap.

REFERENCES

1. A.Nayak, G.L.Bhalla, B.Kumar and G.C.Triconaat , Phys State Sol (b) 213,487 (1999) .
2. X.Xiang, Crys Res Technol. 42, No.5,pp 456-459/DoI 10-1002/crat.200610847, (2007).
3. D.S.Bhavsar and K.B.Saraf, Mat, Chem. Phys.78,630 (2003).
4. M.Svatusk, J.Zavadil and M.Matuchova, J.Phys Chem 97,pp.9288, (1993).
5. O.V.Rybak, Yu.O.Lun, I.M.Bordun and M.F.Omelyan, Inorganic Materials, Vol 41, No 10, pp 1124-1127, (2005).
6. D. S. Bhavsar, K. B. Saraf, S. S. Patil, S. R. Patil, and P. S. Sonawane, J. Instrum. Soc. India 34, 14 (2004).
7. D. S. Bhavsar and K. B. Saraf, Mat. Chem. Phys. 78, 630 (2003).
8. N. Balamurugan, M. Lenin, G. Bhagavannarayana, and P. Ramasamy, Cryst. Res. Technol. 42, 151 (2007).
9. T.Ghosh and etal,"optical and structural properties of lead Iodide thin films prepared by vacuum evaporation method",Cryst.Res.Technol.43,No.9,959_963(2008).
10. Ali M.Mousa and etal,"Effect of changing substrate temperature of PbI_2 thin films deposited by spray technique on the structural,optical and electrical properties" ,University of Technology, College of Basic Education ,no 94, folder 22, (2016).
11. X. H. Zhu, Z. R. Wei, Y. R. Jin, and A. P. Xiang, Cryst. Res. Technol. 42, 456 (2007).
12. Shatha Sh.Jamil and Ali M.Mousa,"The Structural Properties of think film of PbI_2 ",Eng .& Tech.Journal,Vol.28,No.6,(2010).
13. Giuseppe,G.;Pastori,P.G.," Solid state physics", Academic press an imprint of Elsevier Science, USA,pp.(394),(2000).
14. AL-Jammal, Y.N.,"Soild state physics" , Higher Education Press in Mosul, AL-Mousul University ,pp.(322). (1990).
15. Hind D.A. Mfarej, and et al," The Effect of Annealing on The Structural and Optical Properties of SnS Thin Films", Journal Ibn Al-Haitham J. for Pure & Appl. Sci, Vol. 28, No. (1) (2015).
16. Zuheer Naji Majeed, and et al," Study the Effect of The Annealing and Doping on the Some Optical Properties of (ZnS) Thin Films", Journal Kirkuk university, Vol.8,No.1,(2013).





Zahraa razaq and Abbas Fadhel Essa

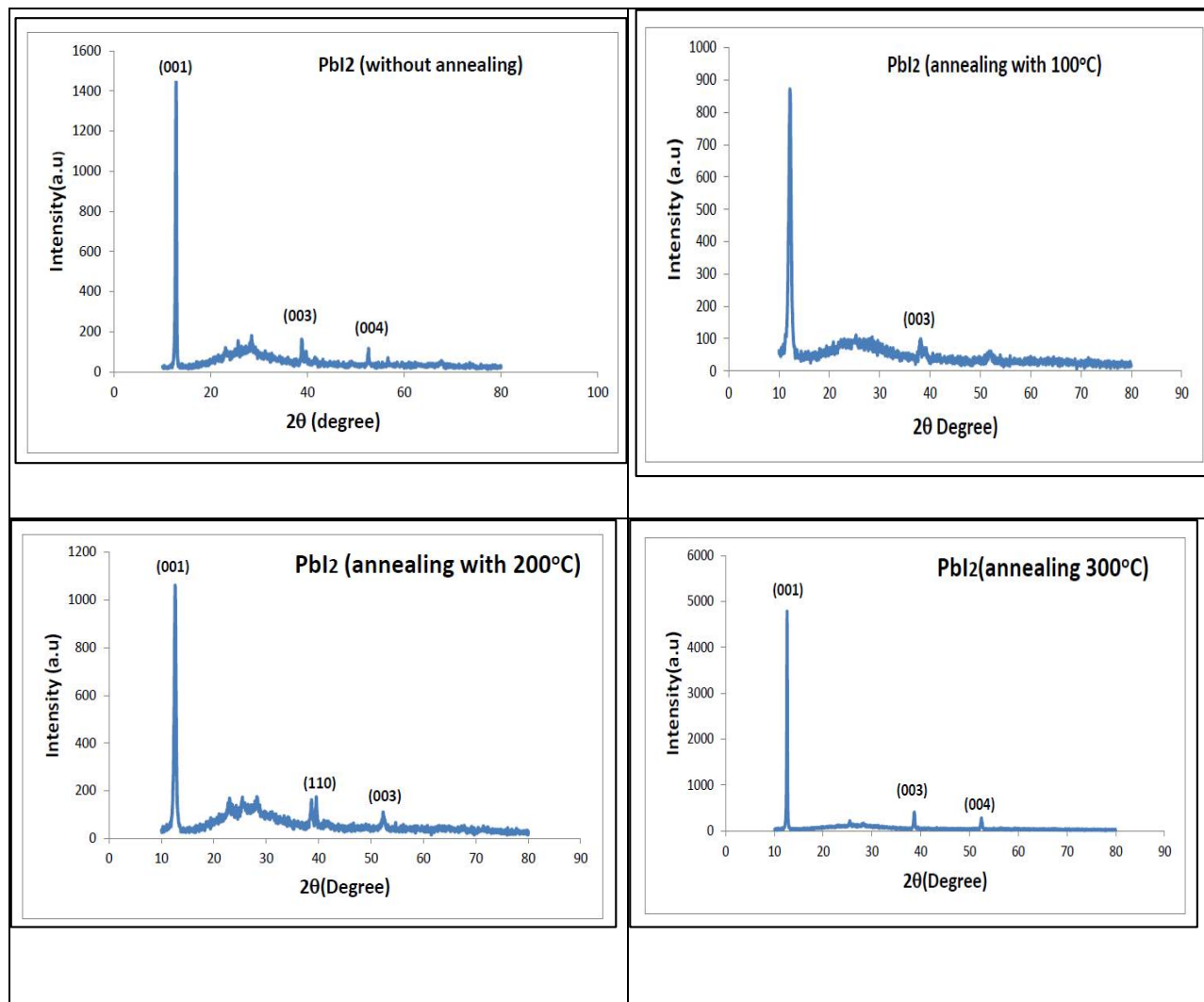


Figure 1. XRD patterns for PbI₂ without annealing and annealing in temperature (0,100,200,300)° C

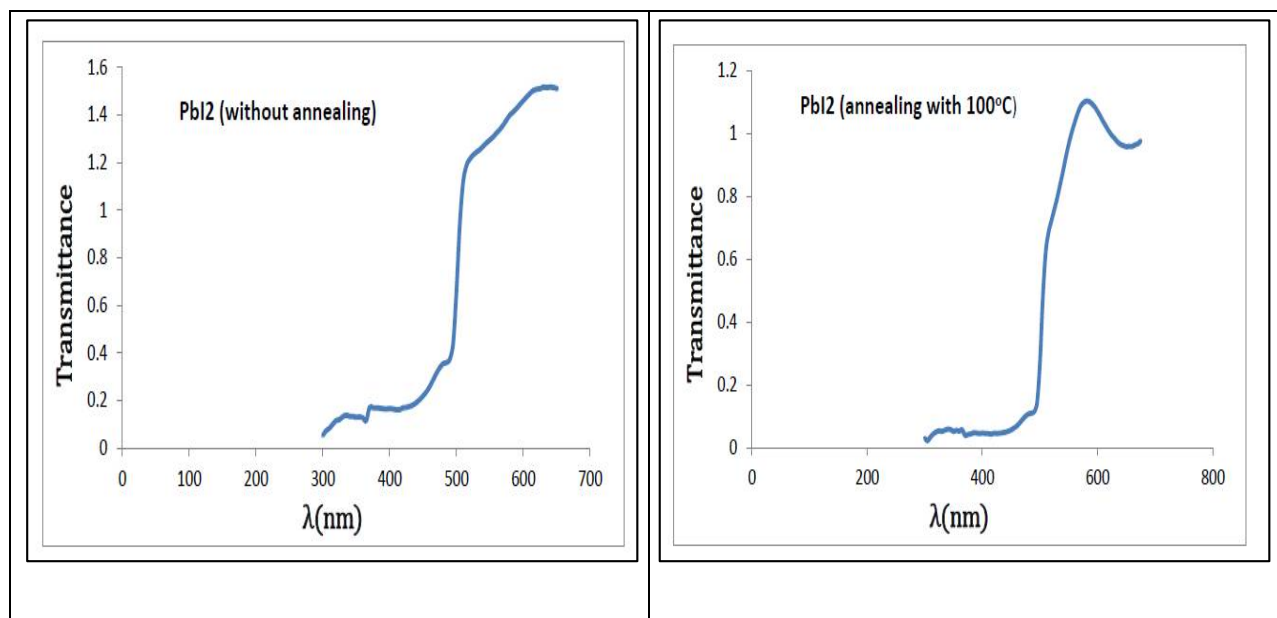




Zahraa razaq and Abbas Fadhel Essa

Table 1. Structural values of PbI₂ thin films without annealing and annealing in temperature (0,100,200,300)0 C

Sample	hkl	2θ (JCPD)	2θ Exp.	I/I ₀	d(A°) (JCPD)	d(A°) Exp.	FWHM (degree)	G.s(nm)
Sample (1) 0 C ⁰	001	12.672	12.8906	100	6.98	6.86208	0.24930	32
	003	38.661	38.8517	10	2.327	2.31609	0.21590	39
	004	52.392	52.5899	6	1.7449	1.73886	0.27820	31.8
Sample (2) 100 C ⁰	001	12.672	12.2328	100	6.98	7.22956	0.55080	14.49
	003	38.661	38.0861	6	2.327	2.36087	0.58930	14.25
Sample (3) 200 C ⁰	001	12.672	12.6776	100	6.98	6.97689	0.41150	19.42
	110	39.527	39.5376	11	2.278	2.27747	0.34320	24.59
	003	38.661	38.6382	10	2.327	2.32839	0.42330	19.88
Sample (4) 300 C ⁰	001	12.672	12.6677	100	6.98	6.98232	0.18150	44
	003	38.661	38.6762	8	2.327	2.32619	0.26030	32.33
	004	52.392	52.4270	6	1.7449	1.74388	0.26850	32.96





Zahraa razaq and Abbas Fadhel Essa

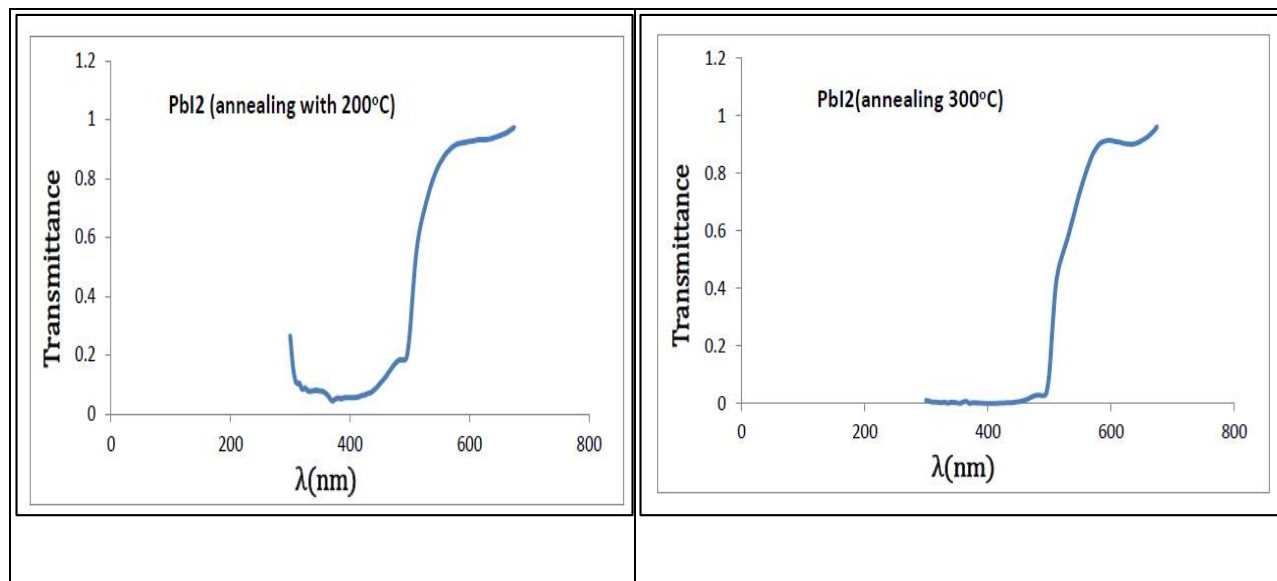
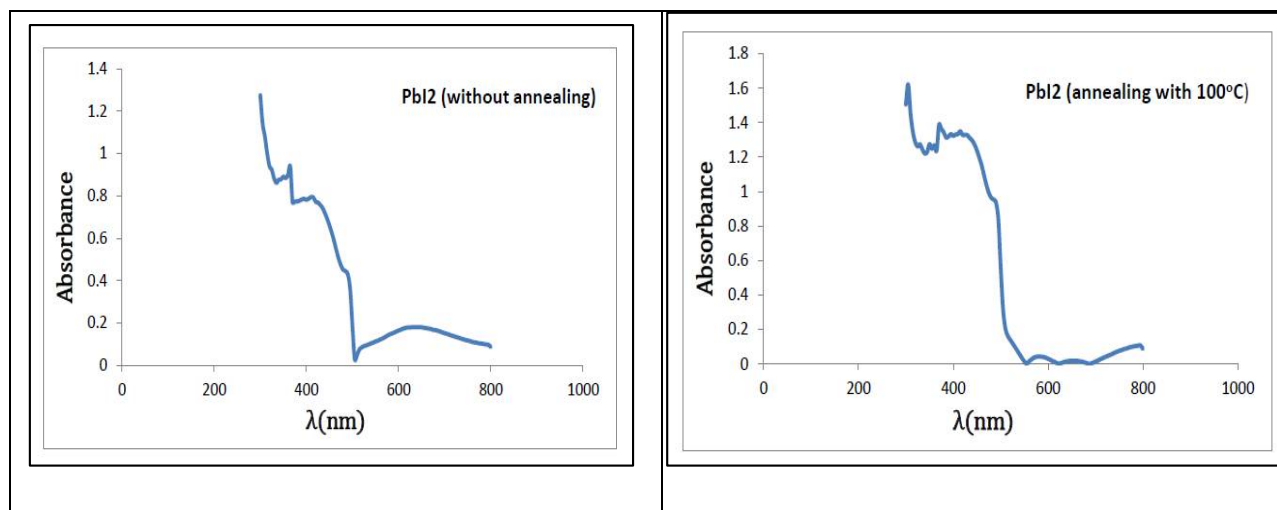


Figure 2 : Optical transmission spectrum vs. wavelength for PbI₂ without annealing and annealing in temperature (0,100,200,300)°C





Zahraa razaq and Abbas Fadhel Essa

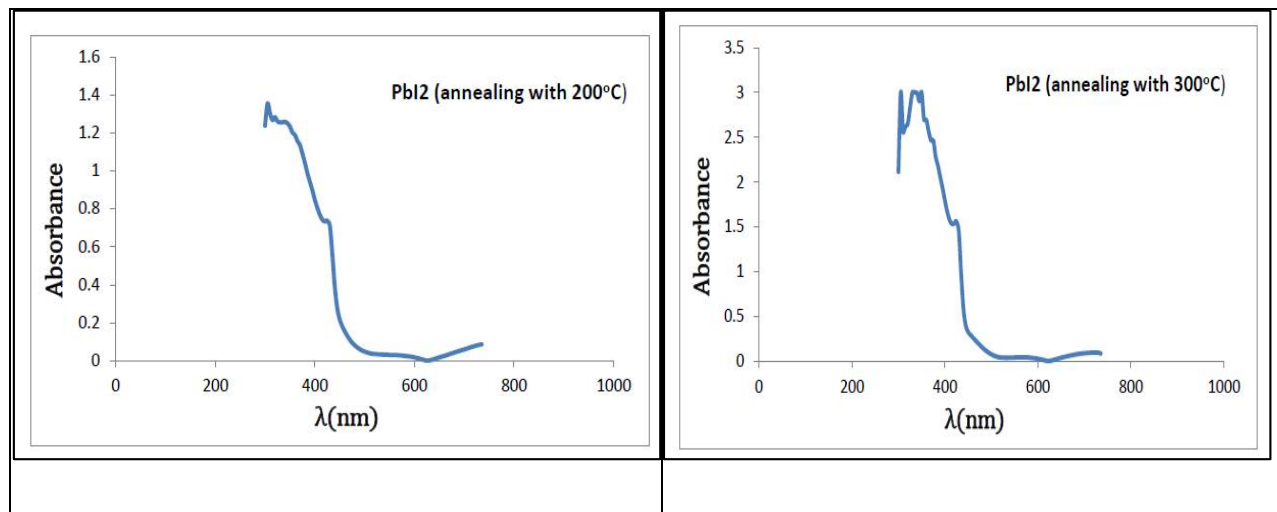


Figure 3 : Absorbance vs. wavelength for PbI₂ without annealing and annealing in temperature (0,100,200,300)^o C

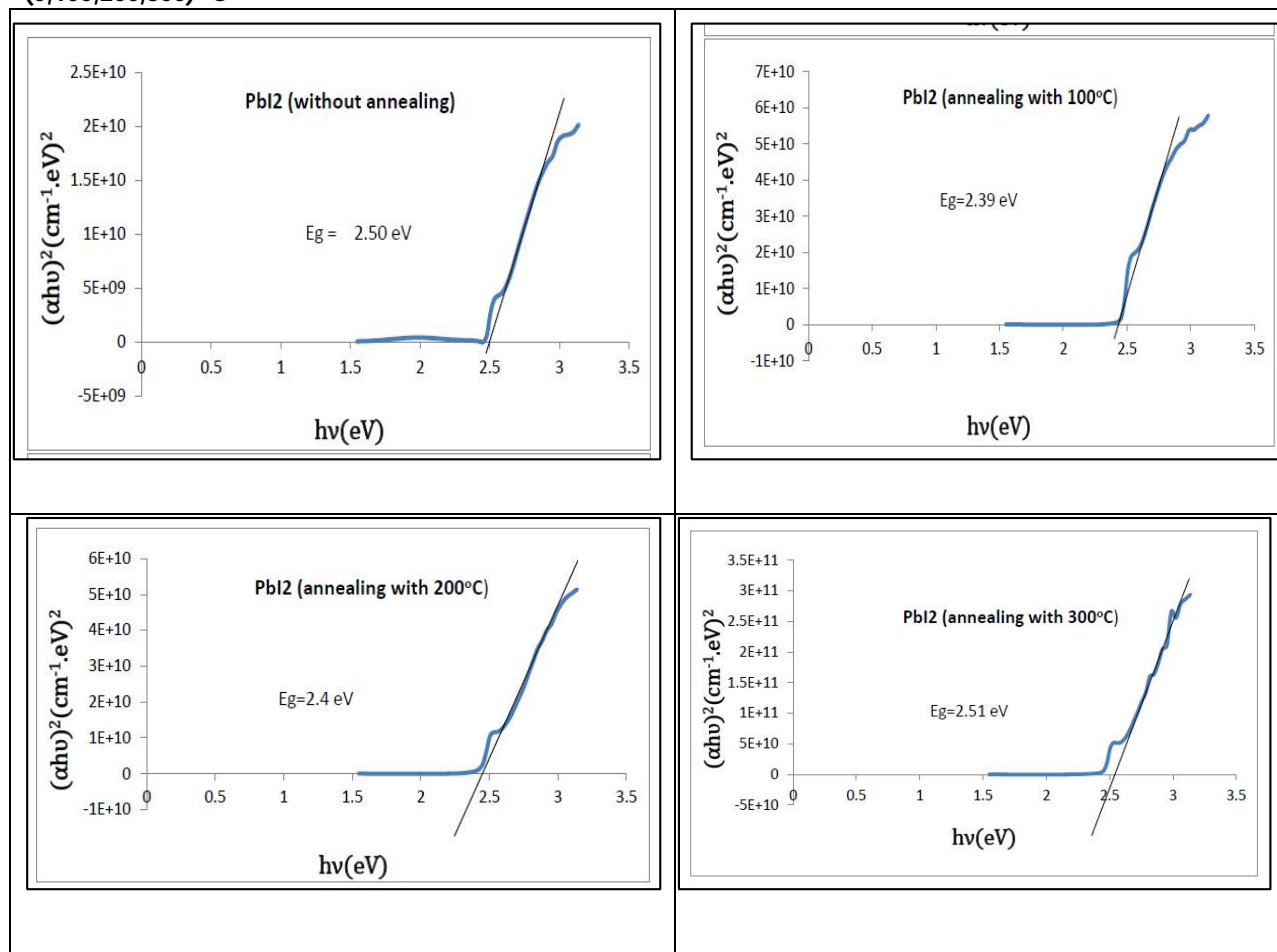


Figure 4: The direct optical energy gap for PbI₂ without annealing and annealing in temperature (0,100,200,300)^o C



**Zahraa razaq and Abbas Fadhel Essa****Table 2. Values of direct optical energy gap for PbI₂ without annealing and annealing in temperature (0,100,200,300)°C**

Sample	E _g (eV)
PbI ₂ without annealing	2.50
PbI ₂ at 100 ⁰ C	2.39
PbI ₂ at 200 ⁰ C	2.4
PbI ₂ at 300 ⁰ C	2.51





A Survey on Canine Oral Neoplasms

M.Sumanth Bedre*, R. Anoopraj, Kavya M., S.Nikhil Rao., Madhura Prashant Naik., Vidyarani H.B., S.Shyam., Krupa T.L., A.J. George and Sajitha I.S.,

Department of Veterinary Pathology, Kerala Veterinary and Animal Sciences University, Pookode, Lakkidi (P.O.), Wayanad, Kerala – 673576, India.

Received: 28 July 2018

Revised: 31 Aug 2018

Accepted: 05 Sep 2018

*Address for Correspondence

M.Sumanth Bedre

Department of Veterinary Pathology,
Kerala Veterinary and Animal Sciences University,
Pookode, Lakkidi (P.O.), Wayanad, Kerala – 673576, India.
Email : sumanthbedre93.vet@gmail.com



This is an Open Access Journal / article distributed under the terms of the **Creative Commons Attribution License** (CC BY-NC-ND 3.0) which permits unrestricted use, distribution, and reproduction in any medium, provided the original work is properly cited. All rights reserved.

ABSTRACT

The incidence of canine oral tumours was studied. Tumour suspected samples from the oral cavity were obtained from the canine cases presented to the Veterinary hospitals under Kerala Veterinary and Animal Sciences University as well as the carcasses brought for post-mortem examination in the Department of Veterinary Pathology of College of Veterinary and Animal Sciences, Pookode and Mannuthy. The samples were collected during the period from December 2016 to June 2018. Out of 252 canine tumours presented during the course of study, 14 tumours of oral cavity were recorded (5.55 per cent; 14 out of 252). Age group of 4 to 6 years showed the highest incidence of tumours (50 per cent; seven out of 14). There was no significant difference in the occurrence of tumours in males and females. Breed-wise analysis revealed that non-descript dogs (35.72 per cent; five out of 14) were the most affected, followed by Labrador, German shepherd, Rottweiler and Spitz. Benign tumours comprised 64.28 per cent (nine out of 14) and malignant tumours were 35.72 per cent (five out of 14). The benign tumours encountered were viral and squamous oral papilloma, ameloblastoma and peripheral odontogenic fibroma. Malignant tumours included oral melanoma, oral fibrosarcoma, oral squamous cell carcinoma, oral basal cell carcinoma and extramedullary plasmacytoma.

Key words: Incidence; Canine; Oral cavity; Tumours.

INTRODUCTION

Neoplastic conditions are frequently encountered in pet animal practice and are important causes of death in companion animals. About 16 to 24 per cent deaths in canines are attributed to neoplasia (Soodet *al.*, 2008). The incidence of tumours of oral cavity is less common than tumours affecting other regions. Among different species of



**Sumanth Bedre et al.**

domestic animals, the occurrence of digestive system tumours is higher in dogs (Frgelecovaet al., 2014). Like in other tumours, the age is considered as one of the risk factors and data on breed-wise and gender-wise incidence helps us to identify genetic factors associated with these tumours. Except few reports, no systematic studies have been carried out on the occurrence and pathology of canine oral tumours in India.

MATERIALS AND METHODS

Out of 252 canine tumours presented during the course of study (December 2016 to June 2018), a total of 17 tumour suspected samples involving oral cavity were collected. Tumour suspected samples were fixed in ten per cent neutral buffered formalin (10 % NBF) for a minimum of 48 hours. Identification of the animal, detailed description of lesion pertaining to location, size, colour and consistency of the samples were recorded at the time of sample collection. The samples were processed in a bench top tissue processor and paraffin embedded blocks were prepared according to the standard procedure. Serial sections were cut from the blocks at 4 µm thickness using rotary microtome. Formalin fixed paraffin embedded (FFPE) sections were stained with Hematoxylin and Eosin (H&E). Histopathological examination was performed to diagnose and classify the tumours.

RESULTS

Out of 17 tumour suspected samples, 14 were diagnosed as tumours (5.55 per cent; 14 out of 252) and three were diagnosed as non-neoplastic proliferative lesions. Benign tumours constituted 64.28 per cent (nine out of 14) and the malignant tumours comprised 35.72 per cent (five out of 14) of the tumours. Age-wise incidence of canine oral tumours is presented in Figure 1. In the present study, the highest risk of development of tumours was seen the age group of 4-6 years (50 per cent), followed by the age group of 0-3 years (21.42 per cent). Age groups of 7-9 years (14.29 per cent) and above 10 years (14.29 per cent) showed fewer incidences. Among malignant tumours, 60 per cent (three out of five) occurred in 4-6 years age group and 20 per cent (one out of five) were encountered in the age groups of 7-9 years and above 10 years. The incidence of benign tumours was 33.33 per cent (three out of nine), 44.44 per cent (four out of nine), 11.11 per cent (one out of nine) and 11.11 per cent (one out of nine) in the age groups of 0-3 years, 4-6 years, 7-9 years and above 10 years respectively.

In the present study, there was no difference in the incidence of tumours between male and female dogs. Among the presented cases, oral papilloma, ameloblastoma, fibrosarcoma, extramedullary plasmacytoma, peripheral odontogenic fibroma were observed in female dogs. Male dogs were presented with oral papilloma, oral melanoma, ameloblastoma, oral squamous cell carcinoma and oral basal cell carcinoma. Breed-wise incidence of canine oral tumours is presented in Figure 2. In the present study, the incidence of tumours was more in non-descript dogs (35.72 per cent; five out of 14), followed by Labrador (28.58 per cent; four out of 14), Rottweiler (14.28 per cent; two out of 14), German shepherd (14.28 per cent; two out of 14) and Spitz (7.14 per cent; one out of 14). Non-descript and Labradors were found to be presented with more benign tumours, whereas in Spitz and Rottweiler only malignant tumours were recorded. There was no difference in the incidence of benign and malignant tumours in German shepherds.

Tumour-wise incidence of canine oral tumours is presented in Table 1. Among all the tumours of oral cavity, five cases of oral papilloma (35.72 per cent) were observed. It was followed by three cases of ameloblastoma (21.44 per cent) and one case of other type of tumours (7.14 per cent).

DISCUSSION

In the present study, oral tumours comprised 5.55 per cent of all canine neoplasms presented. Bastianello (1983) found similar results and reported that oral tumours represented only 5 per cent of all canine neoplasms. The highest





Sumanth Bedre et al.

risk of cancer development was seen in the age groups of 4-6 years (50 per cent). These findings are in agreement with Babuet *et al.* (2012) who reported that the highest incidence was seen in the age group of 5 to 8 years (55 per cent). In the present study the incidence of tumours in the age group of above 10 years was less, this is likely due to the shorter life span of large breeds of dogs as reported by Capiket *et al.* (2008). In the present study there was no significant difference in the incidence of oral tumours in male and female dogs. This is in agreement with the findings of Roshini *et al.* (2013). But, Singh *et al.* (2004) observed the higher incidence in male dogs (76.47 per cent). Lather *et al.* (2017) reported that female dogs showed higher incidence of tumours (53.4 per cent). Rungsipipat *et al.* (2003) opined that the incidence of tumours was not influenced by the sex of dog, except the mammary gland tumours in females and perianal adenoma in male due to the involvement of sex hormones. The highest incidence of neoplasms was observed in non-descript dogs (35.72 per cent), followed by Labrador (28.58 per cent), Rottweiler (14.28 per cent), German shepherd (14.28 per cent) and Spitz (7.14 per cent). Similar observations were recorded by Simon *et al.* (2016), who reported higher incidence of tumours in non-descript dogs (32.87 per cent). In contrary, Babuet *et al.* (2012) reported the higher incidence of tumours in German shepherd dogs. Incidence of tumours might be attributed to population and popularity of different breeds in different geographical areas. In the present area of the study, the population of non-descript dogs was more followed by the popularity of Labrador retriever breed. This might be the reason for higher representation of incidence in these two breeds. A total of nine benign tumours (55.55 per cent) and five malignant tumours (45.45 per cent) were recorded. Komazawa *et al.* (2016) reported that the ratios of benign and malignant tumours varied with different dog breeds and the smaller breeds of dogs showed higher proportion of benign tumours.

The incidence of neoplastic conditions is increasing day by day. The data on age-wise, gender-wise, breed-wise incidence of oral tumours in dogs may help to identify genetic risk factors related to different tumours. Accurate diagnosis and grading of the tumours is very essential to adopt proper treatment regimen.

REFERENCES

1. Sood, N.K., Singh, A., Mekibib, B. and Gupta, K. 2008. Cytopathological diagnosis of canine superficial neoplasia. *Indian J. Vet. Path.* **32**: 206-216.
2. Frgelecová, L., Škorič, M., Fictum, P. and Husník, R. 2014. Canine gastrointestinal tract tumours: a retrospective study of 74 cases. *Acta Veterinaria Brno.* **82**: 387-392.
3. Bastianello, S.S. 1983. A survey on neoplasia in domestic species over a 40-year period from 1935 to 1974 in the Republic of South Africa. VI. Tumours occurring in dogs. *The Onderstepoort J. Vet. Res.* **50**: 199-220.
4. Babu, P., Abraham, M.J. and Lalithakunjamma, C.R. 2012. An epidemiological study of canine neoplasms. *Indian J. Anim. Res.* **46**: 196-198.
5. Capik, I.T., Sevdik, A.T. and Sevdikova, Z. 2008. Tumour diseases in dogs. *Folia Veterinaria.* **52**: 194-198.
6. Roshini, S., Kadam, D.P., Moregaonkar, S.D., Sawale, G.K., Tripathi, S.D., Pawar, A.A., Thakur, D. and Chavan, S.R. 2013. Occurrence of different neoplasms of dogs in Mumbai region. *Indian J. Vet. Path.* **37**: 138-140.
7. Singh, R., Mohindroo, J., Banga, H.S., Singh, S.S. and Kansal, S.K. 2004. Occurance of neoplasms in canines. *Indian J. Vet. Path.* **28**: 54-57.
8. Lather, D., Gupta, R. and Sharma, S., Retrospective studies on tumor conditions in dogs over a period of ten years (2005-2014). 2017. *Haryana Vet.* **56(1)**: 47-49
9. Rungsipipat, A., Sunyasootcharee, B., Ousawaphlangchai, L., Sailasuta, A., Thanawongnuwech, R. and Teankum, K. 2003. Neoplasms of dogs in Bangkok. *Thai. J. Vet. Med.* **33(1)**: 59-66.
10. Komazawa, S., Sakai, H., Itoh, Y., Kawabe, M., Murakami, M., Mori, T. and Maruo, K. 2016. Canine tumor development and crude incidence of tumors by breed based on domestic dogs in Gifu prefecture. *J. Vet. Med. Sci.* **78**: 1269-1275.





Sumanth Bedre et al.

Table 1. Tumour-wise incidence of canine digestive system tumours

Sl. No.	Tumour type	Total	Percentage (%)
1	Oral papilloma	5	35.72
2	Ameloblastoma	3	21.44
3	Peripheral odontogenic fibroma	1	7.14
4	Oral melanoma	1	7.14
5	Oral fibrosarcoma	1	7.14
6	Oral squamous cell carcinoma	1	7.14
7	Oral basal cell carcinoma	1	7.14
8	Extramedullary plasmacytoma	1	7.14

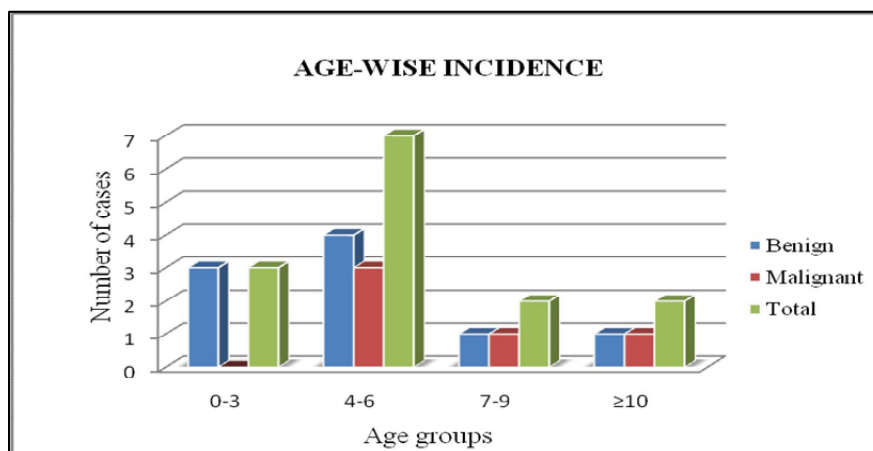


Fig 1. Age-wise incidence of canine oral tumours

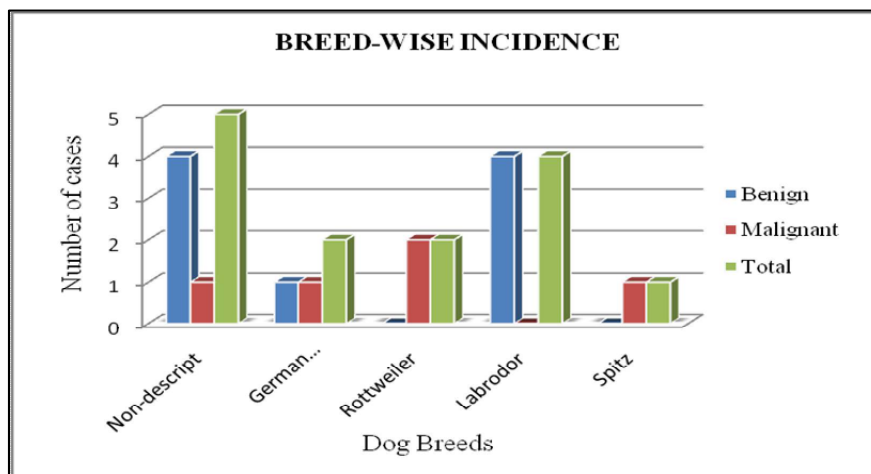


Fig 2. Breed-wise incidence of canine oral tumours





Investigation Structural, Morphological and Optical Properties CdO Thin Film by PVD Method

Amenah Ali Salman*

Applied Science Department, University of Technology, Baghdad, Iraq.

Received: 09 July 2018

Revised: 12 Aug 2018

Accepted: 17 Sep 2018

*Address for Correspondence

Amenah Ali Salman

Applied Science Department,
University of Technology, Baghdad, Iraq.
Email: zamonalisman@yahoo.com



This is an Open Access Journal / article distributed under the terms of the **Creative Commons Attribution License** (CC BY-NC-ND 3.0) which permits unrestricted use, distribution, and reproduction in any medium, provided the original work is properly cited. All rights reserved.

ABSTRACT

Nanostructure of CdO thin films prepared using thermal Evaporation technique on glass substrate. Effect of oxidation time (30, 60, 90 min) on the optical structural and morphological properties was studied and investigated. The optical properties show the decreases of the direct energy band gap from (2.2 - 1.9 eV) for Cadmium oxide thin films with increases in the oxidation time. From AFM measurement, the average grain size found to be in the range of nanometer and increase from (70.79, 73.77, 79.29 nm) with increase of oxidation time (30, 60, 90 min) respectively. XRD pattern confirm the formation of polycrystalline films with preferential orientation along (111, 222) planes and the intensity of the CdO peak of increase with the increasing in the time.

Keywords: CdO thin film, nanostructure, PVD method, oxidation time.

INTRODUCTION

The Oxides of a many metals such as Indium, Tin, Cadmium, Zinc and their alloys. It's used as TCO's possessing transparent conducting property. A studied of transparent conducting metal oxides are anion-deficient (i.e., Oxygen deficient) and it's always n-type conductor [1]. The transparent conducting metal oxides are indicate as oxide semiconductors also. CdO is a material with attractive properties such high transmission coefficient in the visible spectral domain, marked luminescence characteristics, large band gap etc. CdO bulk is n-type semiconductor broadband gap (2.3 eV) [2]. CdO has many applications such as flat panel display, solar cells, phototransistors, windows etc. [3 - 4]. Cadmium oxide thin films prepared by several techniques, spray pyrolysis [5], r.f. sputtering [6], solution growth [7] as chemical bath deposition [8], pulsed laser deposition (PLD) [9], The chemical vapor deposition [10], Sol-gel [11] and thermal evaporation [12], etc. (PVD) A physical vapor deposition permits to prepare small and large area metallic coating films. Also, A temperature for their moreover thermal oxidation is moderate to be easily applied of the thin-film, besides deposition technique, substrate temperature, and oxidation time are an important role in the quality of nanostructures. In this work, the CdO thin films prepared by thermal evaporation technique (pvd). this work present characterization properties of CdO films prepared by (pvd) a





Amenah Ali Salman

thermal evaporation method, such as structural, morphological and optical properties. A influence of oxidation time of films characteristic properties are investigated.

EXPERIMENTAL PART

The high purity cadmium metal deposited on a clean glass substrate by physical vapor deposition (PVD) at normal incidence $\theta = 0^\circ$ (θ represent the angle between the normal Of the substrate and direction of incidence of a evaporated atoms). Glass slides used were held at an angle to a direction of evaporation source, evaporation of cd film was carried out on a substrates at room temperature in the vacuum about (1×10^{-5}) torr from a molybdenum boat heater, which was clean, and located at a distance of 15 cm from the substrate. Then oxides in convention furnace type (Nabertherm) at 500°C for (30, 60, 90 min). After deposition, a surfaces of CdO samples characterized by using atomic force microscope (AFM) AA300 scanning probe microscope Angstrom Advanced Inc. The structure of the CdO is studied from X-ray diffraction (XRD) (SHIMADZU JAPAN, XRD – 6000) with Cu $K\alpha$ radiation ($\lambda = 1.542 \text{ \AA}$) was used. The optical testing of the film was investigated by using a double beam UV-Vis spectrophotometer (CECIL C.7200(France) and SHIMADZU) with respect to a piece of glass of the same kind of the substrate.

RESULTS AND DISCUSSION

The Structural Properties

XRD patterns of CdO thin films deposited on glass substrate at the different time of oxidation (30, 60, 90 min) as shown in figure 1 (a, b and c) respectively. It's clear from the figures, cubic phase formation as compared with the X-ray diffraction data file (standard) [JCPDS file No. 75-0594] [13]. A sharp and strong Bragg's peaks prepared in all the diffractogram confirms the polycrystalline nature of the CdO thin films at diffraction angles (2θ) of (33.27, 38.51, 55.5, 69.51) corresponded to the (111), (200), (202), (222) planes respectively. In addition, the intensity of the (111), (222) plane increases with increase in the oxidation time, while the intensity of the (200), (202) planes decreases with increase in the time. This shows an improvement in the structural properties observed which have the better degree of crystallinity as compared with the less oxidation time. The structure, properties such as (hkl) interplanar distance corresponding to XRD peaks and JCPDS card, grain size of deposited CdO films that obtained from the formula of Scherer's and from AFM listed in the table (1), it's clear from a table, the decreases in the value of grain size from 79.29 to 70.79 nm when oxidation time decreases from (90 to 30 min), this behavior leads to the large surface area to volume for CdO Nanostructure films and large energy conservation in detector and solar cell. This shows the structure enhancement in the less oxidation time at temperature 500°C .

Morphological properties

The morphology of CdO thin films at different oxidation time (30, 60, 90 min) is shown in figure 2 (a, b and c). Where high purity cd metal thermally evaporated at room temperature on clean glass substrates, then oxides in the air at 500°C for different oxidation time to produce CdO nanostructure. Figure 2(a, b and c) shows The surface morphology, and hence particles size distribution of the cadmium oxide thin film is prepared at three different oxidation time shows in Figure (3 a, b and c) As it is clear from Figure, the crystallinity of the samples has been improved by oxidation time. Furthermore, it's clearly seen that at low oxidation time the Mean size of nearly circular shaped grains is about 70 nm Figure (2a) smaller than That of 60 and 90 min Figure (2b and c). The size of the grains decreased as the Oxidation time decreases. This technique confirms the crystalline structure Improves in low oxidation time of films this is usefully in solar cell application

Optical properties

Absorbance spectra recorded for cdo films as a function of wavelength range 300-900 nm for various oxidation time as shown in Figure 4 (a, b and c). It's clear that the absorbance decreases with an increase of the wavelength and the





Amenah Ali Salman

absorbance decreases with the increase of the time oxidation. Oxidation with 30 min shows higher absorbance compare to 90min. The typical plots of $(\alpha h\nu)^2$ versus $(h\nu)$ for CdO for various oxidation time on a glass substrate as shown in Figure 5(a,b and c). The value of the optical E_g decreases from 2.2 eV to 1.9 eV with increasing time to all samples and that may be due to the increased grain size and a decrease in defect states near a bands and this, in turn, decreased value of E_g . The results are in agreement with a theoretical calculations of a band structure and agree within ± 0.1 eV with a previous values, calculated for a films that prepared from other methods [14-15].

CONCLUSION

Polycrystalline CdO thin films with peak intensity corresponding the cubic phase at (111),(200) and (202) plans was obtained successfully via oxidation process at different time. The intensity of the (111),(222) plane increases with increasing in the oxidation time, while the intensity of the (200),(202) planes decreases with increasing in the time. From optical results reveals a decreased in the band gap value with oxidation time this was reflect on the grain size of CdO nanoparticles which found to increase with oxidation time.

REFERENCES

1. Andrease Stadler, "Transparent Conducting Oxides-An Up-To-Date Overview, Materials, 5,661-683,2012.
2. K. Gurumurugan, D. Mangalaraj, And Sa. K. Narayandass, "Structural Characterization Of Cadmium Oxide Thin Films Deposited By Spray Pyrolysis," J. Cryst. Growth 147, 355 (1995).
3. Zheo Z, Morel D.L., Ferekides C.S., "Electrical And Optical Properties Of Tin-Doped Cdo Films Deposited By Atmospheric Metalorganic Chemical Vapor Deposition" Thin, Solid Films, 413(1-2), Pp 203-211, 2002.
4. Su L.M., Grote N, Schmitt F, Electron Lett; 20,(18),716-7,1984.
5. R.L.Mishra, A.K.Sharma, S.G.Prakash, "Gas Sensitivity And Characterization Of Cadmium Oxide Semiconducting Thin Film Deposited By Spray Pyrolysis Technique", Digest Journal Of Nanomaterials And Biostructures, 4(3), Pp 511-518, 2009.
6. Kannianen, T. S.Lindroos, J.Ihanus, M.Leskela, "Growth Of Lead Selenide Thin Films By Successive Ionic Layer Reaction And Reaction (SILAR) Technique", J.Mater.Chem.6, Pp161, 1996.
7. K.Gurumurugan, D.Mangalraj And S.K.Narayanandas, "Correlations Between The Optical And Electrical Properties Of Cdo Thin Films Deposited By Spray Pyrolysis" Thin Solid Films, 251, 7 1994.
8. Al-Ogili, H. K. J. "Effect Of Thickness To The Structure Properties Of Cdo Thin Films" Eng. & Tech. Journal 29, 2011, 1536.
9. Yahya, K. Z. & M. Adel "Influence Of Substrate Temperature On Structure And Optical Properties Of Cdo Thin Films Prepared By Pulsed Laser Deposition" Eng. & Tech. Journal, 30, 2012, 416.
10. Young, X. Li, D. L.H. Moutinho, Y. Yan, C. Narayanswamy, T. A. Gessert & T. J. Coutts "Properties Of Cdo Thin Films Produced By Chemical Vapor Deposition" Electrochem. Solid-State Lett. 4, 2001, C43.
11. Ilcan, S. M. Caglar, Y. Caglar, & F. Yakuphanoglu, "Cdo:Al Films Deposited By Sol-Gel Process: A Study On Their Structural And Optical Properties", Opto. Adv. Material-Rapid Commun., 3, 2009, 135.
12. Dakhel, A. A. & F. Z. Henari, "Optical Characterization Of Thermally Evaporated Thin Cdo Films", Cryst. Res. Tech. 38, 2003, 979. JCPDS "Powder Diffraction File" No. 96-101-1052.
13. K.C. Lalithambika*, K. Shanthakumari And S. Sriram, "Optical Properties Of Cdo Thin Films Deposited By Chemical Bath Method", International Journal Of Chemtech Research, Vol.6, No.5, Pp 3071-3077, Aug-Sept 2014.
14. K.C. Lalithambika*, K. Shanthakumari and S. Sriram. "Optical Properties of CdO Thin films Deposited by Chemical Bath Method", International Journal of Chemtech Research, Vol.6 No.5 Pp 3071-3077, Aug-Sep 2014
15. Waffa K. Khalef, Hasan Hadi Hussein, Amna A. Salman, Uday Mushin Nayef, " Morphology, chemical and electrical properties of CdO Nanoparticles on porous silicon". Iraqi Journal of Physics, Vol 11 No.21, PP.22-107, 2013.





Amenah Ali Salman

Table 1 : Comparison between experimental and standard dhkl, grain size (nm) of CdO thin films.

Oxidation temperature (C)	Oxidation Time(min.)	2θ Exp. (degree)	(hkl)	d _{hkl} STd. (Ao)	d _{hkl} Exp. (Ao)	Average grain size (D)nm from AFM	Average grain size (D)nm From Scherer's formula	Eg(ev)
500	30	33.27	111	2.711	2.69	70.79	15.98	2.2
		69.51	222	1.331	1.35			
	60	33.25	111	2.711	2.69	73.77	18.46	2.1
		69.33	222	1.331	1.35			
	90	33.28	111	2.711	2.68	79.29	27.45	1.9
		69.53	222	1.331	1.35			

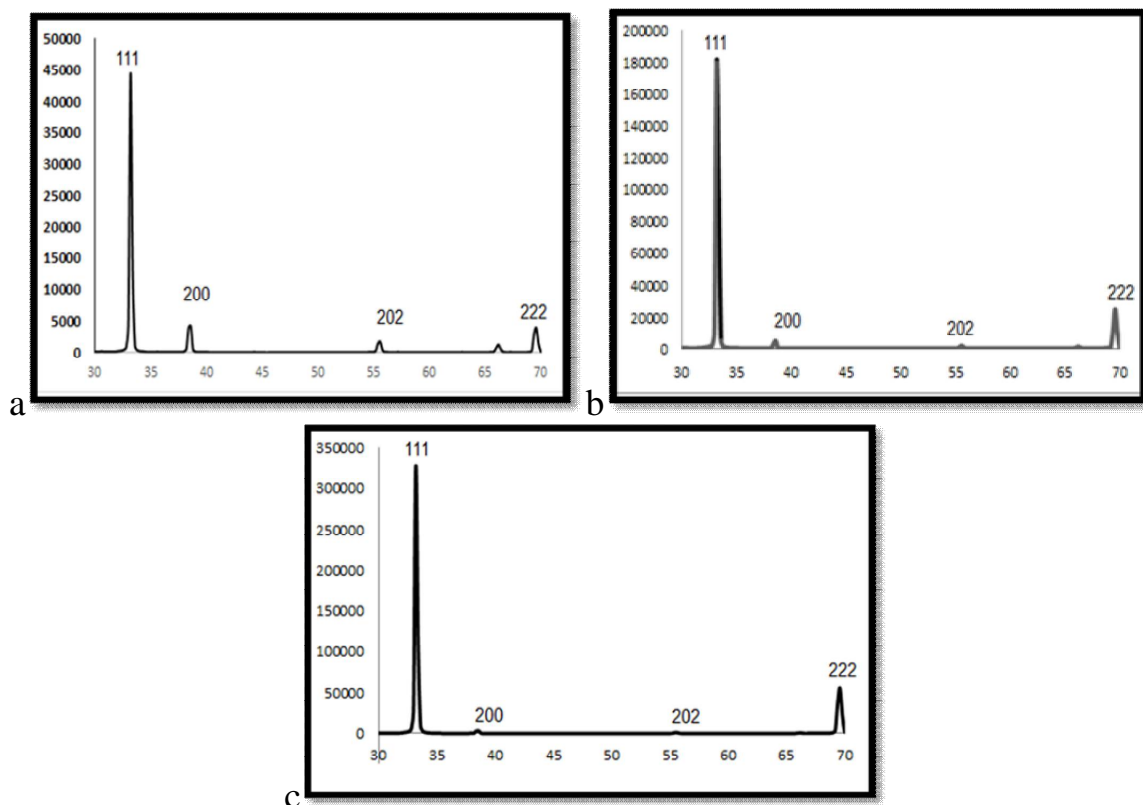


Fig.1:XRD patterns of CdO films deposited byPVD method at different time of oxidation a)30, b)60,c)90min.





Amenah Ali Salman

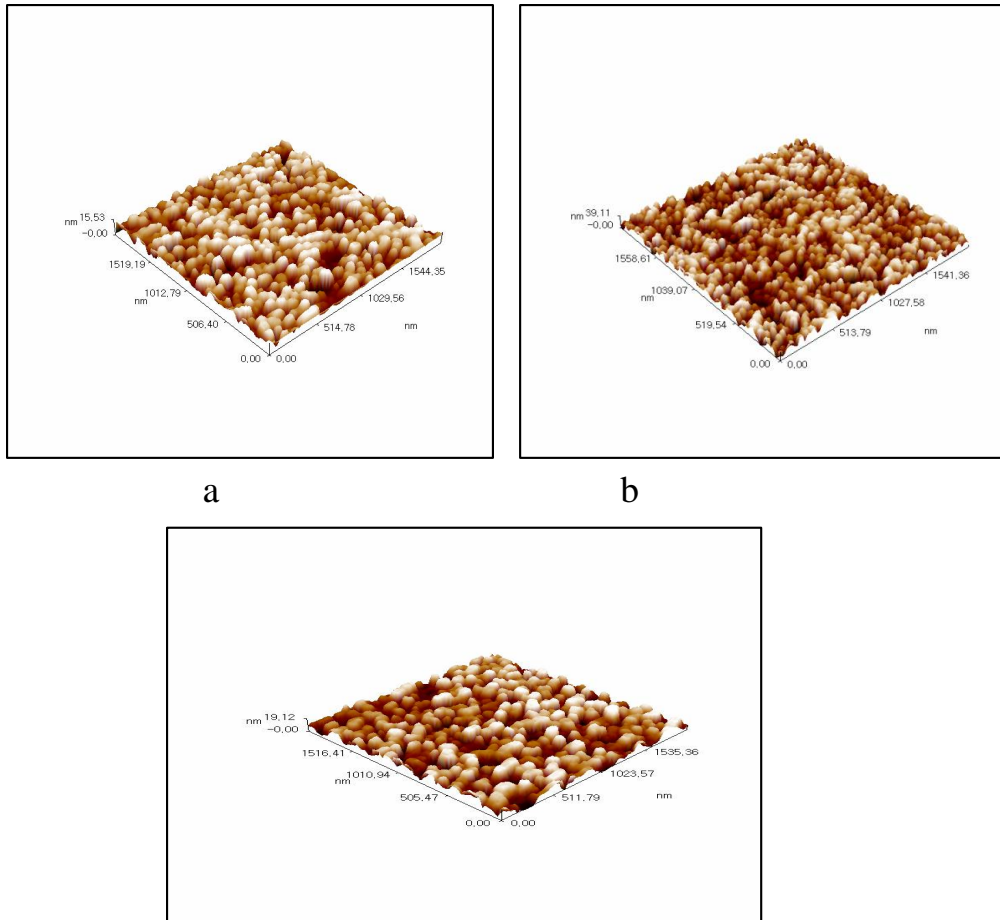
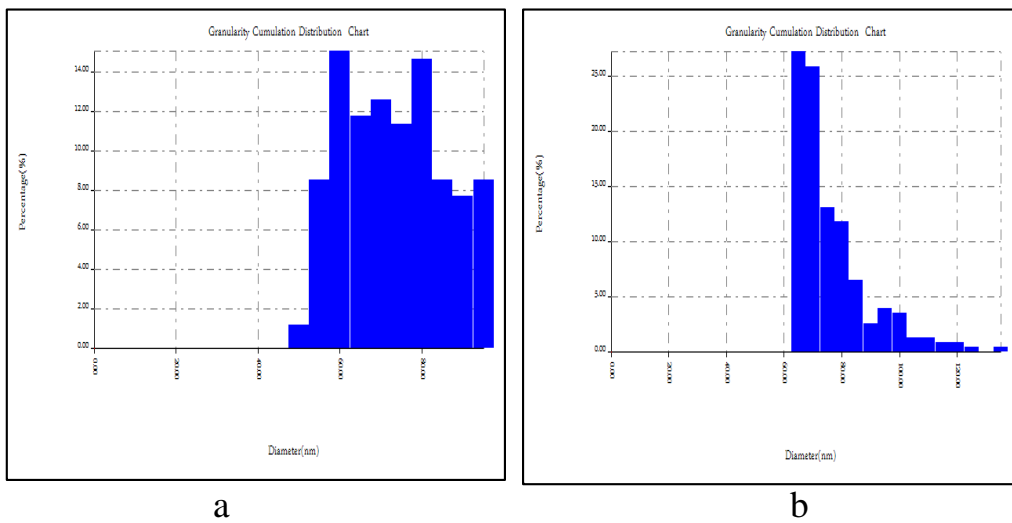
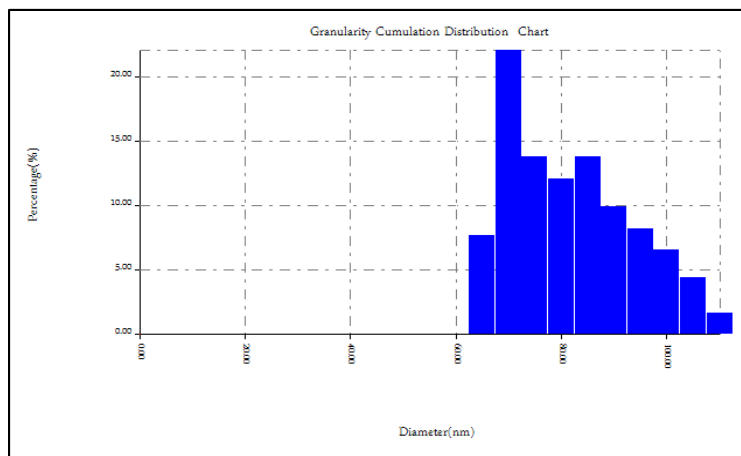


Figure 2 : AFM image of cdo thin film 3DAFM image .a)30,b)60,c)90 min





Amenah Ali Salman



C

Fig.3. The particles size distribution histograms for cdo thin film.a)30,b)60,c)90min.

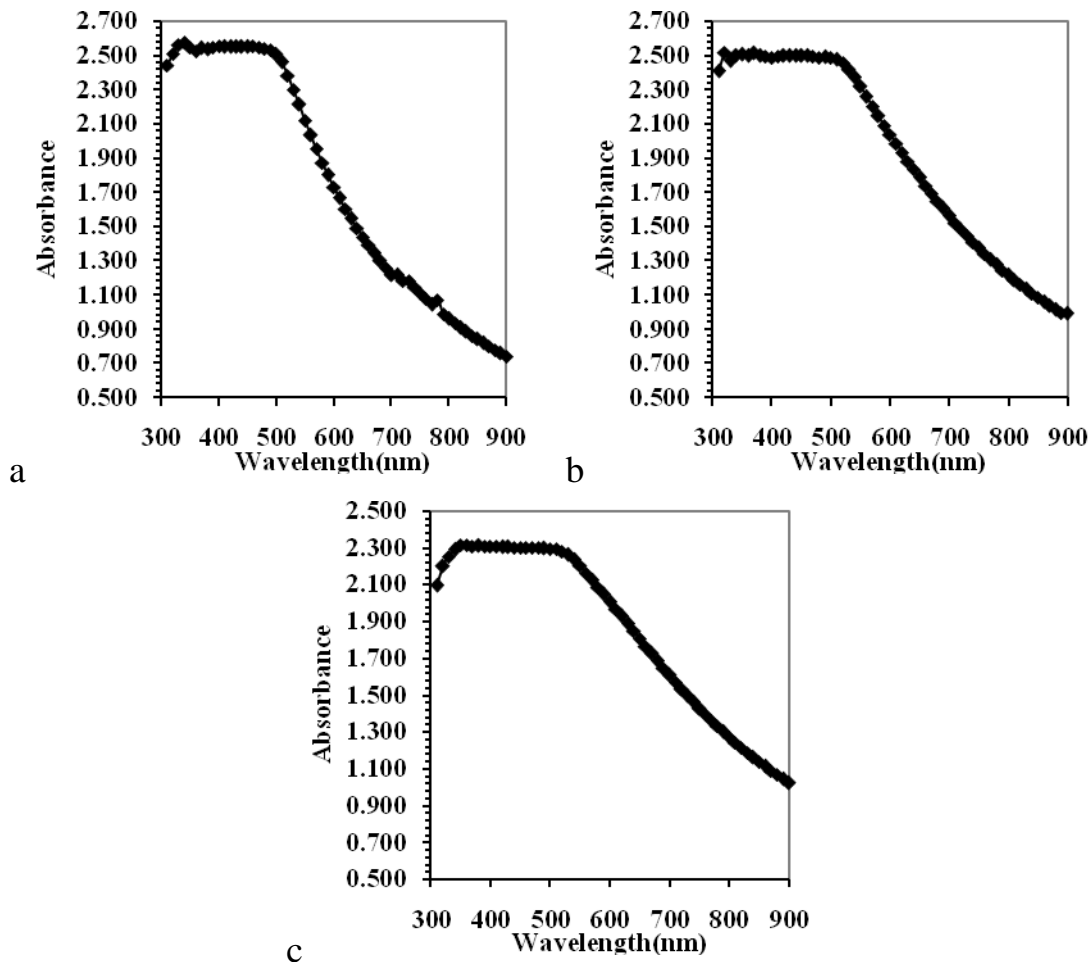


Figure 4 : absorption spectrum for CdO thin film prepared by by PVD Method .a).30min,b)60 min,c)90min.





Amenah Ali Salman

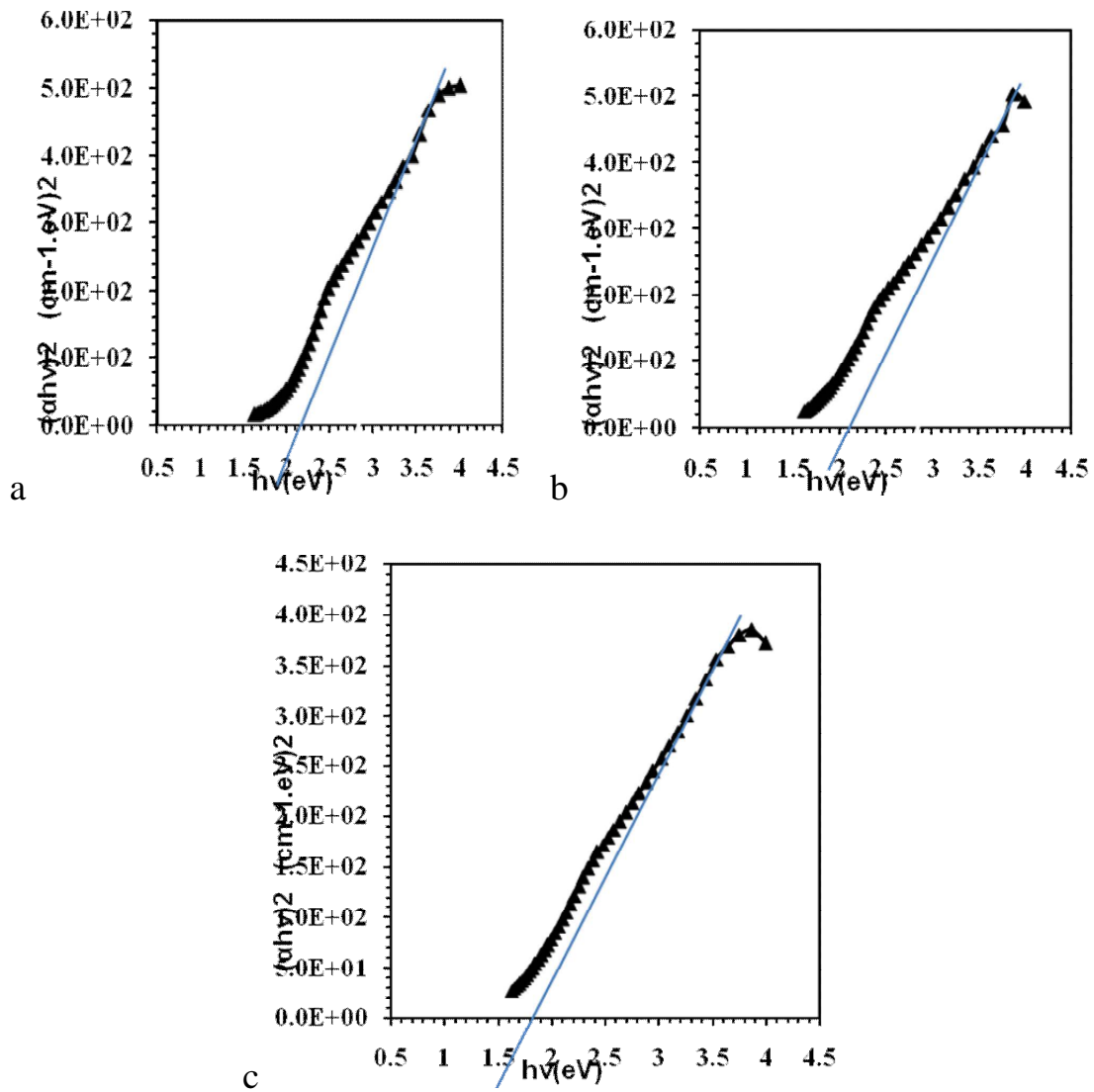


Figure 5: Energy gap of cdo thin film prepared by bypvdMethod.a)30.b)60.c)90min





RESEARCH ARTICLE

Morphometric Analysis of Talha River Basin East of Iraq Using Remote Sensing and GIS Techniques

Mutasim Ibrahim Malik *

Department of Physics , College of Science, University of Wasit, Iraq

Received: 11 July 2018

Revised: 14 Aug 2018

Accepted: 17 Sep 2018

*Address for Correspondence

Mutasim Ibrahim Malik

Department of Physics ,
College of Science,
University of Wasit, Iraq.



This is an Open Access Journal / article distributed under the terms of the **Creative Commons Attribution License** (CC BY-NC-ND 3.0) which permits unrestricted use, distribution, and reproduction in any medium, provided the original work is properly cited. All rights reserved.

ABSTRACT

The aim of this study is to reveal the capability of remote sensing techniques and geographic information system (GIS) to analyzing the morphometric properties of Talha River Basin. The digital elevation model (DEM) were used to draw the drainage pattern of the studied area. The study shows that the drainage pattern was dendritic of five orders and the relation between orders of streams and the numbers of streams was inversely. The morphometric properties shows the faraway from circular shape and the closeness from rectangular shape of Talha River Basin that means the danger of floods is small. The basin texture of Talha River Basin is (1.38 v/km) and that regarded as rough basin texture.

Key words: Talha River Basin, Morphometric Analysis, Remote sensing, GIS, DEM.

INTRODUCTION

Remote sensing techniques and geographic information system (GIS) techniques regarded as a one of the strongest modern techniques in extracting the morphometric properties throughout the capability in determining the shapes, dimensions, and gradients of the earth surface [1]. The study of morphometric properties represent one of the modern directions to study the basins. The morphometric properties are directly related to the natural factors such as water resources for the basins [2]. The morphometric studies help in determining the shape of basins and the earth appearances that developed according to the shape of the basin so that the river drainage basin is the essential unit to make the quantified researches [3]. The geographic and geomorphic characteristics of a drainage basin are important for study the hydrological status involving the assessment of groundwater potential, watershed controlling and environmental assessment [4]. "The morphodynamic calculations" of drainage data gives good amounts clarifications of basin geometry used to reveal the geological and geomorphic history of each drainage basin. This imposes the analysis of diversity drainage parameters such as ordering of various streams, measurement of drainage area and perimeter, length of drainage channels, drainage density (Dd), stream frequency (Fs), bifurcation ratio (Rb), texture





Mutasim Ibrahim Malik

ratio (T_R), Lemniscate Factor (K) and Channel Maintenance Constant (C) to predict the approximate behavior of the watersheds during periods of heavy rainfall [5]. The present study area is drained for a variety of agricultural fields, industrial purposes and also major source for the water supply to Marshes and groundwater.

Describing Studied Area

The studied area is a basin contains a river named Talha River Basin. The basin rises from the Iranian lands and flow in the direction of Iraqi lands and pour in Tigris River. The basin located between latitudes ($33^{\circ}50'$, $32^{\circ}55'$) and longitudes ($46^{\circ}22'$, $46^{\circ}18'$) as shown in figure (1).

Geology of Basin

The geology of the study area indicates various litho units dating from Oligocene to Recent. The studied area is mostly dominated by dolomite, limestone, sandstone, silt, red and gray marls, gypsum, anhydrite and recent alluvial. The formations cropping out in the study area are, Euphrates formation, Fatha formation, Injana formation, and Mukdadiya formation [6].

Data & Software Used

- 1- Digital Elevation Model (DEM) of (30 m) resolution.
- 2- Satellite Image for The Region.
- 3- ArcGIS software (10.2.2).

Extraction of Basin Boundaries

It is needed to extract a DEM cover the basin to use it in drawing the drainage pattern. Firstly, a DEM were prepared and a polygon cover the basin were sketched to use it as a mask as shown in figure (2).

The polygon and the DEM were used as an inputs for the tool Extract by Mask in ArcGIS software. The result of extraction is illustrated in figure (3).

Morphometric properties of the basin

Morphometric properties defined as the geometrical properties of the basin which include the area and the distances related to the basin and its tributaries. These measurements regarded as essential variables for the morphometric relations.

Dimensions of studied basin

Basin perimeter denoted by (P), it is measured in (Km). It is regarded as one of the essential morphometric variables because it is related to many morphometric properties [7]. The perimeter of the basin can be found by using Spatial Analysis tool in ArcGIS software and depending on DEM, so it is found that the perimeter of the basin is 341.19Km. The area of the basin is measured in square kilometers and it is denoted by (A). The area of the basin is 21448Km². Also the width can be measured by determining the maximum width of the basin and compared it with maximum length of drainages basins. It is also can be measured using equation (1) [8].

$$Bw = \frac{A(Km^2)}{L(Km)} \quad (1)$$





Mutasim Ibrahim Malik

Where:

Bw: width of the basin.

A: area of the basin.

L: length of the basin.

By applying equation (1) it is found that the width of studied basin is 167.64 Km.

The length of the basin denoted by (L) and it is measured in (Km). It can be calculated by using the morphometric relation (equation (2)) [9].

$$L = \frac{A(Km^2)}{Bw(Km)} \quad (2)$$

Where:

L: length of the basin.

A: area of the basin.

Bw: width of the basin.

By applying equation (2) it is found that the length of the basin is 127.94 Km. Table 1 shows all previous parameters.

Form factor Ratio

Quantitative expression of drainage basin outline form was made by [10] through a form factor ratio (F) and it's measured by dividing the area of the basin by square of basin length as in equation (3) [10].

$$F = \frac{A(Km^2)}{L^2(Km)} \quad (3)$$

Where:

F: form factor (dimensionless).

A: area of the basin.

L: length of the basin.

It is clear that the form factor is related to the length and area of the basin and that imply the format range between basin parts and regularity of its shape. The high value of the form factor reflect the closeness of basin shape from square or nearly spherical shape which mean quickly of transforming rainfall to floods, while low value of form factor closeness of basin shape from triangle shape. The form factor of Talha river basin is (1.31) which imply the expansion of the basin in source and tight in estuary which poses increasing the danger of floods.

Basin circularity (Circularity ratio)

defined a dimensionless circularity ratio (Rc) and it's measured by dividing the area of the basin by area of circle has the same circumference of the basin as in equation (4) [11].

$$Rc = \frac{4\pi A}{P^2} \quad (4)$$

Where:

Rc: the Circularity ratio.





Mutasim Ibrahim Malik

A: the area of the basin.

P: the circumference of the basin.

The closeness of the circularity ratio from (2) mean the shape of the basin nearly circular and vice versa [12]. The circularity ratio of the basin is (2.3) which is small ratio and that reflect the estrangement of the basin form the circular shape.

Elongation ratio

Elongation ratio (E) is measured by dividing a diameter of circle area represents the area of the basin to maximum basin length. If the ratio is less than 1 the basin shape is close to the rectangular shape, while larger than 1 indicate to estrangement from rectangular shape and closeness from circular shape. The elongation ratio is given by equation (5) [13].

$$E = 2 \sqrt{\frac{A}{L}} \quad (5)$$

Where:

E: Elongation ratio.

A: area of the basin.

L: Maximum basin length.

The elongation ratio of the basin is (1.29) which indicate the elongation of the basin and that compatible with form and circular factors.

Lemniscates Factor

Lemniscates Factor is denoted by (K) and it is measured by dividing the square of basin length by 4 times the area of the basin as in equation (6) [14].

$$K = \frac{L^2}{4A} \quad (6)$$

Where:

K: lemniscate factor.

L: Maximum basin length.

A: Area of the basin.

Lemniscate factor indicate to the similarity between the shape of the basin and pear shape, because most of the basins tend to have pear-shaped rather than the completely circular shape [6]. The high values of this factor indicate the increasing in the elongation of the basin, while the low values indicate to the flattening of the basin which cause increasing in length and numbers of low order streams. Lemniscate factor of the basin was (0.19) and that mean the basin is closest to the elongation.

Compactness factor

It is another factor to emphasizing the estrangement of the basin from circular shape. As this factor estrangement from 1 the basin will be of more elongation [15]. The compactness factor is denoted by (C) and can be measured by equation (7).

$$C = \frac{P}{2\sqrt{M\pi}} \quad (7)$$





Mutasim Ibrahim Malik

Where:

C: compactness factor.

P: perimeter of the basin.

M: circumference of a circle has the same area of the basin.

The compactness factor of the basin is (0.66) and this value indicate to closeness of the basin shape from the elongation.

All previous factors of the basin are summarized in table 2.

Morphometric properties of water net

It is the properties of a set of tributaries and valleys that comprise drainage basin.

Drawing the drainage pattern

Drainage pattern can be drawn from digital elevation model (DEM) and by using ArcMap software as in figure (4) which illustrate the main steps for drawing drainage pattern [16].

In ArcMap software the hydrology tools were used to model the flow of water across a surface. When modeling the flow of water, we may want to know where the water came from and where it is going. After drawing the drainage pattern of the studied basin depending on Strahler method, it is observed that the basin has a dendritic drainage pattern of five orders as shown in figure (5).

Bifurcation Ratio

The term bifurcation ratio is denoted by (R_b), and it is given by equation (8) [10].

$$R_b = \frac{Nu}{Nu + 1} \quad (8)$$

Where:

R_b : Bifurcation Ratio.

Nu : number of streams for a certain order.

$Nu + 1$: the number of steams for order post Nu .

It is defined as the ratio between the numbers of streams for a certain order to the number of streams for an order follow the previous order [15]. The increasing of bifurcation ratio lead to increasing the dangerous of floods during high rainfall [17]. Table 4 summarize the bifurcation ratios for each order.

Streams Frequency

Stream frequency or channel frequency is denoted by (F_s). It is measured by dividing the sum of streams number by the area of the basin as in equation (9) [18].

$$F_s = \frac{\sum N_U}{A_U (Km^2)} \quad (9)$$

Where:

F_s : stream frequency.

Nu : Number of steams.





Mutasim Ibrahim Malik

Au: Area of the basin.

The high values of streams frequency indicate the existence of a large number of tributaries which increase the capability of grouping the water as surface runoff, while the low value of streams frequency indicate a small number of tributaries which decrease the chance of surface runoff and increase the infiltration of water to the underground water [19]. The streams frequency of studied area was (0.013) which regarded as relatively low value and that means decreasing of surface runoff.

Drainage Density

The study of land topography for the draining water regarded as one of the studies which illustrate the operation of diversity and changing from one region to another according to climate, weather, rock nature, and rock structure. the drainage density It is denoted by (Dd) and it's measured by using equation (10) [20].

$$Dd = \frac{\sum Lu}{Au} \quad (10)$$

Where:

Dd: drainage density.

Lu: sum of streams lengths.

Au: area of basin.

The drainage density indicates the breaks in region. The drainage density of the basin (0.069).

Channel Maintenance Constant

Channel Maintenance Constant is denoted by (C) and it's measured by equation (11) [21].

$$C = \frac{1}{Dd} = \frac{Au}{\sum Lu} \quad (11)$$

The channel maintenance constant of the basin is (14.29 Km), and that indicates there is no area of basin hasn't water net in the future.

Texture Ratio

Texture ratio (T_R) is an important factor in the drainage morphometric analysis which is depending on the underlying lithology, infiltration capacity and relief aspect of the terrain. and it is given by equation (12) [20].

$$T_R = \frac{Nu}{P} \quad (12)$$

Where:

Nu : Total number of order streams.

P : Perimeter of watershed

In the present study the texture ratio of the basin is (0.844 valley / Km) and categorized as bad land topography in nature [19].

RESULTS AND DISCUSSION

The mathematical morphometric equations had been applied in this study to obtain the values of morphometric variables as in (schematic features, net features and features of Al Talha Basin topography). Basin of Al Talha river ending in fifth class according to Strahler classification, the basin is one of the biggest basins, basin space about





Mutasim Ibrahim Malik

(21448km²) and in surroundings at (341.19 km), crosswise of the basin are (167.64 km) and lengthwise at (127.94 km). Basin consist of (288) sub-grades, starting from first grade and ending of fifth grade, where we found that the number of first grade riverbed is (142) grade, the number of second grade riverbed is (78) grade, the number of third grade riverbed is (45) grade, the number of fourth grade riverbed is (13) grade, finally fifth grade riverbed is one grade, so the totaling of all grades of the long riverbeds (1500.61 km) for all grades, mainly drainage patterns classified of arboreal to semi arboreal. Basin Properties contain of contrast or divergence of formalism, cadastral and morphologies properties and Drainage network properties, and network of drainage, the Morphometric properties of basin at Talha River Basin according to natural factors of basin. The shapes of the drainage generally were dendritic to semi-dendritic.

It is clear from the studying of the morphometric Analysis properties that the basin tend to the elongation more than the circular shape and that is proven from the circularity ratio (2.3) which indicates the estrangement from the circular shape. While the elongation ratio (1.29) indicates the elongation in basin, and that is proven from the other morphometric factors such as (compactness factor, lemniscate factor, and form factor). The Drainage Density of Talhab river basin reaches to (0.069 km/km²) and that mean for all (0.069 km) from the longest riverbeds of Drainage network of Talha River Basin taken a space about (1 km²).

The texture of the basin was (0.844 v/km) and for that it is considered as rough because it has (0.844) valleys per kilometre. After drawing the drainage pattern of studied basin it is clear from morphometric factors of water network that the basin has a lot of breaks which increase the number of tributaries and distribute of these tributaries randomly throughout the basin. From the studying of morphometric properties of the basin and water network it is clear that the basin in the dangerous of floods.

CONCLUSIONS AND RECOMMENDATIONS

Generally, this study aims to show the possibility of Remote Sensing and Geographic Information Systems Technics in analysing the Morphometric Changes of Talha River Basin. An advantage took from the different applications system to obtain the morphometric treatments to Talha Basin. This study neglect the ratio of generalization that affect the morphometric measurements in classical methods by using accurate data of a high local clarity degree represented by Digital Elevation Model instead of paper topographic maps. The Digital Elevation Model helped us in drawing the water drainage net accurately and clearly, that led to get results which was distinctive of accuracy than the results of morphometric analysis, and saved time and effort, The study concluded the following results: -

- 1) The maximum high level in Talha Basin River reached at (2016 m) above sea level, while the minimum high level of basin reaches at (6 m).
- 2) the formalism properties of Talha River Basin (Form factor, Circular factor, Elongation ratio, Lemniscate Factor and Compactness factor) are refer to the basin living outside of circular form and closing to rectangular form , so that mean the risks of floods happened are in a small percentage happen , and the line of water network of basin are irregular extension , but in zigzag form and clearly.
- 3) This study will help the locals to use water resources for a constant growth in the area of drainage basin, and to know the amounts of water drainage and deposits that held by side streams of the basin and deposit as economical deposits like soil (for agriculture) and quarries of sand and gravels (for building).

REFERENCES

- [1] A. K. Al-khafaji, "Using Digital Elevation Model (DEM) and it's applications in morphometric analysis for the upper part of Tigris River basin northern west of Iraq", Diyala Journal For Pure Sciences, Vol: 9 No: 1, ISSN: 2222-8373, pp. 20-39, 2013.





Mutasim Ibrahim Malik

[2] H. A. Hamed, "Morphometric Parameters study for the lower part of lesser zap using GIS technique", Diyala Journal For Pure Scinces, Vol: 7, No: 2, ISSN: 2222-8373, pp. 127-157, 2010.

[3] T. S. Mohamed "geomorphological analysis of the morphometric characteristics of the top part of the basin and the Valley Alrmedin and Tkala River Basin," Journal of Human Sciences, University of Bahrain, No. 20, pp. 238, 2011.

[4] N.S. Magesh, N. Chandrasekar, "Morphometric evaluation of, Papanasam and Manimuthar watersheds", parts of Western Ghats,Tirunelveli district, Tamil Nadu, India: a GIS approach, 2010.

[5] R. Kumar, S. Kumar, Lohani AK, Nema RK, Singh RD., "Evaluation of geomorphological characteristics of a catchment using GIS". GIS India9(3):13–17, 2000.

[6] T. Budy, S. Jassim, "The regional geology of Iraq. Vol. 1, stratigraphy and paleogeography".I.I.M., Kassab and S.Z. Jassim (ed) SOM. Baghdad.45p, 1980.

[7] J.C. Doornkamap, C. A. King, "Numerical Analysis in Geomorphology – Introduction" ; London , pp.1-112, 1971.

[8] D. Thomas, M. Benson, "Generalization of Steam flow Characteristics From Drainage Basin Characteristics" Geological Server Water Supply , Library of Congress catalog - card No. 77, pp.1-55, 1970.

[9] K. J. Gregory, D. E. Walling, "Drainage Basin Form and Process: A geomorphological Approach"; Edward Arnold Ltd. London , p49, 1973.

[10] R. E. Horton, "Drainage Basin Characteristics"; Trasn, Amer, Geophysics, Union 13, p350-361, 1932.

[11] K. Parata, U. Pareta, "Quantitative Geomorphological Analysis of a Watershed of Ravi River Basin", H.P. India, International Journal of Remote Sensing GIS, 1, I(1) , p 47-62, 2012.

[12] H. Alan Strahler, "Introducing Physical Geography", 6th Edition, John Wiley & Sons, Inc. p 234-341, 2015.

[13] S. A. Schumm, "The evaluation of drainge systems and Slopes in badlands at Perth Amboy", New Jersey; Bull. Geol. Soc. Amer. vol 67, p597-646, 1956.

[14] R. J. Chorley, D. E. Malm, H. A. Pogorzelski, "A New Standard for Estimating Basin Shape"; Amer. Journ. Sci. 255, p138-141, 1957.

[15] K. Pareta, U. Pareta, "Hydro morphological Study of Karawan Watershed Using GIS and Remote Sensing Techninques", E-International Scientific Research Journal, III.I, (4): P243-268, 2011.

[16] R. Salman, "Determining the Optimum Site of Small Dams Using Remote Sensing Techniques and GIS," International Journal of Scientific Engineering and Research, vol. 3 Issue 9, pp. 69-73, 2015.

[17] F.E. Hammad, M. Ghazwi, E. Korany. A. Shabana, "Morphometric Analysis and water Resources Development in El Quseima Area Northern Sinai". Egypt J. Geol. Vol .38 , No.2. P 597-612, 1994.

[18] V. T. Chow, "Handbook of Applied Hydrology"; a Compendium of water-resources technology, McGraw-Hill Book Compagny, New York, pp. 132, 1957.

[19] K. J. Gregory, D. E. Walling, "Drainage Basin form and process Geomorphological Approach", Edward Arnold. London, pp.458, 1994.

[20] R. H. John, "Applied Geomorphology", Amsterdam- Oxford New York, pp.120, 1995.

[21] R. E. Harton, , "Erosional Development of Streams and their Basins": Hydro physical approach to quantitative morphology, Geological Society of America Bull 56: p283, 1945.

Table 1: All dimensions of studied basin.

Basin	Perimeter (Km)	Area (Km ²)	Length (Km)	Width (Km)
Talha	341.19	21448	127.94	167.64





Mutasim Ibrahim Malik

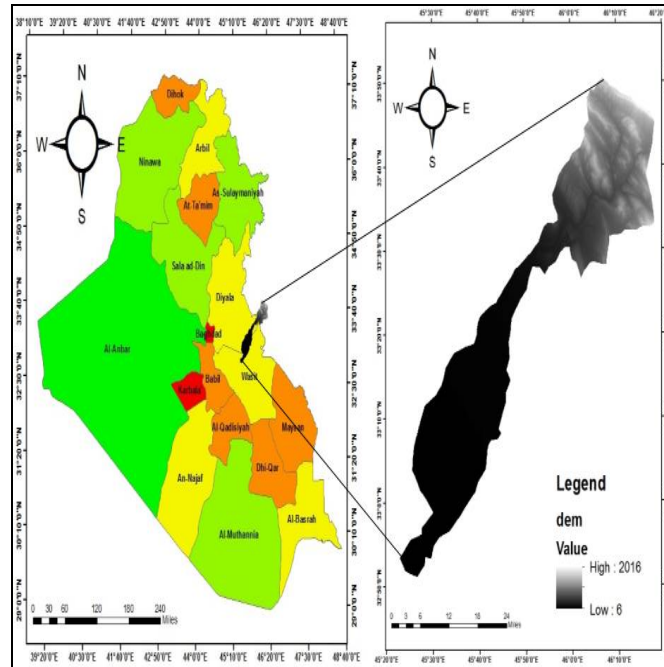


Figure 1: Location of studies area.

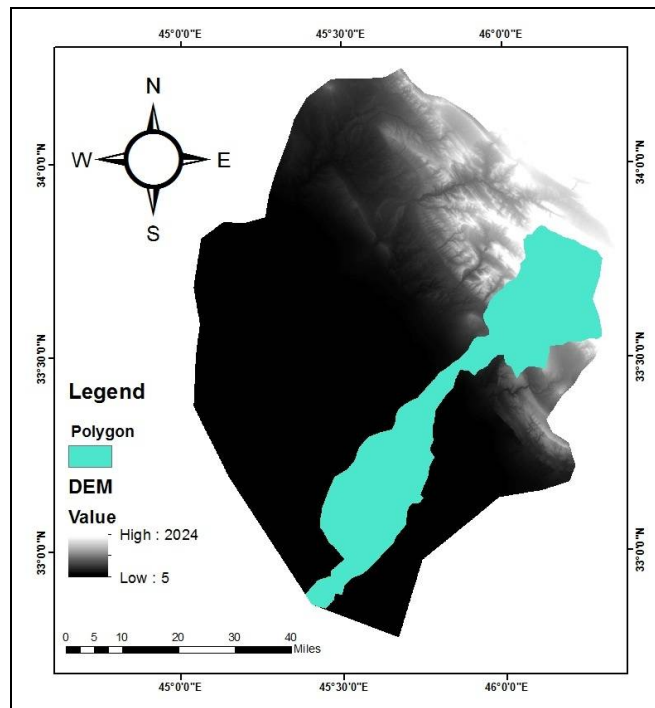


Figure 2: DEM & a polygon represent the basin.





Mutasim Ibrahim Malik

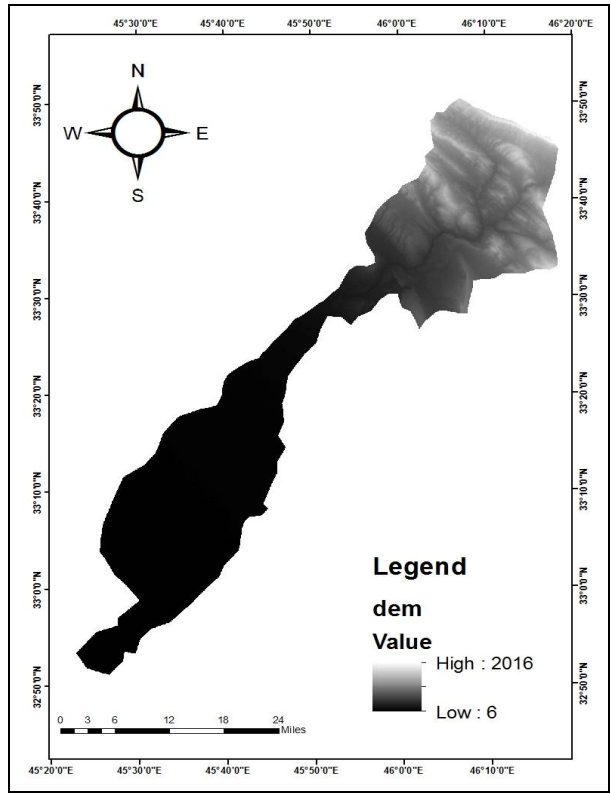


Figure 3: DEM for studied basin.

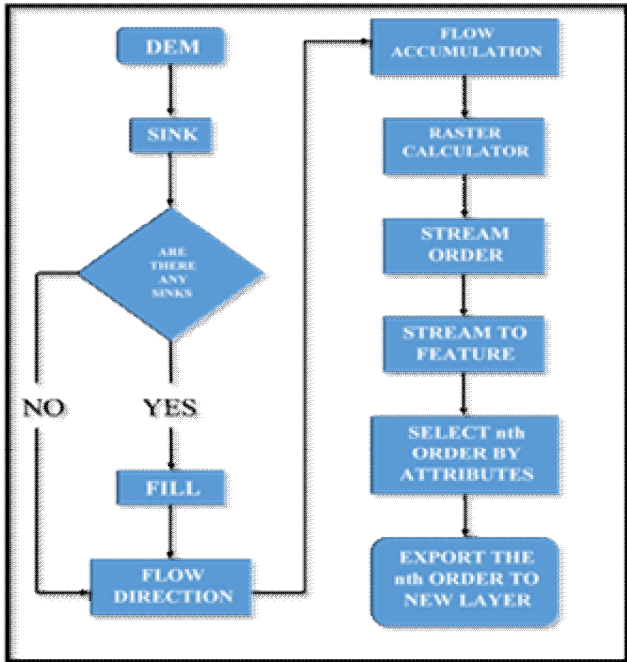


Figure 4: The main steps for drawing drainage pattern.





Mutasim Ibrahim Malik

Table 2: Morphometric factors of studied basin.

Form factor	Circular factor	Elongation ratio	Lemniscate Factor	Compactness factor
1.31	2.3	1.29	0.19	0.66

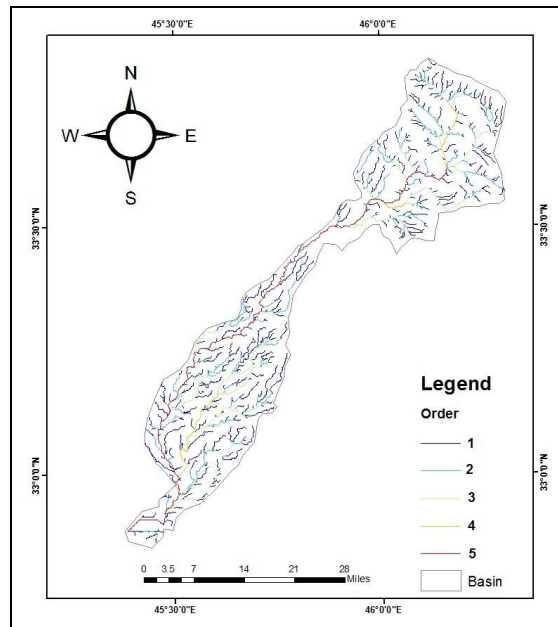


Figure 5: Orders of streams.

Table 3: Numbers of streams

Order	1 st	2 nd	3 rd	4 th	5 th	Aggregate
Number	142	78	45	13	1	288
Percentage%	49.3	27.08	15.6	4.51	0.34	100
Length (km)	775.14	306.8	211.5	54.72	152.45	1500.61
Percentage %	51.6	20.4	14.09	3.6	10.15	100

Table 4: Bifurcation Ratio for each order

Order	1 st	2 nd	3 rd	4 th	5 th	Aggregate	Average
Rb	---	2.35	1.34	3.60	0.41	17.07	7.79





Synthesis Co-Zn Ferrite at 6 Hour via Hydrothermal and Study the Antibacterial Effect

Nada Suheel Ahmade¹*and FalahA-H Mutlak²

¹Teacher, College of Science Physics, University of Diyala, Iraq.

²Assistant Professor, College of Science Physics, University of Bagdad, Iraq.

Received: 10 July 2018

Revised: 15 Aug 2018

Accepted: 19 Sep 2018

*Address for correspondence

Nada Suheel Ahmade

Teacher, Department of Physics,
College of Science, University of Diyala, Iraq.
Email: nada1982210@gmail.com



This is an Open Access Journal / article distributed under the terms of the **Creative Commons Attribution License** (CC BY-NC-ND 3.0) which permits unrestricted use, distribution, and reproduction in any medium, provided the original work is properly cited. All rights reserved.

ABSTRACT

Via the hydrothermal method, preparation the(Cobalt Zinc) ferrite powders and crystallite estimate, The imagein(FESEM) demonstrated that the greater part of the nanoparticles have molecule measure between (16-36)nm., attractive properties of integrated items are gotten by (VSM). All the incorporated ferrites are Nano crystalline single stage materials.Combined Co-Zn ferrites are portrayed by the immersion charge MS of 60-75 (emu/g), leftover polarization Mr of 02.- 0.5(emu/g) and coercivityHc of 300-900 (Oe) (Co-Zn) ferrite have effected on theBacteria *Escherichia coli* observed by inhibition zone increasing with increasing the concentration of ferrite .

Key words:- hydrothermal method, crystallite estimate, *Escherichia coli*.

INTRODUCTION

Soft magnetic materials is spinel ferrite particles, a kind of with structural formula of MFe_2O_4 (M = divalent metal ion, e.g. Mn, Mg, Zn, Ni, Co, Cu, etc.), duo to have interesting and important properties such as low melting point, high specific heating, large expansion coefficient, low saturation magnetic moment and low magnetic transition temperature, etc.[1,2].Hydrothermal synthesis ferrites with many advantages with respect to mechanicchemical methods [3]. or thermolysis in organic solvents,Truth be told, aqueous union empowers to limit time and vitality utilization and is practicable for scale-up with the demonstrated innovation of weight fixed reactors. Limiting response time and lessening/taking out sintering practices is the new test going for encourage diminishment of vitality utilization.[4] Besides, the most limited precipitation of solidified powders from arrangement guarantees consistency of nucleation, development, and aging[5].



**Nada Suheel Ahmade and FalahA-H Mutlak**

(Hydrothermal) method enhances the control of morphology and size of crystallites, diminishing conglomeration and deciding a fine particles dispersion [6]. In specific, the utilization of surfactants can permit the control of morphology and size of nanoparticles entirely relying upon the particular concoction sythesis of the response medium [7]. The properties of nano_materials meander from it morphology, molecule measure and microstructure and it is vital to examine strategies for blend of nanoparticles, and also acquire new metallic oxides with new properties. Materials as nanowires, nano_sheets, and so forth., are particularly critical, as a result of their better optical, electronic and attractive properties permitting to broaden application limits [8].

Ferrites with spinel structure are critical materials being developed of a few innovative applications, where materials with awesome thickness and low porosity are important [9]. (Ferrites), as the majority of clay materials, are gotten in strong stage responses from divergent oxides. By enhancing nanotechnology, a few fluid stage and gas stage blend strategies have been produced – hydrolysis, aqueous union [10], pyrolysis, microwave amalgamation [1], (co-precipitation) technique [11], sol-gel strategy [12], ignition [13]. One of the procedures in amalgamation of materials is aqueous oxidation. The strategy depends on the reality on the numerous oxides are dissolvable in a soluble base arrangement. The strategy has been most very much connected to get ready ferrites. The preferred standpoint in the aqueous technique is that it allows the recrystallization of the powder. It is likewise conceivable to screen the grain size and shapes. Anyway this technique is time overwhelming [14].

MATERIALS AND METHODS

Cobalt- Zinc ferrite nanoparticles was preparation by hydrothermal. Stage one by (co-precipitation) technique cobalt-zinc ferrites were combined with (hydrothermal) method: $\text{Fe}(\text{NO}_3)_3 \cdot 9\text{H}_2\text{O}$, $\text{Co}(\text{NO}_3)_2 \cdot 6\text{H}_2\text{O}$, $\text{Zn}(\text{NO}_3)_2 \cdot 6\text{H}_2\text{O}$, this material were blending and afterward add NaOH to blending material is gradually accelerated until the point that pH of the suspension is of 11 the cooler is darker hasten was then centrifuged and washed with distilled water. A Finally the got arrangement was stayed at 80 °C and its shading goes from dark colored to black. two step is Put the got blend of hydroxides was dealt with hydrothermally at various administrations ($T = 200^\circ\text{C}$, $t = 6 \text{ h}$,). After (hydrothermal) treatment the framed (precipitate) is, washed via (distilled water) and dried at 100 °C.

Bacterial inspect

Movement of bacterial for the (cobalt-zinc) ferrite nanoparticles is attempted on Gram negative Bacteria *Escherichia coli* E. coli by (Well dissemination strategy) with three unique focuses (200, 400, 600 mg/mL) which is discrete in the Distal Water dissolvable for the simple dispersion into the Agar. Each Well is stacked with arranged example arrangement. The plates are brooded at 37 °C for 24 hours. After this period zone of restraint is watched.

Bacterial examine

The bacterial test is completed by well dispersion technique against (cobalt-zin) ferrite nanoparticles. Bacterial measure requested that cobalt-zinc ferrite nanoparticles hindered the and gram negative microorganisms. The unadulterated societies are exchanged to sterile tryptone soup, which is hatched medium-term at 37 °C. The stock culture is utilized for advance assurance of Minimum Inhibition Concentration (MIC). The way of life are swabbed on the sterile Muller Hinton (MH) agar plates with four wells made by sterile stopper borer. The plates are hatched to watch the unmistakable zone of hindrance around the wells. The zone of restraint for bacterial societies is estimated utilizing the equation given beneath [14].





Nada Suheel Ahmade and FalahA-H Mutlak

RESULTS

XRD estimations are performed for the auxiliary portrayal of the incorporated nanoparticles. XRD investigation are performed with Cu K α illumination ($\lambda=1.5418 \text{ \AA}$) in the 2θ range (10– 80°). The crystallite size of the (CoFe₂O₄) NPs depends on X-beam diffraction line expanding and ascertained by utilizing Scherrer's condition [9].

$$D = B\lambda / \beta \cos \theta \quad (15)$$

where D is the normal crystallite size of the stage under scrutiny, B is the Scherrer's steady (0.89), λ is the wave length of X-beam pillar utilized, β is the full-width half most extreme of diffraction pinnacle and θ is the Bragg's angle. the cross section parameter "an" is ascertained by the formula:[9].

$$a = dhkl (h^2 + k^2 + l^2)^{1/2} \quad (16)$$

the XRD designs given in Fig. 2, thin and sharp reflection tops are seen in the deliberate co-precipitation innovation, joined with the aqueous most huge beneficial outcome on the gem structure [9]. The diffraction examples of (CoZnFe₂O₄) comprised of pinnacles relating to crystallographic planes (220), (311), (400), (422), (511) and (440). All the watched pinnacles and Miller files (hkl) of the fcc grid are in concurrence with the revealed values[10]. The crystallite size of the examples arranged by various techniques was in the scope of (20-33) nm. The distinction in the crystallite measure is because of various planning conditions for ferrite synthesis[2]. The grid parameter of as-arranged examples, as per the cubic precious stone structure figured from the primary pinnacle of spinel structure (311) utilizing condition (2). The substituted zinc particles in cobalt ferrite prompted vast increment in the cross section steady, after this esteem the cross section parameter have little increment in the qualities. while crystallite measure diminish with zinc particles this allude to the zinc particles supplanted with cobalt particles which might be credited to the littler ionic radii of Zn²⁺ particles (0.6 \AA) when contrasted with co²⁺ (0.79 \AA) cations[11].

VSM estimations

The polarization of the present examples is acquired by utilizing VSM at R.T. with a connected field ± 10 kOe. The watched hysteresis circles from VSM are appeared in Fig. (7,8,9,10). The attractive properties of the readied tests are examined by utilizing a magnetometer (VSM) at room temperature. Fig (7,8,9,10) demonstrates the M-H bends of the readied tests. The circle is restricted which implies the papered tests are delicate attractive material. The immersion charge (Ms) and coercivity (HC) values have been straightforwardly removed from these bends as in embed of figures, and have been recorded in different Co. the immersion charge and coercivity increment with Co content. The conduct of the immersion charge can be clarified on account of cations appropriation and super-trade associations. The immersion polarization increments by expanding the crystallite estimate with a most extreme estimation of Ms = 75.245emu/gm by co-precipitation innovation, joined with the aqueous and after that decline with additionally increment in the crystallite measure. The coercivity change with (D). Then again, to clarify the effect of lessening area, squareness proportion Mr/Ms is processed 0.2-0.4, 0.5. Estimations of squareness proportion fluctuate somewhere in the range of 0.2 and 0.5. At the point when the proportion amongst remanence and immersion charge under (0.5) the materials have single area, yet in the event that the proportion bigger than (0.5) the materials have multi space blend [19,20], Mr/Ms proportion showed underneath the range that is implied the examples have single area structures.[21]

FESEM estimations

Fig (10) demonstrates the FESEM pictures. Note that the normal grain size of the example got from FESEM pictures is bigger than nanocrystals estimate which dictated by the XRD estimation, which is essentially demonstrates to the agglomeration in the nanoparticles. The examples are circular, uniform and having a conveyance estimate (17-49).





Nada Suheel Ahmade and FalahA-H Mutlak

Bacteria inhibited

There are a few conceivable instruments for the antibacterial activity to ferrite nanopowders. It has been proposed that ferrite nanopowders tie to the films of microorganisms, like mammalian cells, drawing out the slack period of the development cycle and expanding the age time of the life forms with the goal that it requires every living being greater investment to finish cell division [19]. In the Fig.(4) the primary reason is that the murdering rate is personally connected with the surface zone of nanopowders scattered into the E.coli suspension media. The second impact may emerge from the basic attributes of the co-zn ferrite nanopowders. The infiltration rate in the fig(5) of a functioning oxide through the microscopic organisms cell divider may have an influence in the murdering rate of ferrite nanopowders against microbes [20].

CONCLUSION

Hydrothermal synthesis method is wonderful to produce Single phase cobalt ferrite nano-powders. Crystalline size of the nano-powders obtained via hydrothermal method is in the range of (17-49)nm. (VSM) is the magnetic saturation values of these samples depend on method of preparation and oven temperature and (time) and reach up to 60-75 (emu/g). (Co-Zn) possesses very high effect on bacteria due to the nano-particle size.

REFERENCES

- [1] A. Rabenau, "The Role Hydrothermal Synthesis in Preparative Chemistry", *Angew. Chem., Int. Eng. Ed.*, 24, 1026-1040, 1985.
- [2] R.A. Laudise, *The Growth of Single Crystals*, (Prentice-Hall, Englewood Cliffs, NJ, 1970).
- [3] A.N. Lobachev, *Crystallization Processes under Hydrothermal Conditions*, (Consultants Bureau, New York, 1973).
- [4] R. Roy, "Speeding up the Kinetics of Low-Temperature Inorganic Syntheses", *J. Strong State Chem.*, 111, 11-17, 1994.
- [5] P. L. Leng, M. G. Naseri, A. H. Shaari and M. A. Kamaruddin, "union and portrayal of Ni-Zn ferrite nanoparticles (Ni_{0.25}Zn_{0.75}Fe₂O₄) by warm treatment strategy", *Adv. Nanopart.*, 2, 378-383, 2013.
- [6] M.M. Eltabey, W.R. Agami, H.T. Mohsen, "Change of the attractive properties for Mn- Ni- Zn ferrites by uncommon earth Nd³⁺ particle substitution", *Journal of Advanced Research*, 5, 601- 605, 2014.
- [7] S. S. Yattinahalli, S. B. Kapatkar and S. N. Mathad, "Basic and Mechanical properties of a nano-ferrit", *Adv. Sci. Center.*, 2, 42-46, 2014.
- [8] S. F. Wang, Y. Fu Hsu and K. M. Chou, "impacts of Li⁺ and Mg²⁺ dopants on the attractive properties of Ni-Zn ferrites", *IEEE Transactions on Magnetics*, 67, 1-25, 2014.
- [9] A. Kumar, P. Kumar and M. Kumar, "Amalgamation and Characterization of Nickel Doped Zinc Ferrite Nanoparticles", *J. Appl. Phys.*, 09, 228-230, 2014.
- [10] P. Parsons, K. Duncan, A. K. Giri, J. Q. Xiao and S. P. Karna, "electromagnetic properties of Ni-Zn ferrite nanoparticle and their polymer", *J. Appl. Phys.*, 115, 173905, 2014.
- [11] R. Kumar, R. R. Singh and P. B. Barman, "Cobalt Doped Nickel Zinc Ferrite Nanoparticles – XRD Analyses an Insight", *International Journal of Scientific and Engineering Research*, 5, 12-20, 2014.
- [12] A. Kumar, P. Kumar, G. Rana, M. S. Yadav and R. P. Gasp, "An investigation on basic and attractive properties of Ni_xZn_{1-x}Fe₂O₄ (0 ≤ x ≤ 0.6) ferrite nanoparticles", *Appl. Sci. Lett.* 1(2), 33-36, 2015.
- [13] N. H. Kumar, N. Venkatesh, G. Aravind, S. Goud, T. Somaiah and D. Ravinder, "FTIR studies and dielectric properties of Cu substituted nanocrystalline Ni-Zn ferrites incorporated by citrate-gel auto burning specialized", *J. Appl. Phys.*, 7, (79-83), 2015.
- [14] N. Sanpo, J. Wang and C. Berndt "Sol-Gel Synthesized Copper-Substituted Cobalt Ferrite Nanoparticles for Biomedical Applications" *J. of Nano Research.*, Vol. 22, p.p 95-106, 2013.





Nada Suheel Ahmade and FalahA-H Mutlak

- [15] C. Stein,, M.. Bezerra, A. Holanda, J. Andr'e-Filho, and P. Morais" Structural and agnetic properties of cobalt ferrite nanoparticles blended by co-precipitation at expanding temperatures" AIP Advances ,vo8, p.p056303,2018.
- [16]L.Zhong L. Xiao,X. Zhong, R.Wang,and X. Qiang "Basic, attractive and electrical properties of Zr-substituedNiZnCo ferrite nanopowders" J. Magn. Mater.Vol.. 435 ,p.p58-63,2017.
- [17]K.VijayaBabu, M. Ravi C. Gondu, V.Santosh , andK., Kantamsetti "Impact of cobalt substitution on basic, electrical and attractive properties of NiFe₂O₄", Processing and Application of Ceramics,Vol. 11,p.p 60-66,2017.
- [18] N. Sanpo, C.Wen, C. Berndt, and J. Wang" Antibacterial properties of spinel ferrite nanoparticles" , Microbial pathogens and techniques for fighting them: science, innovation and education,Vol.6p.p239-250,2013.
- [19]A. Hathout, A.,Bassem A. Sabry, A. El-Nekeety, M. Roby N. Deraz, S. Aly, and A. Abdel-Wahhab " Synthesis and portrayal of cobalt ferrites nanoparticles with cytotoxic and antimicrobial properties" Journal of Applied Pharmaceutical Science, Vol. 7 (01), pp. 086-092, January, 2017.
- [20]K. kapadnis"Synthesis, Characterization& Antimicrobial Activity of Mixed Metal Oxides of Iron Cobalt Nickel and Zinc" , International Journal of Chemical and Physical Sciences , Vol. 4, p.p357-360, 2015.

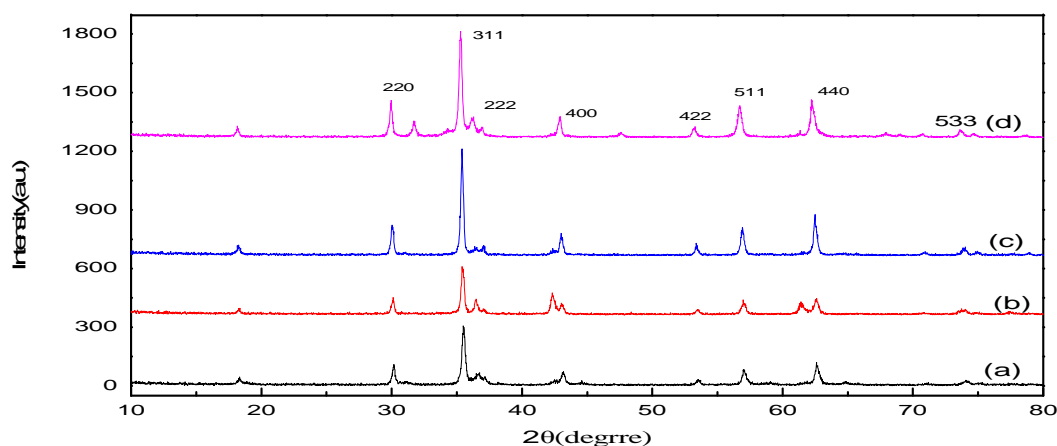


Figure 1:XRD patterns of the samples obtained by hydrothermal. (a- CoFe_2O_4),(b- $\text{Co}_{0.9}\text{Zn}_{0.1}\text{Fe}_2\text{O}_4$),(c- $\text{Co}_{1.1}\text{Zn}_{0.1}\text{Fe}_2\text{O}_4$)(d- $\text{Co}_{0.3}\text{Zn}_{0.7}\text{Fe}_2\text{O}_4$).

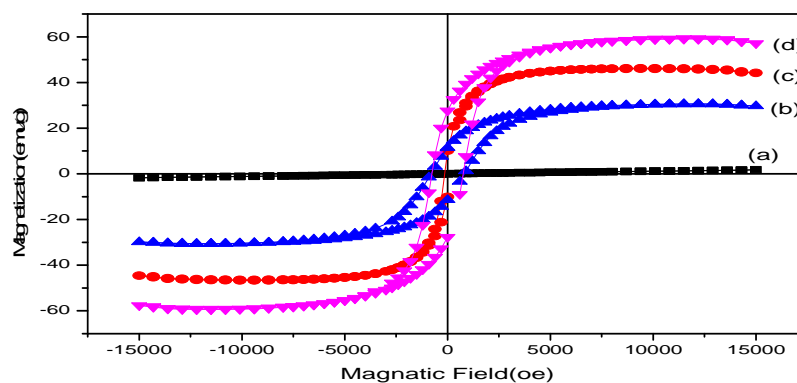


Figure 2: Magnetic hysteresis loops (a) CoFe_2O_4 (b) $\text{Co}_{0.9}\text{Zn}_{0.1}\text{Fe}_2\text{O}_4$ (c) $\text{Co}_{1.1}\text{Zn}_{0.1}\text{Fe}_2\text{O}_4$ (d) $\text{Co}_{0.3}\text{Zn}_{0.7}\text{Fe}_2\text{O}_4$ hydrothermal.





Nada Suheel Ahmade and Falaha-H Mutlak

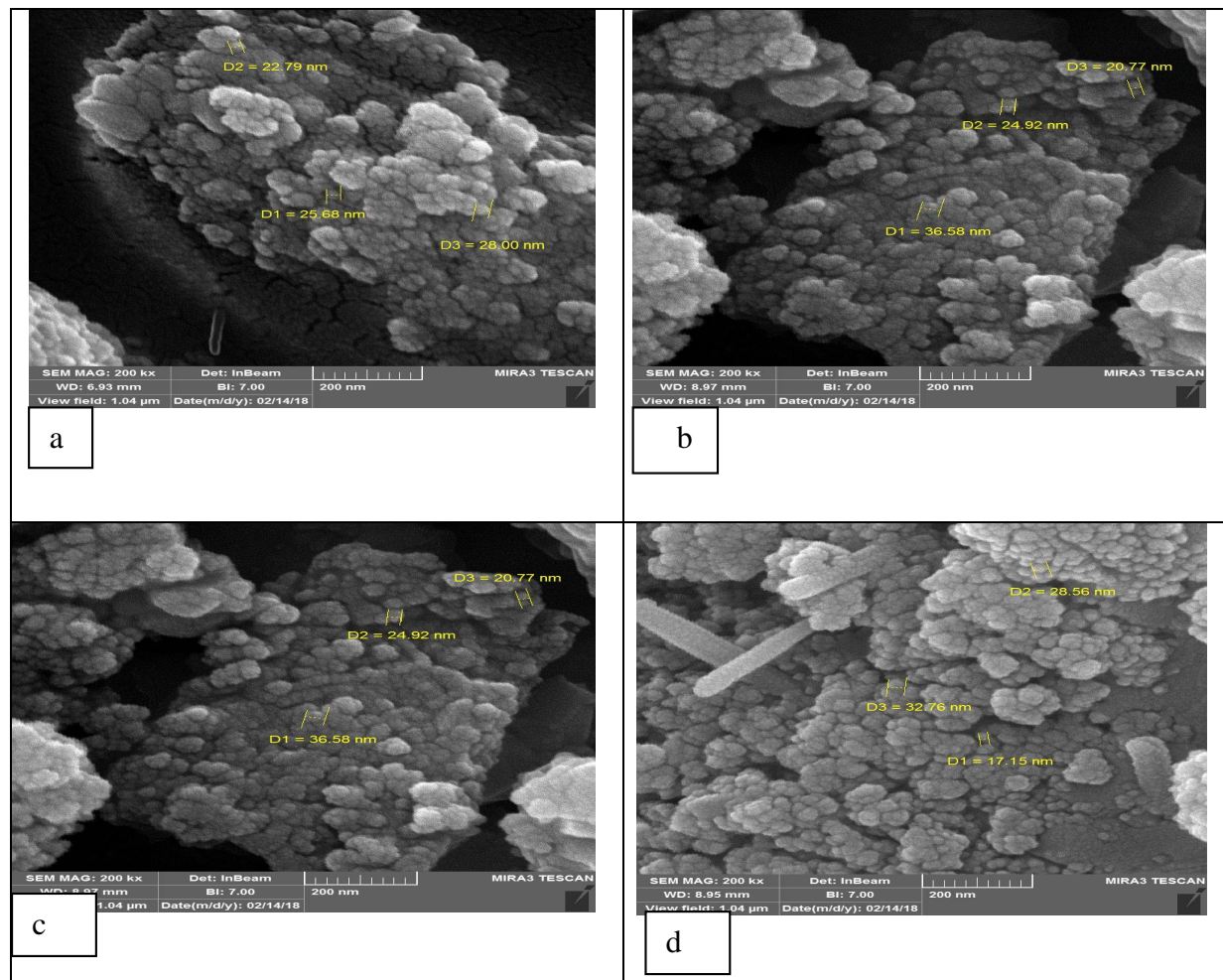


Figure 3: FESEM image (e) CoFe_2O_4 (f) $\text{Co}_{0.9}\text{Zn}_{0.1}\text{Fe}_2\text{O}_4$ (g) $\text{Co}_{1.1}\text{Zn}_{0.1}\text{Fe}_2\text{O}_4$ (h) $\text{Co}_{0.3}\text{Zn}_{0.7}\text{Fe}_2\text{O}_4$ by hydrothermal.





Nada Suheel Ahmade and FalahA-H Mutlak

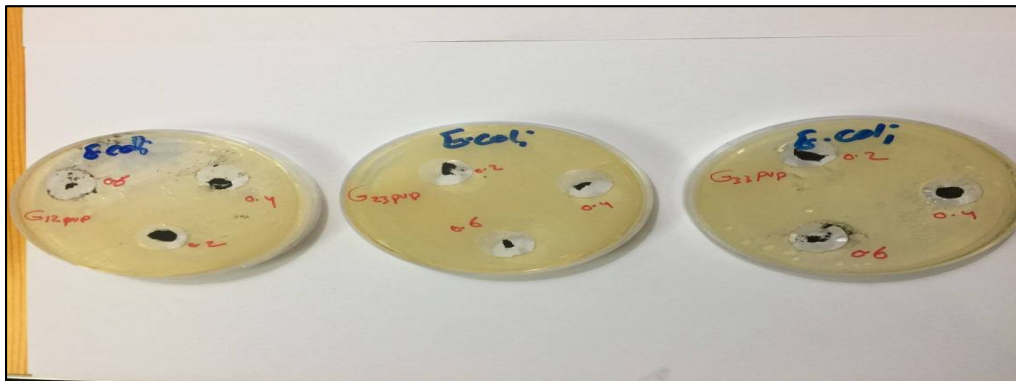


Fig 4: Inhibition zone of (Co-Zn) ferrite nanoparticles.

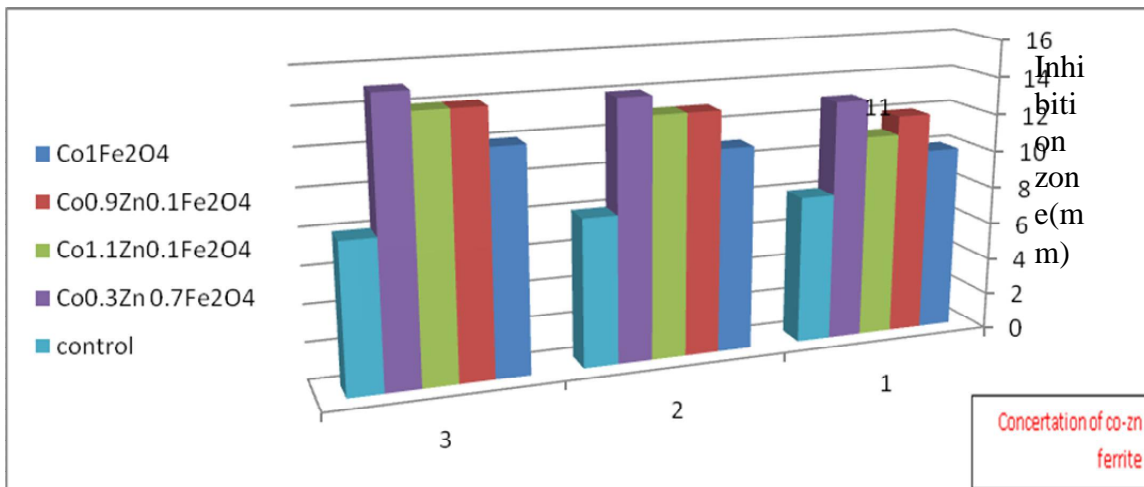


Fig 5: Inhibition zone of *E.coli* bacteria).





Evaluation of Iron Stores in Iraqi Chronic Renal Failure Patients

Dhelal Abdul khaliq Jumma*

Al-Imam khadhim (a.s) University College for Islamic Sciences, Iraq

Received: 12 June 2018

Revised: 15 July 2018

Accepted: 18 Aug 2018

*Address for correspondence

Dhelal Abdul khaliq Jumma

Al-Imam khadhim (a.s) University College for Islamic Sciences,
Iraq.



This is an Open Access Journal / article distributed under the terms of the **Creative Commons Attribution License** (CC BY-NC-ND 3.0) which permits unrestricted use, distribution, and reproduction in any medium, provided the original work is properly cited. All rights reserved.

ABSTRACT

Anemia is the most common finding among the hematological manifestations in chronic renal failure and its severity increases with disease progression. Iron is a key component of haemoglobin in red blood cells, myoglobin in muscle, and many metalloproteins and enzymes. It is essential for uptake of oxygen and its delivery to tissues, utilization of oxygen by muscle cells, and mitochondrial energy production. The aim of this study is to evaluate the iron stores in chronic renal failure. The study included 108 Iraqi subjects with age range (20-69 years) who have chronic renal failure. The subjects involved in this study included 42 conservative patients (21 Males and 21 Females) and 66 hemodialysis patients (44 Males and 22 Females). Results showed that the ferritin, iron and transferrin saturation levels were increased significantly in hemodialysis patients as compared with conservative patients but unsaturation iron-binding capacity, total iron-binding capacity and transferrin levels were decreased significantly in hemodialysis patients when compared with conservative patients. In conclusions: Ferritin levels increased in chronic renal failure patients not involved iron overload.

Keywords: Iron stores ,Anemia,Chronic renal disease

INTRODUCTION

Renal diseases are associated with a variety of hematological changes. (Sureshet *et al.*, 2012). Anemia is the most common finding among these hematological manifestations and its severity increases with disease progression. Iron is a key component of haemoglobin in red blood cells, myoglobin in muscle, and many metalloproteins and enzymes. It is essential for uptake of oxygen and its delivery to tissues, utilization of oxygen by muscle cells, and mitochondrial energy production (Frazer and Anderson, 2014). Patients with ESRD received blood transfusions to maintain hemoglobin levels. (Besarab *et al.*, 1998). The main markers of iron status are serum ferritin, transferrin saturation (TSAT) and total iron binding capacity (TIBC). By determining both the serum ferritin concentration and the transferrin saturation, are used to direct anemia therapy in CKD and are associated with clinical outcomes in patients on dialysis (Kovesdy *et al.*, 2009). Serum ferritin adequately reflects iron stores in bone marrow of HD patients and also functions as an acute phase reactant (Birgegard *et al.*, 1978). Despite the ferritin values ranging from



**Dhelal Abdul khaliq Jumma**

approximately 80 - 480ng/mL, the iron stores were absent on bone marrow aspiration in ESRD patients starting dialysis and may have functional iron deficiency (FID) (Fudin *et al.*,1998).Ferritin is the intracellular storage form of iron. A very small amount is found in serum, in inflammation, liver disease, and malignancy, ferritin levels can rise because ferritin is an acute phase protein (Adams and Barton, 2011).Serum iron refers to ferric ions (Fe 3+) bound to serum transferrin. Serum iron concentration is highly variable and is affected by dietary iron intake, inflammation, and infection (Fairbanks, 1991). Transferrin is the principal iron transport protein in plasma. It increases in iron deficiency to maximize utilization of available iron. (Adams and Barton, 2011).TIBC is an alternative test to transferrin. TIBC reflects the availability of iron binding sites on transferrin. Values increase in iron deficiency and decrease in iron overload. Some laboratories measure unsaturated iron binding capacity (UIBC) and calculate TIBC by adding serum iron to UIBC. TSAT, is calculated from serum iron and either TIBC or transferrin measurements. Typically, transferrin is 30% saturated with iron. (Fairbanks, 1991). Transferrin saturation rises in iron overload and falls in iron deficiency, but does not quantitatively reflect iron stores (EASL, 2010).

MATERIALS AND METHODS

The study was designed on 108 Iraqi subjects age range (20-69 years) with chronic renal failure in Baquba teaching hospital in Ibn Sina Center for Dialysis during the period from 28 February to 23 May 2017. The subjects involved in this study 42 conservative patients (21 Males and 21 Females) and 66 hemodialysis patients (44 Males and 22 Females).Iron store compound were estimated in serum of all subjects by using were using an automated quantitative COBAS INTEGRA 400 plus test (from Roche, Germany), while ferritin were estimated in serum of all subjects by using an automated quantitative COBAS e411 test (from Roche, Germany).

Statistical Analysis

Data were analyzed using SPSS 20 for windows.Data were expressed as mean \pm standard error (M \pm SE). Differences between means of two major groups were compared by using t-test and the significance was tested at two- tail P value.The P <0.05 is considered significant.

RESULTS

The results which illustrated levels of ferritin were higher than the upper limit of normal range (Male15-200ng/mL and Female12-150ng/mL) in conservative group (377.54 \pm 83.74ng/mL) and hemodialysis group (1450.61 \pm 217.52ng/ml) and also increased significantly (p<0.01) in hemodialysis group when compared with conservative group. Iron level was decreased than the lower limit of the normal range (13-32 μ mol/L) in conservative group (9.94 \pm 0.78 μ mol/L), but was within limit of the normal range in hemodialysis group (14.56 \pm 1.05 μ mol/L), and also showed a significant (p<0.01)increase in hemodialysis group when compared with conservative group. Unsaturated iron binding capacity levels were within limit of the normal range (22.3-70.1 μ mol/L) in both conservative (42.17 \pm 1.67 μ mol/L) and hemodialysis groups (27.87 \pm 1.54 μ mol/L) and also was decreased significantly (p<0.01) in hemodialysis group when compared with conservative group. Total iron binding capacity and transferrin levels were within limit of the normal range (45-70 μ mol/L and 2.0-3.6g/L) in conservative group (52.21 \pm 1.43 μ mol/L and 42.73 \pm 1.37 μ mol/L) respectively, while less than the lower limit of the normal range in hemodialysis group (42.73 \pm 1.37 μ mol/L and 1.62 \pm 0.02 μ mol/L) and significantly (p<0.01) decrease in hemodialysis group were compared with conservative group. The percentage of TSAT levels were decreased than the lower limit of the normal range (20-50%) in conservative group (19.61 \pm 1.68%), but was within limit of the normal range in hemodialysis group (36.17 \pm 2.91%), and also increased significantly (p<0.01) in hemodialysis group when compared with conservative group Table (1).



**Dhelal Abdul khaliq Jumma****DISCUSSION**

Ferritin had been elevated in both groups, but more increased levels were showed in HD group that ferritin is an intracellular iron storage protein and a marker of iron stores. Low ferritin values provide absolute evidence of iron deficiency. Raised levels often indicate iron overload, but they are not specific, as ferritin is an acute phase protein and is also released from damaged hepatocytes; thus levels are elevated in inflammatory disorders (Koperdanova and Cullis, 2015). Most patients (90%) with hyperferritinaemia will not have iron overload. Many conditions are associated with “reactive” high ferritin levels, elevated ferritin levels are usually due to causes such as acute or chronic inflammation, chronic alcohol consumption, liver disease, renal failure, metabolic syndrome, or malignancy rather than iron overload, as HD group suffering from CRF in our study. (Mitchell and Mendes, 2013; Chifman *et al.*, 2014). So diminished iron transport and accumulated iron stores are manifested as low transferrin saturation and elevated serum ferritin level as observed in conservative group, (Kakey and Abdoulrahman, 2016).

Iron decreased in conservative group while HD group showed normal values TSAT, also was lower in conservative group and was within normal value in HD group this means, low iron levels and low TSAT in conservative group. The TSAT is a score that indicates how much iron is available, or circulating, to make red blood cells. A TSAT score below 20 percent is another sign of iron deficiency that transferrin saturation rises in iron overload and falls in iron deficiency as observed in conservative group but does not quantitatively reflect iron stores (Kelly *et al.*, 2017). The decrease of iron in conservative group that the iron deficiency which may occur when iron stores are depleted as a result of loss or decreased intake, however, functional deficiency occurs when there is a need for a greater amount of iron to support hemoglobin synthesis than can be released from iron stores (Koshy and Geary, 2008).

In HD group showed normal iron levels indicated that CRF patients were not iron deficient. This coincides with the report of Steffensen *et al.*, in which 15 ESRD patients were recruited in the study, all of whom were not iron deficient, regardless of the type of dialysis (Steffensen *et al.*, 1996). On the other hand, in an earlier report by Karivone and Izuya (1988) decreased iron levels were found in CRF patients. However, the presence of anemia, as measured by other parameters, associated with these apparently normal iron levels in HD CRF patients group suggests poor utilization of iron by the bone marrow; iron-deficiency was not a dominant condition among those patients, and many of the patients who had normal serum iron and high ferritin levels with lower TIBC, also had lower EPO levels (Karivone and Izuya, 1988). Thus it is concluded that poor iron utilization occurred in CRF patients due to the defective erythropoiesis. Poor iron utilization in CRF patients was also reported by Seguchi *et al.*, 1992.

UIBC decreased in HD group that UIBC may also be used as a marker for altered iron metabolism. UIBC represents the portion of iron binding sites on transferrin that are not occupied by iron therefore, a low UIBC indicates that transferrin is highly saturated with iron. These results are in consistence with other studies, which showed significant lowering of UIBC, TSAT and TIBC in CRF patients before hemodialysis, and significant increase of the levels of these parameters after hemodialysis with lowering the ferritin level (Jelic *et al.*, 2013; Bojana *et al.*, 2014). The decrease of serum transferrin in this group may be caused by three factors, high iron requirements as a result of an enhanced erythropoiesis, an insufficient release of iron from the body iron stores, and insufficient iron absorption. The first factor, a high demand for iron, exists when erythropoiesis is enhanced by EPO treatment. The second factor, a disturbed release of iron from ferritin and haemosiderin molecules in the mononuclear phagocytic system and from hepatocytes, is known to occur in patients with the anemia of inflammation (Brock, 1994).

CONCLUSION

This study indicated ferritin levels increased in chronic renal failure patients, this raised not caused by iron overload. Iron deficiency common in chronic renal failure patients.





Dhelal Abdul khaliq Jumma

REFERENCES

1. Adams, P.C.; and Barton, J.C. (2011). A diagnostic approach to hyperferritinemia with a non-elevated transferrin saturation. *J Hepatol* 2011; 453-8. doi:10.1016/j.jhep.2011.02.010 pmid: 21354228.
2. Besarab, A.; Bolton, W.K. and Browne, J.K. (1998). The effects of normal as compared with low hematocrit values in patients with cardiac disease who are receiving hemodialysis and epoetin. *N Engl J Med*; 339: 584–590.
3. Birgegard, G.; Hallgren, R.; Killander, A.; Stromberg, A.; Venge, P. and Wide, L. (1978). Serum ferritin during infection. A longitudinal study. *Scand J Haematol*; 21(4):333-340.
4. Bojana, K.; Dijana, M.; Radojica, S.; Aleksandra, I.; Julijana, R.; Mirjana, M. and Ilija, D. (2014). Investigation of lipid peroxidation products and antioxidant enzyme activities in end-stage renal disease patients. *Advances in Chemical Engineering and Sci.*; 4(1): 73-80.
5. Brock, J.H. (1994). Iron in infection, immunity, inflammation and neoplasia. *Iron metabolism in health and disease*, 353.
6. Chifman, J.; Laubenbacher, R. and Torti, S.V. (2014). A systems biology approach to iron metabolism. *Adv Exp Med Biol*; 844:201-25.
7. European Association for the Study of the Liver. EASL. (2010). clinical practice guidelines for HFE hemochromatosis. *J Hepatol*; 357:3-22. doi:10.1016/j.jhep.2010.03.001 pmid: 20471131.
8. Fairbanks, V.F. (1991). Laboratory testing for iron status. *Hosp Pract (Off Ed)*; 357(Suppl 3):17-24. doi:10.1080/21548331.1991.11704280 pmid: 2010484.
9. Frazer, D.M. and Anderson, G.J. (2014). the regulation of iron transport. *Biofactors*; 357:206-14. doi:10.1002/biof.1148 pmid: 24132807.
10. Fudin, R.; Jaichenko, J.; Shostak, A.; Bennett, M. and Gotloib, L. (1998). Correction of uremic iron deficiency anemia in hemodialyzed patients: a prospective study. *Nephron*; 79(3):299-305.
11. Jelic, M.; Cvetkovi, T.; Djordjevi, V.; Damnjanovi, G.; Vlahovi, P.; Koci, G.; Djindji, N. and Jovovi, B. (2013). Hepcidin and iron metabolism disorders in patients with chronic kidney disease. *Vojnosanitetski pregled*, 70(4), 368–373.
12. Kakey, M.I.S. and Abdoulrahman, k.k. (2016). Estimation of Anemia parameters in chronic renal failure patients on hemodialysis in Erbil Governorate. *ZJPAS*; 28 (6); 57-08.
13. Karivone, S. and Izuya, S. (1988). Relationship between erythropoietin and chronic renal failure. *Kidney Dialysis (suppl 1)*, 144–148.
14. Kelly, A.U.; Sorley, S.T.; Patel, P. and Talwar, D. (2017). Interpreting iron studies *BMJ* 357:1-6. doi: 10.1136/bmj.j2513.
15. Koperdanova, M. and Cullis, J.O. (2015). Interpreting raised serum ferritin levels. *BMJ*; 351:h3692.
16. Koshy, S.M. and Geary, D.F. (2008). Anemia in children with chronic kidney disease. *Pediatric Nephrology*, 23(2), 209-219.
17. Kovesdy, C.P.; Estrada, W.; Ahmadzadeh, S. and Kalantar-Zadeh, K. (2009). Association of markers of iron stores with outcomes in patients with nondialysis-dependent chronic kidney disease. *Clin J Am Soc Nephrol*; 4(2):435-441.
18. Mitchell, S. and Mendes, P.A. (2013). Computational Model of Liver Iron Metabolism. *PLoS Comp Biol*; 9(11):e1003299.
19. Seguchi, C.; Shima, T.; Misaki, M.; Takarada, Y. and Okazaki, T. (1992). Serum erythropoietin concentrations and iron status in patients on chronic hemodialysis. *Clin. Chem.* 38, 199–203.
20. Steffensen, G.; Aunsholt, N.A. and Povlsen, J.V. (1996). Evidence that treatment of ESRD patients with recombinant human erythropoietin induces immunosuppression without affecting the distribution of peripheral blood mononuclear cell subpopulations. *Clin. Nephrol.* 45(2), 98– 103.
21. Suresh, M.; Mallikarjuna, R. N.; Singh, S.M.; HariBandi, H.K.; Keerthi, S.G. and Chandrasekhar, M. (2012). Hematological Changes in Chronic Renal Failure. *International Journal of Scientific and Research Publications*; 2(9): 1-4.





Dhelal Abdul khaliq Jumma

Table 1. Iron Store Biomarkers in Conservative and Hemodialysis Groups.

Biomarker	Normal range	Conservative (n=42) Mean ± SE	Hemodialysis (n=66) Mean ± SE	t-test P value
Ferritin	Male 15-200ng/mL Female 12-150ng/mL	377.54 ± 83.74	1450.61±217.52	0.001
Iron	13-32µmol/L	9.94 ± 0.78	14.56 ± 1.05	0.002
UIBC	22.3-70.1µmol/L	42.17 ± 1.67	27.87 ± 1.54	0.001
TIBC	45-70µmol/L	52.21 ± 1.43	42.73 ± 1.37	0.001
Transferrin	2.0-3.6g/L	2.30 ± 0.06	1.62 ± 0.02	0.001
TSAT	20-50%	19.61±1.68	36.17±2.91	0.001
UIBC Unsaturation Iron-Biding Capacity, TIBC Total Iron-Biding Capacity and TSAT Transferrin Saturation.				





RESEARCH ARTICLE

Comparative Evaluation of Diuretic Activity of Ethanolic Extracts of (Celery) *Apium graveolens* and (Parsley) *Petroselinum crispum* in Male Rats

Jawad Kadhim Faris, Ali, I. Al-ameedi*, Rawaa Safaa and Shatha m. Abbas

Department of Physiology and Pharmacology, College of Veterinary Medicine, Alqasim Green University, Iraq.

Received: 10 July 2018

Revised: 15 Aug 2018

Accepted: 18 Sep 2018

*Address for Correspondence

Ali, I. Al-ameedi

Department of Physiology and Pharmacology,
College of Veterinary Medicine,
Alqasim Green University, Iraq.
E.mail: ali.alameedy89@yahoo.com



This is an Open Access Journal / article distributed under the terms of the **Creative Commons Attribution License** (CC BY-NC-ND 3.0) which permits unrestricted use, distribution, and reproduction in any medium, provided the original work is properly cited. All rights reserved.

ABSTRACT

The current study is an trial to search the diuretic effect of Ethanolic extracts of the plants *Apium graveolens* (Ag) and *Petroselinum crispum* (Pc) , with furosemide as a standard and normal saline as control in male rats at a single dose of (200) mg/Kg, b.w. orally for each extract. The urine volume (in mL) measured at (6) hours and urinary electrolyte excretion. The urine volume and urinary electrolyte excretion (Na⁺ , K⁺ and Cl⁻) were found to be significantly higer in rats treated with (Pc) extracts than in (Ag) extracts as compare to normal rats. This current study suggest that Ethanolic extract of (Pc) and (Ag) possess diuretic activity .

Key words: *Petroselinum crispum* , *Apium graveolens*, diuretic activity, urine volume

INTRODUCTION

Drug-induced diuresis is beneficial in many life threatening disease conditions such as congestive heart failure, nephritic syndrome, cirrhosis, renal failure, hypertension. Most diuretic drugs such as the high-ceiling loop and thiazides with several side effects, such as electrolyte and metabolic changes (1,2). A search for better drugs with lesser adverse effects, which are more effective effective and economical is need of the hour. Plants are source for various drugs , therefore this study has been carried out to look for diuretic potential of commonly available plants. *Apium graveolens* (Celery) are medicinal plants are used in traditional medicine to treat many diseases. Observations of scientific studies on medicinal plants are used to cure various diseases including: cancer, infectious diseases, diabetes and atherosclerosis. (Ag) is a medicinal plant in traditional medicine with numerous health



**Jawad Kadhim Faris et al.**

benefits . (3). All parts of this plant contain an aromatic essential oil and the main constituents of the essential oil of celery are limonene, selinene, α - and β -pinene, and myrcene (4). The active substances of (Ag) act as, antibacterial, antifungal, antiparasitic and antioxidant activity. (5), and reduces blood pressure, relieves indigestion, anti-inflammatory, arthritic pain (6). The ripe seeds, herb and root are laxative, carminative, diuretic, nerve stimulant and tonic(7).

Petroselinum crispum (Parsley) is a species of flowering plant in the family Apiaceae, native to the central Mediterranean region, naturalized elsewhere in Europe, and widely cultivated as a herb, a spice, and a vegetable (8). Active ingredients and content of (Pc) are essential oil, ferulic acid, (apiol, myristicin), terpenes (alpha and beta-pinene). Flavonoids: apioside, luteolol, apigenol, Vitamins A, B, C, minerals (iron, calcium, phosphorus, magnesium, sodium, potassium, iodine, manganese, sulfur), furanocoumarins (9). Medicinal use of (Pc) are, chew the leaf raw to freshen the breath and promote healthy skin, infuse for a digestive tonic. Bruised leaves have been used to treat tumors, insect bites, lice and skin parasites and contusions. Other traditional uses reported include the treatment of diseases of the prostate, liver and spleen, in the treatment of anemia, arthritis and cancers, and as an expectorant, antimicrobial aphrodisiac, hypotensive, laxative and as a scalp lotion to stimulate hair growth and reduces inflammation by inhibiting histamine. The seeds may be substituted for (Ag) seeds in the treatment of gout, rheumatism and arthritis.(10),(11).

MATERIALS AND METHODS

This study was conducted at the period between January 2018 and June 2018 in physiology department of veterinary medicine of AL-Qassim green university.

Experimental animals

The number of laboratory animals used in the experiment are twenty healthy male rats aged (100-120) days and weighted (190-210) grams, obtained from the animal house of the College of Veterinary Medicine, AL-Qadisiya University, were kept for one week as acclimatization period before the starting of the experiment, all rats were fed on concentrated food (pellets) and were given plain water, the animals room temperature was (19-23)°C, and the humidity was (45-55), that room was washed and sterilized once a week. Before the administration of the extract and control, the bladder of the rats was evacuated by gentle compressing of pelvic area and pulling of tails (12).

B-Collection and Preparation of Plant Extract

The healthy fresh leaves of (Ag) and (Pc) were purchased from local markets in Baghdad and identified by national herbarium at Abu-Ghraib, first washed separately very carefully and clearly with water and then leaves were dried at room temperature for (14) days and powdered, then extracted by (70)% ethanol using magnetic stirrer for (72) hrs at (50)°C then the extract was filtered and evaporated to dry it by rotary evaporator (45)°C under reduced pressure (13).

Acute Toxicity Studies

To study the toxic effects of (Ag) and (Pc) to carry out the remarkable behavioral effects and safety effects of the ethanolic extract of (Ag) and (Pc) was carried on mice weighing about (22-26)gm, overnight fasted mice and received the two test extract at a dose of (5) mg/kg.bw orally and mortality was observed for first (24) hrs, with keeping for the first (4) hrs and daily then, for a total of (14) days. If mortality was not observed, the same procedure was repeated in each group for each extract for further higher doses as (100, 300, 600, 1000, 2000) mg/Kg b.w. (14) (15).





Jawad Kadhim Faris et al.

Diuretic activity

Twelve male rats were divided into (4) groups of (3) animals each and prohibit of food and water for (18) hrs. All the rats received priming dose of normal saline (25ml/kg) orally. Both the extracts (Ag) and (Pc) and Furosemide as a standard were dissolved in a normal saline. Group (I) served as control in which only normal saline (25)ml/kg was administered intraperitoneal route (i/p). Group (II) served as standard received Furosemide (20)mg/kg. Group III and Group IV received (200) mg/Kg, b.w. of ethanolic extract of (Ag) and (Pc) of leafs respectively, directly after administration, the rats (one in each cage) were placed in metabolic cages specially designed to separate urine and faeces and kept at room temperature of (24-25)°C. The urine was collected in a measuring cylinder up to (6) hrs (16). The content of Na⁺, K⁺ and Cl⁻ in the urine was evaluated and results were compared with standard Furosemide. The concentration of Na⁺ K⁺ and Cl⁻ ions in the fresh urine samples was evaluated using Urine Electrolyte Measurement. Diuretic index and diuretic activity will be calculated as below(17).

$$\text{Diuretic index} = \frac{\text{Mean urine volume of the test group}}{\text{Mean urine volume of the control group}}$$

$$\text{Lipschitz value} = \frac{\text{Mean urine volume of the test group}}{\text{Mean urine volume of the furosamide group}}$$

Statistical analysis

The results were analyzed by a using Complete Randomized Design(C.R.D) (18). In order to determine the effect of level of both extracts of (Ag) and (Pc) and comparison of furosamide drug for male rats comparing the mean of the studied traits using the Duncan test (19) of probability level of (0.001) to test the significance of the differences between the averages of the studied traits by applying the (SAS,2010) (20).

RESULTS

Acute toxicity study

In the acute toxicity study, of both extracts of (Ag) and (Pc), no clear signs of toxicity or any abnormal behavior were observed and none of the treated animals died in (24) hrs in the test animals at the dose of (2000) mg/kg of body weight.

Diuretic effects

The oral administration of Ethanolic extracts of (Ag) and (Pc) increased the urinary flow in (Table 1) When compare with the control group, (1.91±) and (2.42±) fold increase in urine output was observed in group (Ag) and (Pc), respectively. The diuretic index values of the test groups group (Ag) and (Pc) were (2.17) and (2.75) which indicated a good diuretic activity at the dose of (200) mg/kg of (Ag) extracts and (Pc) extracts (Table 2). The Lipschitz values demonstrate that, at the doses of (200) mg/kg of (Ag) extracts and (Pc) extracts appear 50% and 64% of diuretic activity respectively, compare with furosemide (Table 2). The results appear that ethanolic extract of (Ag) and (Pc) rise the urinary electrolytes excretion of Na⁺, K⁺ and Cl⁻ ions show electrolytes when compared to normal control. Group (Pc) more potent than group (Ag) according to results in (Table 1 and 2).





Jawad Kadhim Faris et al.

DISCUSSION

Diuretics are the agents which rise production of urine and are used to treat many cases like heart failure, liver cirrhosis, certain kidney diseases hypertension and poisoning (21). Ethanolic extracts of (Ag) and (Pc) showed the diuretic activity and significantly rise urinary electrolyte excretion may be due to contain numerous compounds which could be responsible for the plant's diuretic effects such (flavonoids, Phthalide compounds or organic acids) (22), or may be act by Inhibiting vasopressin secretion (23) or may work by causing dilation of glomerular arterioles, thereby increasing glomerular filtration rate (24 and 25). The diuretic activity is considered to be good if the diuretic index values are greater than (1.50), moderate if the values are in between (1.00-1.50) and, mild if the values lie in between (0.72 - 1.00) and there is no diuretic activity if the value is (< 0.72) (26). In our study, the diuretic index values of the treated group (Ag) and (Pc) were (2.17) and (2.75) respectively, this indicates more than 2-fold increase in the urine volume. Lipschitz values also showed that, at the maximal dose (200 mg/kg), treated group (Ag) and (Pc) showed (50)% and (64)% of diuretic activity compared with furosemide. The good diuretic activity of extract of (Ag) and (Pc), as compared to the standard drug.

REFERENCES

- 1-Agunu, A. ; Abdurahman, EM. ; Andrew, GO. ; Muhammad Z. (2005). Diuretic activity of the stem-bark extracts of *Steganotaenia araliaceae* Hoehst. J Ethnopharmacol 96 :471-475.
- 2-Gasparotto, JA. ; Boffo, MA. ; Lourenço, ELB. ; Stefanello, MEA. Kassuya, CAL. ; Marques, MCA. (2009). Natriuretic and diuretic effects of *Tropaeolum majus* (Tropaeolaceae) in rats. J. Ethnopharmacol 122 (3):517-522.
- 3-Wesam Kooti, ; Majid Asadi-Samani, ; Hosna Ghadery ; Damo Ashtary-Larky, ; Sara Ali-Akbari. (2014). A review on medicinal plant of *Apium graveolens*. Advanced Herbal Medicine, 1 (1): 48-59
- 4-Sowbhagya, H.B. ; Sampathu, S.R. ; Krishnamurthy, N. (2007). Evaluation of size reduction on the yield and quality of celery seed oil. J. Food Eng., 80, 1255–1260.
- 5-Baananou, S. ; Bouftira, I. ; Mahmoud, A. ; Boukef, K. ; Marongiu, B. Boughattas, N.A. (2013). Antiulcerogenic and antibacterial activities of *Apium graveolens* essential oil and extract. Nat. Prod. Res., Form. Nat. Prod. Lett., 27, 12, 1075–108
- 6-Nagella, P. ; Ahmad, A. ; Kim, S.J. ; Chung, I.M. (2012). Chemical composition, antioxidant activity and larvicidal effects of essential oil from leaves of *Apium graveolens*. Immunopharmacol.
- 7-Satyanand Tyagi, ; Patel Chirag, J. ; Mangukia Dhruv, ; Mangukia Ishita, ; Mohammed Rageeb, ; Mohammed Usman Bhupendra Nimbiwa Anil Kumar Gupta, Raaz K Maheshwari. (2013). Medical benefits of *Apium graveolens* (celery herb). Journal of Drug Discovery and Therapeutics 1 (5), 36-38
- 8-Meyer, H. ; Bolarinwa, A. ; Wolfram, G. ; and Linseisen, J. (2006). Bioavailability of apigenin from apigenin-rich parsley in humans". Annals of Nutrition and Metabolism. 50 (3): 167–172
- 9-Ashraf, M. ; Ahmad, R. ; Mahmood, S. ; and Bhatti M.K. (1980). *Petroselinum crispum*. Pakistan J. Sci. Ind. Res. 23(3/4):128–129
- 10-Andi Clevely, ; Katherine Richmond. (1995). The Complete Book of Herbs. Amness Publishing
- 11-Julia Lawless. (1995). The Illustrated Encyclopedia of Essential Oils. Element Books.
- 12-Abeywickrama, KRW. ; Ratnasooriya WD. ; Amarakoon, AMT. (2010). Oral diuretic activity of hot water infusion of Sri Lanka black tea (*Camellia sinensis* L.) in rats. Pharmacogn Mag. 6 (24): 271–277.
- 13-Harbone, JB. (1998). Phytochemical methods. a guide to modern techniques. Kluwer Academic Publishers Imprint. Dordrecht, NI.
- 14-BHABANI SHANKAR NAYAK, ; SUBAS CHANDRA DINDA, P. ELLAIAH (2012). Evaluation of diuretic activity of *Gmelina arborea* roxb fruit extract. Asian J Pharm Clin Res, Vol 6, Suppl 1, 111-113
- 15-Fathima, SN. ; Salwa, A. ; Anusha, S. ; and Fatima S. (2016). Study of antiasthmatic activity of ethanolic extract of *Alternanthera sessilis* leaves. Int J Pharma Res Heal Sci., 4: 1478–1482.





Jawad Kadhim Faris et al.

- 16-Hemant Swami , ; Mahendra Kumar Panigrahi, ; and Supriya Pradhan .(2017).Diuretic activity of ethanolic extract of plant *Solanum surattense* seeds . World Journal Of Pharmaceutical Research, Vol. 6, Issue 01,835-840
- 17- Asif ,M. ;Jabeen, Q. Abdul Majid A.M.S. ; Atif ,M. (2015). Diuretic of activity of aqous extract of *Nigella sativa* in albino rats. Drug Research, Vol. 72 No. 1 pp. 129-135.
- 18-AL-Rawi,K.M. and Abdul-Aziz,M.K. (2000).Design and Analysis of Agriculture Experiments. Dar AL-Kutob press for printing and publishing , Mosul University .
- 19-Duncan, C.B.(1955). Multiple range and multiple (F)test. Biometrics.11:1- 12.
- 20-SAS.(2010).Statisttical Analysis System.SAS institute Inc.Release, Virgin7.12 Tsozo North Carolina state University of Cary , NC, USA.
- 21- Ahmed, HQ. ; Rida, K. ;and Robert WS. (2015) . Clinical Use of Diuretics in Heart Failure, Cirrhosis and Nephrotic Syndrome, International Journal of Nephrology .
- 22- Muhammad Asif ,;Muhammad Atif; Amin Shah Abdul Maliki. ; Zahari Che Dan ,;Irshad Ahmad ;and Ashfaq Ahmadi.(2013).Diuretic ActivityTropical Albino Rats of *Trianthema portulacastrum* Crude TropicalJournal of Pharmaceutical Research December; 12 (6): 967-972.
- 23-Brunton ,LL;. Goodman, LS. ; Blumenthal, D. ; Buxton, I. ; Goodman and Gilman's (2007). Manual of pharmacology and therapeutics. United States: McGraw-Hill Professional;. Chapter 28 Diuretics; 477-500.
- 24-Schilcher, H. 91987a). Moglichkeiten und grenzen der phytotherapie ambeispiel pflanzlicher urologika. Urologe B 27: 316-319.
- 25-Schilcher, H. 91987b). Pflanzlicher diuretika. Urologe B27: 215-222.
- 26-Abdala, S. ; Martin-Herrera, D. ; Benjumea, D. ; Perez-Paz,P. (2008).Diuretic Activity of Smilax canariensis, An Endemic Canary Island Species. J. Ethnopharmacol; 119: 12-16

Table 1:Effect of oral administration of Ethanolic extracts of *Apium graveolens* and *Petroselinum crispum* on urine volume and electrolytes excretion in male rats .

Traits	Control	Furosamide	Ag	Ps
Urine volume (ml)	0.880 ± 0.03 D	3.77 ± 0.08 A	1.91 ± 0.03 C	2.42 ± 2.02 B
Na ion (mmol/L)	55.80 ± 1.24 C	72.00 ± 2.39 A	61.00 ± 2.43 BC	66.00 ± 2.21 AB
K ion (mmol/L)	8.40 ± 0.22 C	11.20 ± 0.17 A	9.10 ± 0.18 B	9.60 ± 0.29 B
Cl ion (mmol/L)	34.0 ± 1.73 C	69.00 ± 1.30 A	40.00 ± 1.84 B	43.00 ± 1.79 B

The average of traits which have carried different letters horizontally indicates high significance differences at level of probability 0.0001



**Jawad Kadhim Faris et al.****Table 2: Effect of oral administration of Ethanolic extracts of *Apium graveolens* and *Petroselinum crispum* on Diuretic index and Lipschitz value in urine male rats**

Groups	Dose (mg/kg)	Diuretic index	Lipschitz value
Control (T1)	-	-	-
Standard (T2) (Furosemide)	20	4.28	-
Ethanolic Extract of (Ag)	200	2.17	0.50
Ethanolic Extract of (Pc)	200	2.75	0.64





RESEARCH ARTICLE

Study the Histopathologic and Cytogenetic Effects of Glyphosate in Mice

Ahmed Tayyeh Hattat and Zainab Ismail Ibrahim*

Department of Pathology and Poultry Diseases, College of Veterinary Medicine ,University of Baghdad,Iraq.

Received: 15 July 2018

Revised: 17 Aug 2018

Accepted: 19 Sep 2018

*Address for Correspondence

Zainab Ismail Ibrahim

Department of Pathology and Poultry Diseases,
College of Veterinary Medicine,
University of Baghdad, Iraq



This is an Open Access Journal / article distributed under the terms of the **Creative Commons Attribution License** (CC BY-NC-ND 3.0) which permits unrestricted use, distribution, and reproduction in any medium, provided the original work is properly cited. All rights reserved.

ABSTRACT

The aims of present study is to investigate the genotoxicity effect by a single gel electrophoresis technique (comet assay) and the histopathologic lesions in lung, heart, and liver post oral administration of glyphosate in mice. The experiment included twenty four (24) adult albino mice (female and male) aged between 6-8 weeks and weighed about 20-25 gm. Mice subdivided into three equal groups (n=8); A, treated with (250 mg/kg/daily, B treated with (500 mg/kg/daily for 12 weeks, respectively, and C left on access water as control group. The animals of all treated groups sacrificed at the end of experiment of each treated group. The comet assay of A and B group improved its effect in the treated mice as compared with control negative group in head and tail comet areas. In G6B the lesions became severe and hypertrophy and sometimes hyalinized walls of small blood vessels of heart, myocardial infarction (coagulative necrosis) the predominant lesion with MNCs infiltration between myocardial fibers. In conclusion; the present results improved the potent genotoxic effect of glyphosate and its role in the histopathologic changes in lung, heart and liver in mice.

Keywords: glyphosate, histopathology, geontoxic effect (comet assay).

INTRODUCTION

Herbicides are just one of many types of pesticides. They are chemical substances used by farmers to kill unwanted plants (Simmons, 2010). The herbicide glyphosate, N-(phosphonomethyl) glycine, is a biocide with a broad spectrum activity that was introduced for weed control in agricultural production fields in 1974 (Benbrook, 2016). Industry studies show that when livestock are fed glyphosate at levels allowed in feed, glyphosate residues may be present at low levels in milk and eggs from the animals, as well as in the liver and kidneys (FAO/WHO, 2005). In fact; the European Food Safety Authority was explained, the

14841



**Ahmed Tayyeh Hattat and Zainab Ismail Ibrahim**

issue of glyphosate residues in animal products, because considering the wide use of glyphosate on feed crops, a significant livestock exposure to glyphosate and its metabolites might be expected, resulting in a carry-over of residues in the food of animal origin (EFSA, 2012). Comparisons between the cells of different organisms *in vivo* and *in vitro* using the comet assay system can be important in assessing the genotoxicity of glyphosate. The comet assay, which was first used in human lymphocytes, is very efficient in detecting genotoxicity (Singh *et al.*, 1988) because it allows the visualization of damage directly in the genetic material of individual cells. This test has also been used in plants and fish (Guilherme, Gaivão, Santos, & Pacheco, 2012).

MATERIALS AND METHODS

Glyphosate: used in experiment produced by Monsanto Europe N.V. Belgium as in (table-1).

Experimental animals

Twenty-four (24) adult albino mice (female and male) aged 6-8 weeks with an average body weight of 25-30 gm., obtained from the animal house colony of the animals housed and maintained in the clean and septic cages and supplied with optimal conditions from light, temperature and foods with water.

Single Cell Gel electrophoresis (SCGE) or Comet assay

Comet assay was performed for genotoxicity and were made from whole blood cells, the assay was carried out in Ministry of Science and Technology-Iraq and was performed according to the ITRC: the SCGE protocol (Dhawan *et al.*, 2007) with few modifications.

Evaluation of DNA Damage

1. For visualization of DNA damage, observations are made of EtBr-stained DNA using a 40x objective on a fluorescent microscope.
2. Although any image analysis system may be suitable for the quantitation of SCGE data, we use a Komet 5 image analysis software developed by Kinetic Imaging, Ltd. (Liverpool, UK) linked to a CCD camera to assess the quantitative and qualitative extent of DNA damage in the cells by measuring the length of DNA migration and the percentage of migrated DNA. Finally, the program calculates tail moment. Generally, 50 to 100 randomly selected cells are analyzed per sample.
3. Compare the amount of migration per cell, the number of cells with increased migration, the extent of migration among damaged cells, and viability.

Experimental design

After two weeks adaptation, the animals (n=24) divided randomly into three groups and administered orally and glyphosate daily as following:

- A:** (n=8) 250 mg/kg B.W (0.3 µl) daily for 12 months
- B:** (n=8) 500 mg/kg B.W (0.3 µl) daily for 12 weeks
- C:** (n=8) administered D.W as control negative group



**Ahmed Tayyeh Hattat and Zainab Ismail Ibrahim**

All animal groups sacrificed at the end of experiment (12 weeks) anesthetized to obtain the whole blood samples by heart punctures and kept in EDTA containers for comet protocol, then done postmortem examination to get autopsies (1cm³) from internal organs of lung, heart and liver, preserved in 10% formalin, all specimens were processed with alcohol ethanol, clearing by xylol and staining (Hematoxylin and Eosin stain) were carried on routine procedure to study the histopathologic changes (Luna and Lee, 1968).

Statistical Analysis

The Statistical Analysis System- SAS (2012) program was used to assess the effect of difference factors on studied parameters. Least significant difference –LSD test was used to compare the differences between means. P<0.05 is considered significant.

RESULTS**Genotoxicity of Glyphosate by Single gel electrophoresis (Comet assay)**

The table, 4-6; expressed significant values of DNA damage at the head and tail of comet length and area when compared with control negative group, was high % DNA in head groups G6A & B (65.46 ± 3.91 , 27.94 ± 14.20), respectively, while % DNA in tail was significantly highest at 12 weeks in group G6B then A (38.72 ± 19.53 , 34.53 ± 3.91), respectively, when compared with control group (82.94 ± 2.10 , 17.06 ± 2.10), respectively. Table- 2: normal cell(control) Figure -1, DNA light damage Figure-2 and DNA more damage Figure-2.

Histopathologic examination

Glyphosate (A) 250 & (B) 500 mg/kg B.W):the microscopic lesions of internal tissue sections in groups A and appeared more severe in B; were mostly moderate focal MNCs aggregations around degenerated and necrotic bronchioles (Figures-4&5), also diffuse in pulmonary tissue in interalveolar and perivascular cuffing in group B (500 mg/kg), extend to pleural membrane to cause pleuritis (Figure-6), congestion of blood vessels in myocardium with inflammatory cells also there was hypertrophy and sometimes hyalinized wall of small blood vessels of heart in group B and focal myocardial necrosis (Figure-7), the hepatic sections of group A & B revealed severe dilation of central and portal veins and sinusoidal capillaries with perivascular cuffing (Figure-8), The hepatocytes severely degenerated and necrotized (Figure-9), enlargement of kupffer's cells (Figure-10) and infiltration of MNCs as focal infiltration (Figure-11).

DISCUSSION

The comet assay is an important and touchy instrument for identifying hereditary harm in singular cells (Alvarez *et al.*, 2001) detailed a convention that improves this test in Tradescantia stamen cores. Hereditary harm initiated by glyphosate has been accounted for reported (Vera-Candiotti *et al.*, 2013) and the comet assay has been used to demonstrate genotoxicity in fish hepatic cells and Tradescantia nuclei (Guilherme *et al.*, 2012).The percentages of DNA damage estimated by SGEF, in present results due to oral administration of glyphosate may agree with Guyton *et al.*, (2015), was based on two experiments where mice had developed malignant tumors as a result of exposure to glyphosate alone, one revealing a rare case of cancer (kidney), which is extremely important in assessing human risk. Furthermore, the experts took into consideration the strong evidence of genotoxicity (DNA damage) and oxidative stress (tissue/cell damage) in humans and laboratory animals following exposure to glyphosate-pesticides and its



**Ahmed Tayyeh Hattat and Zainab Ismail Ibrahim**

metabolites. Zúñiga, (2001) and Poletta *et al.*, (2009), they are demonstrate that glyphosate is genotoxic, contingent upon the time and focus used.

Wink *et al.*, (1995) and Muriel, (1998), shows that glyphosate increases the levels of nitric oxide (NO) and proinflammatory cytokines such as TNF- α than Roundup. NO can function as a cellular antioxidant and protect against ROS induced toxicity while TNF- α plays an important role in regulating the inflammatory responses (Elenkov and Chrousos, 2002). Roundup or glyphosate produced an increase in TNF- α production during treatment time that explained the infiltration of mononuclear cells in pulmonary tissue of the present study and peribronchial or in diffuse form also between the myocardial fibers to cause degeneration and necrosis.

Hepatic effects of glyphosate have been known since the 1980s, among them the ability of glyphosate to disrupt liver mitochondrial oxidative phosphorylation from 15 mg/kg B.W in rats (Olorunsogo *et al.*, 1979), from that time until ours the glyphosate effects appeared severe in hepatic lobules from the degeneration and necrosis of hepatocytes with 250 and 500 mg/kg B.W, mononuclear cells infiltration as focal areas in responded to injured cells by the stimulation of T_H cells, cytokines released by Kupffer cells in response to toxic chemicals. This can explain the leakage of enzymes from liver; this detects the liver injury by glyphosate and Roundup. However, excessive amounts of the cytokine are released into circulation in response to infection, inflammation and other environmental insults, often resulting in tissue injury (Jing *et al.*, 2008).

The liver and kidneys are among the first of the final stage of a processes of alimentary intoxications, increases the frequency of chronic kidney disease among farmers (Jayasumana *et al.*, 2015) possible kidney and liver effects of GlyBH exposures is a matter of concern.

REFERENCES

1. Guyton KZ, Loomis D, Grosse Y, *et al.* (2015). Carcinogenicity of tetrachlorvinphos, parathion, malathion, diazinon, and glyphosate. *The Lancet Oncology*, 16: 490 – 491.
2. Jayasumana, C., Paranagama, P., Agampodi, S., Wijewardane, C., Gunatilake, S. Siribaddana, S., (2015). Drinking well water and occupational exposure to Her Bicides is associated with chronic kidney disease, in Padavi-Sripura, Sri Lanka Environ. Health 14, 6.
3. Olorunsogo, O.O., Bababunmi, E.A., Bassir, O., (1979). Effect of glyphosate on rat liver mitochondria in vivo. *Bull. Environ. Contam. Toxicol.* 22, 357e364.
4. Alvarez C, Santerre A, Zúñiga G, Torres O, Padilla E and Feria A (2001) Evaluation of the genotoxic activity of maleic hydrazide, ethyl methane sulfonate, and N nitrosodiethylamine in Tradescantia. *Salud Pública Méx* 43:563-569.
5. Benbrook, C. M. (2016). Trends in glyphosate herbicide use in the United States and globally. *Environmental Sciences Europe*, 28(1), 1–15. <https://doi.org/10.1186/s12302-016-0070-0>
6. Dhawan, A., Ph, D., Bajpayee, M., Sc, M., Pandey, A. K., & Parmar, D. (2007). PROTOCOL FOR THE SINGLE CELL GELELECTROPHORESIS / COMET ASSAY FOR RAPID GENOTOXICITY ASSESSMENT Prepared by: *Electrophoresis*, 17(3), 1–10.
7. EFSA. (2012). Modification of the existing MRL for glyphosate in lentils. *European Food Safety Authority Journal*, 10(1), 1–25. <https://doi.org/10.2903/j.efsa.2012.2550>.
8. Guilherme, S., Gaivão, I., Santos, M. A., & Pacheco, M. (2012). DNA damage in fish (*Anguilla anguilla*) exposed to a glyphosate-based herbicide - Elucidation of organ-specificity and the role of oxidative stress. *Mutation Research - Genetic Toxicology and Environmental Mutagenesis*, 743(1–2), 1–9. <https://doi.org/10.1016/j.mrgentox.2011.10.017>
9. Simmons L:(2010). Herbicide Safety.. [www.ehow.com/ way_5417453_herbicide-safety.html](http://www.ehow.com/way_5417453_herbicide-safety.html) (accessed August 2010).




Ahmed Tayyeh Hattat and Zainab Ismail Ibrahim

10. FAO/WHO Joint Meeting on Pesticide Residues (2005) Evaluation of glyphosate (158) Available at http://www.fao.org/agriculture/crops/core_themes/theme/pests/lpe/lpe-g/en/
11. Vera-Candioti J, Soloneski S and Larramendy ML (2013) Evaluation of the genotoxic and cytotoxic effects of glyphosate-based herbicides in the ten spotted live-bearer fish *Cnesterodon decemmaculatus* (Jenyns, 1842). *Ecotoxicol Environ Saf* 89:166-173.
12. Zúñiga GG (2001) Sistemas de detección de daño genético. In: Álvarez C (ed) *Genética, Ambiente y Salud*. 2nd edition. Universidad de Guadalajara, Guadalajara, pp 127-150..
13. Singh N, McCoy M, Tice R and Schneider L (1988) A simple technique for quantitation of low levels of DNA damage in individual cells. *Exp Cell Res* 175:184-199..
14. Poletta, G. L., Larriera, A., Kleinsorge, E., & Mudry, M. D. (2009). Genotoxicity of the herbicide formulation Roundup®(glyphosate) in broad-snouted caiman (*Caiman latirostris*) evidenced by the Comet assay and the Micronucleus test. *Mutation Research - Genetic Toxicology and Environmental Mutagenesis*, 672(2), 95–102. <https://doi.org/10.1016/j.mrgentox.2008.10.007>.
15. SAS. (2012). *Statistical Analysis System, User's Guide*. Statistical. Version 9.1th ed. SAS. Inst. Inc. Cary. N.C. USA.
16. Olorunsogo OO, Bababunmi EA, Bassir O. (1979). Effect of glyphosate on rat liver mitochondria in vivo. *Bull Environ Contam Toxicol*. 1979;22:357–64..
17. Muriel, P., (1998). Nitric oxide protection of rat liver from lipid peroxidation, collagen accumulation, and liver damage induced by carbon tetrachloride. *Biochem. Pharmacol*. 56, 773–779.
18. Jing, Y., Shishkov, A., Ponnappa, B.C., (2008). Inhibition of tumor necrosis factor alpha secretion in rat Kupffer cells by siRNA: in vivo efficacy of siRNA-liposomes. *Biochim. Biophys. Acta* 1780 (1), 34–40.
19. Elenkov, I.J., Chrousos, G.P., (2002). Stress hormones, proinflammatory and anti-inflammatory cytokines, and autoimmunity. *Ann. N. Y. Acad. Sci*. 966, 290–303.
20. Wink, D.A., Cook, J.A., Pacelli, R., Liebmann, J., Krishna, M.C., Mitchell, J.B., (1995). Nitric oxide (NO) protects against cellular damage by reactive oxygen species. *Toxicol.Lett*. 82/83, 221–226.
21. Dhawan, A., Ph, D., Bajpayee, M., Sc, M., Pandey, A. K., & Parmar, D. (2007). PROTOCOL FOR THE SINGLE CELL GEL ELECTROPHORESIS / COMET ASSAY FOR RAPID GENOTOXICITY ASSESSMENT Prepared by: *Electrophoresis*, 17(3), 1–10.
22. Luna and Lee, G. (1968). *Manual of Histopathological Staining Methods of the Armed Forces Institute of Pathology*. 3rd Edn., McGraw-Hill, New York,.

Table-1: Glyphosate composition / 1000 ml are listed below according to manufacturer's industry

SUBSTANCE	CONCENTRATION
glyphosate	360 g Per 1000 ml
Salt isopropyl amine glyphosate	480g Per 1000 ml



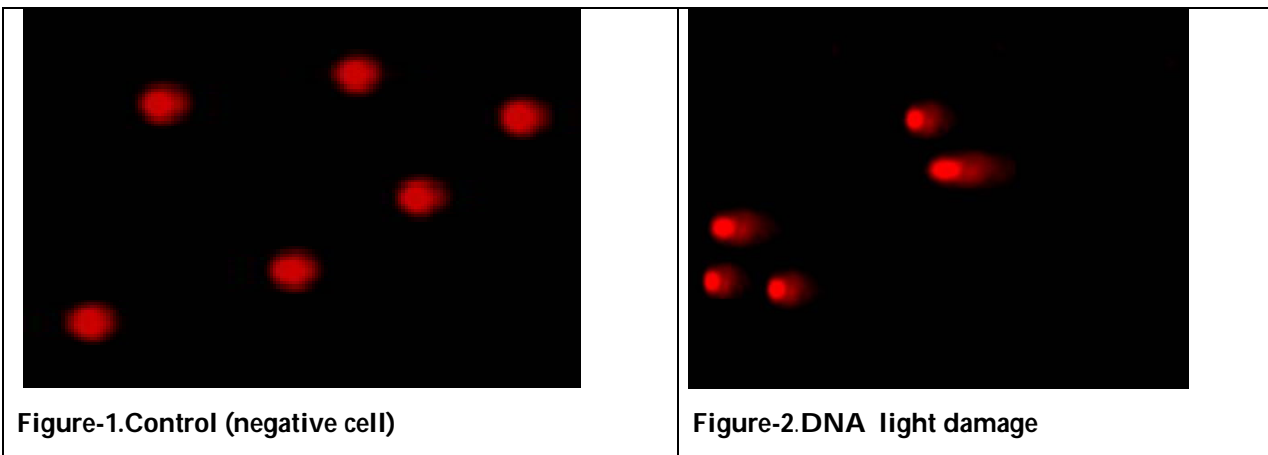


Ahmed Tayyeh Hattat and Zainab Ismail Ibrahim

Table- 2: single gel-electrophoresis (comet assay) to investigate the genotoxicity of Glyphosate in A&B on DNA of whole blood compared with control group.

Groups	Mean ± SE					
	Comet length	Comet area	%DNA in head	Tail area	%DNA in tail	Tail moment
C	35.13±1.86 a	664.36± 103.63 a	82.94 ± 2.10 a	76.89 ± 0.70 a	17.06 ± 2.10 a	0.628 ± 0.04 a
A	68.80±10.25 a	2455.62±782.50 a	65.46 ± 3.91 a	475.51±64.85 a	34.53 ± 3.91 a	5.58 ± 1.87 a
B	40.93±20.49 a	1365.72±684.99 a	27.94 ± 14.20 b	558.97±281.69 a	38.72 ± 19.53 a	8.41 ± 4.30 a
LSD value	56.97 NS	2586.90 NS	36.71 * NS	717.87 NS	49.55 NS	11.65 NS

* (P<0.05), NS: Non-Significant.
Means having with the different letters in same column differed significantly





Ahmed Tayyeh Hattat and Zainab Ismail Ibrahim

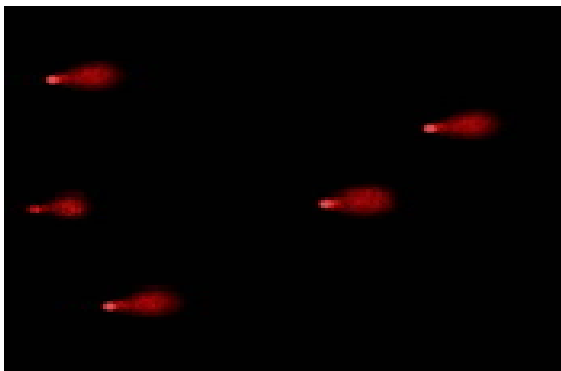


Figure-3. DNA more damage

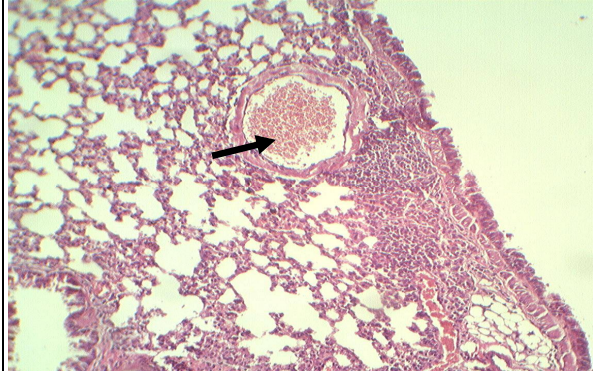


Figure-4: Histomicrograph of lung in mouse treated with glyphosate (250 mg/kg)/ daily; with broncho interstitial pneumonia and necrotic bronchial epithelium (—→) seen, (H&E stain, 10X

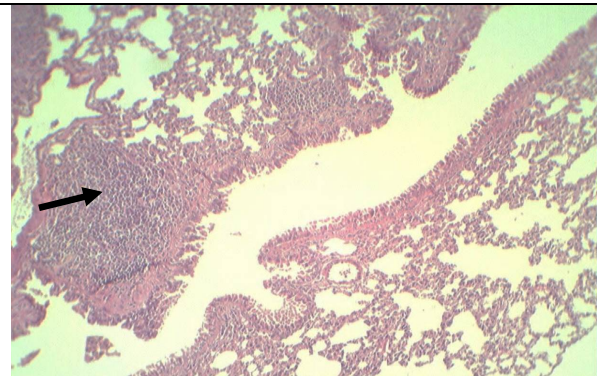


Figure-5: Histomicrograph of lung in mouse treated with glyphosate (250 mg/kg)/ daily; showed focal MNCs (—→) peribronchial, (H&E stain, 10X).

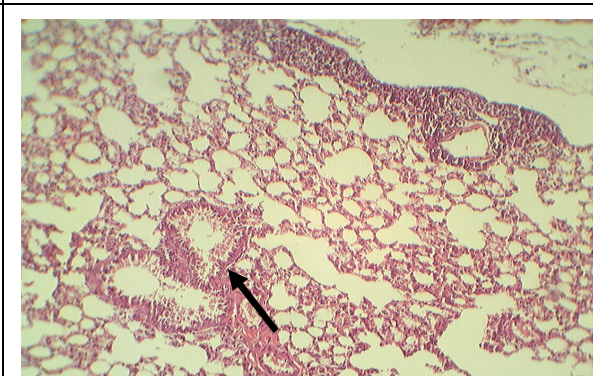


Figure-6: Histomicrograph of lung in mouse treated with glyphosate (500 mg/kg)/ daily; showed pleuritis (—→) , (H&E stain, 10X).

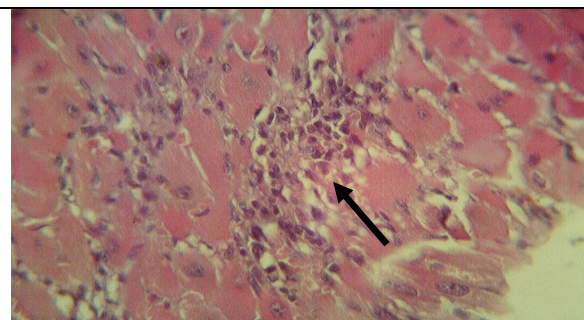


Figure-7: Histomicrograph of heart in mouse treated with glyphosate (500 mg/kg)/ daily; showed focal myocarditis with MNCs infiltration (—→), (H&E stain, 40X).

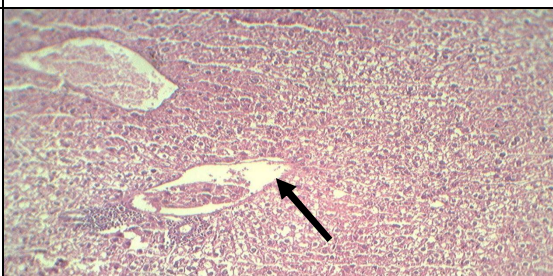


Figure-8: Histomicrograph of liver in mouse treated with glyphosate (250 mg/kg)/ daily; showed severe central vein and dilated portal vein contained inflammatory cells (—→) and focal MNCs periductal, (H&E stain, 10X).





Ahmed Tayyeh Hattat and Zainab Ismail Ibrahim

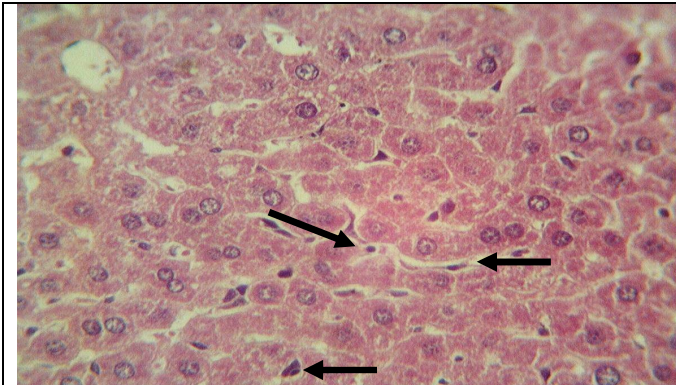


Figure-9: Histomicrograph of liver in mouse treated with glyphosate (250 mg/kg)/ daily; showed enlargement of kupffer's cells (→), (H&E stain, 40X).

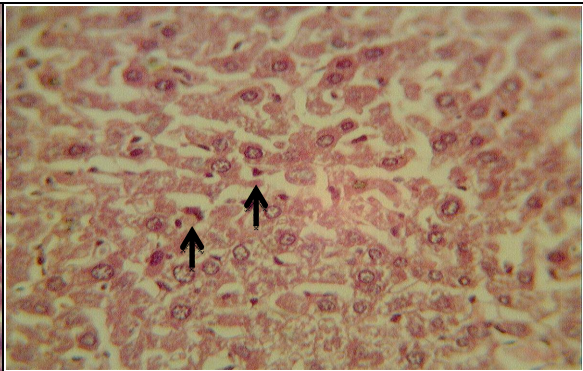


Figure-10: Histomicrograph of liver in mouse treated with glyphosate (500 mg/kg)/ daily; severe dilation of sinusoids and enlarged kupffer's cells (→), (H&E stain, 40X).

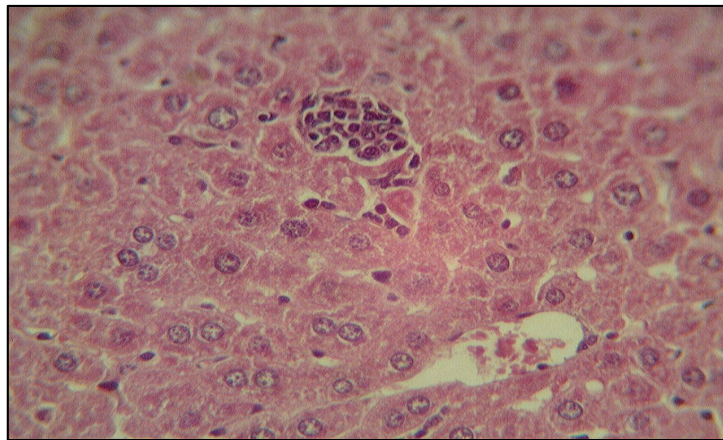


Figure-11: Histomicrograph of liver in mouse treated with glyphosate (500 mg/kg)/ daily; small focal MNCs aggregation (→), (H&E stain, 40X).





RESEARCH ARTICLE

Anatomical and Chemical Study of (*Scorpiurus muricatus* L.)NisreenSabbarHashan^{1*}, Dhifaf Khalil Salam² and Aiyemen Ahmed A.K.AL-Abassi³¹Collage of Education for Pure Science Biology, University of Diyala, Iraq.²Biology Collage of Science, University of Diyala, Iraq.³Education Directory of Diyala, Iraq.

Received: 14 July 2018

Revised: 16 Aug 2018

Accepted: 19 Sep 2018

Address for Correspondence*NisreenSabbarHashan**Collage of Education for Pure Science .Biology,
University of Diyala, Iraq.

This is an Open Access Journal / article distributed under the terms of the **Creative Commons Attribution License** (CC BY-NC-ND 3.0) which permits unrestricted use, distribution, and reproduction in any medium, provided the original work is properly cited. All rights reserved.

ABSTRACT

The objective of the study is to know the anatomical and chemical components of *Scorpiurus muricatus* L. of the legume family. The anatomical study showed that the anatomical characteristics of the leaves and necks of the leaves and the stems of the plant are of remarkable importance, such as the spindle cells of the blades of leaves skin and the serrated dermis layer, which are encrusted by the torn or convex crevices of the stem cells. The wood texture is characterized by an inverted conical, squared and ovarian cells of thoracic skin surrounded by denture metal. The chemical study of the Alcoholic extract of air parts of the plant by using the chromatography method of gases - GC-MS is the most important chemical compounds in it. 80 chemical compounds that reflect the importance of therapeutic and medicinal plants, and the value of fodder and its importance in improving soil fertility and quality.

Keywords: *Scorpiurus muricatus*, Iraqi plant, fabaceae, Anatomical study and chemical study.

INTRODUCTION

Biodiversity is a national natural resource that is no less important than other natural resources and is a renewable resource for any country that provides sustainability and survival (Wahhab et al.). Wild plants are one of the most important aspects of this diversity because they are at the forefront of the plants that are invested in grazing (As it is spread in the Iraqi mountains and fields with mud clay soil and have a high nutritional value palatable by sheep and cows (Khatib, 1978). As well as food production such as (black bean, beans, cowpea, lentils, pistachio and others), And animal feed processing Such as jute and alfalfa including wild plant and some of decorative plants such as bauhinia, acacia, gum extracts, medical drugs and aromatic products, a source of wood and dyes (Musawi, 1987) and other economic fields. The rank of corneas or foliage is one of the broadest plants of dicotyledons and the most notably economically, with some 700 species and 1800 species (Habib, 2013). The corneas are composed of three families: the mimosa, the Sababa and the Fabaceae family, which is the second largest family among flora after the compound family. It has 550 sexes and 300 types. It has a global presence in Iraq. 24 species include 300 wild species



**NisreenSabbarHashan et al.**

and 76 species are cultivated for economic purposes. (Alkatib,2000). In addition to its importance in protecting the land from the encroachment of desertification and improve the quality of the fact that its roots consist of coexisting contract with raazoubiom bacteria which proving atmospheric nitrogen as proven in the soil about 250 kg of atmospheric nitrogen per acre in Chapter (Habib 2013), which raises their use in agricultural courses fertilizer (Green), which contributes to enriching the soil reserves of nitrogen and raising plant productivity. Despite the great importance of the legume family plants, there are some wild species classified in the Iraqi flora and the lowlands of Iraq (Rechinger), (1964), but did not get the specialized study, including the plant *Scorpiurus muricatus* L. locally known in Iraq by several names are Khuzima, , Siege, Mametik (Chakravarty, 1976) and Townsend and Guset (1974). (Al-Mahdawi, 2014), also called locally in the Levant, in the name of Scorpio's sin (Habib, 2013) and Libya in the name of the Jambian Bean (and the free encyclopedia of Wikipedia).

MATERIALS AND METHODS

The selected plant samples were collected to study *Scorpiurus muricatus* L. from the gardens of the University of Diyala in a clear atmosphere during the period of flowering between (March - June). After filming the fields were healthy and free of infections and fungal diseases and measured their parts Metric ruler for the purpose of describing the appearance and after shaking and washing the dust. The study was divided into two sections of the anatomical study, which were based on soft samples only. The vertical sections of leaf leaves were found in the method (Thammathaworn, 1996). The stems and stalks were studied according to the method (AL-Khafaji, 2004), and then studied the layers of these sections using the microscope. And the other part of the samples suspended in the shade for several days at room temperature until dry and conducted the chemical study of GC-MS in the laboratories of Ibn al-Bitar Center - Industrial Research and Development Authority and was extracted based on the method Alwan. Et al (2015), with some Modifications including:

Chemical extraction

Extract the plant with high purity ethyl alcohol for the analytical test by following the these steps:

- 1 - dry the total vegetation (roots, stems and leaves) and grinding with an electric mill.
2. Take 1 g dry powder of the plant and add 20 ml of 100% pure ethanol.
3. After shaking in the shaking incubator for 8 hours and 37-30 ° C on the strength of 9-6 cycles and then depositing for 32 hours.
4. Apply the filtration with the filter paper and leave the filter to dry at room temperature.
5. Dry matter mixed with special alcohol for HPLC.

Analysis by gas chromatography device - GC-MS mass spectrometer

Four microliters of ethanoic extract were injected using a precision silicone syringe. Soon after the injection, the temperature of the source of the device reaches 350 m while the sample is evaporated at a temperature of 150 m. Helium gas, an inert gas, is used to carry the material to represent the mobile phase to drive material to a column whose length varies from one device to another. In this study, the length of column 60 m, which contains different materials in the polar in the Stationary phase, the materials with the lowest molecular weight of the column first, followed by the materials with the largest molecular weight, then move all the materials to the detector after exposure to fixed voltage difference of 70 V to diagnose the compounds to their components, leaving an electronic signal to detect the compound, and the greater the concentration of the compound, the greater the signal. Then calculate the weight of its molecular weight through the mass-to-charge ratio (M / Z) where the constant Z (70 volts) is obtained from the graph. The diagram is then plotted by the GC-MS calculator, which is called the scatter diagram. The y axis represents the signal intensity to determine the element in the injection sample and the x-axis represents



**NisreenSabbarHashan et al.**

the retention time. The identification of the compounds is compared with the compounds stored in the computer library GC-MS device.

RESULTS

Morphological description of *Scorpiurus muricatus* L.

Herbaceous plant, up to 15-40 cm in diameter, is covered with concentrated hair follicles. The leaves are green, elongated and spherical. Its sharp peaks contain a cluster nectar containing (1-4) flower, pink flowers or red side-by-side symmetry. The coriander is made up of five large petals, the Standard Flag, two separate wings, and two interiors keel. The pustule is simple, consisting of a single high-grade single-chamber ovary and a marginal marigold. It has one stylus and one stigma. The fruit is oddly curled, sometimes free of capillaries, and sometimes the ribs are smooth and foreign, with long, thick spines (Kazem et al., 2016) First: Anatomical study of *Scorpiurus muricatus* L.

Blade leaf

The results of the anatomical study showed that the vertical sections of blade leaves (Fig. 1) were skin-shaped and had a mean thickness of 0.99 μm , The outer layer of the skin is coated with a slightly serrated layer of thickness (5.94-9.93) micrometer. The bottom layer of the epidermis reaches the top of the skin is a layer of 11.88 micrometers. The spongy layer consisted of semi-scattered layers of three to four layers with a thickness of 24.75 to 27.72 micrometers. It was also characterized by a lack of interstitial space for both layers. The middle race contained one-pack vesicles with two oval. For the lower skin, the cells are oval to a length of thickness of (1.98) micrometer. The current study also showed that the dimensions and shapes of the cells vary and on the upper and lower surfaces of the paper.

Stem

The study showed that the general shape was an oval with convex or concave projections (Fig. 2) It is externally encrusted with a peritoneal cilia and is formed by protrusions and is formed from the skin with a thickness of 5-7.5 micrometers, which is peripheral to the layer of skin cells of varying size and shape. And oval are longitudinal or square, and when the nuts are your name of the cells that are above the cells Chlorenchyma containing chloroplast, which consists of two layers and the average thickness (4.95) micrometer followed by two to three ribbons of coliform cells with function supporting both legs and other young areas such as stalks and middle sweat areas (Mcmah et al., 2011) with a thickness of 9.9-12.87 μm . The interior of the veneer area and the wood texture was clear and distinct as it filled a wide area of the beam and had a thickness of 12.87 -29.7 μm and was cone-reversed. The inner bark of the bark is arranged by an inverted pyramidal pyramid and it's thickness 9.9 - 29.7 micrometers (Figure 6). The number of beams in the cross section was between six and fifteen packages, followed by the area of the pulp that occupies the center in the sections.

Petiole

The leaves in the type under study are of the type mobile on the petiole so I took the cross section petiole (Fig. 3). The skin cells are square to oval-shaped oval and have a thickness of 1.98 -2.97 micrometers. The skin is surrounded by a layer of toothy cottle. Below the skin layer are two to four rows of the bronchial tissue cells, which are more prevalent than the base of the suiq and are large in size in the middle and are small towards the two sides of the skin and these cells are irregular in shape. As for the number of vascular bundles, they are classified according to the part of the section. In general, these numbers are lower. The lower the number of beams, the more the number of beams is three to six. The number of vascular units of wood is 3-10 rows, and the beams are oval.





NisreenSabbarHashan et al.

The chemical study of *Scorpiurus muricatus* L.

DISCUSSION

The results of GC-MC analysis led to the identification of number of compounds from the ethanolic extract of Iraqi *Scorpiurus muricatus* L. Plant GC-MC chromatogram showed 80 peaks, indicating the presence of 80 compounds (figure -1) and (table -1), the concentration of this secondary metabolites are varying from plant to plant belong to the same genus and even in the different parts of the same plant (Abdul et al, 2009), this is due to many factors like environmental heterogeneity (pauses et al, 2001), or high complexity and heterogeneity of soil create a big variation in the chemical constituents even in the same country (Karlovsky, 2008). In the present study methanolic extract of Iraqi *Scorpiurus muricatus* L. analyzed appeared presence of different chemical constituents which could be medicinal and economic value and antioxidant activity of this plant as well as evaluation their safety or otherwise (toxicity) for human and other animal use.

REFERENCES

1. Townsend, C.C. and E. Guest (1974). Flora of Iraq. Vol 3: Leguminales, Ministry of agriculture and Agrarian Reform, Baghdad, Iraq. 662pp.
2. Rechinger, K.H (1964). Flora of Lowland Iraq. Weinheim Verlag Von J. Cramer. New York Hofener Co : 685 pp.
3. McMahon, M.J.; Kofranek, A.M. and Rubatzky, V.E (2011) Plant science hall: 674pp.
4. Alwan et al (2015).
5. Chakravarty, H.L. (1976). Plant Wealth of Iraq, (Dictionary of Economic Plants). Vol 1: Ministry of agriculture and Agrarian Reform, Baghdad, Iraq, 505 pp.
6. Alwan et al (2015).
7. Thammathaworn, A. (1998). Handbook by paraffin method. Department of biology Faculty of science, KhonKaen University, Thailand.
8. AL-Kafaji, B.A. (2004). Taxonomic study of *Crepis* L. (Compositae) in Iraq. M.Sc. thesis. College of Science Univ. Babylon. Iraq (In Arabic).
9. Abdul K.K.; Palwasha A.; Ayeesha M.; Safdar Ali K.; Rasool B.T.: Response of plant parts and age on the distribution of secondary Metabolites on plants found in Quetta. Pak J Bot 2009; 41 (5): 2129-35.
10. Pausas J.G.I., Austin M.: Patterns of plant species richness in relation to different environment: An appraisal Journal of Vegetation Science 2001; 12: 153-293 p.
11. Karlovsky P.: Secondary Metabolites in Soil Ecology. Volume 14, 1st ed., Springer-Verlag Berlin, Heidelberg, 2008, 293 p.

Table 1. phytochemicals identified in the methanolic extracts of *Scorpiurus muricatus* L.

Peak #	R.Time	Area%	Name
1	7.798	0.03	Disiloxane, 1,3-diethoxy -1,1,3,3-tetramethyl-
2	7.949	0.04	2-p-Tolylisoindole-, 3-dione
3	9.343	2.57	Benzyl chloride
4	11.702	0.01	Benzyl chloride
5	16.449	0.09	1-Butanole, 3-methyl-, formate
6	16.622	0.06	Propanoic acid
7	18.370	0.15	Benzene, 2-methoxy -1,3,4-trimethyl
8	19.448	0.06	1-(3,6,6-Trimethyl -1,6,7,7a-tetrahydrocyclopenta [c]pyran-1-yl)ethanone
9	20.804	0.16	1-Decanol, 2-hexyl-
10	21.136	0.24	Oxirane, [(dodecyloxy)methyl]-





NisreenSabbarHashan et al.

11	21.475	0.14	4-Trifluoroactoxyhexadecane
12	21.633	0.50	Fluoroaceticacid,dodecyl ester
13	22.372	11.03	1- Dodecanamine,N,N-dimethyl-
14	25.318	0.10	1-Methyl-3,6-diazahomoadamantan-9-One
15	25.966	0.12	Silicic acid,diethylbis (trimethylsilyl) ester
16	26.508	0.24	Cinnamaldehyde, .alpha.-pentyl-
17	26.961	0.26	Pentafluoropropionic acid ,undecyl ester
18	27.262	0.53	Pentafluoropropionic acid ,dodecyl ester
19	27.948	5.11	1-Tetradecanamin, N,N-dimethyl-
20	28.385	0.02	6-Methyl-2-tridecanone
21	28.611	0.11	Hexatriacontylpentafluoropropionate
22	31.022	1.77	Hexanoic acid,3-fluorophenyk este
23	31.489	0.24	.alpha.-D-Glucopyranose,4-o-.beta.-D-galactopyranosyl-
24	31.761	0.40	Didodecyl phthalate
25	31.866	0.29	Methyl 4,6 -ethylidene-.alpha.-d-galactopyranoside
26	32.017	0.55	Acetylcysteine
27	32.401	0.16	3,6,9,12-Tetraoxahexadecan-1-o1
28	32.469	0.20	Ethylamine ,N,N-dimethyl-2-((o-methyl-.alpha.-phenylbenzyl)oxy)-,N-oxide
29	32.793	0.70	Lidocaine
30	32.883	0.47	Cis-4-Hydroxy-L-proline
31	33.124	0.40	Methoxyacetic acid,4-tridecyl ester
32	33.237	0.73	Mythyltridecyl ether
33	33.622	0.61	Oxirane,2-methyl-3-propyl-,cis-
34	33.780	0.37	N-Isopropoxy -2-carbomthoxyaziridine
35	34.006	0.60	Octanamide,N,N-dimethyl-and 3-Bromobutyric acid
36	34.187	0.71	N-Isopropoxy-2-carbomethoxyaziridine
37	34.292	0.54	Undecanoic acid,2,4,6.-trimethyl -.methyl ester
38	34.579	1.52	Pentadecanoic acid
39	34.669	1.49	n-Hexadecanioc acid
40	34.971	1.77	Decanioc acid ,3- methyl-
41	35.362	2.52	Valeric acid ,2,3-epoxy -3,4-dimethyl -,ethyl ester ,cis-
42	35.897	1.84	3-o-Methyl -d-glucose
43	36.169	1.44	2-Trimethylsilyl-1,3-dithiane
44	36.704	8.13	1,3,4-oxadiazole-2-(3H)-thione,5-2-bromophenyl)-3-benzyl(methyl)aminomethyl-
45	37.254	0.52	4-o-Methylmannose
46	37.518	0.26	6- Ethoxy-6-methyl-2-cyclohexenone
47	37.623	0.31	6- Ethoxy-6-methyl-2-cyclohexenone
48	37.924	0.80	Methacrylicacid,hexadecyl ester
49	38.015	0.34	Oxirane,2-methyl-3-propyl-,cis-
50	38.105	0.34	Methacrylic acid ,nonadecyl ester
51	38.173	0.31	Methyl 7,9 -tridecadienyl ether
52	38.248	0.38	Methyl tridecyl ethers
53	38.459	0.77	Propanioc acid,3-methoxy-.methylester and tetra-Hexadecanethiol
54	38.572	0.74	Triethylene glycol monododecyl ether
55	38.829	0.95	2-Nonadecanol
56	39.115	1.02	Hexanal ,2- methyl-
57	39.364	1.12	Triethylene glycol monododecyl ether





NisreenSabbarHashan et al.

58	39.575	0.29	2-[2-[2-[2-[2-(Trimethylsilyloxy)ethoxy]ethoxy]ethoxy]ethoxy]ethoxy]ethanol
59	39.680	0.29	2-[2-[2-[2-[2[2[2]2-(2-methoxy ethoxy)ethoxy]ethoxy]ethoxy]ethoxy]ethoxy] ethoxy] ethoxy] ethoxy]ethoxy]ethanol
60	39.816	0.68	Triethylene glycol monododecyl ether
61	40.200	1.27	Octyl -.beta .-D-glucopyranoside
62	40.366	3.05	Benzene ,1- ethynyl -3-methoxy – andBenzene,1- ethynyl-4-methoxy-
63	40.833	0.44	n-Decanoic acid
64	41.933	0.54	Cyclohexyl -15- crown-5
65	42.589	0.98	Monomethyl –trimethylene-.beta.-sedoheptitol
66	43.395	1.40	Hexaethylene glycol
67	43.847	3.31	Glycerol 1-palmitate
68	44.028	0.96	Bis (tridecyl)phthalate
69	44.284	0.87	3,6,9,12,15,pentaoxanonadecan-1-o1and Heptaethylene glycol
70	44.473	0.78	Heptaethylene glycol monododecyl ether
71	44.714	0.43	Pentaethylene glycol monododecyl ether
72	44.854	0.55	Hexaethylene glycol
73	45.204	0.30	2-[2-[2-[2-[2[2(2-methoxy ethoxy)ethoxy]ethoxy]ethoxy]ethoxy]ethoxy]ethoxy] ethoxy]ethanol
74	45.656	0.84	Inden,1,3-bis(2-ethylhexyl)-and 6-Methyl -2-tridecanone
75	45.882	0.18	1- Naphthalenol,1,2,3,4,-tetrahydro-,acetatee
76	46.191	1.02	1H-Indole,4-Methyl-
77	46.477	2.45	n-Decanoic acid
78	49.047	1.20	22-Tricosseonic acid
79	50.870	0.26	1,4,7,10,13,16- Hexaoxanonadecane,18-propyl-
80	53.101	0.22	2-[2-[2-[2-[2-[2-[2-[2-(Trimethylsilyloxy)ethoxy]ethoxy]ethoxy] ethoxy] ethoxy] ethoxy] ethoxy]ethoxy]ethoxy] ethoxy]ethanol

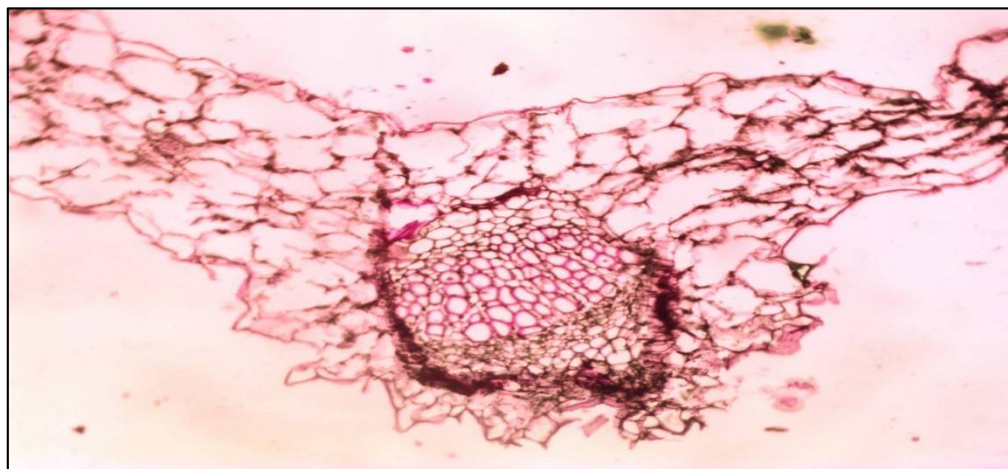


Fig.1.vertical sections of blade leaves





NisreenSabbarHashan et al.

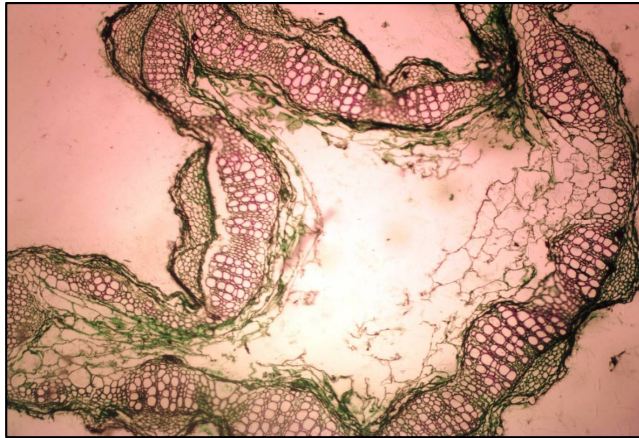


Fig. 2. Oval with concave projections

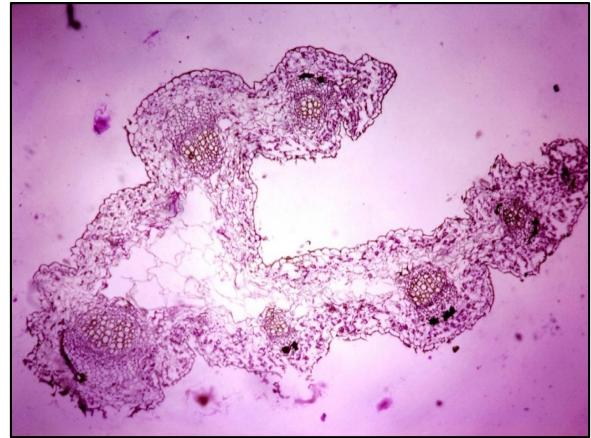
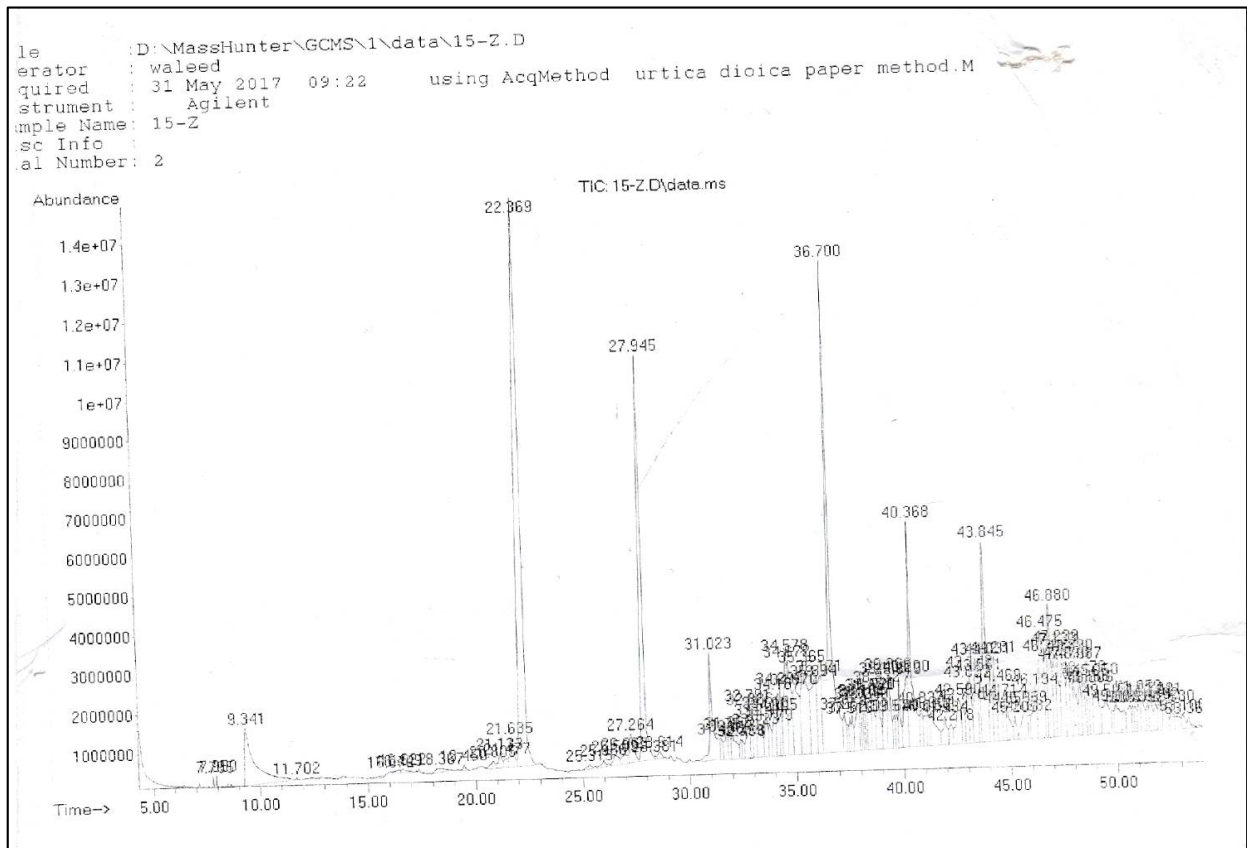


Fig 3. Cross section of petiole





RESEARCH ARTICLE

Fabrication of Functionalized Single Wall Carbon Nanotubes Gas Sensor

Waleed k. Mahmood*, Asama N. Naje and Murad Mohammed Kadhim

Department of Physics, College of Science, University of Baghdad, Iraq.

Received: 10 July 2018

Revised: 18 Aug 2018

Accepted: 20 Sep 2018

Address for Correspondence*Waleed k. Mahmood**

Department of Physics,

College of Science,

University of Baghdad, Iraq.

E-mail : waleed.kh@yahoo.com, Naje.as75@gmail.com, muradmohammed56@gmail.com



This is an Open Access Journal / article distributed under the terms of the **Creative Commons Attribution License** (CC BY-NC-ND 3.0) which permits unrestricted use, distribution, and reproduction in any medium, provided the original work is properly cited. All rights reserved.

ABSTRACT

Functionalized single wall carbon nanotubes (F-SWCNTs) films have been utilized to the manufactured hydrogen gas sensor. CNTs films have been deposited on porous substrate by drop method. The sensor shows high sensitivity to hydrogen gas. The F-SWCNTs gas sensor shows high sensitivity ($S = 12\%$) at R.T. with response time 11sec.

Keywords: F-SWCNTs; reducing gas; sensitivity; response time; silicon.

INTRODUCTION

Chemical gas sensors have been widely used to recognize and monitor various gaseous analytes in numerous applications including flammable and toxic gas detection, environmental monitoring, space exploration, industrial emission, public security, medical diagnosis and food quality control[1-2]. Gas sensors with high sensitivity and selectivity are required for leakage detections of explosive gases such as hydrogen, and for real-time detections of toxic or pathogenic gases in industries [3-4]. In gas sensors, the dynamic component that is sensitive to the target gas molecules is the key part and thus receives intensive attention. For example, after realizing the resistance of some semiconductor materials can be drastically changed by the presence of gas molecules, many works have been directed to research them in gas sensors [5]. Upon exposure to certain gases, the change in the properties of CNTs or CNTs-based composites can be detected by various methods. As a result, CNTs-based gas sensing systems and the theoretical analyses of gas adsorption and collision effects on the nanotubes have been the subjects of intense research [6-7].





Waleed k. Mahmood *et al.*

MATERIALS AND METHODS

Materials

In this work, (2x2 cm²) dimensions primary n-type silicon wafer substrates were thoroughly cleaned to decontaminate their surface from any available stains and dirt. To prepare CNT sample, 0.010 g of CNT was dispersed in Dimethylformamide (DMF). A magnetic stirrer was incorporated for this purpose for 15 minutes, followed by 2 hour sonication. The obtained solution was used for film deposition on porous silicon by the drop casting method.

Characterization

X-ray diffraction (XRD) patterns of the PFO (EFO) products were recorded at a XRD-6000 X-ray diffract meter (XRD, Shimadzu, Kyoto, Japan) by using Cu K radiation (λ : 1.54056 Å).

RESULTS AND DISCUSSION

Fig.1 displays the XRD patterns for the SWCNTs powder. The diffraction pattern SWCNTs appeared at 2θ of 26° and 44.5°. The 2θ peaks correspond to (002) and (100) reflection planes or also known as the interlayer spacing between adjacent graphite layers and these peaks reflect hexagonal structure. This is in agreement with results reported by other researchers [8]. Table (1) shows the crystalline size of SWCNTs from X-ray diffraction pattern and by using Scherer's formula Eq formula:

$$D = (0.89\lambda) / (\beta \cos\theta) \dots \dots \dots (1)$$

Where λ is the X-ray wavelength (1.54056 Å), θ is the Bragg diffraction angle and β is the peak width at half maximum. The sensitivity of SWCNT-gas sensor is defined as the resistance (or conductance) difference between after and before gas exposure $[(R_m - R_0)/R_0]$, where R_m and R_0 are the measured and the initial resistances, respectively. The sensitivity S% of CNTs was measured upon exposure to different gases, the test performed at 1:1 (air: gas) mixing ratio and at room temperature. It is shown that the sensitivity of F-SWCNT for H₂ (12%). The observed resistance shown in Fig. 1 increases while uncovering the F-SWCNT networks to H₂, which can be explained as follows: In the case of electron-donating induced spillover (e.g., reducing gases, H₂, NH₃, CO), these energy levels are likely donor gap states. In the donor gap states, on the other hand, electrons can be transport from the energy state to a conduction band of the p-type CNT, followed by recombination between majority hole-carriers and transferred electrons, decreasing the free net (hole) charge density. This procedure results in increased resistance of the CNTs in agreement with other researchers. From the gas sensing data, the result was expected and can be explained by the following: an H₂ molecule is reduced agent that donates an electron to another species. Therefore, H₂ can play a role as an electron-donor and/or hole-acceptor. When the CNT gas sensor was exposed to H₂, electrons were transferred from H₂ molecules to the CNTs. H₂ then donated its electrons to the valence band of the CNTs, thereby decreasing the number of holes by recombination, reducing the conductivity of CNTs, and increasing electrical resistance. Therefore, it is reasonable to assume that CNTs are a p-type semiconductor.

CONCLUSION

The best performance of F-SWCNTs as gas sensing was realized in the study. The best performance of (F- SWCNTs) as hydrogen sensing was realized in the study. F-SWCNTs film provides good sensitivity to hydrogen gases (S = 12%). The sensor room temperature reduces the response to hydrogen gases from (11 Sec).





Waleed k. Mahmood et al.

REFERENCES

1. Sari Lakkis, Rafic Younes, Mazen Ghandour, Yasser Alayli . New Optical Gas Sensor for Gas Concentration Measurement Using Digital Image Processing. *Sensors and Actuators B*, 2015,Vol. 207 ,pp 321–329.
2. Jae-Hong Lim, Nopparat Phiboolsirichit, Syed Mubeen, Marc A Deshusses, Ashok Mulchandani and Nosang V Myung . Electrical and gas sensing properties of polyaniline functionalized single-walled carbon nanotubes. *Nanotechnology*, 2010, Vol.21 , 075502 (7pp).
3. YunWang and John T. W. Yeow. A Review of Carbon Nanotubes-Based Gas Sensors. *Journal of Sensors*, 2009, Article ID 493904, 24 pages.
4. Chun-Shin Yeh. Carbon Nanotubes Gas Sensor for Ethanol Detection. *International Journal of Science and Engineering*, 2012, Vol.2 , No.1.
5. P. Feng , F. Shao, Y. Shi and Q. Wan. Gas Sensors Based on Semiconducting Nanowire Field-Effect Transistors .*Sensors*, 2014, Vol. 14, p.17406.
6. N. Sinha, J. Ma, and J. T. W. Yeow. Carbon nanotube-based sensors. *Journal of Nanoscience and Nanotechnology*, 2006, vol. 6, no. 3, pp. 573–590.
7. J. Li and H. T. Ng. . Carbon nanotubes sensors. *Encyclopedia of Nanoscience and Nanotechnology*, 2004, vol. 1, pp. 591–601.
8. Yukihiro Yoshida, Masato Tsutsui, Ayar Al-zubaidi, Yosuke Ishii and Shinji Kawasaki. In Situ Synchrotron X-ray Diffraction Studies of Single-walled Carbon Nanotubes for Electric Double-layer Capacitors. *J. Chem. Chem. Eng.* 9 (2015) 509-513.

Table 1 Crystalline size of the CNTs powder as estimated via the Scherer formula.

CNT type	2Theta (degree)	Cos θ	β (rad)	Crystalline size D (nm)	hkl	Average crystallite size (nm)
SWCNTs	26	0.974	0.122	1.16	002	1.325
	44.5	0.925	0.104	1.49	100	

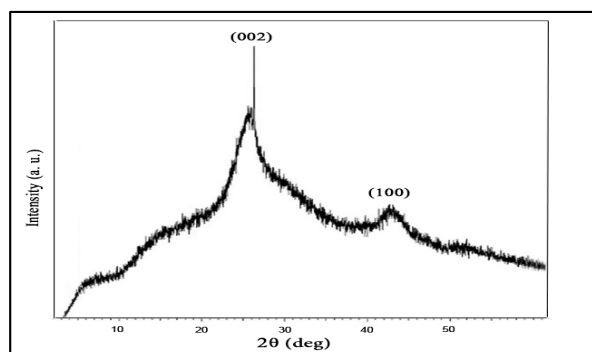


Figure 1. X-Ray diffraction of SWCNTs

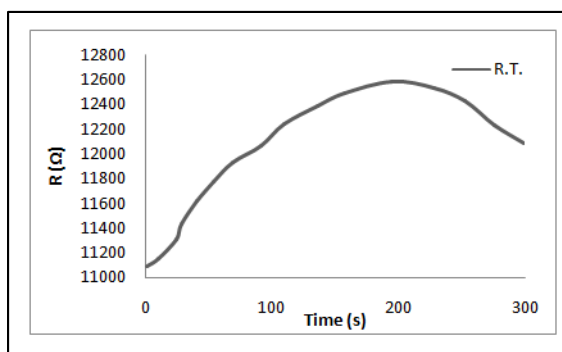


Figure 2. Resistance-time change of F-SWCNTs gas sensor at room temperature upon exposure to H₂ gas





RESEARCH ARTICLE

Utilizing Ground Penetration Radar to Detect Buried Human Remains at Two Different Depths

Faleh H. Mahmood^{1*}

Remote Sensing Unit, College of Science, University of Baghdad, Baghdad, Iraq.

Received: 10 July 2018

Revised: 18 Aug 2018

Accepted: 20 Sep 2018

*Address for Correspondence

Faleh H. Mahmood

Remote Sensing Unit,

College of Science,

University of Baghdad,

Baghdad, Iraq.

Email: faleh70@gmail.com



This is an Open Access Journal / article distributed under the terms of the **Creative Commons Attribution License** (CC BY-NC-ND 3.0) which permits unrestricted use, distribution, and reproduction in any medium, provided the original work is properly cited. All rights reserved.

ABSTRACT

Ground-penetrating radar (GPR) is considered as one of the best shallow detection geophysical methods because of its instantaneous radargram profile collecting from the recorded traces of the subsurface and its capability of preservation the underground sensitive features during the survey process. GPR surveys were conducted to identify unmarked mass graves belonging to unknown persons who have died since long periods of time and buried at different depths. According to these aspects it was utilized to simulate the process of locating and detecting old human remains in AL-Khamessiyia location southern of Iraq with a similar bodily condition model. The work was partitioned into four phases, the first phase was the pre-digging field testing searching for subsurface anomalies and antennas penetration depth determination, next phase was the calculation of the radar velocity below the field surface to calibrate the depth scale of the remains, next one was human remains burying at (2 and 4) meter depths in individual and clustered form to achieve the GPR survey task. This research clarify that the dielectric constant contrast between the buried feature and host medium is the major factor in the detection process, also it prove the success of GPR low frequencies to locate and detect the mortal remains in shallow burying depths. Based on the positive results obtained from this study, GPR data can be interpreted to identify possible hundreds of unmarked burial sites.

Keywords: ground penetrating radar, data simulation, collective cemetery sites, and relative dielectric permittivity contrast





Faleh H. Mahmood

INTRODUCTION

Geophysical techniques, such as ground-penetrating radar (GPR), have been successfully used by law enforcement agencies to locate graves and forensic evidence. Ground Penetrating Radar (GPR), Ground Impulse Radar (GIR) [1], Ground Probing Radar (GPR) [2], or Subsurface Interface Radar (SIR) [3] are the same terms for the geophysical scheme that create shallow subsurface image using radar pulses. There are generally three main components of a standard GPR unit: the antenna which both transmits and receives electromagnetic waves, the control unit, and the monitor which displays results in real time. The GPR unit generates radar waves that permeate the subsurface. When the radar waves encounter an object in the subsurface, a resulting reflected wave will occur that will be received by the receiving portion of the antenna. However, the amplitude of the returning wave is directly dependent on the contrast in dielectric permittivity between adjoining two materials. A stronger contrast between two horizons, or a strong contrast between a feature and the surrounding soil, will result in a stronger reflection, [4,5].

In this technique Ultra High Frequency and/ or Very High Frequency radiation of the microwave band is adopted to execute underground survey (i.e. remote sensing Non-Destructive Technique NDT) [6], underground natural burials or man-made subsurface structure features would be well-protected during the detection process, so that its valid to be applied in urban districts or in highly sensitive environments. The applicable GPR frequencies lays in 10-1000 MHz [7], its transmitter emits wave train of radio waves to ground surface; if electromagnetic pulse encountered an object or an interface between two layers with (electric permittivity, magnetic permeability, or electric conductivity) variation. The pulse refracted, scattered, and reflected to energy source point. Variations of the reflected signal could be recorded then using receiver antenna [8]. First experiments on this technique implemented by Leimbach and Löwy in the 1st decade of last century utilizing continuous waves, then after Hülsenbeck used radar pulses to detect burials in 1926 [9].

The efficiency of GPR system influenced by some factors such as host medium conductivity due to water and/or soil salinity content or scattering of the signal in rocky media [10], also the voids existence (in non-compacted or in high porosity soil) decrease the detecting efficiency [11] and finally radargram poor interpretation due to user experience lack causes underground features detection failure [12]. The detection dependence on physical properties variation between target and host medium, the wide range of utilized frequencies, the non-destroying survey, and the three dimensional illustrating are the main factors to make this technique the optimum one for archeological and unknown collective cemetery sites investigating and mapping [13].

MATERIALS AND METHODS

The work of this point was divided into eight stages as follow:

In the first stage electromagnetic wave reflection was explained, when the wave encounters underground point-type object that had different permittivity than the host medium or a boundary interface between two adjacent layers, this wave will suffered a change in character and direction called reflection, as the contrast of permittivity between these layers increased the reflected amplitude of a radar signal increased too and vice versa [14], in the case of no other signal losses; the signal reflection coefficient (R) quantify the ratio of reflected amplitude from the incident one according to equation:

$$R = \frac{\epsilon_{r2}^{1/2} - \epsilon_{r1}^{1/2}}{\epsilon_{r2}^{1/2} + \epsilon_{r1}^{1/2}} \quad (1)$$

Where ϵ_{r1} is the relative dielectric constant of the overlying material; and ϵ_{r2} is the relative dielectric constant of the underlying material as reflection coefficient converges to 1 the GPR survey improves. Thus, the reflection





Faleh H. Mahmood

coefficients grades are: weak reflection coefficient ($-0.2 < R < 0.2$); intermediate reflection coefficient ($0.2 < R < 0.35$) or ($-0.35 < R < -0.2$); and high reflection coefficient ($0.35 < R < 1.0$) or ($-1.0 < R < -0.35$). In the second stage electric permittivity was illustrated, (ϵ_m) of a medium is the ratio of electric flux density to the electric field strength in it, the charge that can be held in a medium is dominated by the value of its electric permittivity, In practice the medium relative permittivity (m_r) (well-known as the relative dielectric permittivity RDP) utilized which is the ratio of the medium electric permittivity to the one of the air [15]. In the third stage energy loss and medium phase velocity was discussed, they are the factors that illustrate the propagation of high-frequency radio waves in the ground [16]. The factors that are responsible of GPR radio waves energy losing can be classified into geometrical and physical ones. The geometrical configuration of the underground (i.e. the layers multiplicity) causes energy loss due to the consequence of reflection-transmission process about each layer boundary, another geometrical factor is the energy spreading of the radio waves in the propagation process, the electromagnetic waves speared in a cone with energy reduction per unit area at a rate of $1/r^2$, where r is the distance from the transmitter. The physical factors gathered to make the attenuation factor (α) which depends upon electric conductivity (σ), magnetic permeability (μ), electric permittivity (ϵ), and radio wave angular frequency (ω). The attenuation factor equation is given:

$$\alpha = \omega \left[\dots \right] \quad (2)$$

This equation explains the severely GPR signal attenuation in sea water or in a clay soil (conductive medium) and the high penetration in fresh water (Resistive medium) [17]. Velocity and attenuation are the factors that describe the propagation of high-frequency radiowaves in the ground. The speed of radiowaves (V_m) in any medium is dependent upon the speed of light in free space ($c = 0.3 \text{ mns}^{-1}$), the relative dielectric constant (i.e. permittivity ϵ_r) and the relative magnetic permeability (μ_r) [15]. But the main factor that effect on medium phase velocity (V_m) is the medium electric permittivity; other factors with less effect are the magnetic permeability and electric conductivity of the host medium. The relationship between phase velocity and medium physical properties is given by:

$$V_m = c / \sqrt{\left[\left(\frac{\epsilon_r \mu_r}{2} \right) (1 + P^2) + \dots \right]} \quad (3)$$

Where P is the loss factor, such that ($P = \sigma / \omega \epsilon_m$)

σ is the conductivity (S/m),

$\omega = 2\pi f$, f is the frequency (Hz),

$\epsilon = (\epsilon_r \epsilon_0)$ is the permittivity and

ϵ_0 is the permittivity of free space ($8.854 \times 10^{-12} \text{ F/m}$).

Most geological material is non-magnetic ($\mu = 1$) and a lot of them are low-loss ones ($P \approx 0$), so the equation (3) simplified to:

$$V_m = c / \sqrt{\epsilon_r} \quad (4)$$

For most geological materials ϵ_r ranging from (3-30), so V_m ranges from (0.06-0.175 m/ns) [18]. Table 1 illustrates some of the physical properties for common materials and their radar parameters. In the fourth stage GPR data acquisition was explained; after GPR signal amplitude being reflected from underground layers and objects; it has been recorded and managed in the control unit. Each longitudinal sample of radar data called a trace which present amplitude versus signal in the displaying unit, the movement of the device produces stacked series of traces commonly called radargram profile [18, 4].



**Faleh H. Mahmood**

In the fifth stage GPR data processing was illustrated; in many situations there is no need to make any processing on the acquired data to illustrate the subsurface features while in others it must be achieved in a way similar to that done on the seismic ones. The general processing stages are [19]:

- Removing or minimization of direct and air waves from the data.
- Data amplitude adjustments.
- Gain adjustments.
- Normalization of the signal distance;
- Horizontally scale.
- Filtering of the vertical frequencies.
- Horizontally filter.
- Correcting process for the velocity.
- Migrating process.

These stages make radargram more interpretability by removing the noisy signals and enhancing the interested features brightness [20]. In the sixth stage GPR data visualizing was illustrated; three varying schemes are used to visualize Ground Penetrating Radar data.

- The A-scan which is a one dimensional representation of reflected signal samples (trace).
- The B-scan which is a two dimensional representation of a series of stacked reflected signal samples (profile).
- The C-scan which is a three dimensional representation of a series of profiles (tomography) [21].

In the seventh stage the study area was illustrated; the study area is AL-Khameesiya location which falls in AL-Khameesiya marsh; AL-Nasiriya city, Thi-Qar Province in the southern part of Iraq. The borders and topography of the region and its surroundings was identified by utilizing the Differential Global Position System (Topcon Hyper-II DGPS). The region extends between the north latitudes 30°44'12.509" and 30°45'47.082", the east longitudes 46°26'13.25" and 46°28'42.604". It covers an area of 5.282 km². the general outlet (the third river), which is an artificial river of 656 km length made for collecting the salinity irrigation water from farms in the middle and south part of Iraq pass near the study area, the study area can be shown in figure 1. In the eighth stage methods of the work were explained, the aim of this work was the use of the radar simulation to evaluate the GPR system capabilities to detect human mortals which were buried in shallow depths (individually or in clustered) for long time (i.e. sufficient time for decadence of the human body), and the determination of the appropriate frequency for detection in salinity soil (the soil in the middle and southern parts of Iraq). Old human remains from 1986 were adopted as a model in the reflected radar data simulation process. It is worth mentioning the utilized antennas had 250 MHz and 500 MHz frequencies and the burying depths was 2 meter and 4 meters respectively, for each hole individual and clustered Iraqi remains had been put in

The first step in this work was the pre-digging testing of the subsurface medium to determine if there were any anomalies among the layers at the region and to state the penetration depth for each antenna as can be shown in figures 2, and 3. This test clarify that the location subsurface construct of multiple sediment layers with no obvious solid objects or voids to make a radargram anomaly, also it shows that the approximate penetration depth in the study area was four and a half meters for 250 MHz frequency and decreased to three meters for 500 MHz one. Next step was the determination of the radar phase velocity in the location (this is important to correct the depth scale of the detected objects). In the field the appropriate software was not available to make the migration process, so that an iron piece with known depth (2 m) was used to recognize the radar wave velocity in the medium. This step can be shown in figures 4 and 5, For the study area (i.e. AL-Khameesiya location) the penetration velocity was 140 nm/sec., Next after a hole with two meters depth was made and the mortals had been buried in individual and cluster form each time, for each burying process the GPR survey achieved with 250 MHz and 500 MHz frequencies respectively.



**Faleh H. Mahmood**

This task can be seen in figures 6 and 7 Finally a hole with four meters depth was made and the same procedure had been implemented as shown in figures 7 and 8,

For AL-Khameessiyia location the radargram profile processing begin with the air separation distance between the antenna and ground surface removing, then depth scale calibration using calculated host medium phase velocity, next after the (DC signal removing, background removal, automatic gain, band pass, and running average) filters were utilized respectively, the filters application in this arrangement was to overcome the environment conditions that weaken radar signal such as soil high conductivity because of the shallow groundwater movement toward the surface and the seepage of the salinity irrigation water from the neighborhood third river and soil voids due to flipping.

RESULTS AND DISCUSSION

This section illustrates the major result of this work as follow:

Study area penetration depth

The approximate penetration depth in AL-Khameessiyia location was 4.5 m using 250 MHz frequency antenna and decreased to 3 m using 500 MHz frequency antenna because its signal suffered from the double valued attenuation than the 250 MHz antenna according to equation (2) that had been proved in the first methodology step as shown in figures 8 and 9

The first burial depth testing

In the situation of two meters depth burying both antennas had almost the same radargram with low significance hyperbolas indicting to remains existence in individual or clustered form, the reason beyond that was the little contrast between the remains and soil dielectric constants (due to the decadence process of the human body after long time burying) which yield to reflected radar signal amplitude decrement as shown in figures 6 and 7.

The second burial depth testing

In the four meters depth burying; for both cases (individual or clustered) only 250 MHz antenna radargram had low significance hyperbola with its echo ones while the 500 MHz antenna radargram was severely confused with non-obvious hyperbola due to the high attenuation according to equation (2).

CONCLUSION

In this work it had been demonstrated that the reflected amplitude of GPR wave depend majorly on the dielectric constant difference between the host medium, the buried object and minor on the signal frequency or object physical properties, also this research clarify that penetration depth of 250 MHz frequency was approximately 4.5 m and less than 3 m for 500 MHz one because of the high salinity in AL-Khameessiyia location soil. These facts indicate that shallow locating and detection of human mortals in hard environment such as middle and southern parts of Iraq is possible with GPR but must be executed using low frequency antennas 100 MHz or 250 MHz. So that GPR technique is valid to be applied for many locations all over Iraq that are suspected to be collective cemetery locations. Based on the positive results obtained from this study, GPR data can be interpreted to identify possible hundreds of unmarked burial sites.





REFERENCES

1. Sun J.; Young R.A. Recognizing surface scattering in ground-penetrating radar data. *Geophysics* 1995, 60, 1378–1385.
2. Perez-Gracia, V.; Caselles, O.; Salinas, V.; Pujades, L.G.; Clapé s, J. GPR applications in dense cities: Detection of paleochannels and infilled torrents in Barcelona GPR applications in dense cities. In Proceedings of the IEEE 13th International Conference on Ground Penetrating Radar (GPR), Lecce, Italy, 21–25 June 2010; pp. 1–5.
3. Harbi, H.; McMechan, G.A. Conductivity and scattering Q in GPR data: Example from the Ellenburger dolomite, central Texas. *Geophysics* 2012, 77, H63–H78.
4. Santos-Assuncao, S.; Perez-Gracia, V.; Gonzalez-Drigo, R. GPR backscattering applied to urban shallow geology: GPR application in seismic microzonation. In Proceedings of the IEEE 8th International Workshop on Advanced Ground Penetrating Radar (IWAGPR), Florence, Italy, 7–10 July 2015; pp. 1–4.
5. Chandler, V.W.; Lively, R.S. Utility of the horizontal-to-vertical spectral ratio passive seismic method for estimating thickness of Quaternary sediments in Minnesota and adjacent parts of Wisconsin. *Interpretation* 2016, 4, SH71–SH90
6. Takahashi, K.; Igel, J.; Preetz, H.; Sato, M. Sensitivity analysis of soil heterogeneity for ground—Penetrating radar measurements by means of a simple modeling. *Radio Sci.* 2015, 50, 79–86.
7. Panzera, F.; D'Amico, S.; Lombardo, G.; Longo, E. Evaluation of building fundamental periods and effects of local geology on ground motion parameters in the Siracusa area, Italy. *J. Seismol.* 2016, 20, 1001–1019.
8. Alfaro, A.; Pujades, L.G.; Goula, X.; Susagna, T.; Navarro, M.; Sanchez, J.; Canas, J.A. Preliminary Map of Soil's Predominant Periods in Barcelona Using Microtremors. *Pure Appl. Geophysics.* 2001, 158, 2499–2511.
9. Daniels, D.J. *Ground Penetrating Radar*, 2nd ed.; the Institution of Electrical Engineers: London, UK, 2004.
10. Jol, H.M. (Ed.) *Ground Penetrating Radar Theory and Applications*; Elsevier: Amsterdam, the Netherlands, 2008.
11. Leuschen, C.J.; Plumb, R.G. A Matched-Filter-Based Reverse-Time Migration Algorithm for Ground-Penetrating Radar Data. *IEEE Trans. Geosci. Remote Sens.* 2001.
12. Almeida, E.R.; Porsani, J.L.; Catapano, I.; Gennarelli, G.; Soldovieri, F. Microwave tomography-enhanced GPR in forensic surveys: tropical environment. *IEEE J. Sel. Top. Appl. Earth Obs. Remote Sens.* 2016, 9, 115–124.
13. Grasmueck, M.; Weger, R.; Horstmeyer, H. Three-dimensional ground-penetrating radar imaging of sedimentary structures, fractures, and archaeological features at submeter resolution. *Geology* 2004, 32, 933–936.
14. Reynolds, J., M., *An Introduction to Applied and Environmental Geophysics*, West Sussex, John Wiley & Sons, 1997.
15. Charlton M. B., principles of Ground-Penetrating radar for Soil Moisture Assessment', *Journal of Hydrology review* on 31 st May 2006, 2006.
16. Davis, J.L., Annan, A.P., Ground Penetrating Radar for High-Resolution Mapping of Soil and Rocks Stratigraphy, *Geophysical Prospecting* Vol. 37, PP. 531-551, 1989.
17. Du, S., and Rummel, P., "Reconnaissance Studies of Moisture in the Subsurface with GPR, Proceedings of The Fifth International Conference of Ground Penetrating Radar, Kitchener, Ontario, 12-16 June 1994, 1241-1248, 1994.
18. Busby, J.P.; Merritt, J.W. Quaternary deformation mapping with Ground Penetrating Radar. *J. Appl. Geophysics.* 1999, 41, 75–91.
19. CFLHD, and Blackhawk GeoServices Inc., Subsurface Geophysical Imaging of Lava Tubes, Lava Beds of National Monuments, CA, 2003.
20. Daniels, J., Ehsaani, M. R., and Allred, B., I., *Handbook of Agricultural Geophysics*. Chapter 7, Ground- Penetrating Radar (GPR), 2008.
21. Picco, V.; Gennarelli, G.; Negishi, T.; Soldovieri, F.; Erricolo, D. Experimental validation of the quadratic forward model for RF tomography. *IEEE Geosci. Remote Sens. Lett.* 2015, 12, 1461–1465.





Faleh H. Mahmood

Table 1. Some well-known materials with their physical properties and radar parameters [15].

Material	ϵ	σ ms/m	Vm m/ns	α dB/m
Air	1	0	0.30	0
Ice	3-4	0.01	0.16	0.01
Fresh water	80	0.05	0.033	0.1
Salt water	80	3000	0.01	1000
Dry sand	3-5	0.01	0.15	0.01
Wet sand	20-30	0.01-1	0.06	0.03-0.3
Shales and clays	5-20	1-1000	0.08	1-1000
Silts	5-30	1-100	0.07	1-1000
Limston	4-8	0.5-2.0	0.12	0.4-1
Granite	4-6	0.01-1	0.13	0.01-1
(Dry) salt	5-6	0.01-1	0.13	0.01-1

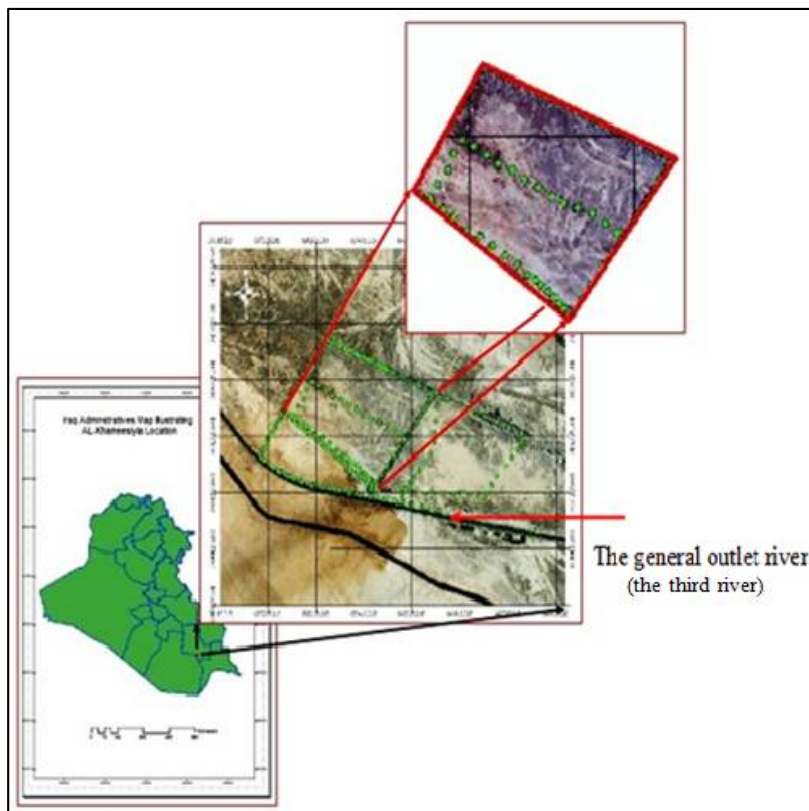


Figure 1. Iraq administrative map illustrating the study region position using Quick bird composite bands 1, 2, and 3 imagery.





Faleh H. Mahmood

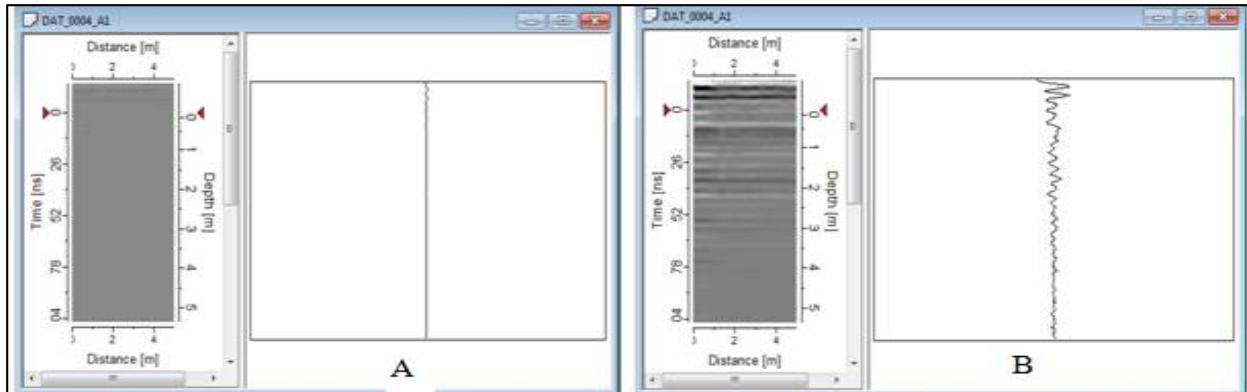


Figure 2. (A)AL-Khamessiyya location pre-processed radargram using 250 MHz; (B)AL-Khamessiyya location processed radargram using 250 MHz;

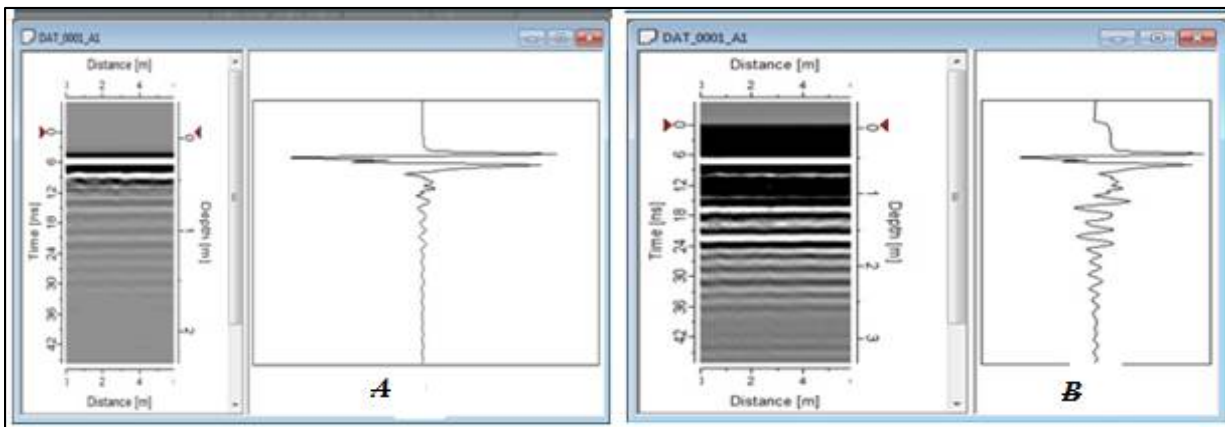


Figure 3 (A) AL-Khamessiyya location pre-processed radargram using 500 MHz; (B) AL-Khamessiyya location processed radargram using 500 MHz

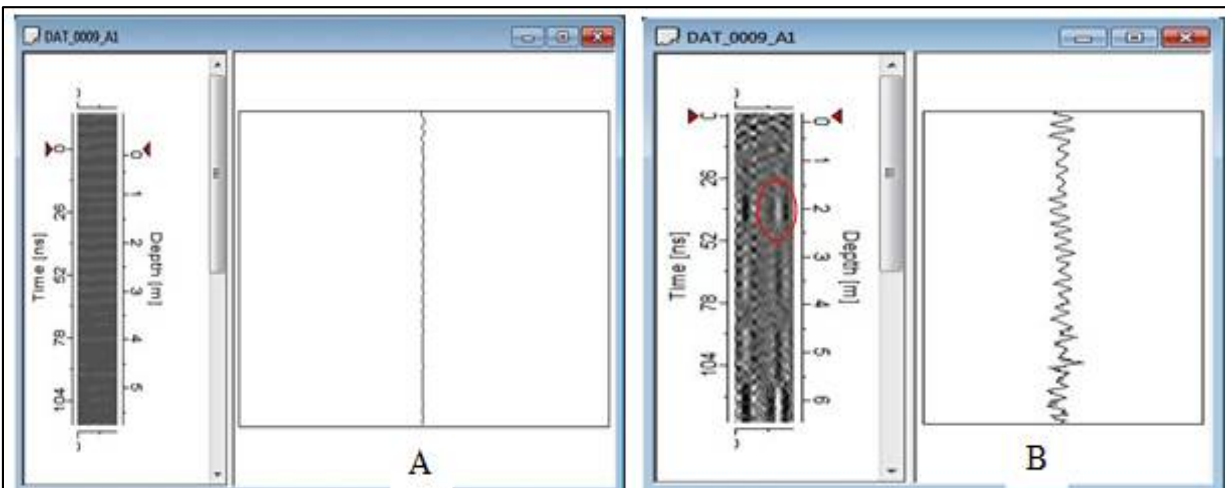


Figure 4. (A) The pre-processed soil with iron piece radargram using 250 MHz; (B) The processed soil with iron piece radargram using 250 MHz;





Faleh H. Mahmood

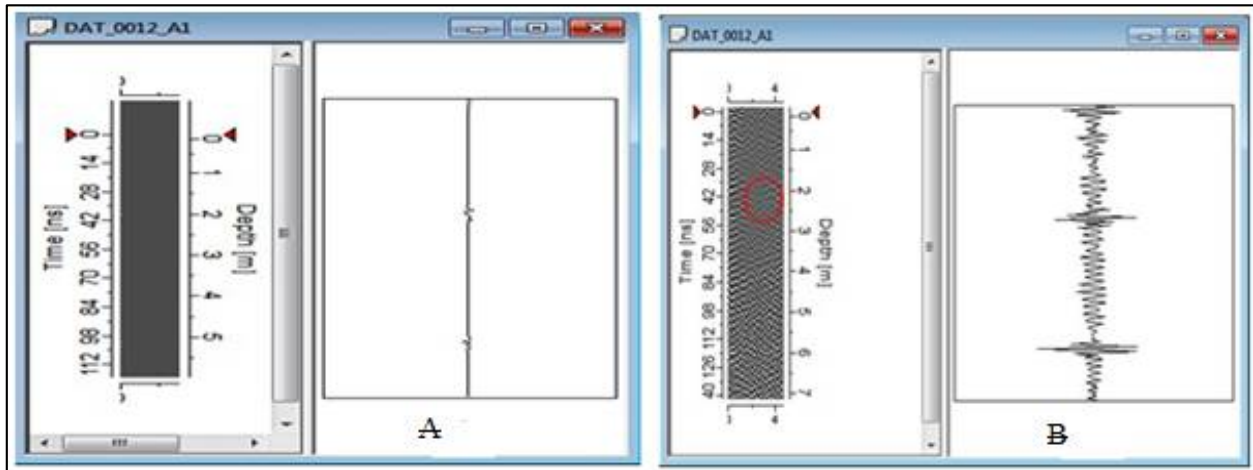


Figure 5. (A) The pre-processed soil with iron piece radargram using 500 MHz; (B) The processed soil with iron piece radargram using 500 MHz

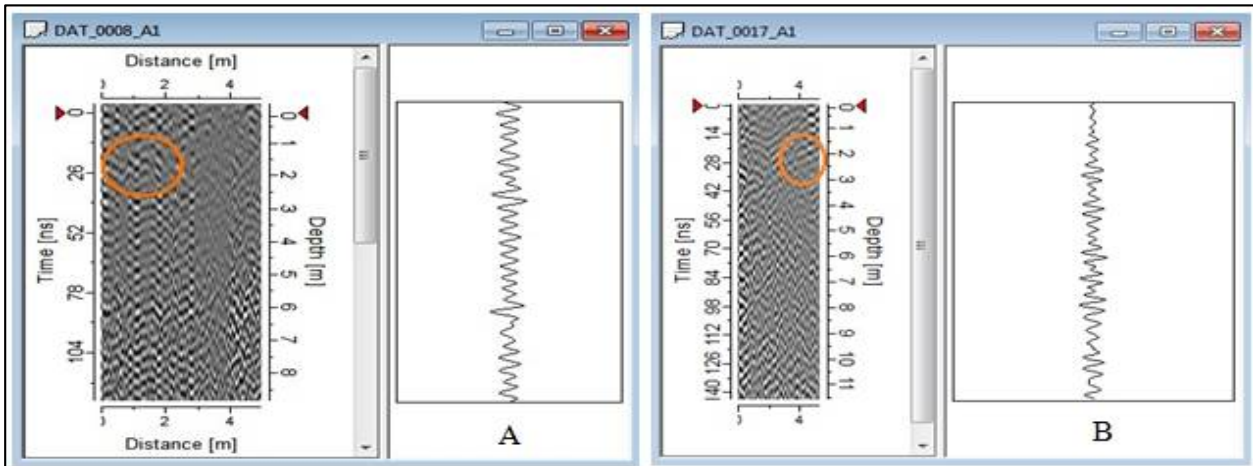


Figure 6. (A) The processed radargram of one mortal using 250 MHz; (B) The processed radargram of one mortal using 500 MHz;

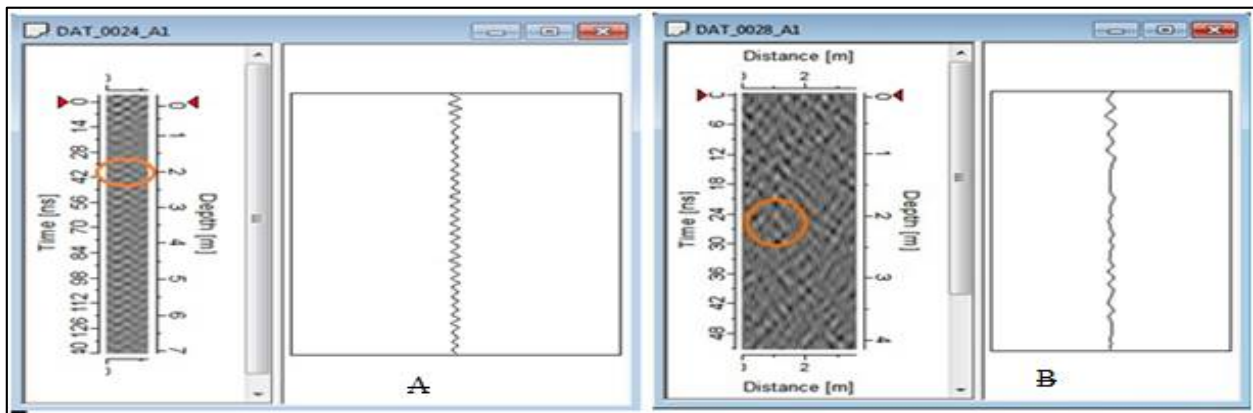


Figure 7. (A) The processed radargram of clustered mortals using 250 MHz; (B) The processed radargram of clustered mortals using 500 MHz





Faleh H. Mahmood

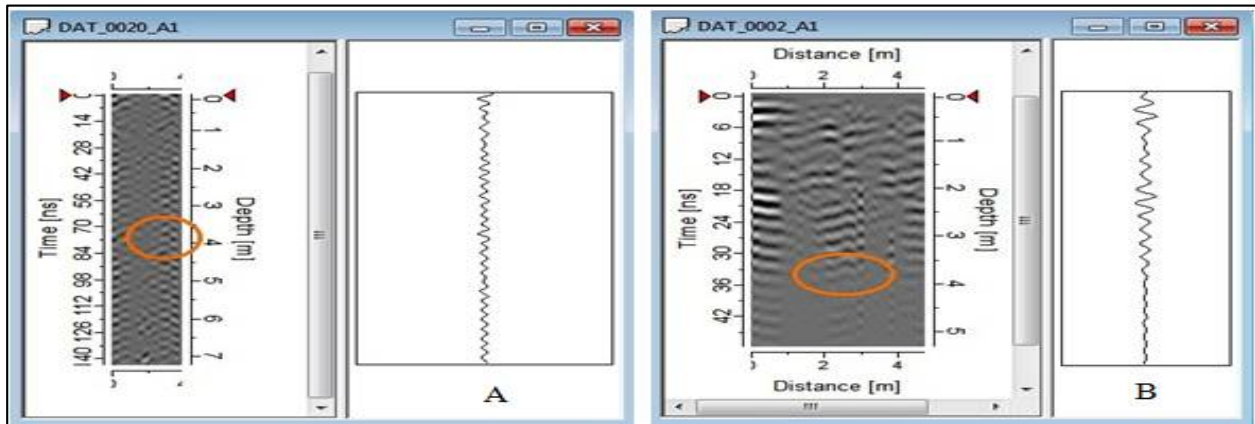


Figure 8. (A) The processed radargram of one mortal using 250 MHz; (B) The processed radargram of one mortal using 500 MHz;

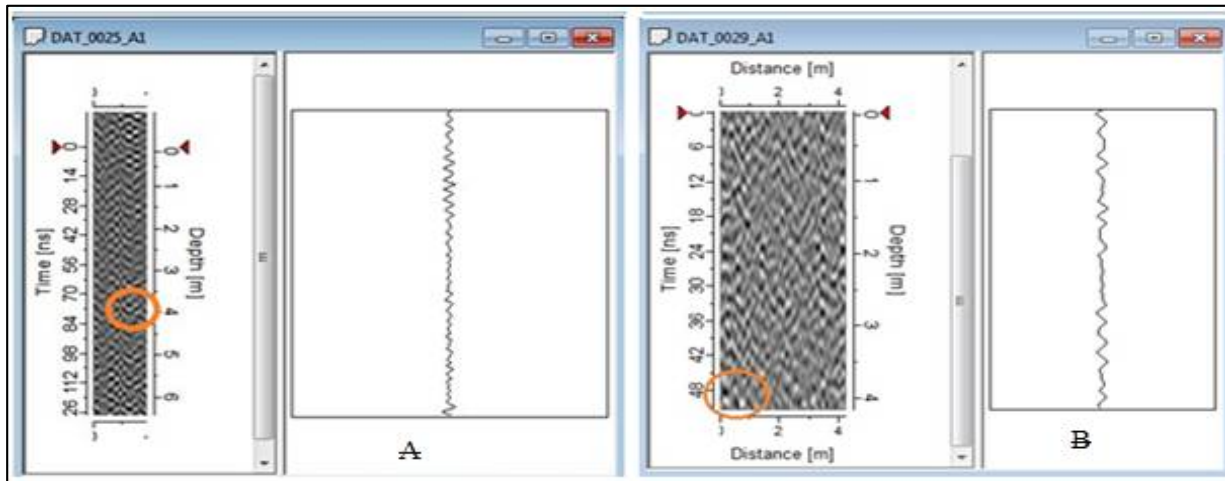


Figure 9.(A) The processed radargram of clustered mortals using 250 MHz;(B) The processed radargram of clustered mortals using 500 MHz





RESEARCH ARTICLE

Assessment of Groundwater Quality Using Heavy Metal Pollution Indices and Statistical Analysis in Lailan Basin, Southeast Kirkuk Governorate, Iraq

Ousai Y. Al-Kubaisi¹ and Arjan A. Rasheed^{2*}

¹Department of Geology, College of Science, University of Baghdad, Baghdad, Iraq

²General Commission for Groundwater, Ministry of Water Resources, Baghdad, Iraq.

Received: 19 July 2018

Revised: 22 Aug 2018

Accepted: 25 Sep 2018

* Address for Correspondence

Arjan A. Rasheed

General Commission for Groundwater,
Ministry of Water Resources,
Baghdad, Iraq.
Email: aahydro77@gmail.com



This is an Open Access Journal / article distributed under the terms of the **Creative Commons Attribution License** (CC BY-NC-ND 3.0) which permits unrestricted use, distribution, and reproduction in any medium, provided the original work is properly cited. All rights reserved.

ABSTRACT

The main objective of this study is to assess the groundwater pollution with heavy metals in Lailan basin using pollution indices according to the WHO standards. To get the extent of groundwater pollution, 22 samples from tube wells were collected and analyzed for 8 heavy metals including Iron, Copper, Cadmium, Manganese, Lead, Zinc and Chromium. The obtained data were subjected to heavy metal pollution Index (HPI) and contamination index (C_d) in conjunction with multivariate statistical analysis. The results showed that the HPI values were found to be under the critical pollution index level of 100 except samples W_1 and W_2 were above the critical limit. Similarly the computed contamination index (C_d) values showed that the groundwater samples were within low pollution levels except the samples (W_1, W_2, W_3 and W_4) which showed a high pollution index ($C_d > 3$). In both methods the highest pollution value was recorded at sample W_2 while sample W_{11} recorded the lowest pollution value. Pearson's analysis showed both positive and negative correlations among all metals. Also cluster analysis showed the state of similarity and correlation between metals and also between groundwater samples.

Keywords: Groundwater quality, heavy metals, pollution index, WHO standards, correlation matrix.

INTRODUCTION

Groundwater has always been used as a readily accessible and stable source of water supply for domestic, industrial and agricultural uses throughout the world. Rapid urbanization, incorrect waste disposal and landfill, excessive application of fertilizers and unhealthy conditions has threatened groundwater quality and consequently human health in many parts of the world by naturally occurring pollutants and anthropogenic pollutants [1]. Groundwater

14869



**Qusai Y. Al-Kubaisi and Arjan A. Rasheed**

as an important environmental indicator of hydrochemical contamination receives heavy metals from various sources such as industrial discharges from chemical and metallurgic factories, leakage from landfills and excessive application of fertilizers as well as natural geochemical resources [2]. For most geochemical components anthropogenic sources contribute more to pollution than the natural source [3,4,5]. Groundwater is a significant source of drinking and other domestic water uses in Lailan basin. Hence, considering the rapid growth of the population coupled with a steady increase in water requirements for agricultural and industrial development as well as climatic changes, it becomes necessary to regularly monitor the quality of groundwater to identify ways and means of protecting it. The study evaluates groundwater quality of Lailan basin using pollution indices as a tool for assessing the environmental condition of the study area. There are many previous works included the study area such as, Sogiria [6], studied the hydrology of Kirkuk and northern part of Al Adhaim Basin. Araim [7], studied the hydrogeological basins of Iraq. Al-Nakash et al. [8], they designed an operational program for wells in Kirkuk. The State Company of Geological Survey and Mining studied the hydrogeology and hydrochemistry of groundwater of Kirkuk quadrangle sheet (NI-38-2)[9]. Saud [10], studied the Hydrogeology and hydrochemistry of groundwater of Kirkuk governorate. The General Commission for Groundwater / Branch of Kirkuk, studied the hydrochemistry of groundwater of Lailan sub-basin [11].

Location and Geology

Lailan basin which covers an area of 436 km² is situated within the southeast part of Kirkuk governorate, north of Iraq, between longitudes (44° 18' 30" E - 44° 40' 30" E) and latitudes (35° 7' 30" N - 35° 29' 30" N) (Fig. 1). Geologically, The most important geological formations that are exposed in the basin are Bai Hassan and Mukdadiyah Formations in addition to Quaternary deposits (Fig. 2) [12]. The basin is located between two structures; Kirkuk structure from the northeast side and Jambur Anticline from the southwest side. The study area is characterized by the districts and small villages scattered over the basin mostly depending on the agriculture and livestock, poultry and fish breeding. As well as the industrial projects such as cement, asphalt and refinery factories which are circulating in the basin.

Groundwater Aquifer

Bai-Hassan formation and Quaternary deposits forms the major aquifer unit in the basin. Bai- Hassan Formation is characterized by thick layers of conglomerates interbedded with sandstone, siltstone, and claystone. While Quaternary deposits are characterized by layers of gravel, sand, silt and clay [8] [13]. The aquifer unit is characterized by rapid variation of subsurface sediment sequence, in the form of multi aquifers interceded with clay layers. These aquifers are classified into two main aquifers, unconfined and semi-confined or leaky aquifer. The general groundwater flow direction is from northeast to southwest and west similar to the direction of regional groundwater flows in the region.

MATERIALS AND METHODS

In order to assess the groundwater pollution with heavy metals in Lailan basin, Twenty-two groundwater samples were collected in April 2017 from wells distributed in the study area, their locations and depths are shown in (Table.1) and (Fig.1). The water samples were stored in plastic bottles with one liter capacity. One ml of concentrated nitric acid was added to it for preservation. The heavy metals constituents in groundwater samples (Iron, Cobalt, Nickel, Copper, Zinc, Cadmium, Lead and Manganese) were analyzed in the water analysis department in North Gas Company using Atomic Absorption Spectrophotometry (AAS) method. The environmental impact of metals and the pollution level in the groundwater can be assessed with the help of two indices; the heavy metal pollution index (HPI) and contamination index (C_d).





Ousai Y. Al-Kubaisi and Arjan A. Rasheed

Heavy Metal Pollution Index (HPI)

Heavy metal pollution index (HPI) is an effective tool to assess the ground water pollution on the basis of heavy metal concentration as it combines several parameters to reach at a particular value which can be compared with the critical value to assess the level of pollution load. The index system selection depends upon the importance of individual quality considerations or it can be defined as inversely proportional to the standard permissible value [14] [15]. HPI is determined by using the expression (Eq.1)[15] [16] :

$$HPI = \frac{\sum_{i=1}^n W_i Q_i}{\sum_{i=1}^n W_i} \dots\dots\dots(Eq.1)$$

Where, Qi is the sub-index of the ith parameter; Wi is the unit weightage of the ith parameter; n is the number of parameters. The sub-index (Qi) is calculated by(Eq.2):

$$Q_i = \sum_{i=1}^n \frac{M_i}{S_i} \times 100 \dots\dots\dots(Eq.2)$$

Where Mi is the monitored value of heavy metal, Si is the standard value of the ith parameter. Generally, the critical pollution index value, above which the overall pollution level should be considered unacceptable, is 100 [17].

Contamination Index (Cd)

Contamination index (Cd) is one of the approaches to calculate contamination of water bodies, which takes into consideration both the number of parameters exceeding the upper permissible limits or guide values of the potentially harmful elements [18]. Contamination index can be calculated by (Eq.3)and(Eq.4)[18][5]:

$$Cd = \sum_{i=1}^n C_{fi} \dots\dots\dots(Eq.3)$$

$$C_{fi} = \frac{C_{Ai}}{C_{Ni}} \dots\dots\dots(Eq.4)$$

Where C_{fi} is the contamination factor for the ith component; C_{Ai} is the analytical value of the ith component ; C_{Ni} is the upper permissible concentration of the ith component. The value scale for contamination index consists of 3 ranges; C_d< 1 (low contamination), 1 < C_d< 3 (medium contamination) and C_d> 3 (high contamination)[18]. In computing the Cd and HPI values for the present water quality data, the concentration limits, i.e. the standard permissible value (Si) for each parameter were according to the WHO standards [19].

Statistical Analysis

To identify the relationship between various heavy metals in the water samples, statistical analysis has been done by using Pearson’s correlation matrix and cluster analysis with the help of XLSTAT 2018 software.

RESULTS AND DISCUSSION

A statistical summary of heavy metals analysis of the groundwater samples taken from the Lailan basin is presented in (Table 2) and (Fig. 3). The resultsshow that the mean concentrations of the examined parameters (Fe, Co, Ni, Cu,



**Qusai Y. Al-Kubaisi and Arjan A. Rasheed**

Zn, Cd, Pb and Mn) were (0.08, 0.01, 0.02, 0.01, 0.01, 0.00, 0.01, 0.01 ppm) respectively. Among the investigated heavy metal constituents Fe shows the highest mean, while Cd remained the least. The quality of groundwater was assessed using heavy metal pollution index (HPI) and contamination index (C_d). The heavy metal pollution index HPI have been calculated separately for each sampling according to the WHO standards. The weightage (W_i) was calculated as the inverse of standard permissible value (S_i). The components considered include Fe, Co, Ni, Cu, Zn, Cd, Pb and Mn. The results of HPI are presented in (Table 3). Results revealed that the highest HPI was 334 at sample W_2 and the lowest was 0.001 at sample W_{11} with mean concentration value 47.05 (Fig.4). The result of the index showed that the HPI for all the samples were under the critical limit of 100 except the samples W_1 and W_2 were above the critical limit, indicating that the groundwater quality in Lailan basin is not seriously polluted with respect to these heavy metals except the samples W_1 and W_2 . HPI distribution in the study area presents in (Fig.5).

Also contamination index (C_d) was used to estimate the metal pollution of groundwater of the study area by computing all measured metals according to the WHO standards. All samples display, low contamination level based on a contamination index ($C_d < 1$) ranging between (0.02 – 0.94), except the samples ($W_7, W_8, W_9, W_{12}, W_{13}, W_{21}$ and W_{22}) are moderately contaminated ($C_d = 1 - 3$) ranging between (1.03 – 2.81), while the samples (W_1, W_2, W_3 and W_4) show high contamination index value ($C_d > 3$), ranging between (3.56 - 13.71) (Table 3) and (Fig.6). (C_d) distribution in the study area presents in (Fig.7). The high contamination source in samples (W_1, W_2, W_3 and W_4) may be due to anthropogenic sources, because they are located in urban areas in Kirkuk city. While contamination in a remaining groundwater samples may be due to agricultural activities. Multivariate statistical analysis was applied to understanding the relationship between various heavy metals in groundwater of the study area. The correlation matrix has been calculated based on the Pearson's correlation coefficient (Table 4).

The matrix showed both positive and negative correlations among different metals. It is clear from the results that Cu and Cd have positive correlated with most of the other metals, whereas Fe and Pb shows a strong correlation between them. Suggesting that these variables may have similar hydrochemical characteristics or similar sources of input. Cluster analysis was also used for investigating the similarities among various heavy metals found in groundwater in the study area. Evaluations of similarity were based on the average linkage between groups. The results of the cluster analysis were presented as dendograms in (Fig.8). The results of cluster analysis of heavy metals showed two clusters types, first cluster consists of 7 metals (Co, Ni, Cu, Zn, Cd, Pb and Mn) with two sub-clusters while the second cluster consists of Fe. Indicating the state of correlation between these metals. On the other hand the cluster analysis of groundwater samples showed two clusters, first consists of 18 wells while the second consists of 4 wells. The analysis reflects the interconnections between these wells.

CONCLUSIONS

In present work, the calculated HPI values of groundwater samples were under the critical level of 100 which reveals that the water is unpolluted with respect to heavy metals except samples W_1 and W_2 were above the critical limit. The highest HPI value was recorded at sample W_2 is 334, while sample W_{11} recorded the lowest contamination value in the study area. Similarly the calculated contamination index (C_d) values showed that the ground water samples were within low or medium pollution levels ranged between (0.02 – 0.94) and (1.03 – 2.81) respectively, except the samples (W_1, W_2, W_3 and W_4) showed a high pollution degree ($C_d > 3$) ranged between (3.56 - 13.71). The highest C_d value was recorded at sample W_2 is 13.71, while sample W_{11} recorded the lowest contamination value in the study area. The high contamination source in samples (W_1, W_2, W_3 and W_4) may be due to anthropogenic sources, because they are located in urban areas in Kirkuk city. Whereas the sources of metals in a remaining samples may be due to agricultural activities. Pearson's correlation analysis showed both positive and negative correlations among different metals. The cluster analysis was also reverses the state of similarity and correlation between metals and also between groundwater samples.





Qusai Y. Al-Kubaisi and Arjan A. Rasheed

REFERENCES

1. Keishiro, H., 2006. Groundwater Contamination and Quality Management Policy in Asia. *Int.Rev. Environ. Str.*, (6), 291-306.
2. Smedley, P. L. and Kinniburgh, D. G. , 2002. A review of the source behavior and distribution of arsenic in natural waters. *Appl. Geochem.*, 17: 517-568.
3. Appelo, C. A. G. and Postma, D. , 2005. *Geochemistry groundwater and pollution*. 2nd Edition, A.A. Balkema publishers, 649 p.
4. Longe, E. O. and Balogun, M. R. , 2010. Groundwater Quality Assessment near a Municipal Landfill, Lagos, Nigeria. *Res. J. App. Sci. Eng. Tech.*, 2 (1): 39-44.
5. Akoteyon, I. S. , 2012. Evaluation of groundwater quality using contamination index in parts of Alimosho, Lagos-Nigeria. *American Academic & Scholarly Research Journal*, V.4 (N.4).
6. Sogiria, 1981. Hydrologic Study of Kirkuk Basin. Baghdad, Al – Furat Center.
7. Araim, H.I. 1984. Regional Hydrogeology of Iraq. Vol. 6. GEOSURV, int. rep.no. 1450.
8. Al-Naqash, A. B., Ismaeel, S. K., Hassan, A. H. and Rahey, K. M. 2003. Evaluation study of wells operation of national campaign project for watered wells drilling in Kirkuk governorate. Technical Final Report, Ministry of Irrigation, p.185.
9. Saud, Q. J. and Mohammed, R. A. 2007. Hydrogeological and hydrochemical study of Kirkuk quadrangle sheet (NI-38-2). Scale 1:250 000 , GEOSURV, Baghdad , Iraq. internal report, No. 2986.
10. Saud, Q. J. 2009. Hydrogeological and hydrochemical study of Kirkuk governorate; Northern Iraq. *Geol. Min. Irq. Jour.*, 5(1): 1-15.
11. Al-Hamdani, J.A., Wely, H.A., Khorshed, S.A. and Nief, A.J. 2012 . Hydrochemical study of groundwater Lailan sub-basin , Kirkuk , Ministry of water resources ,General Commission for Groundwater , internal report , 144p.
12. Sissakian, V.K. 1993. The Geology of Kirkuk Quadrangle, sheet NI-38-2. scale 1: 250 000. GEOSURV, Baghdad, Iraq.
13. Jassim, S. Z. and Goff, J. C. 2006. *Geology of Iraq*. 1st Edition, Doline, Prague and Moravian Museum, Brno, Czech Republic, 341 P.
14. Reddy, S.J. , 1995. *Encyclopedia of environmental pollution and control*. - Environmental media, Karela, India.
15. Mohan, S.V., Nithila, P., Reddy, S.J. , 1996. Estimation of heavy metal in drinking water and development of heavy metal pollution index. - *Journal of Environmental Science and Health* 31: 283-289.
16. Pal R., Dubey R.K., Dubey S.K., and Singh A.K., 2017. Assessment of Heavy Metal Pollution through Index Analysis for Yamuna Water in Agra Region, India; *Int.J.Curr.Microbiol.App.Sci*, V.6 (N.12), 1491-1498 PP.
17. EqbalDohanChalap Al- Grawi and Ghaidaa Raheem Lateef Al-Awsi (2018). Expression of CDKN2A (p16/Ink4a) among Colorectal Cancer Patients: A cohort study. *Journal of Pharmaceuticals Sciences and Research*. Vol. 10(5), 2018, 1145-1147.
18. Amalraqibshamran, Zinahhadi Shaker, Ghaidaa Raheem Lateef Al-Awsi, Ammar S. Khamis, Zainab A. Tolaifeh and ZahraalsamJameel, 2018. RAPD-PCR IS A GOOD DNA FINGERPRINTING TECHNIQUE TO DETECT PHYLOGENETIC RELATIONSHIPS AMONG STAPHYLOCOCCUS AUREUS ISOLATED FROM DIFFERENT SOURCES IN HILLA CITY, IRAQ. *Biochem. Cell. Arch*. Vol. 18, Supplement 1, pp. 1157-1161.
19. Ibraheem, Lujain Hussein and Abed, Salwan Ali (2017) Accumulation detection of some heavy metals in some types of fruits in the local market of Al-Diwaniyah City, Iraq. *Rasayan J. Chem*.10 (2), 339 -343. DOI: <http://dx.doi.org/10.7324/RJC.2017.1021641>.
20. Prasad, B. and Kumari, S. , 2008. Heavy metal pollution index of ground water of an abandoned open cast mine filled with fly ash: A case study. *Mine Water Environ.*, 27(4): 265-267.
21. Backman, B., Bodis D., Lahermo P., Rapant S. , and Tarvainen T., 1998. Application of a Groundwater Contamination Index in Finland and Slovakia. *Environmental Geol.*, 36, 55 – 64p.
22. Ewaid, S. H., & Abed, S. A. (2017) Water Quality Assessment of Al-Gharraf River, South of Iraq Using Multivariate Statistical Techniques. *Journal of Al - Nahrain University* Vol. 20 (2), June , 201 7 , pp. 114 – 122.





Qusai Y. Al-Kubaisi and Arjan A. Rasheed

23. Ewaid, S. H., & Abed, S. A. (2017). Water quality index for Al-Gharraf River, southern Iraq. The Egyptian Journal of Aquatic Research, 43(2), 117-122. <https://doi.org/10.1016/j.ejar.2017.03.001>.
24. WHO, 2011. World Healthy Organization , Guideline for drinking water quality Recommendation , 4rd ed. , Geneva,541p.

Table 1: Locations and depths of wells in the study area

Well	Coordinates		Well depth m
	longitudes	latitudes	
1	44°24'30.00"	35°26'30.00"	90
2	44°23'13.77"	35°24'24.36"	108
3	44°25'25.55"	35°24'3.82"	156
4	44°22'32.40"	35°22'18.43"	150
5	44°25'16.34"	35°22'19.25"	150
6	44°28'44.72"	35°22'20.04"	130
7	44°28'40.57"	35°20'58.58"	102
8	44°25'27.22"	35°19'57.42"	127
9	44°23'55.73"	35°20'11.58"	100
10	44°30'8.42"	35°18'28.07"	100
11	44°30'58.52"	35°19'52.57"	110
12	44°28'59.35"	35°18'10.09"	157
13	44°26'1.80"	35°18'4.42"	140
14	44°32'24.79"	35°18'22.83"	160
15	44°30'56.69"	35°17'21.33"	200
16	44°33'52.43"	35°17'13.49"	110
17	44°31'26.81"	35°16'28.73"	150
18	44°34'11.74"	35°16'0.46"	120
19	44°31'52.79"	35°15'11.29"	96
20	44°32'43.01"	35°14'13.92"	96
21	44°35'35.04"	35°14'6.45"	110
22	44°36'38.95"	35°13'38.23"	120

Table 2: Heavy metals concentrations in groundwater samples in(ppm)

Well	Fe	Co	Ni	Cu	Zn	Cd	Pb	Mn
1	0.303	0.012	0.014	0.095	0.015	0.009	0.05	0.04
2	0.551	0.01	0.098	0.066	0.011	0.008	0.07	0.052
3	0.109	0.07	0.023	N.D	N.D	N.D	0.012	0.002
4	0.124	N.D	0.091	N.D	0.015	0.004	N.D	0.051
5	0.053	N.D	0.014	0.003	0.003	N.D	N.D	0.004
6	0.039	0.002	N.D	0.002	N.D	N.D	N.D	0.007
7	0.06	0.003	0.01	0.007	N.D	N.D	0.019	N.D
8	0.025	N.D	0.003	N.D	0.005	N.D	0.01	N.D
9	0.084	N.D	0.002	0.003	0.0197	N.D	0.01	0.007
10	0.05	N.D	N.D	0.005	0.014	N.D	N.D	0.006
11	N.D	N.D	N.D	0.004	0.055	N.D	N.D	N.D
12	0.035	N.D	N.D	0.005	0.02	0.003	0.001	0.005
13	0.044	0.06	0.011	N.D	0.004	N.D	0.01	N.D





Qusai Y. Al-Kubaisi and Arjan A. Rasheed

14	0.062	N.D	0.001	0.005	0.073	N.D	N.D	0.004
15	N.D	N.D	0.019	0.004	0.032	N.D	N.D	0.001
16	0.056	N.D	0.001	0.002	N.D	N.D	N.D	0.009
17	0.067	N.D	0.05	0.004	N.D	N.D	N.D	N.D
18	0.04	N.D	N.D	0.002	N.D	N.D	N.D	0.015
19	0.056	N.D	0.01	0.003	N.D	N.D	N.D	0.017
20	0.01	N.D	0.01	0.004	N.D	N.D	N.D	0.037
21	0.021	0.008	N.D	0.006	0.02	0.002	N.D	0.008
22	0.017	N.D	0.048	N.D	0.023	N.D	0.01	0.003
Min.	0	0	0	0	0	0	0	0
Max.	0.551	0.07	0.098	0.095	0.073	0.009	0.07	0.052
Mean	0.08	0.01	0.02	0.01	0.01	0.00	0.01	0.01
Median	0.0515	0	0.01	0.0035	0.008	0	0	0.0055
Stdev.	0.12	0.02	0.03	0.02	0.02	0.00	0.02	0.02
WHO Std.	0.3	0.04	0.07	2	3	0.003	0.01	0.1

N.D: Not detected

Table 3 : HPI and Cd values for groundwater samples

Well	HPI	Class	Cd	Class
1	311.6	Polluted	9.96	High
2	334.0	Polluted	13.71	High
3	34.9	Unpolluted	3.66	High
4	96.4	Unpolluted	3.56	High
5	0.8	Unpolluted	0.42	Low
6	0.5	Unpolluted	0.25	Low
7	40.0	Unpolluted	2.32	Medium
8	20.7	Unpolluted	1.13	Medium
9	21.0	Unpolluted	1.39	Medium
10	0.2	Unpolluted	0.23	Low
11	0.001	Unpolluted	0.02	Low
12	70.7	Unpolluted	1.28	Medium
13	28.8	Unpolluted	2.81	Medium
14	0.3	Unpolluted	0.29	Low
15	0.8	Unpolluted	0.29	Low
16	0.4	Unpolluted	0.29	Low
17	2.2	Unpolluted	0.94	Low
18	0.4	Unpolluted	0.28	Low
19	0.9	Unpolluted	0.50	Low
20	1.2	Unpolluted	0.55	Low
21	46.9	Unpolluted	1.03	Medium
22	22.6	Unpolluted	1.78	Medium





Qusai Y. Al-Kubaisi and Arjan A. Rasheed

Table 4 : Correlation matrix for heavy metals concentrations

Variables	Fe	Co	Ni	Cu	Zn	Cd	Pb	Mn
Fe	1	0.129	0.629	0.828	-0.084	0.843	0.925	0.694
Co	0.129	1	0.036	0.024	-0.216	0.009	0.191	-0.119
Ni	0.629	0.036	1	0.303	-0.099	0.510	0.484	0.621
Cu	0.828	0.024	0.303	1	0.013	0.898	0.875	0.607
Zn	-0.084	-0.216	-0.099	0.013	1	0.016	-0.091	-0.142
Cd	0.843	0.009	0.510	0.898	0.016	1	0.807	0.757
Pb	0.925	0.191	0.484	0.875	-0.091	0.807	1	0.550
Mn	0.694	-0.119	0.621	0.607	-0.142	0.757	0.550	1

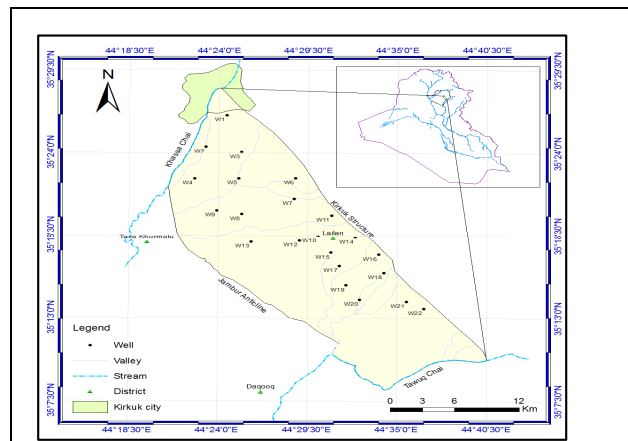


Figure 1: Location of the study area showing the sampling points

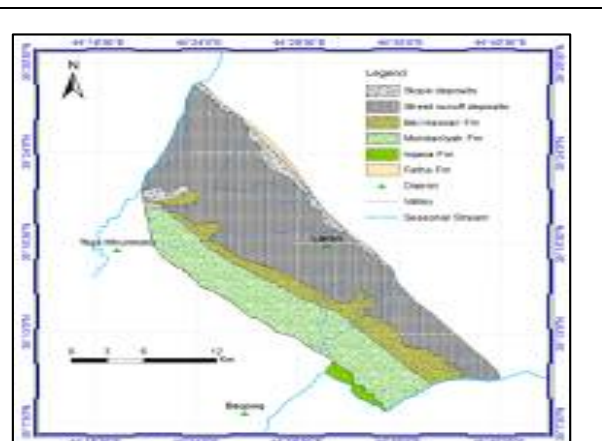


Figure 2: Geologic map of the study area

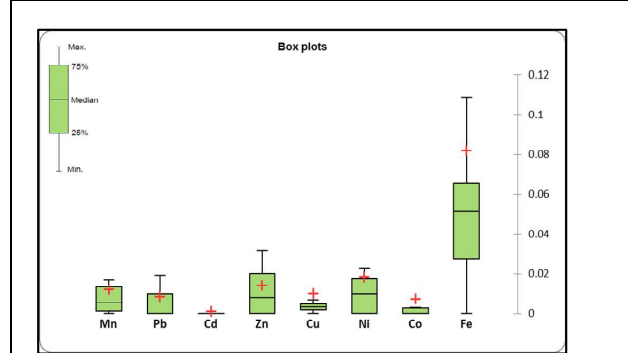


Figure 3: Box - Plots diagram for heavy metals concentrations

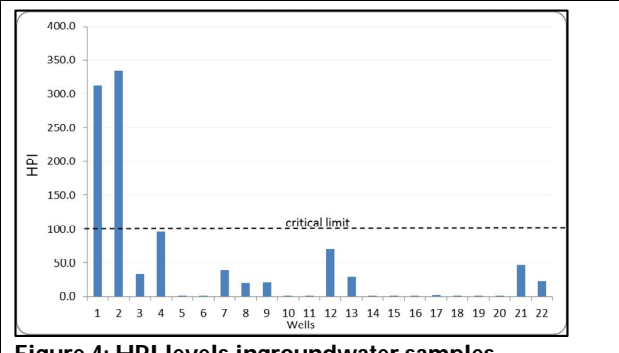


Figure 4: HPI levels ingroundwater samples





Qusai Y. Al-Kubaisi and Arjan A. Rasheed

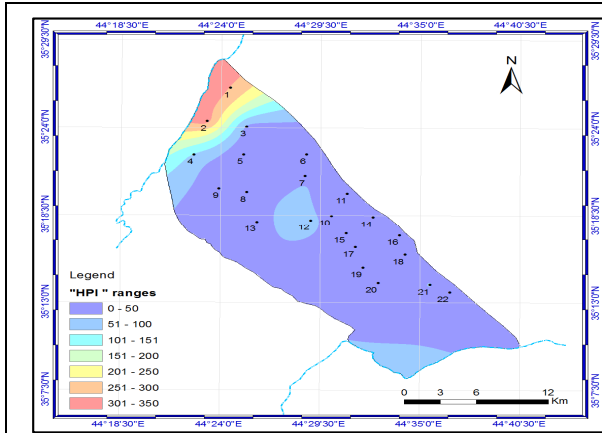


Figure 5: Spatial distribution of HPI in the study area

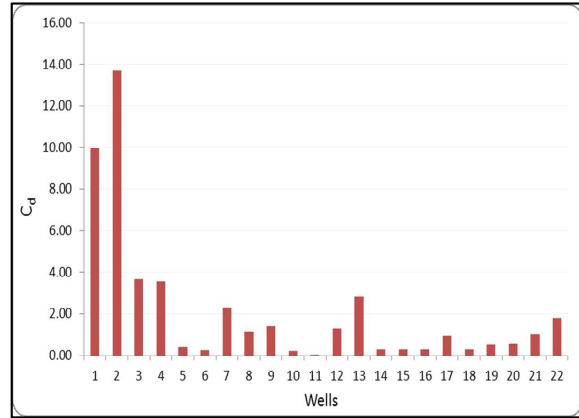


Figure 6: Cd levels in groundwater samples

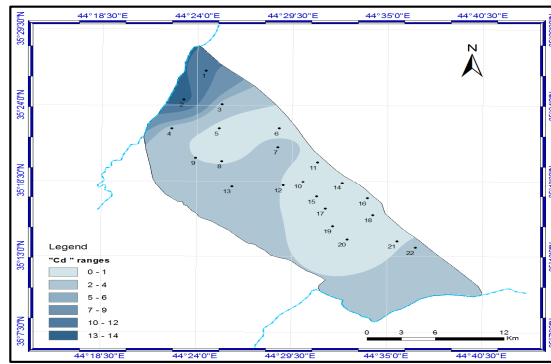


Figure 7: Spatial distribution of Cd in the study area

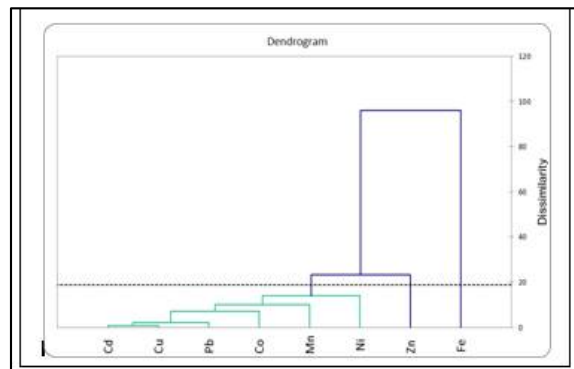
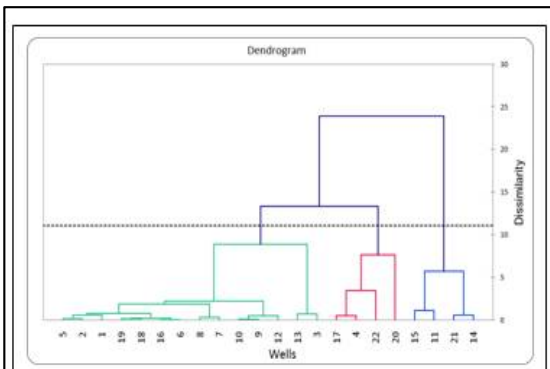


Figure 8: Cluster analysis of heavy metals concentrations in groundwater samples





RESEARCH ARTICLE

Study of Boron, Phosphate, Nitrate and H₂S Gas Pollution in the Water of Tigris River From Al Suwayra to Al Hayy City, Wasit, Iraq

Murtadha J. Issa^{1*}, Basim Shaker Obaid², and Ruaalssa Muslim³

¹Department of Geology, College of Science, University of Baghdad, Baghdad, Iraq

²Department of Soil and Water Science, College of Agriculture, University of Tikrit, Iraq

³Departments of Chemistry, College of Science, University of Wasit, Iraq

Received: 17 July 2018

Revised: 20 Aug 2018

Accepted: 24 Sep 2018

* Address for Correspondence

Murtadha J. Issa

Department of Geology,

College of Science,

University of Baghdad,

Baghdad, Iraq.

Email: aarr217@yahoo.com



This is an Open Access Journal / article distributed under the terms of the **Creative Commons Attribution License** (CC BY-NC-ND 3.0) which permits unrestricted use, distribution, and reproduction in any medium, provided the original work is properly cited. All rights reserved.

ABSTRACT

The main objective of this study is to determine of boron, Phosphate, Nitrate, H₂S gas and chemical, biological oxygen demands parameters pollution of Tigris River and wastewater that discharged to it from Al Suwayra to Al Hayy cities, Wasit Governorate / Iraq. In addition to draw the spatial distribution maps of these parameters. Twenty of water samples (15 surface and 5 waster waters) from studied area are collected and studied. Samples are from wastewaters are drainages canal, rain stream, sewages pipes and cooling tower pipes of Wasit thermal Power Plant. Field work of these samples has been completed in the March 2017. This paper reviews Boron, Phosphate, Nitrate, H₂S gas and chemical, biological oxygen demand parameters. There are many different analyzed techniques such as using Atomic Emission Spectrometry (ICP-AES) in inorganic Chemist ALS Arabia. - Kuwait – Environmental Division in boron different. The result appears, the Tigris River is polluted with phosphate (0.09 - 24 ppm), Nitrate (5.7-38 ppm), Boron (0.15- 0.26 ppm) and H₂S gas (1.5-17 ppm). These polluted parameters exceed the Iraqi and global standards limits. This has agreed with significant high BOD (3.5-13 ppm) and COD (20- 50 ppm), this turn to decrease content of oxygen dissolved level to be 4.5- 9.67 ppm in Tigris River. Wastewater contains high concentration of phosphate (1.5- 13 ppm), nitrate (5-29.8 ppm), boron (0.15- 1.43 ppm) and H₂S gas (1.7- 23 ppm) caused by agricultural, industrial activities, petroleum industry and domestic sewage pipes, chemical wastes from fertilizers, releasing large amounts of sewage untreated into the river; considered as the main cause of river water pollution in Wasit Governorate.

Keywords: Biological properties. Nutrients. Pollution. Wastewater. Phosphates.



**Murtadha J. Issa et al.**

INTRODUCTION

Tigris River and some of its branches appear to be widely used as both a prime water resource and disposal of waste discharged by industrial, agricultural, and domestic activities. Industrial processing is considered to be the main anthropogenic sources of metal and organic pollutants, the agriculture may be the main cause of pollution by the generation of chemical wastes from fertilized land, as well as the effluents from domestic activities due to large volumes of untreated sewage dumping into the river (1). In addition to pollution from human sources in this area, the river also receives saline groundwater from the floodplains that extend to the south-west until Basrah(2). In recent decades, Iraq's agricultural and water resources policies have focused on land reclamation with the expansion of irrigation networks and drainage systems to improve soil productivity. Wastewater from urban areas is released into the river, carrying discharges from domestic and industrial users, as well as hotels and hospitals (3).

water quality of rivers is degradation by various forms of pollutants. Water resources have become increasingly limited, difficult to exploit, and often affect of the major problems of human activities on water quality of rivers. Problems arise from discharges sewage and industrial waste waters, incorrect locations of industrial plants, poor land use practices, uncontrolled and poor agricultural practices, excessive use of fertilizers, and a lack of integrated water resources management (4). Poor water quality in in Tigris River after the confluence with the river Diyala indicates deterioration in the quality of this water and its incapability to support water life, which means a negative impact on biodiversity in the study region. (5).

Most freshwaters would naturally have low nutrient concentrations, and since freshwater plants and animals have evolved over millions of years in these conditions, the majority of species require low nutrient environments. Today, nutrients, particularly phosphate and nitrate, are amongst the most pervasive pollutants of freshwater across the globe. High levels of nutrients in the water result in excessive growth of aquatic plants, including algae, which suppresses less tolerant species. This, in turn, causes a raft of biological, health and economic impacts, including loss of plant, invertebrate and fish diversity, declines in the visual appeal and amenity value of water bodies, and in some cases the development of toxic blue-green algae blooms that are harmful if ingested by humans and animals. As a result of their wide ranging effects, levels of phosphate and nitrate are widely used measures for assessing waterbody quality in international monitoring programmers such as the Water Framework Directive (6).

Evidence of nutrient pollution is also a marker for other types of pollution which are still too difficult or expensive to measure. For example, waterbodies affected by nitrate pollution caused by farming in their catchments are quite likely to also be exposed to unnaturally high sediment runoff and intermittent pesticide pollution. Likewise, nutrient rich runoff from urban areas will often have high levels of heavy metals, sediment, pesticides and sewage waste(7).

Discharge points of wastewater are continuous sources of pollution for rivers, where making the rivers exposed to pollution and being contaminated. Raw sewage contains urine and faeces from toilet flushing as well as other types of human waste; it may also contain such things as toilet paper and wipes. The pathogens in raw sewage can contaminate ecological systems in addition to sickening humans and animals. In addition, raw sewage contains a variety of other constituents, including oxygen-demanding organics, which can deplete dissolved oxygen in receiving waters; pathogenic microorganisms and nutrients, which can stimulate the growth of aquatic plants (8).

The rain stream and sewages are that flow into the Tigris River inside the governorate, which are 31 pipes wastewater and there drainage rate ranging from 150 m³ / h to 750 m³ / h. The total number of sewage pipes in Wasit Governorate, which discharges its water to the Gharraf River without passing through treatment units is 14 pipes (9). Cooling towers pipes of Wasit power plant contain chemicals opened daily to the river directly to maintain the connection to the cooling water. The waste water to the Tigris River reaches a minimum of 5 tons. Main river water and its branches can be used for public consumption after the elaborate treatment. On other hand, the shortage of water in the river and discharge domestic sewage and runoff water from agricultural has negatively impacted on the



**Murtadha J. Issa et al.**

quality of water (10). Reducing of Tigris discharges in the past decades due to drought conditions and upstream damming, in addition to the increasing tension of wastewater emissions from anthropogenic activities, controlled to degradation of the downstream in water quality south of Iraq in terms of physico-chemical and biological properties (11). The amount of boron in fresh water depends on such factors as the geochemical nature of the drainage area, proximity to marine coastal regions and inputs from industrial and municipal effluents, The borate content of surface water can be increased as a result of wastewater discharges, because borate compounds are ingredients of domestic washing agents. Naturally occurring boron is present in groundwater primarily as a result of leaching from rocks and soils containing borates and Borosilicates. Boron could be released into the environment by both natural weathering processes and anthropic sources (12).

Significant sources of nitrate are chemical fertilizers, sewage sludge disposal to land, industrial discharge, and leachates from refuse dumps and atmospheric washout. Depending on the situation, these sources can contaminate streams, rivers, lakes and ground water (13). Phosphorus is the principal growth-limiting nutrient for macroplankton and phytoplankton growth in freshwater rivers and lakes and is the main cause of eutrophication in rivers and lakes. Additional phosphorus encourages algal growth beyond the natural levels. This growth depletes the dissolved oxygen in the water, causes algal blooms in lakes and fish kills in rivers (14). H₂S gas arises from sulfate reduction by bacterial action. The areas of degraded land reduced by 75,373 ha from 2000 to 2010 and were in the reversion situation as a whole. On the other hand, the rapid growth in population and the development of regional industry (such as the exploitation of oil) put considerable pressure on limited land and water resources of the region) (15).

Further investments in wastewater treatment plants, reduction of excessive fertilization (implementation of the Nitrate Directive), and agricultural development on the ecological basis are the driving forces in water quality improvement (16). The aim of this research is to study of Phosphate, Nitrate, Boron and H₂S gas pollution in the water of Tigris River from Al Suwayra to Al Hayy city / Wasit / Iraq. Compare these parameters to national and international standards and determine the suitability of the River for use in drinking and drawn spatial distribution maps for the results.

Geological and hydrological setting

Wasit region Located within unstable Shelf. The north eastern part is characterized by High Mountain when Iranian-Iraqi borders which are within low folded zone and other parts of Wasit Governorate in Mesopotamian zone. The Mesopotamian plain is covered mostly by Quaternary deposits and is considered as a part of it. The old geological outcrops in the area belong to the Pliocene age represents Bai Hassan and Mukdadiya Formations show in figure 1A. From the topographic point of view the area can be divided into two regions. The highland area is in the northeastern part and the Mesopotamian plain area, Between Tikrit and Samarra, the effluent conditions along the river seem to be retained on its western bank only, while the eastern bank becomes influent (17).

Between Fatha and Tikrit in north-western Iraq, the Tigris River drains groundwater from the Neogene and Quaternary aquifers on both banks (1). Groundwater moves in the Quaternary aquifer from the Tigris River to local depressions in the east figure 1A and B. In general, the direction of the groundwater movement coincides with the topography of the region; it is from the north and north-east to the south and south-west. Most of the groundwater in the study area is unsuitable qualitatively for human (Drinking purpose), but it can be used for livestock and irrigation purposes. The Paleocene depositions, represented by Bai Hassan and Al-Mukdadiyah formations, are the main aquifer of the eastern and north-eastern parts of the plate. The majority of wells dug up to a depth of 20 meter provide conclusions about the nature of the aquifers and their distribution within the Quaternary deposits, especially in upper parts. While the presence of deep wells, these wells reach up to 200 meter within the region give a clear perception about the nature and distribution or extension of these reservoirs within the alluvial plain deposits (18) internal report of (19)



**Murtadha J. Issa et al.****Wasit area**

Wasit province is located in the southern part of the central region of Iraq between 31.934210-33.486720 N and 44.533030-46.597930 E. Wasit is crossed via the Tigris River, the river has length of 327 km in the borders of the province, where most of the districts and areas of the province on both banks of the river. Present study covered Tigris River, its branches and drainages canal throughout from Al Suwayra to Al-hayy city in this area (Table 1). Wasit has a dry, desert climate, with temperatures easily exceeding 40°C in summer. Rainfall is rare and intense in the winter months (21).

MATERIALS AND METHODS**Field work and sampling**

Field and sampling works were achieved in March 2017, included twenty sites of the superficial Tigris River and its branches in addition to wastewater that discharged directly to the river. The field work covered throughout the study area from Al Suwayra to Al-hayy within Wasit Governorate in Iraq. Geological formations, geography, and drainage system are clearly observed during field trip in order to support for data interpreting. The sample sites are selected on the base of cities distribution (Figure 2), population community, wastewater drain sites (electrical thermal station) and other affected sites like agricultural areas on banks of the Tigris River. The field work comprises survey trips for defining the effective sampling sites along the studied area.

Laboratory Works

The water samples from Tigris River, drainage, cooling tower pipers of Wasit power plant, rainfall and sewage pipes are analyzed by numerous methods in Ministry of Municipalities and Public Work Laboratory of Wasit Sewerage Directorate. PO_4^{3-} and NO_3^- were determined by colorimetric method by Spectrophotometer 470nm and 410nm respectively (22). H_2S was measured using Sodium Thiosulfate titration. Dissolved Oxygen has been measured by means of Membrane Electrode Method (DO – Meter. YSI AMECCAN). BOD concentration has been estimated 5-day BOD test (Oxitop Bottle) as well as COD concentrations in a method of Open Reflux (titration with Standard ferrous Ammonium Sulfate Solution 0.1 N + thermoreactor that has been identified (23)). Boron was investigated using Atomic Emission Spectrometry (ICP-AES) in In-Organic Chemist ALS Arabia. - Kuwait – Environmental Division.

RESULTS AND DISCUSSION**Chemical parameters**

Assigning a class of a river reach is not simple, only in rare cases; all the relevant variables are found to be within the permissible limits (24). Concentrations of boron vary widely and depend on the surrounding geology and wastewater discharges. Boron may be derived from evaporate dissolution and carbonate weathering (25). Boron is released into surface waters through weathering processes, volcanic emission, and, in variable amounts, from anthropogenic sources that include sewage outfalls, especially with detergent products, leaching salt deposits and fertilizers. The average of boron rates in ground water in Karbala-Najaf areas with time is 3 mg/l and this average is more than the average of boron in sediment filtration of the same localities (2.6 mg/l) (26). Boron in Tigris River of studied area was ranged from 0.15 to 0.26 ppm; at PH 7.2-7.8 these results were within permissible limits of (27) are resulting from weathering process of carbonate rocks of river sediments (Table 2). Boron in waste water records high concentration in drainage canal water may be of a real agricultural activities and agricultural fertilizers in some areas. Boron concentration reaches 0.15 ppm in Rain stream and sewage pipes at PH 6.9- 8.1 in Wasit Governorate



**Murtadha J. Issa et al.**

(Figure 3). Dujaila River in study area Water, nitrate ion concentration of the river water samples in August 2015, with an average value of (4.43 ppm), in the drainage water samples with an average value of (17.9 ppm). Phosphate ion concentration in the river water August 2015 was an average value is 0.12 ppm (32). In study area, There were bacterial contamination in water exceeded the Iraqi and international standards criteria in in Al-Haay and Al-Bashaar water within Wasit governorate (33). Al-Dujaila and Al-Gharraf, BOD values affected evidently by excreta untreated wastewater because they decrease in non-contaminated positions and rise in the contaminated sites (8) and (34). Nitrate is the most highly oxidized forms of nitrogen compounds, and is commonly existent in surface and groundwater since it is the final product of the aerobic decomposition of organic nitrogenous matter. The nitrate itself is not a direct toxicant but is a health hazard because of its conversion to nitrite which reacts with blood haemoglobin to cause methaemoglobinaemia (14). Irregular variation pattern in concentration of nutrients in surface water are subjected to intense anthropogenic activities (35).

Anthropogenic activities are major sources of phosphate and nitrate pollution in aquatic ecosystems. These nonpoint sources of nutrients are difficult to measure and regulate because they are derived from activities dispersed over large expanse of land and are variable in time because of weather and climate changes. In rivers, lakes and streams they cause various problems such as toxic algal blooms, hypoxia, fish deaths, loss of biodiversity and species composition, loss of aquatic plant beds and coral reefs, and other problems. Nutrient enrichment seriously impairs aquatic ecosystems usage, purposes and functions (36).

In present study, the concentration of nitrate was from 5.7 to 38 ppm as range in Tigris River. These are due fertilizers and releasing of untreated sewages in the end of river in Wasit Governorate this agreed with (37). Nitrate in Tigris River exceeds permissible limits of (29). Nitrate in wastewater pipes was about 5-29.8 ppm as range (Figure 4). Nitrate content increase in river water could be related to the impact of several sewage effluents and drainages canal that discharged into the river without treatment. This is clear significant; the sources of nitrate are chemical fertilizers, domestic effluents, sewage sludge disposal to land, industrial discharge, leachates from refuse dumps and atmospheric washout. Depending on the situation, these sources can contaminate streams, rivers and ground water. Unpolluted natural water contains minute amounts of nitrate (13).

Phosphates can enter aquatic environments from the natural weathering of minerals in the drainage basin, from biological decomposition, and runoff from human activities in urban and agricultural areas (38). In present study, the concentration of phosphates ranged from 0.09 to 24 ppm in Tigris River, The maximum concentration was in Sheik Saad station due to the flood impact. Wastewater that flowed to the river in Wasit Governorate was varied from 1.5 to 13 ppm (Figure 5). From the above results, Phosphate concentration in Tigris River exceeds permissible limits of (27), (28) and (29). So, In relation to study area increasing of phosphate content comes from, industrial activities especially cooling tower pipes of Wasit thermal power plant in Al Zubaydia Station which has the highest content of Phosphate. Fertilizers, pesticides as a result of many waste water pipes that discharged into the long of river from rainfall, sewages and Wasit as well large agricultural areas along the Tigris River especially in Al Shuhaymiya Station. The high concentrations of phosphates in river water are indicated there are various sources of phosphate to rivers, such as firm rock deposit, runoff from surface catchments, and interaction between the water and sediment from dead plant and animal remains at the bottom of rivers (39). In Al Ahrarr area the concentration of (PO_4^{2-}) are detected in surface water as the result of industrial and urban wastes from the Al Ahdeboil field (40). High level of Phosphates concentration attributed to fertilizers and detergents which contain a high content of PO_4^{2-} from petroleum activities where they use considerable amounts of detergents that contains high rate of phosphates.

Hydrogen sulfide gas (H_2S gas) also occurs naturally in some groundwater. It is formed from decomposing underground deposits of organic matter such as decaying plant material. It is found in deep or shallow wells and also can enter surface water through springs, although it quickly escapes to the atmosphere. Hydrogen sulfide often is present in wells drilled in shale or sandstone, or near coal or peat deposits or oil fields. Hydrogen sulfide is flammable and poisonous. Usually it is not a health risk at concentrations present in household water, except in very



**Murtadha J. Issa et al.**

high concentrations. While such concentrations are rare, hydrogen sulfide's presence in drinking water, when released in confined areas, has been known to cause nausea, illness and, in extreme cases, although many impurities are regulated by Primary or Secondary Drinking Water Standards set by the EPA, hydrogen sulfide is not regulated because a concentration high enough to be a drinking water health hazard also makes the water unpalatable (41). In studied area, H₂S gas concentrated Al Ahrarrstation Record 17 ppm (Sample num. 9AHR) and lower concentration was 1.5 ppm. All results values of this research higher than permissible limits of WHO 2011, this intersected with study of (42) in the Baiji Area where H₂S is below detection limits, which is within national and world standards. This elevation in H₂S gas in water river attributable to the presence of sulfur which decant directly to Tigris River especially in Al Ahrarrstation near Al Ahdeb Oil Field (Figure 6), Wastewater contain large concentration of H₂S gas, this may be due to the oil production activity of the in Al Ahrarrstation near Al Ahdeb Oil Field reduction by bacterial action in these waters (Sample Num. 19KSP).

Biological properties

Dissolved Oxygen

The concentration of dissolved oxygen in the water is controlled by numerous factors which involving: temperature, hydrodynamic characteristics, air pressure, and process of photosynthesis respiratory activity of aquatic organisms. Decrease in the dissolved oxygen content during summer season could also be attributed to increase in temperature will result in a decrease in the concentration of dissolved oxygen, photosynthesis and aquatic organisms respiration also play an important role with fluctuations of dissolved oxygen concentration in water because self-purification occur when the decomposing organisms use the dissolved oxygen to degrade the organic matter (43). This evident in present study, the dissolved oxygen for the river water samples in Wasit governorate area ranged between 4.57 to 9.67 ppm. Waste water is that flowed to the river in the governorate ranged from 3.6 -8.1 ppm. The low concentration of dissolved oxygen was in rain stream and sewages water pipes because the water is polluted with huge amount of organic matter, an amount of dissolved oxygen would be rapidly consumed in the biological aerobic decay which would affect the water quality; then reduced DO in water and affect the river lives. In another meaning, these wastewaters have low of DO value in some sites in study area belongs to the density of organism which consumes the DO for their living activities and the high concentration of BOD and COD.

Biological Oxygen Demand

Biological oxygen demand is defined as the change in the concentration of dissolved oxygen when a sample is incubated in the dark at 20 °C for five days. BOD₅ tests measures only biodegradable fraction of the total potential DO consumption of a water sample. High BOD₅ levels indicates decline in DO, because the oxygen that is available in the water is being consumed by the bacteria leading to the inability of fish and other aquatic organisms to survive in the river (44). In this study, the BOD values for surface water samples in Wasit governorate area ranged between 3.5 to 13 ppm for the Tigris River. Waste water that flowed to the river in Wasit Governorate ranged from 8.2 to 180 ppm; the result indicates that the Tigris River can be described as critical water whereas wastewater of pollution water according to (45). Organic matter is oxidized to CO₂ and H₂O by organism. These may be come from the waste water pipes that flowed directly without treatment to the river which are Polluted. These lead decrease in the amount of DO. DO decreases with increase BOD indicating strong negative relationship (Figure 7).

Chemical Oxygen Demand (COD)

Consequently, it is an indicator to measure the amount of water pollution and more applications for chemical oxygen requirement in determining the quantity of organic pollutants in water High organic materials in water discharge appear by (COD) parameter, this is due to the higher use of chemical compounds, solution (46). In present study, the





Murtadha J. Issa et al.

lower COD value for surface water samples in Wasit governorate area are 20 ppm for the Tigris River. The COD in Tigris River in study area record the highest value in Al Zubaydiya station sample. 6ZDR_c (50ppm) was near Wasit thermal power plant. This elevation due to the chemical compounds that came from the wastewater pipes are collected and dissolved in the water which is carried out to the river directly without any treatment, especially the cooling water and rainfall- sewages pipes which contain many chemical materials. Wastewater contains high concentration of COD reach 258ppm in rain stream and sewages pipes comparison with lower contain record in drainages (21ppm)

CONCLUSIONS

This study revealed evidently Tigris River is polluted water in the Phosphate, Nitrate, H₂S gas and biological parameters. Nitrate in Tigris River more than permissible limits of (29) Nitrate content increase in river water could be related to the impact of several sewage effluents and drainages canal that discharged to the river without treatment. Phosphate concentration in the River is greater than permissible limits of (27), (28) and (29) Increasing of phosphate content comes from cooling tower pipes of Wasit thermal Power Plant in Al Zubaydiya station and chemical fertilizers from large agricultural areas along the Tigris River especially in Al Shuhaymiya station. Also many waste water pipes that discharged along the river from rain stream and sewages system.

It should be noticed that the station of Sheik Saad show an increase in nitrate and phosphate concentration are double from other stations because of the floods that swept the governorate from Iran during the sampling period. Besides the Rule of the detergents materials which are used in the petroleum production processes in the Ahdab oil field. All results values of H₂S in this research higher than permissible limits of (28). This due the presence of sulfur which decant directly to Tigris River especially in Al Ahrar station near Al Ahdeb Oil Field as associated gas, besides oil spills, Distribution of hydrogen sulfide ion in river stations. Wastewater contains large concentration of H₂S gas. (Sample Num. 19KSP) because a lot of organisms such as bacteria that reduction sulfate to H₂S gas. The BOD and COD values affected clearly by excreta untreated different types wastewater (drainages canal, rain stream, sewages and cooling tower pipes) in this research because they decrease in non-contaminated sites, increase in the contaminated sites with low DO in the same time. In the conclusion we can say that the water of the river is not suitable for drinking in the term of studied properties.

REFERENCES

1. ESCWA-BGR Cooperation, 2013. Inventory of Shared Water Resources in Western Asia (Online Version). Chapter 4: Shared Tributaries of the Tigris River. Beirut
2. ACSAD and UNEP-ROWA (Arab Center for the Studies of Arid Zones and Dry Lands; United Nations Environment Programme- Regional Office for West Asia). 2001 Surface Water Resources in the Euphrates and Tigris River Basin. Unpublished work.
3. Al-Rawi, S. M. 2005. Contribution of Man-made Activities to the Pollution of the Tigris within Mosul Area, Iraq. International Journal of Environmental Research and Public Health, 2 (2): p. 245-250.
4. Al-Mayah, W. T. J. 2018. Evaluating of Water Quality in Al-Gharraf River Southern of Iraq Using Different Environmental Indices, Remote Sensing Technique, and Geographical Information System. Ph.d . Thesis. College of Science, University of Baghdad, Iraq.
5. AL-Doulaimy, A. Q. H. 2015. The Environmental Impacts of Diyala Tributary in the Quality of the Tigris River Water – Baghdad City M. Sc. Thesis. College of Science, University of Baghdad, Iraq.
6. Brahney, J., N. Mahowald, D. S. Ward, A. P. Ballantyne, and J. C. Neff (2015), Is atmospheric phosphorus pollution altering global alpine Lake stoichiometry?, Global Biogeochem. Cycles, 29, 1369–1383, doi:10.1002/2015GB005137





Murtadha J. Issa et al.

7. Biggs, J., McGoff, E., Ewald, N., Williams, P., Dunn, F. and Nicolet, P. 2016. Clean Water for Wildlife technical manual. Evaluating PackTest nitrate and phosphate test kits to find clean water and assess the extent of pollution. Freshwater Habitats Trust, Oxford
8. Al-Zamili H. A. A. 2014. Effect of local domestic sewage in water quality of Al-Dujaila River in Al-Kut city/ Iraq. M. Sc. Thesis. College of Science, University of Baghdad, Iraq.
9. Ministry of Municipalities and Public Work, Wasit Sewerage Directorate Internal report, 2018.
10. Wisam Th. Al-Mayah, Adel M. Rabee. 2018. Application of Overall Index of Pollution (OIP) for the Evaluating of the Water Quality in Al-Gharraf River southern of Iraq. Iraqi Journal of Science, 2018, Vol. 59, No.2A, pp: 660-669 DOI:10.24996/ij.s.2018.59.2A.4
11. Al-Gburi H.F.A, Al-Tawash, B. S, Al-Lafta, H. S. 2017. Environmental assessment of Al-Hammar Marsh, Southern Iraq. Heliyon 3 (2017) e00256 Article No-e00256.
12. Salih, W. M. Saadi K. Alnasri, and Ali Abdulameer Al Abdalaali, 2012: Removal of Boron from Simulated Iraqi Surface Water by Electrocoagulation Method. Journal of Engineering. Volume 18 November 2012.
13. Foglar, L. 2013. Nitrate removal in continuous-flow stirred reactor. Chem. Biochem. Eng. Q. 27 (1): 7-13.
14. EPA (Environmental Protection Agency). (2013). Domestic waste water treatment systems, Ireland. www.epa.ie/whatwedo/advice/wastewater.
15. Jabbar1, Dr. Ammar S. Dawood. 2015. Evaluation of Sandy Land Degradation Based on Geo-Information Techniques: a case Study South Part of Iraq. International Journal of Engineering Inventions e-ISSN: 2278-7461, p-ISSN: 2319-6491 Volume 5, Issue 5 [May 2015] PP: 39-45
16. Ami .A , and Tadi.L , 2018. Analysis of Basic Physical-Chemical Parameters, Nutrients and Heavy Metals Content in Surface Water of Small Catchment Area of Karašica and Vučica Rivers in Croatia. <http://dx.doi.org/10.3390/environments5020020>
17. Jassim, S. Z. and Goff, J. C., 2006: Geology of Iraq. Published in Heritage Oil Corporation, 337p.
18. Al Jubory, H.K.S. 2005. HYdrochemical and hydrological study of Kut plate (NI-38-15). Scale 1: 250000. Geosurvey. Internal report. 45p.
19. Ministry of sciences and technology. Space and Communications Service. 2015. Water Harvesting in Wasit Governorate. Internal reports. 209p
20. Varoujan k. Sissakian (Export) and Dr. Saffa F. Fouad (Export) 4th Edition, 2016. Geological Map of Iraq, Scale 1:1 1000000, 2016, GEOSURV. Boszke, L., Sobczynski, T., Kowalski, A. 2004. Distribution of Mercury and Other Heavy Metals in Bottom Sediments of the Middle Odra River (Germany/Poland). Polish Journal of Environmental Studies, 13: 495-502.
21. Iraqi Meteorological Organization and Seismology (I.M.O.S). 2017 Department of Climate, Al Kut, Al Aziziya, Al Hayy and Badrah Stations Data, Unpub. Statistical Reports, Baghdad (1994-2017).
22. Kenkel, J., 2003: Analytical chemistry for technicians 3rd, CRC phess LLC, FL, USA, 198p
23. APHA, AWW and WPCF, 1996: Standard Methods for the examination of water and waste water. American public Health Association 9 19thed) Washington
24. Asadollahfardi, G. 2015. Application of water quality indices to define surface water quality in Tehran. Int J Water 5(1):51-69.
25. Xi'an .J, Jin. Z, Wang. J. 2014. Geochemistry of trace elements and water quality assessments of natural water within the tarim river basin in the extreme arid region, NW China. Journal of geochemical Exploration. V 136. 118-126p
26. Al-Dabbas, M. A. and Al-Jumili, K.A., 2005: Alternate Relationship between Sediments and Ground water by using Boron as Indicator in Kerbala – Nejaf Area – Middle of Iraq. Report on the Magazine of Kerbala University Vol. 3, no. 12, pp. 106-119.
27. Iraqi standard, 2009: Iraqi Standard of Drinking Water No. 417 modification No. 1.
28. WHO (World Health Organization), (2011), "Guidelines for drinking-water quality". 4th edition. World Health Organization. 564p.
29. USEPA (US Environmental Protection Agency), (2011), "2011 Edition of the Drinking Water Standards and Health Advisories". Office of Water. U.S. Environmental Protection Agency. Washington, DC. 18p..





Murtadha J. Issa et al.

30. Iraqi Standards, 1996: Iraqi Standard for Drinking Water, No 417, 1996.
31. ARC Map 10.6, 2018 of maps distribution for chemical parameters
32. Maiws. S.U. 2016. Assessment of Dujaila River Water and Its Relationship with the Agricultural Soils of Dujaila Project Wasit Governorate - Central Of Iraq. M. Sc. Thesis. College of Science, University of Baghdad, Iraq.
33. Al-Tmemy, W.B.M. 2014. Investigation of drinking water quality in Al-Haay and Al-Bashaar water treatment plants in Wasit province southern Iraq.
34. Al-Grawi, E.D.C., and G.R.L. Al-Awsi. 2018. "Expression of CDKN2A (P16/Ink4a) among Colorectal Cancer Patients: A Cohort Study." *Journal of Pharmaceutical Sciences and Research* 10 (5).
35. Ewaid, S. H., & Abed, S. A. (2017). Water quality index for Al-Gharraf River, Southern Iraq. *The Egyptian Journal of Aquatic Research*, 43 (2), 117-122. <https://doi.org/10.1016/j.ejar.2017.03.001>
36. AL-NASHI, A.P. Ali Abed Raheem; AL-AOSI, Ghaidaa Raheem Lateef (2013). Isolate and diagnose the bacteria present in the hospital in the city of Diwaniyah and the statement of the mechanisms to control the use of antibiotics and antiseptics. *Al-Qadisiyah Journal of Pure Science*, V. 18 (3): 11-20.
37. Al-Mayah, W. T. 2013. Effect of domestic sewage on water quality of Al-Gharraf River in Al-Haay city. M. Sc. Thesis. College of Science, University of Baghdad, Iraq.
38. Al Saady, Y.I.I. 2016. *Environmental impact assessment of land use on lesser Zabriver basin, north east of Iraq*. PH.D. Thesis. College of Science, University of Baghdad, Iraq.
39. Adesuyia, A., Nnodu V.C., Njoku K.L., Anuoluwapo, Jolaoso, 2015. Nitrate and Phosphate Pollution in Surface Water of Nwaja Creek, Port Harcourt, Niger Delta, Nigeria. *International Journal of Geology, Agriculture and Environmental Sciences Volume – 3 Issue – 5 October 2015 Website: www.woarjournals.org/IJGAES ISSN: 2348-025*
40. Al-Dabbas M. A. Maiws S.U. 2016 Validity of Dujaila River Water within Wasit Governorate - Central Iraq *Iraqi Journal of Science*, 2016, Vol. 57, No.2C, pp:1452-1461.
41. Flores, M. J. L. and Zafaralla, M. T. (2012). An assessment of the physicochemical parameters of mananga River, Cebu, Philippine. *Intern.P. Rev. J.*, ISSN 2244-1581.
42. Abed, Salwan Ali. 2017. "Occurrence of Anataidae in Sawa Lake: A Ramsar Wetland Site in Southern Iraq." *Journal of Advanced Zoology* 38 (1). Taru Publications: 43–51.
43. Adeyemo, O. K.; Adedokun, O. A. and Yusuf, R. K. (2008). Seasonal changes in physico-chemical parameters and nutrient load of river sediments in Ibadan city, Nigeria. *Global NEST J.* Vol.10 (3) pp: 326-336.
44. Hassan, R. A. A. 2018 The Impact of Al Ahdeb Oil Field on The Environment Pollution in Al Ahrar District, Wasit Governorate, Iraq. M. Sc. Thesis. College of Science, University of Baghdad, Iraq.
45. Oram, B., Professional Geologist (PG). 2018. Water Research Center B.F. Environmental Consultants Inc 15 Hillcrest Drive, Dallas, PA 18612 <https://www.water-research.net/index.php/sulfur>
46. Abed, M.F. 2016. Environmental Risk Assessment of Industrial District, Baiji Area. PH.D. Thesis. College of Science, University of Baghdad, Iraq. Mushtak T.
47. Toma, J. J. 2013. Limnological study of Dokan, Derbendikhan and Duhok lakes, Kurdistan region of Iraq. *Open J. Eco.* Vol.3 (1): 23-29.
48. Vaishali, P. and Punita, P. 2013. Assessment of seasonal variation in water quality of River Mini, at Sindhrot, Vadodara. *Int. J. Environ.Sci.* Vol.3 (5), ISSN 0976 – 4402
49. Pandey, K. J.P., Shula, S.P., Trivedi, 2005: Fundamental of Toxicology. New book Agency (P.Ltd), 356p. Abawi, S. A, and Hassan, M.S., 1990: Environmental Engineering Water analyses. International Library, Baghdad, Iraq, 296p.
50. Ma'alah, W. N. 2013. Examining the Effects of Baghdad Medical City Waste Water on the Quality of Tigris River. Ms.c. Thesis. College of Science, University of Baghdad, Iraq.





Murtadha J. Issa et al.

Table.1: Geographic coordination of the studied water sampling location

Num.	water	Location	description	Coordination		
				N	E	
1	1SUR	Al Suwayra	Surfaces water	RiverTigris	32.92094	44.795635
2	2TJR	TajAldin		TigrisRiver	32.985134	44.859647
3	3AZR	Al Aziziya		Tigris River	32.901216	45.065334
4	4ShR	Al Shuhaymiya		Tigris River	32.753249	45.215423
5	5ZDR _b	Al Zubaydia		Tigris River	32.794961	45.088997
6	6ZDR _c	Al Zubaydia		Tigris River	32.793793	45.088591
7	7ZDR _a	Al Zubaydia		Tigris River	32.770125	45.113997
8	8NMR	Al Numaniya		Tigris River	32.55492	45.420234
9	9AHR	Al Ahrarr		Tigris River	32.527463	45.604188
10	10KR _a	Al Kut		Tigris River	32.5058	45.806376
11	11KR _b	Al Kut		Tigris River	32.486788	45.826392
12	12KR _c	Al Kut		River Tigris	32.497285	45.816092
13	13WaR	Nahyat Wasit/		Dujaila River	32.518771	46.405741
14	14HYR	Al Hayy		Al Garaf River	32.171627	46.038678
15	15SdR	Sheik Saad		Tigris River	32.571094	46.274087
16	16LD	Al Suwayra	wastewater	Al- ling Drainage	32.998749	44.775478
17	17HD	TajAldin		Drainage Halata	32.924245	44.912627
18	18 CTP	Al Zubaydia		Cowling Tower Pipes / Thermal Power Plant	32.902403	45.062268
19	19KSP	Al Kut		Sewage pipes&Rain stream	32.768	45.171668
20	20HSP	Al Hayy		Sewage pipes&Rain stream	32.556756	45.416407

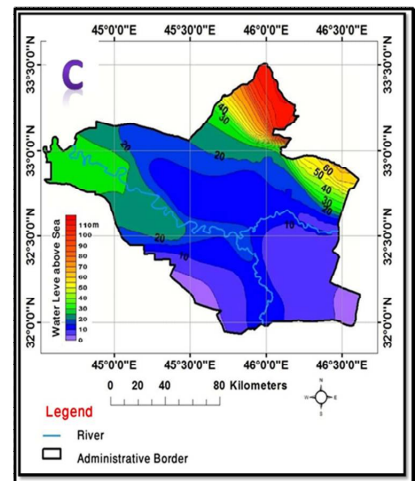
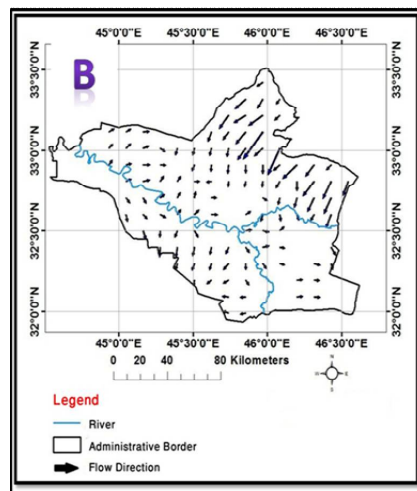
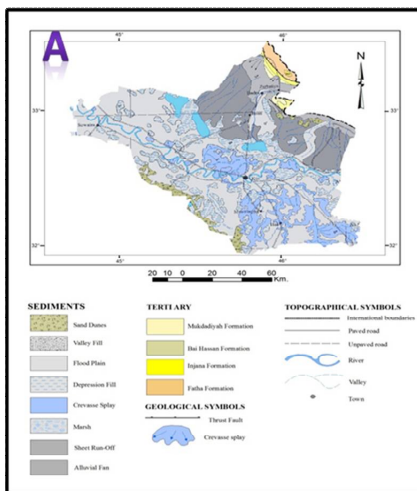


Figure 1 A: Geological map of studied area (Wasit Governorate (20), B: Direction of groundwater, C: Contour map groundwater level (18) in internal reports of Ministry of sciences and technology in 2015 (19)





Murtadha J. Issa et al.

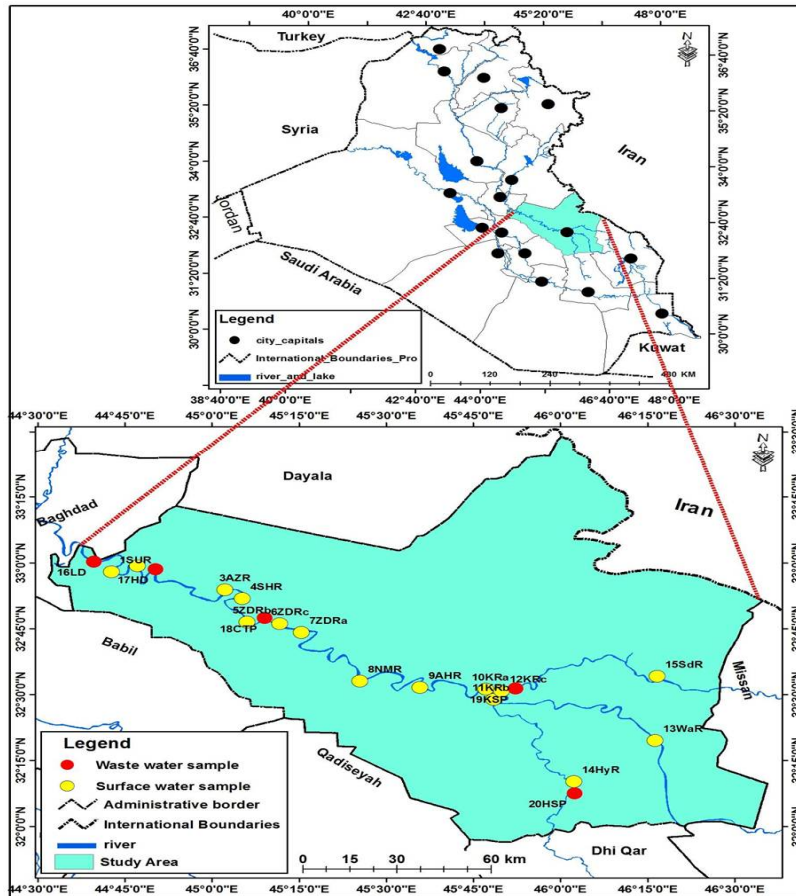
Table 2: Concentration B, NO₃⁻, PO₄⁻³ and H₂S gas and biological test (DO, BOD and COD) parameters in ppm units of surface water samples for the sampling

Sam. Num	Station	Sample Name	PH	Chemical parameters				Biological test			
				ppm							
				B	NO ₃ ⁻	PO ₄ ⁼	H ₂ S	DO	BOD	COD	
1	Al Suwayra	1SR	Tigris River	7.3	0.19	6	1.4	3.4	7.65	4.6	22
2	TajAldin	2TJR		7.8	0.18	17	8	1.7	6.22	5.4	26
3	Al Aziziya	3AZR		7.7	0.22	8	0.8	3.6	9.67	6.2	28
4	Al Shuhaymiya	4ShR		7.7	0.22	23	10	3.8	7.7	10	35
5	Al Zubaydia	5ZDR _b		7.5	0.21	5.7	7.6	3.4	7.3	6.82	40
6	Al Zubaydia	6ZDR _c		7.8	0.21	6.2	7.9	5.1	7.9	7.04	50
7	Al Zubaydia	7ZDR _a		7.7	0.2	9.2	6.8	4.6	7.8	6.13	36
8	Al Numaniya	8NMR		7.2	0.21	8	0.09	3.4	6.91	4.6	22
9	Al Ahrarr	9AHR		7.4	0.2	13	4.8	17	7.36	5.1	27
10	Al Kut	10KR _a		7.8	0.18	10	3.2	1.8	9.61	3.5	20
11	Al Kut	11KR _b		7.4	0.2	14.2	5.6	3.7	9.17	4.2	26
12	Al Kut	12KR _c		7.7	0.2	30.6	10.2	5.1	8.84	4.6	28
13	Nahyat Wasit / Dujaila River	13WaR		7.5	0.22	24	7	3.4	6.37	10	35
14	Al Hayy / Al Gharaf River	14HyR		7.4	0.15	26	5.5	1.5	4.57	13	36
15	Sheik Saad	15SdR		7.6	0.26	38	24	6	9.23	7.2	21
R*			7.2- 7.8	0.15- 0.26	5.7- 38	0.09- 24	1.5 - 17	4.57- 9.67	3.5- 13	20- 50	
16	Al- ling drainage / AISuwayra	16LD	Waste Water	8.1	1.41	29.8	2.2	6.8	7.2	ε	30
17	Haltadrainge / TajAldin	17HD		7.7	1.43	5	1.5	1.7	8.1	14	21
18	Al Zubaydia	18 CTP		8.2	0.71	29	13	3.3	3.6	21	40.7
19	Al Kut	19KSP		6.9	0.16	20	9	23	4.5	180	258
20	Al Hayy	20HSP		7.4	0.15	22	12	21	4.1	130	256
R*			6.9- 8.1	0.15- 1.43	5- 29.8	1.5- 13	1.7- 23	3.6- 8.1	8.2- 180	21- 258	
(27)		-----	Standards Limits		0.5	50			> 5**	> 5**	> 5**
(28)		-----			2.4	50	0.4	0.05- 0.1			
(29)		-----				10					

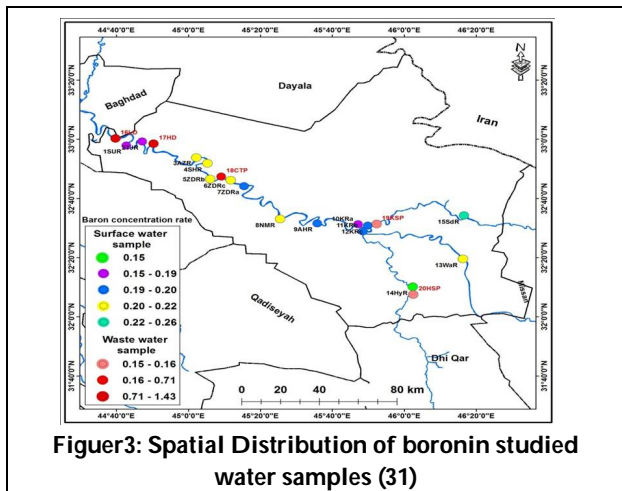




Murtadha J. Issa et al.



Figuer2: Sampling map of studied area according to Arc map program 10.5 (map of Iraq scale 1:1000000)



Figuer3: Spatial Distribution of boronin studied water samples (31)

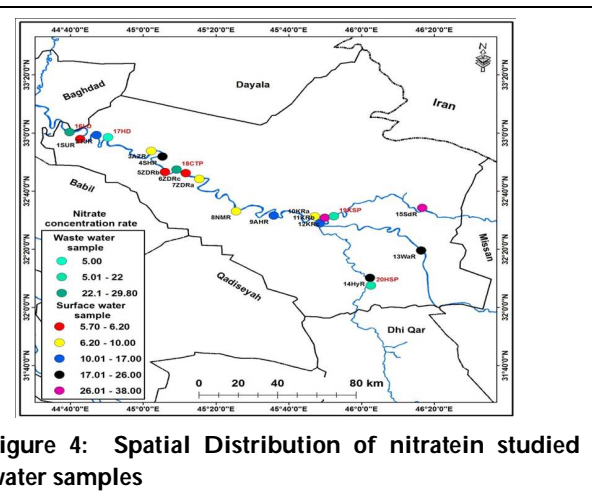


Figure 4: Spatial Distribution of nitratein studied water samples





Murtadha J. Issa et al.

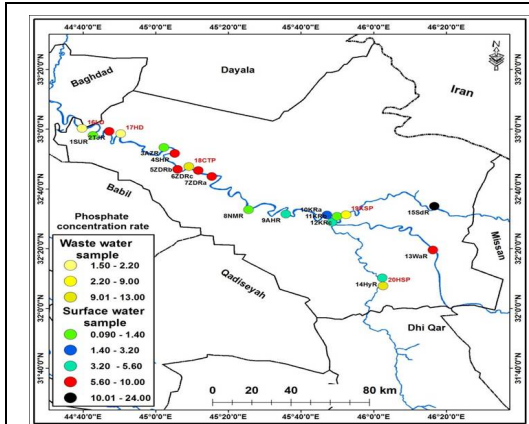


Figure 5: Spatial Distribution of phosphate in studied water samples

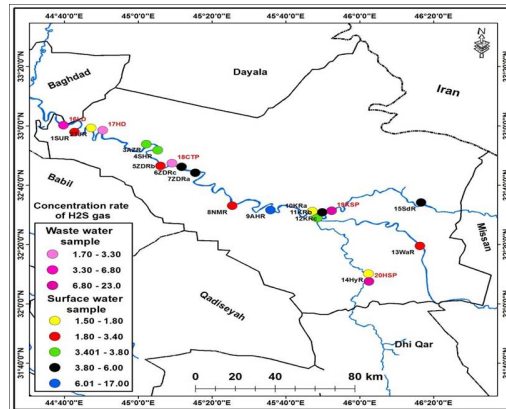


Figure 6: Spatial Distribution of H₂S gas in studied water samples of Wasit governorate

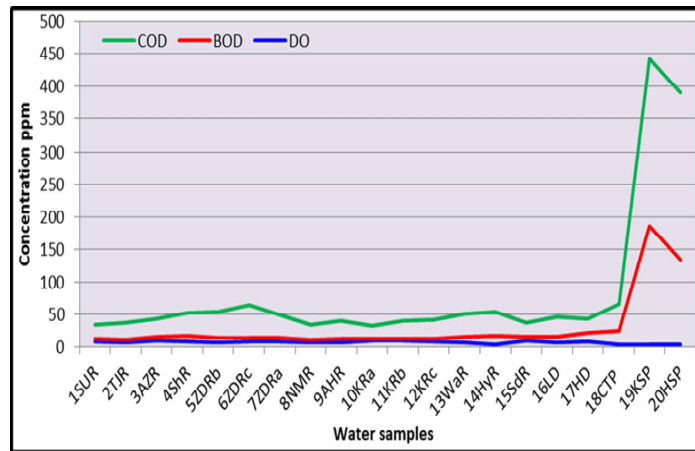


Figure 7: Bar shape for DO, BOD and COD of surface and wastewater in Wasit Governorate.





Investigate the Conductivity and Dielectric Properties of Polymer Electrolytes

Mustafa Kadhum¹, Mohammed K. Jawad^{1*} and Abdulkareem M.A. Alsammarraie²

¹Department of Physics, College of Science, University of Baghdad, Baghdad, Iraq.

²Department of Chemistry, College of Science, University of Baghdad, Baghdad, Iraq.

Received: 13 July 2018

Revised: 17 Aug 2018

Accepted: 19 Sep 2018

*Address for Correspondence

Mohammed K. Jawad

Department of Physics,

College of Science,

University of Baghdad, Baghdad, Iraq.

Email : tophy_007@yahoo.com



This is an Open Access Journal / article distributed under the terms of the **Creative Commons Attribution License** (CC BY-NC-ND 3.0) which permits unrestricted use, distribution, and reproduction in any medium, provided the original work is properly cited. All rights reserved.

ABSTRACT

The effect of mixed iodide salts system with two dissimilar cations by varying the weight ratio of potassium iodide (KI) and cesium iodide (CsI) to enhance the conductivity of polymer blend electrolytes (GPEs) was studied. Two series of polymer blend electrolytes (As and Cs) composed of Poly (methyl methacrylate) (PMMA) / Polyacrylonitrile (PAN), (80/20) wt.% and ethylene carbonate (EC), propylene carbonate (PC) (1:1) as plasticizer have been synthesized using solution cast technique. All the electrolytes based on binary salts have shown conductivity enhancement compared to their single cation counterparts. The ionic conductivity of electrolytes with relatively large cations, Cs⁺, was higher and essentially constant. The highest ionic conductivity at room temperature for sample C4 is found to be (3.4 mS.cm⁻¹) which contain salt KI/CsI (15/20) wt.% at room temperature. The temperature dependence conductivity has been performed in the range of 298–373 K and it is observed that it obeys the Arrhenius behavior. It has been observed that the dielectric constant, increases with temperature in the lower frequency region and is almost negligible in the higher frequency region.

Key words: Ionic conductivity, Polymer electrolyte, Potassium iodide, Cesium Iodide

INTRODUCTION

Polymer electrolytes have gained wide attention due to its potential application in rechargeable lithium-ion batteries during the three decades. For the promising application of polymer electrolyte, lithium-ion polymer rechargeable batteries are applicable in automotive industries, portable devices, aerospace applications, etc. Most of the recent studies have been directed to the preparation and characterization of gel polymer electrolytes which exhibit higher ionic conductivity at ambient temperature. Gel polymer electrolytes prepared by incorporating liquid electrolyte into a matrix polymer such as PAN and PMMA have been employed in quasi-solid-state DSSCs [1,2]. However, such gel polymer electrolytes suffer from poor mechanical strength, making assembly difficult and increasing the incidence of





Mustafa Kadhum et al.

shorting between electrodes, because of impregnation of liquid electrolyte into a polar polymer results in softening of the polymer. To overcome this problem, the porous separators such as microporous polyolefin membranes and nonwoven mats have been used as the supporting framework to make gel polymer electrolyte for lithium-ion batteries. Here the porous separator serves as the mechanical support, while gel polymer electrolyte coated onto the separator provides the necessary ionic conductivity between electrodes [3,4]. Redox electrolytes are ionic conductors in which charges are transported via diffusion or by migration. The ionic salt and plasticizers such as EC and PC offer a compromise between a solid electrolyte and a gel electrolyte. These gel electrolytes possess ionic conductivities close to their liquid counterparts and superior mechanical properties compared to liquid electrolytes [5]. The aim of this work is to optimize the ionic conductivity and dielectric constant systematically by means of varying the KI and CsI salt composition in a PAN/PMMA based electrolyte.

MATERIALS AND METHODS

PAN, PMMA, KI, CsI, I₂, (PC) and (EC) all with purity greater than 98%, purchased from Aldrich. Iodine (I₂ – Breckland Scientific Supplies), were used as starting materials. The electrolyte samples prepared with fixed ratio of PAN (20%), PMMA (80%), EC and PC (1:1) the iodine (I₂=10%) and the weight ratio of KI and CsI were varied as given in Table1. At first, adequacy amount of EC, PC, and iodides (KI and CsI) were medley in a glass container with continuous stirring at 50 °C for approximately 2h. Then PAN was added to the mixture which was stirred further keeping it at 40 °C for about 4 hours after that PMMA was added to the mixture with continues stirrer for 1 h. Finally, iodine was added to the mixture and heated to about 60 °C along with continuous stirring for a few more minutes until a homogeneous viscous solution was obtained. The resulting slurry was then cast onto a glass container. The complex impedance measurements were performed using LCR-8110G/8105G, impedance analyzer in the 50 Hz – 2 MHz frequency range to evaluate the ionic conductivity of the samples, The relationship of the specific ionic conductivity σ with the bulk resistance R_b can be represented by a simple form as shown in equation (1) for the measurement setup with polymer electrolytes film sandwiched between two electrodes [6]:

$$\sigma = \frac{L}{R_b A} \dots \dots \dots (1)$$

where L (cm) represents the separation distance between the electrodes, A (cm²) is the area of the electrode and σ (S.cm⁻¹) is the specific conductivity The sample cell was prepared by sandwiching the electrolyte using two stainless steel electrodes. The temperature of the sample varied from 25 to 60 °C during the measurements. The real parts of dielectric constant (ϵ_r) values were calculated using the following eq. (2) [6]:

$$\epsilon_r = \frac{Z_i}{\omega C_0 [Z_r^2 + Z_i^2]} \dots \dots \dots (2)$$

where ω is the angular frequency ($\omega=2\pi f$), C_0 is vacuum capacitance and Z_r and Z_i are real and imaginary parts of impedance. Arrhenius law equation (3) is a basic relationship, which describes the linear relationship of $\log \sigma$ with $1/T$ as follows [6]:

$$\sigma = \sigma_0 \exp \left[\frac{-E_a}{K_B T} \right] \dots \dots \dots (3)$$

where σ_0 is conductivity at an absolute temperature ($T=0$ K), E_a is the apparent activation energy [J.mol⁻¹], and K_B is Boltzmann constant.



Mustafa Kadhum *et al.*

RESULTS AND DISCUSSION

The ionic conductivities of the electrolyte (A0) owned the lowest value of conductivity with $(0.169\mu\text{S.cm}^{-1})$ at room temperature and increase with increasing temperature up to $(0.376\mu\text{S.cm}^{-1})$ at 333K. Generally, the contribution from the plasticizer towards the enhancement of conductivity is two-fold: a higher percentage of plasticizer would (1) open up the narrow rivulets of plasticizer – rich phase for greater ionic transport, and (2) provide a large free volume of relatively superior conducting phase [7].

The ionic conductivity of plasticized polymer electrolytes (As and Cs) as a function of temperature and different (KI/CsI) (0-25 and 0-35 wt.%), are shown in Figs. (1-2), which appear arbitrarily behavior upon increase the iodides concentration (KI/CsI). Also one can noted that the conductivity raise with rising the temperature for each salt concentration. From Fig. 1 which describe the increasing of ionic conductivity with increasing salts reaching a higher value of (2.42 mS.cm^{-1}) for electrolyte A2 with binary salts (5KI/20CsI wt.%). Whereas the conductivity of electrolytes A1 and A6 with single salt (CsI and KI 25 wt.%) respectively have the values of $(0.94$ and $2.2\text{ mS.cm}^{-1})$ respectively. The ionic conductivity must come from the contributions of both K^+ and I^- ions resulting in the highest conductivity observed for this sample. As the cation Cs^+ is bulky only the iodide ions (I^-) are expected to make a considerable contribution to the ionic conductivity and therefore this sample shows the lowest conductivity. The conductivity values of group C was increase randomly as appear in Fig.2. The sample C4 owned the higher value of conductivity with (3.48 mS.cm^{-1}) which contain binary salt (15KI/CsI20wt.%) at a given salt concentration combination this can be due to the compatibility and contribution the double salts with each other leading promote the ionic conductivity of the polymer electrolyte. The dissociated K^+ and I^- ions from KI salt and I^- ions from CsI salt will take part in the conduction process and contribute to the ionic conductivity of the gel electrolyte. While the conductivity of samples C1(35CsI wt.%) and C8 (35KI wt.%) with single iodide $(1.24$ and $3.11\text{ mS.cm}^{-1})$ respectively at room temperature.

That can be related to the enhancement of both salts which owned nearly same cation size makes the polymer chains spaced apart resulting in an increase of polymer flexibility and size of voids. This reduces viscosity and helps to improve the segmental motion and the transport of ions. For the sequence K^+ and Cs^+ , the size of the ions increases resulting in a drop in the mobility of the ions[4]. Fig. (3-4) showed the conductivity dependence temperature for electrolytes group (A and C) hence the conductivity increase temperature for all electrolyte samples. The number of free ions and ion aggregates increase with increasing salt concentration and thereby giving rise to the observed initial increase in conductivity. This can also be linked to decreasing in viscosity and hence, increase in chain flexibility as temperature increases due to the fact that ions in the systems get more energy and hence their motion increase resulting conductivity increment [8]. It has to be noted that salt separation, polymer crosslinking, the mobility of ions, ion consistency and shielding by polymer chains all are linked to the cation size and charge density. The high molecular weight of CsI (259.81 g/mol) is gradually replaced by low molecular weight KI (166 g/mol), the number of iodide ions will also obviously increase with increasing KI content.

Activation Energy (E_a) is the required energy of an ion to detach from its initial site to become free ion. The conductivity temperature plots values in Fig. (3-4), can be best fitted by Arrhenius equation (equation 3) [9]. The calculated E_a values are listed in Table (1). The electrolytes conductivity are easily raised as temperature increases hence creating more free volume [10]. This phenomenon enhances ionic mobility and polymer segmental motion thus increasing the conductivity [11]. The E_a decrease with increasing conductivity indicates that the ions in higher conducting electrolyte require lesser energy to migrate, from observation activation energy decreases as the iodide salts concentrations increases. From the Table (2) the E_a of electrolyte samples (A1 & A6) that contain single iodide (CsI & KI) with weight ratio (25%) have the values of $(0.07592$ & $0.06762\text{ eV})$ respectively. However the electrolyte samples C1 that contain single iodide (CsI) with weight ratio (35%) have the values of (0.0725 eV) . The decrease in E_a values with increase single iodide weight ratio (25 and 35%) for the same iodide as a result of increase conductivity of the electrolyte samples. The variation in activation energy strongly supports the change in the electrical conductivity.



**Mustafa Kadhum et al.**

It is observed that the minimum activation energy is the characteristics feature of the optimum conductivity value [12]. The E_a of the electrolyte samples groups (A & C) with binary salt have lower values for samples A2 and C4 (0.0655 and 0.0593 eV) respectively. The mixed of the two salts is helpful in improving the electrical conductivity. Originates from two types of ions, namely K^+ ions and iodide (I-/I-3) ions and all these ions contribute to the conductivity of this sample which is higher compared to the GPE containing only single salt [13]. It is observed that the minimum activation energy (0.0593 eV), is the characteristics feature of the optimum conductivity value (3.48 mS.cm⁻¹) for electrolyte sample C4 which contain binary salt. Generally, the activation energy E_a , is a combination of the energy of defect formation and the energy of defect migration. The complete amorphous nature of the particular polymer electrolyte will exhibit low activation energy.

Dielectric analysis is obtained from impedance plot and used to strengthen the conductivity pattern. The dielectric constant (ϵ_r) which represents the material's stored charges and dielectric loss (ϵ_i) which stands for the loss of energy to move ions and align dipoles when the electric field polarity reverses rapidly [14]. The dielectric constant studies are very useful in understanding the behavior of polymers and the electrolyte materials. The relaxation of dipoles in polymer electrolytes is studied through a broad frequency range [15]. To further enhance the understanding in conductivity trend, Fig. (4&5) illustrate the dielectric constant corresponding to the frequency (50Hz - 4GHz), for gel polymer electrolytes A & C, at room temperature, note that the dielectric constant values were calculated using (equation 2). It can be noticed that at low frequencies, the values of ϵ_r are higher compared to that at high frequency, the charge starts to accumulate at the surface of the electrode causing the electrode polarization to occur [16]. High frequency causes a fast rate of periodic reversal of the electric field which reduces the dielectric constant [17]. As the amount of salts concentration increases the values of ϵ_r increase in randomly manner which is attributed to the increment of charge carriers. However, when the salt content exceed 25 wt.%, the value of ϵ_r decrease. At high salt concentration, re-association and recombination of ions is favorable [18].

From Figures we can notes that the higher values to the real dielectric constant for electrolyte samples that contain single salt C1 (4.54*10⁷) and C8 (7.38*10⁷). However the ϵ_r for the electrolytes with binary salts that owned the highest values was A2 (7.6*10⁷). In reality, the addition of iodide salts to the polymer network makes amorphicity within the polymeric fabric and as a result increment in ϵ_r is observed [19]. Since ϵ_r conductivity is known to increase with frequency, permittivity must decrease with frequency so that the flow of charge will not encounter much resistance in the high-frequency region. At lower frequency region, ϵ_r is observed to decrease with increasing frequency and level off at higher frequency region Fig. (4&5). This is because, at lower frequency region, electrode polarization occurs due to the accumulation of ions at the electrode-electrolyte interface, confirming non-Debye dependence. Towards high frequency, the reversal of electric field occurs at a faster rate so that most of the ions are located in the bulk of the sample which decreases the electrode polarization.

The variation of permittivity (ϵ_r) with respect to frequency (50 Hz) for electrolytes A&C, over temperatures range (298-333 K) are depicted in Fig. (6&7). It can be seen that on assist increase of salts weight proportion, there's decrement of ϵ_r due to a lessening in chain segmental mobility. From perceptions, the values of a genuine portion of dielectric steady (ϵ_r) increment with raise temperature. This contributes to the higher carrier thickness whereby the ionic conductivity is expanded [20]. The higher values of dielectric consistent at higher temperature can be ascribed to the separation of particle totals and the next degree of salt separation. The crystallinity of the polymer electrolyte is reduced with an increment within the temperature. This, in turn, impacts the polymer elements and the dielectric behavior [21].

The increase in the dielectric constant with temperature can be attributed to the increase in charge carrier density due to the increase in dissociation of ion aggregates. The ϵ_r values increase with temperature, high temperature promotes more dissociation of ions thus enhances the value of ϵ_r [22].





Mustafa Kadhum et al.

CONCLUSIONS

The electrolyte C4 containing 15/20 wt.% salt have the higher conductivity (3.4 mScm^{-1}) at room temperature. The activation energy decreases with increasing the conductivity of electrolyte while the dielectric increase when temperature increased. The results indicated that the ionic conductivity values increase with increasing salts weight ratio up to 15% KI and lower of CsI down to 20%. The conductivity observed to increase with increasing temperature. The electrolytes are easily expanded as temperature increases hence creating more free volume. The activation energy E_a is a combination of the energy of defect formation and the energy of defect migration. At lower frequency region, ϵ_r is observed to decrease with increasing frequency and level off at higher frequency region, Enhancement in dielectric constant with temperature is mainly due to the decrease in viscosity of the polymeric material. The maximum dielectric constant value is obtained for polymer electrolyte A5 having one order increment in their magnitudes at room temperature. In fact, the addition of iodide salts to the polymer matrix creates amorphicity in the polymeric material and as a result increase in ϵ_r is observed.

REFERENCES

- [1] Y. J. Choi and D. W. Kim, "Photovoltaic Performance of Dye-sensitized Solar Cells assembled with Hybrid Composite Membrane-based on Polypropylene Non-woven Matrix", Bull. Korean Chem. Soc. 2011, Vol. 32, No. 2, pp. 605-608.
- [2] S. Lu et al., "Quasi-solid-state dye-sensitized solar cells with cyanoacrylate as electrolyte matrix", Solar Energy Materials & Solar Cells 2007, Vol.91, No. 1081-1086.
- [3] T. Bandara et al., "Efficiency enhancement in dye-sensitized solar cells using gel polymer electrolytes based on a tetrahexylammonium iodide and MgI₂ binary iodide system", Phys. Chem. Chem. Phys., 2012, Vol.14, No.8620–8627.
- [4] T. Bandara et al., "Effect of the alkaline cation size on the conductivity in gel polymer electrolytes and their influence on photo electrochemical solar cells", Phys. Chem. Chem. Phys., 2016, Vol.18, No. 10873-10881.
- [5] G.P. Kalaigan et al., "Effects of compositions on properties of PEO–KI–I₂ salts polymer electrolytes for DSSC" Solid State Ionics, 2006, Vol.177, No.1091-1097.
- [6] M.K.Jawad, "Synergistic effect of Metal- Phthalocyanine in Gelled Co-Polymer for Energy Conversion Device", 2015, Ph.D. Thesis, Baghdad University, Department of Physics, 87-88.
- [7] B. Cosar et al. " Photovoltaic performance of bifacial dye-sensitized solar cell using chemically healed binary ionic liquid electrolyte solidified with SiO₂ nanoparticles", 2013 Electrochimica Acta, Vol.87,425– 431.
- [8] A. Pathirana et al., "Effect of Binary salt based Gel Polymer Electrolytes on Dye-Sensitized Solar Cells" 2015, Vol. 31, P9-17.
- [9] Arup Dey, et al, "Structure, morphology and ionic conductivity of solid polymer electrolyte", Materials Research Bulletin, Vol.46, pp.2009–2015, 2011
- [10] M.F. Shukur, et.al, "Proton conducting polymer electrolyte based on plasticized chitosan–PEO blend and application in electrochemical devices", 2013, Optical Materials, Vol. 35, pp.1834–1841.
- [11] D., Padalia, et, al., "Study of cerium doped magnetite (Fe₃O₄:Ce)/PMMA nanocomposites" , 2012, Physica B, 407, 838–843 .
- [12] M.S. Su'ait, et. al., "The potential of polyurethane bio-based solid polymer electrolyte for photoelectron- chemical cell application", 2014, International Journal of Hydrogen Energy, 39(6), pp. 3005–3017.
- [13] G. Wang, X. Zhou, et, al., "Gel polymer electrolytes based on polyacrylonitrile and a novel quaternary ammonium salt for dye-sensitized solar cells", 2004, Materials Research Bulletin, Vol. 39(13), pp. 2113-2118.
- [14] AK Arof, et, al., "A method based on impedance spectroscopy to determine transport properties of polymer electrolytes", 2014. Phys Chem Chem Phys 16(5):1856–1867.
- [15] S. Rajendran, and M.R. Prabhu, "Effect of different plasticizer on structural and electrical properties of PEMA-base polymer electrolytes", 2010, J. Appl. Electrochemistry, Vol. 40, pp. 327-332.





Mustafa Kadhum et al.

[16] S. Selvasekarapandian and Chithra DR “Dielectric studies on a solid electrolyte AgI-PbBr₂-Ag₂O-B₂O₃ mater”, 1999. Chem Phys 58:90–93.

[17] MZ Iqbal and S. Rafiuddin “Structural, electrical conductivity and dielectric behavior of Na₂SO₄-LDT composite solid electrolyte”, 2016. J Adv Res 7(1):135–141.

[18] A. Chandra “Synthesis and dielectric studies of PEO-PVP blended solid polymer”, 2013. Indian J Pure Appl Phys 51:788–791.

[19] O.A. Ileperuma, et, al. “Photoelectrochemical solar cells with polyacrylonitrile-based and polyethylene oxide-based polymer electrolytes”, 2004, Solar Energy Materials and Solar Cells, Vol. 84(1), pp.117-124.

[20] L. Othman, et, al., “Impedance spectroscopy studies of poly(methyl methacrylate)-lithium salts polymer electrolyte systems”, 2007, Ionics, Vol.13, pp. 337-342.

[21] A. Awadhi, et, al., “Dielectric investigations in PVA based gel electrolytes”, 2006, Progress in Crystal Growth and Characterization of Materials, Vol.52, pp. 61-68.

[22] RJ Sengwa, et, al., “Effects of plasticizer and nanofiller on the dielectric dispersion and relaxation behavior of polymer blend based solid polymer electrolytes”, 2015, Curr App Phys 15(2):135–143.

Table 1: Assigning and composition of [PAN-PMMA (20:80%)]-KI/ CsI gel electrolytes system

Group A	KI w%	CsI w%	Group C	KI w%	CsI w%
A0	0	0	C1	0	35
A1	0	25	C2	5	30
A2	5	20	C3	10	25
A3	10	15	C4	15	20
A4	15	10	C5	20	15
A5	20	5	C6	25	10
A6	25	0	C7	30	5
			C8	35	0

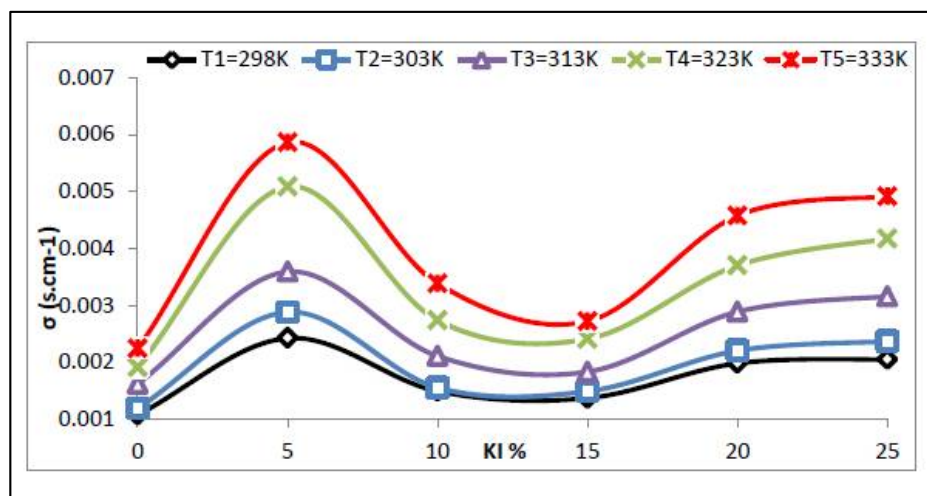


Fig.1: Ionic conductivities dependence of temperature and KI/CsI wt.% of the electrolytes A.





Mustafa Kadhum et al.

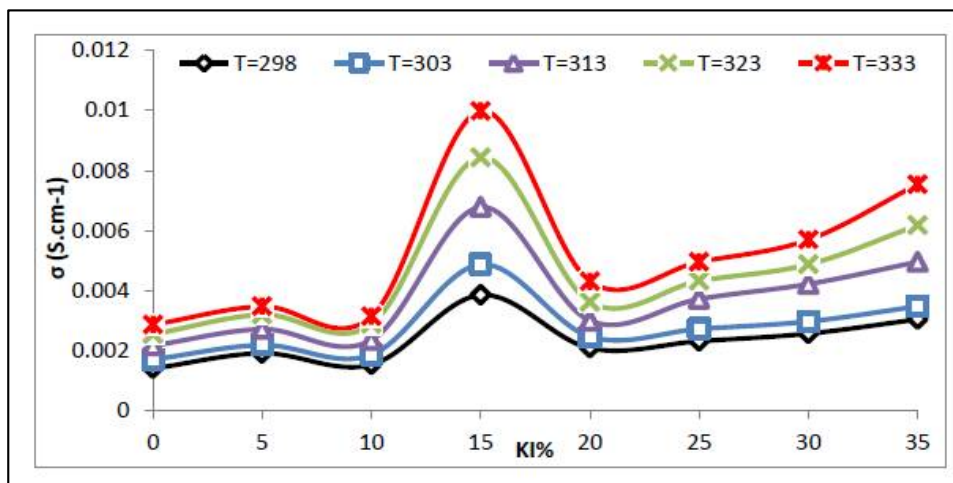


Fig. 2: Ionic conductivities dependence of temperature & KI/CsI wt.%of the electrolytes C.

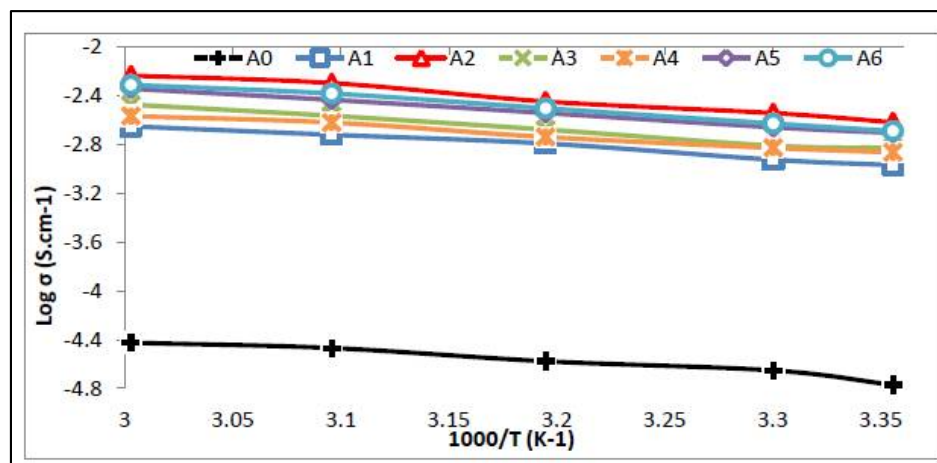


Figure 3: Temperature dependence of the ionic conductivity of electrolytes Group (A)

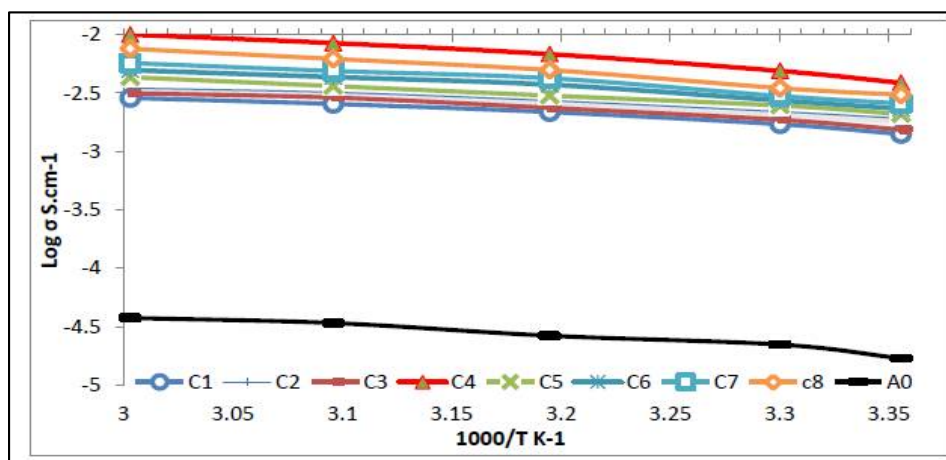


Fig. 4: Temperature dependence of the ionic conductivity of electrolytes Group (C)





Mustafa Kadhum et al.

Table 2: Ionic conductivity and activation energy values of electrolytes group A and C at room temperature

Electrolytes A _s at R.T	σ (S.cm ⁻¹)	Activation energy E _a (eV)	Electrolytes C _s at R.T	σ (S.cm ⁻¹)	Activation energy E _a (eV)
A0	0.000000169	0.12367	C1	0.00124	0.07254
A1	0.00094	0.07592	C2	0.00208	0.0697
A2	0.00242	0.06559	C3	0.00141	0.07143
A3	0.00143	0.07214	C4	0.00348	0.05935
A4	0.00136	0.07355	C5	0.0014	0.06822
A5	0.00204	0.06851	C6	0.00232	0.06649
A6	0.00228	0.06762	C7	0.003	0.06515
			C8	0.00311	0.06281

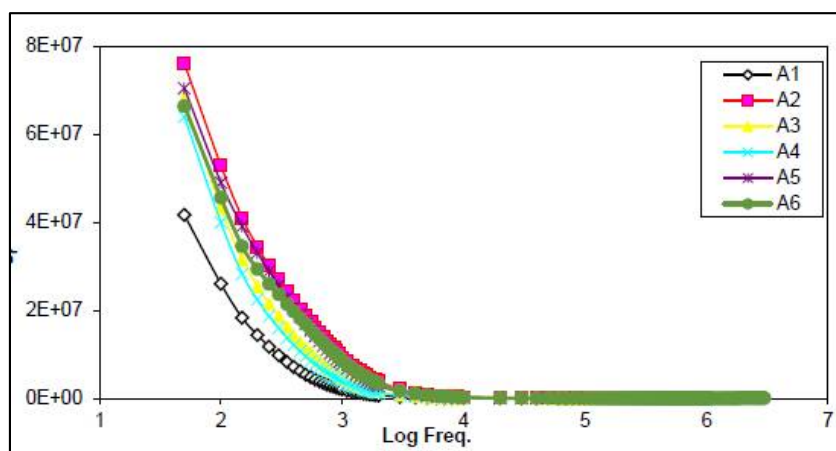


Fig. 5.Real part of dielectric constant (ϵ_r) for electrolytes A at room temperature, corresponding to log frequency.

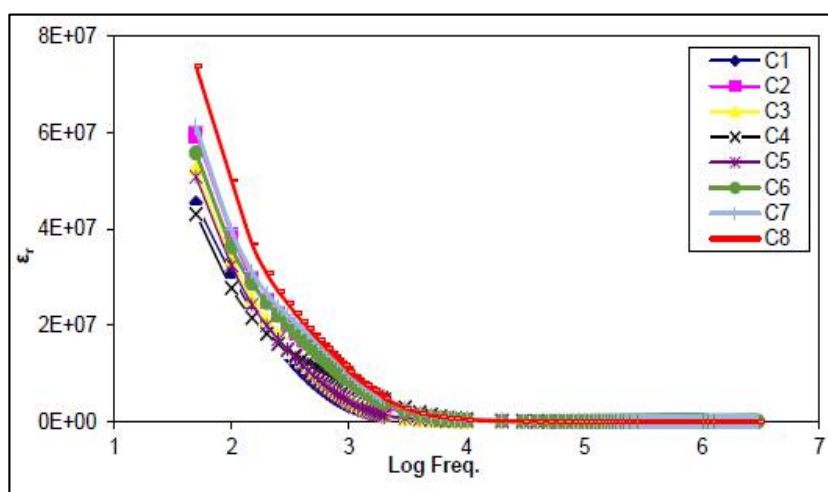


Fig. 6.Real part of dielectric constant (ϵ_r) for electrolytes C, at Room Temperature, corresponding to log frequency.





Mustafa Kadhum *et al.*

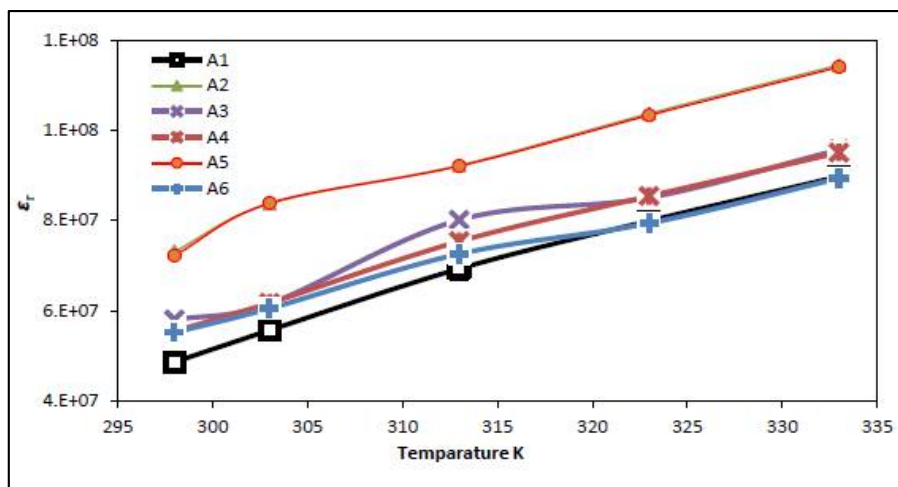


Fig. 7. Real part of dielectric constant (ϵ_r) for electrolytes A corresponding to frequency over a temperature range (298-333K).

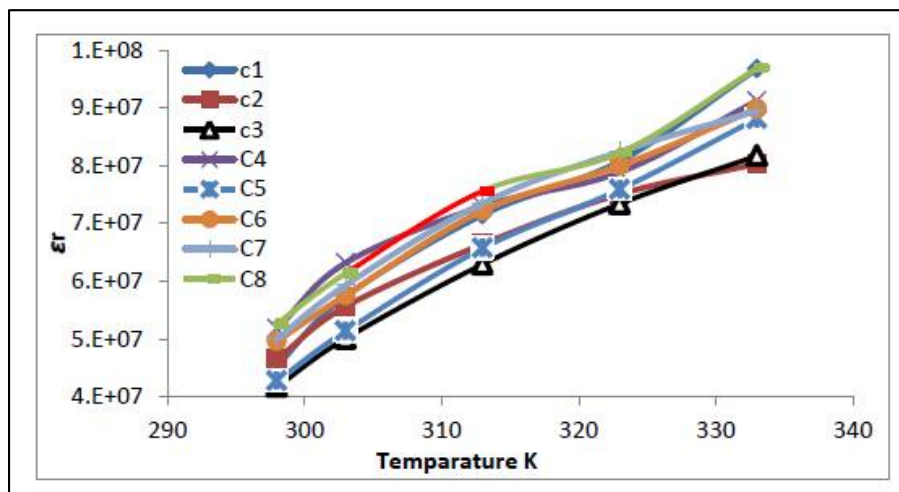


Fig.8. Real part of dielectric constant (ϵ_r) for electrolytes C corresponding to frequency over a temperature range (298-333K).





RESEARCH ARTICLE

Investigation of Toxoplasmosis in Human, Camels and Goats by Using Molecular Methods

GhaidaaAbbas Jasim* and Rasha Imad Ayyal

College of Veterinary Medicine, University of Al-Qadisiyah, Diwaniyah, Iraq.

Received: 14 July 2018

Revised: 20 Aug 2018

Accepted: 25 Sep 2018

*Address for Correspondence

GhaidaaAbbas Jasim

College of Veterinary Medicine,

University of Al-Qadisiyah,

Diwaniyah, Iraq.

Email: Ghaidaa.Abass@qu.ed.iq



This is an Open Access Journal / article distributed under the terms of the **Creative Commons Attribution License** (CC BY-NC-ND 3.0) which permits unrestricted use, distribution, and reproduction in any medium, provided the original work is properly cited. All rights reserved.

ABSTRACT

The current study included the detection of *Toxoplasma gondii* in camels, goats from slaughter house in Al-Qadisiyah province, aborted ewe from owner who attended to the veterinary hospital in Al Diwaniyah and also from aborted women from Maternity and Childhood Teaching Hospital to point to the rate of infection in the human and to study animals and also the organs can be found in animals. A total of 200 samples distributed as a males and females of camels and goats, and from aborted women, the samples were divided into, (70) sample from camels, from (liver, meat and uterus), 70 samples of goats' meat, uterus, placenta and fetus and 60 samples were collected randomly from aborted women who received to the Maternity and Childhood Teaching Hospital. The first method of diagnosis was an impression method for all samples. The result of camels shows that was 48/ 70 positive (68.57%), while the result of goats were 45/70 (64.28%) and the aborted women show 20/60 positive (33.33%), there was a statistically significant among the species in $p < 0.05$. to suspected *toxoplasma gondii* bradizoite. The present study include molecular method to detected small subunit ribosomal RNA (ssRNA) using Nested Polymerase Chain Reaction (nPCR), the results of the nPCR for ssRNA gene showed that 18/32 (54.54%) were positive in the camels, while the result of the goats were 17/33 (51.51%) were positive, the rate of toxoplasmosis in the aborted women was Positive 60%. There is a statistically significant between species in $p < 0.05$.

Keyword: Toxoplasmosis, nPCR, Camel, goat, human, Diwaniyah, Iraq.





INTRODUCTION

Toxoplasmosis is a classic zoonosis, A wide range of vertebrate animals serve as hosts and while human infections are common, serious complications occur primarily in immune compromised hosts, Human infections are caused by accidental ingestion of oocysts, shed into the environment by cats, or tissue cysts contained in undercooked meat, Infections in healthy adults are generally benign, although toxoplasma retinitis is frequently a cause of serious eye disease in otherwise healthy adults (Gilbert et al., 1999). More profound disease occurs in immune compromised hosts or as the result of congenital infections (McLeod et al., 2000). Toxoplasmosis intracellular parasite that has a two stage asexual cycle in warm-blooded animals and a sexual cycle in felidae, the parasite comprises three clonal lineages (I, II and in the main, with type II and III being associated with disease in animals while type II is the predominant form identified in human disease (Howe and Sibley, 1995, Khan et al., 2006). In the asexual cycle, the two developmental stages are the rapidly multiplying tachyzoite and the slowly multiplying bradyzoite, in acute infection, tachyzoites actively penetrate host cells where they multiply causing the cell to rupture and release organisms locally and into the bloodstream As the host develops immunity, the parasite retains its overall size and shape but transforms into the bradyzoite stage and multiplies more slowly within tissue-cysts to establish a persistent infection, These microscopic tissue cysts are present most frequently in brain and skeletal muscle and represent the quiescent stage of the parasite within the host, Viable tissue cysts within muscle (meat) are a significant source of human infection, In animals that succumb to acute infection tachyzoites may be demonstrated in ascitic fluid or in lung impression smears as well as in tissue sections of the liver and other affected organs (Luft et al., 1993).

MATERIALS AND METHODS

Primers

The Nested PCR primers for detection small subunit ribosomal RNA gene in *Toxoplasma gondii* were design by pervious study (Vitale et al., 2008). These primers were provided from Macrogen company, Korea as following table:1

Samples collection

The study was carried out during the beginning of November 2017 until the end of February 2018 in AL-Qadisya provenance, total 200 samples were examined in the current study divided as 70 samples of different camel organs (liver, meat, uterus) in the slaughter house, 70 samples of goat also taken from slaughter house (uterus, meat, Placenta and fetus). Also the present study include 60 human samples from aborted women (placenta and fetus) who attended to the Maternity and Childhood Teaching Hospital. The samples were collected randomly and using two clean containers containing 1st one containing normal saline and kept cool and transferred to the laboratory to make the impression method and the 2nd one then put in deep freeze under for DNA extraction as a target for PCR amplification.

Microscopic Examination

(by stamp method or immersion method) Stamp the tissue on the glass slide and left in air to dry and methanol alcohol was added for (3-5) minute then was stained with Giemsa stain for 30 minutes and was washed by tap water then left to dry, after drying they were examined under the oil immersion lens of light microscope (Zafar et al., 2006).



**GhaidaaAbbas Jasim and Rasha Imad Ayyal****Tissue Genomic DNA Extraction**

Tissue Genomic DNA from tissue samples were extracted by using DNA extraction kit (Tissue DNA protocol) Geneaid. USA and the extraction was done according to company instructions as following steps:

1. Weight of 100mg Human tissue samples was transferred to sterile 1.5ml microcentrifuge tube.
2. Volume of 200µl GST 20µl and proteinase K were added and mixed by vortex. And incubated at 60°C for 1 hour.
3. Volume of 200µl of GSB was added to each tube and mixed by vortex vigorously, and then all tubes were incubated at 70°C for 15 minutes, and inverted every 3 minutes through incubation periods.
4. Volume of 200µl absolute ethanol were added to lysate and immediately mixed by shaking vigorously.
5. DNA filter column was placed in a 2 ml collection tube and transferred all of the mixture (including any precipitate) to column. Then centrifuged at 10000rpm for 5 minutes. And the 2 ml collection tubes containing the flow-through were discarded and placed the column in a new 2 ml collection tube.
6. Volume of 400µl W1 buffer were added to the DNA filter column, then centrifuge at 10000rpm for 30 seconds. The flow-through was discarded and placed the column back in the 2 ml collection tube.
7. 600µl Wash Buffer (ethanol) was added to each column. Then centrifuged at 10000rpm for 30 seconds. The flow-through was discarded and placed the column back in the 2 ml collection tube.
8. All the tubes were centrifuged again for 3 minutes at 10000 rpm to dry the column matrix.
9. The dried DNA filter column was transferred to a clean 1.5 ml microcentrifuge tube and 50 µl of pre-heated elution buffer were added to the center of the column matrix.
10. The tubes were let stand for at least 5 minutes to ensure the elution buffer was absorbed by the matrix. Then centrifuged at 10000 rpm for 30 seconds to elute the purified DNA.

Nested Polymerase chain reaction (nPCR)

The nested PCR technique was performed for detection *Toxoplasma gondii* based small subunit ribosomal RNA gene from all tissue samples of all species. This method was carried out according to method described by (Vitale *et al.*, 2008) as following steps:

Genomic DNA estimation

The extracted genomic DNA was by using Nanodrop spectrophotometer (THERMO. USA), that check and measurement the purity of DNA through reading the absorbance in at (260 /280 nm) as following steps:

1. After opening up the Nanodrop software, chosen the appropriate application (Nucleic acid, DNA).
2. A dry wipe was taken and cleaned the measurement pedestals several times. Then carefully pipette 2µl of free nuclease water onto the surface of the lower measurement pedestals for blank the system.
3. The sampling arm was lowered and clicking OK to initialize the Nanodrop, then cleaning off the pedestals and 1µl of DNA was added to measurement.

3-2-6- Primary PCR master mix preparation

Primary PCR master mix was prepared by using (Maxime PCR PreMix Kit) and this master mix done according to company instructions as following table:2 After that, these PCR master mix component that mentioned in table above placed in standard PCR PreMix Kit that containing all other components which needed to PCR reaction such as (Taq DNA polymerase, dNTPs, Tris-HCl pH: 9.0, KCl, MgCl₂, stabilizer, and tracking dye). Then, all the PCR tubes transferred into Exispin vortex centrifuge at 3000rpm for 3 minutes. Then placed in PCR Thermocycler (T100 Thermal cycler. BioRadUSA).



**GhaidaaAbbas Jasim and Rasha Imad Ayyal****PCR Thermocycler Conditions**

PCR thermocycler conditions by using conventional PCR thermocycler system as following table:3

Secondary PCR master mix preparation

Secondary PCR master mix was prepared by using (Maxime PCR PreMix Kit) and this master mix done according to company instructions as following table:4 After that, these PCR master mix component that mentioned in table above placed in standard AccuPower® PCR PreMix Kit that containing all other components which needed to PCR reaction such as (Taq DNA polymerase, dNTPs, Tris-HCl pH: 9.0, KCl, MgCl₂, stabilizer, and tracking dye). Then, all the PCR tubes transferred into Exispin vortex centrifuge at 3000rpm for 3 minutes. Then placed in PCR Thermocycler (T100 Thermal cycler. BioRad USA).

PCR Thermocycler Conditions

PCR thermocycler conditions by using conventional PCR thermocycler system as following table:5

PCR product analysis

1. The Nested PCR products was analyzed by agarose gel electrophoresis following steps: 1-A percent of 1% Agarose gel was prepared in using 1X TBE and dissolving in water bath at 100 °C for 15 minutes, after that, left to cool 50°C.
2. Volume of 3µL of ethidium bromide stain were added into agarose gel solution.
3. Agarose gel solution was poured in tray after fixed the comb in proper position after that, left to solidified for 15 minutes at room temperature, then the comb was removed gently from the tray and 10µl of PCR product were added in to each comb well and 5ul of (100bp Ladder) in one well.
4. The gel tray was fixed in electrophoresis chamber and fill by 1X TBE buffer. Then electric current was performed at 100 volt and 80 AM for 1 hour.
5. Nested PCR products were visualized by using UV Transilluminator.

RESULTS AND DISCUSSION**Detection of *Toxoplasma gondii* bradyzoite using impression method****Detection of Toxoplasmosis in camel****Incidence of suspected bradyzoites Toxoplasmosis according to organ**

The present study was used impression method for detect suspected toxoplasma bradyzoites in different organs of camel, 70 samples were examined (9 liver, 25 meat and 36 uterus). The results shows the percent of the infection in general 48/70 (68.57%), while the rate of the infection according to the organs were 3/9 (33.33%), 12/25 (48%) and 33/36 (91.66%) in the liver, meat and uterus respectively table (1), figure (6). The present study divided the camel samples based on gender into 28 male and 42 female, the infectious rate of toxoplasmosis according to the gender based on impression method were 9/28 (68.57%) and 39/42 (92.85%) in male and female respectively table (7). In the study found the infectious rate of toxoplasmosis was 68.57%, this result agree with other study using the LAT as a serological test in the Sudan 67% (Elamin et al., 1992), also another prevalence study for *Toxoplasma gondii* seropositivity detection in Sudan using the LAT was (61.7%) (Manal, 2003)



**GhaidaaAbbas Jasim and Rasha Imad Ayyal****Detection of Toxoplasmosis ingoat****Incidence of suspected bradyzoites Toxoplasmosis in the goat according to theorgans**

The current study use impression method to detected suspected toxoplasma bradyzoite in the uterus, meat, placenta and fetus samples from slaughter house. The result of the present study was 45/70 (64.28%) was positive result in the method above., while according to the organs were 46.66 %, 73.33%, 73.33% and 64% in the uterus ,placenta , fetus and meat respectively table(8) figure(2). The preset study divided the goat samples based on gender into 25 male and 45 female, the infectious rate of toxoplasmosis according to the gender based on impression method were 16/25 (64%) and 29/45(64.44%) in male and female respectively table(9).The present study found 64.28% in the goat, On the other hand the result of another study which were nearlyto the result of the present study in Bangladesh reported 61% by used latex method (Rahman etal.,2014) , in Egypt reported 59.4% by used indirect hemaagglutination assay, (Barakat etal.,2009).

Detection of Toxoplasmosis in human**Incidence of bradyzoites Toxoplasmosis according to organ**

The current study used the impression method to detected toxoplasmosis bradyzoite in the placenta and fetus from the same aborted woman who attended to the maternity and childhood hospital in Al Diawanyia province. A total number of placenta and fetus samples were (60 each sample to the single patient) samples exam by impression method, and the result of this study found 20 /60 (33.33 %) positive That means the placenta source of transmission of infection to the fetus. Table (10) figure (3). The present study found 33.33% in the human, In other hand by ues ELISA test the seroprevalence in women was 50% in USA (Stagno, 1980), 54% in Kenya (Griffin and Williams, 1983), 7.5% in Scotland (Jackson and Hutchinson, 1987).

Detection of *Toxoplasma gondii* using Molecular methods.**DNA extraction**

The DNA of positive samples to impression method which are (95) was extracted and purified by using genome DNA purification kit. The results were detected by nanodrop and the result were exelant.

Nested polymerase chain reaction nPCR to detect small sub unit ribosomal RNA gene.

The results of PCR amplification which was performed on the DNA extracted of small subunit ribosomal RNA gene of *Toxoplasma gondii*, the samples were taken from 95 samples which were positive result with impression method as (32,33and 30) camel,goat and human respectively the studied isolates confirmed by electrophoresis analysis. By this analysis the strands of DNA which are resulted from the successful binding between specific primers and extracted DNA of isolates, These successful binding appear as single band together with the 313 pb band product size.The result of nPCR in present study of camel was 18/32 (54.45%) from positive samples to impression method, while the result of goat in the same method was 17/33% figure (4). The electrophoresis also used to estimate DNA weight depending on DNA marker (2000 bp DNA ladder) and the result of this estimation revealed that the amplified DNA figure(5). Out of 95 were taken from impression methodpositive cases, and examined by nested PCR found (53) positive result with a percent (55.20%).In human the number of samples was 18/30 from positive impression method Table (8).





Ghaidaa Abbas Jasim and Rasha Imad Ayyal

The correct study found 54.54% in camel, other study use LAT of Al-Qadisiya province reported 16.34% (Al-Hindawe, 2006), Hilali *et al.* (1998) detect prevalence of 17.4%. The differences among percentages that recorded in the current study and other studies may be due to method of diagnosis or the time of collected samples. The correct study found 51.51% in goat, this result compare with other result use the blood sample for an indirect antibody test in the slaughterhouse in Iran (Sharif *et al.*, 2007) which reported 30%. The present study found 60% in the human, while the result of Al-Kalaby, (2008) who recorded that 83.3% of tested samples from Iraq women was positive by PCR technique using *B1* gene, on the other hand the results of Okay *et al.*, (2009) who reported that 17.65%, the result of present study agreed with the results of Al-Addlan, (2007) who reported that 63.49%

CONCLUSIONS

1. This study determine the proportion of *Toxoplasma gondii* parasite in the organs of slaughter animals and in humans by using the different technique, the study shown that the presence of parasite in a high rate in the camel
2. There is a variation in the incidence of infection among different animals and human
3. There is a variations in the incidence of the infection of *toxoplasma gondii* parasite between different organs of the camel depending on the stage of infection and the importance of the organ relative to the parasite
4. The uterus is considered the best organs as a target of the *toxoplasma gondii* when compared to the other organs.
5. Meat of slaughter animals is an important source of toxoplasmosis and a threat to consumer health.

REFERENCES

1. Howe, D. K. and Sibley, L. D. (1995). *Toxoplasma gondii* comprises three clonal lineages: correlation of parasite genotype with human disease. *Journal of infectious diseases*. 172(6):1561-1566.
2. Khan, A.; Böhme, U.; Kelly, K. A.; Adlem, E.; Brooks, K.; Simmonds, M.; Mungall, K.; Quail, M. A.; Arrowsmith, C. and Chillingworth, T. (2006). Common inheritance of chromosome 1a associated with clonal expansion of *Toxoplasma gondii*. *Genome research*. 16(9):1119-1125.
3. Luft, B. J.; Hafner, R.; Korzun, A. H.; Lepore, C.; Antoniskis, D.; Bosler, E. M.; Bourland, D. D.; Uttamchandani, R.; Fuhrer, J. and Jacobson, J. (1993). Toxoplasmic encephalitis in patients with the acquired immune deficiency syndrome. *New England Journal of Medicine*. 329(14):995-1000.
4. Vitale, S.; Leon, E. Mary, F.; Frederick, L.; Ferris, S. (2008). *Toxoplasma* describe the prevalence of refractive error in the states: 126(8):111-133.
5. Zafar, I.; Sajid, M. S.; Jabbar, A.; Rao and, Z. A. and Khan M N (2006). *Techniques in Parasitology*. 1st Ed., Higher Education Commission, Islamabad, Pakistan.
6. Elamin, E.; Elias, S.; Dauschies, A. and Rommel, M. (1992). Prevalence of *Toxoplasma gondii* antibodies in pastoral camels (*Camelus dromedarius*) in the Butana plains, mid-Eastern Sudan. *Veterinary parasitology*. 43(3-4): 171- 175.
7. Manal, Y. L. 2003. Studies on *Toxoplasma* and *Sarcocystis* from camels (*Camelus dromedarius*) in the Sudan. Ph. D. thesis. University of Khartoum, Sudan.
8. Rahman, M.; Azad, M. T. A.; Nahar, L.; Rouf, S. M. A.; Ohya, K.; Chiou, S.- P.; Baba, M.; Kitoh, K. and Takashima, Y. (2014). Age-specificity of *Toxoplasma gondii* seroprevalence in sheep, goats and cattle on subsistence farms in Bangladesh. *Journal of Veterinary Medical Science*. 76(9):1257-1259.
9. Barakat, A.; Elaziz, M. A. and Fadaly, (2009). Comparative diagnosis of toxoplasmosis in Egyptian small ruminants by indirect hemagglutination assay and Elisa. *Global Veterinaria*. 3(1):9-14.
10. Stagno, S. (1980). Congenital toxoplasmosis. *Amer. J. Dis. Child.*; 134:635-637. Steven, E.; Schmitt, B.; Golovko, A.; Mehdi, E. and Santanu, K. 2008. Toxoplasmosis. Chapter 2. 9. 10. *Terrestrial Manual*. 6th ed. OIE Scientific Publications.





GhaidaaAbbas Jasim and Rasha Imad Ayyal

11. Griffin, L., and Williams, K. A. B. (1983). Serological and parasitological survey of blood donors in Kenya for toxoplasmosis. *Trans. Roy. Soc. Trop. Med. Hyg.*; 6:143-145.
12. Jackson, M. H. and Hutchinson, W. M. (1987). A seroepidemiologic al survey of Toxoplasmosis in Scotland and England. *Ann. Trop. Med.Parasitol.*;81: 365-395.
13. Al-Hindawe, A. J. (2006). Seroprevalence of Toxoplasmosis (*Toxoplasma gondii*) infection in the camels in Al-Qadisiya governorate..*Al-QadisiyaVet. Med. Sci.* 2:71-73.
14. Hilali, M.;Romand, S.;Thulliez, P.;Kwok, O. and Dubey, J.(1998).Prevalence ofNeospora caninum and *Toxoplasma gondii* antibodies in serafromcamelsfrom Egypt. *Veterinary parasitology.* 75(2-3): 269- 271.5
15. Sharif, M.;Gholami, S.;Ziaei, H.;Daryani, A.;Laktarashi, B.;Ziapour, S.; Rafiei, A. and Vahedi, M.(2007). Seroprevalence of *Toxoplasma gondii* in Cattle, Sheep and Goats Slaughtered for Food in Mazandaran Province,Iran,2005. *Journal of Animal and VeterinaryAdvances.*
16. Al-Kalaby, R. (2008). *Sero-epidemiological study of toxoplasmosis among different groups of population in Najaf city*, MSc. thesis, Universityof Kufa.Iraq.
17. Okay, T. S.;Yamamoto, L.;Oliveira, L. C.;Manuli, E. R.;Andrade Junior, H. F. d. and Del Negro, G. M. B.(2009). Significant performance variation among PCR systems in diagnosing congenital toxoplasmosisin São Paulo, Brazil: analysis of 467 amniotic fluid samples. *Clinics.* 64(3):171-176.
18. Al- Addlan, A. A. J. (2007). Diagnostic and serological study on *T.gondii* for women whom had abortion by using PCR technique in Thi-Qar governorate. *M. Sc. Thesis, College of Education, Thi-QarUniversity.*

Table 1. PCR primers RNA gene in *Toxoplasma gondii*

Primer	Sequence		Amplicon
18SrRNA gene First round PCR Primers	F	TGCGGAAGGATCATTACACG	530bp
	R	CCGTTACTAAGGGAATCATAGTT	
18SrRNA gene Second round Nested PCR Primers	F	GATTTGCATTCAAGAAGCTGATAGTAT	313bp
	R	AGTTAGGAAGCAATCTGAAAGCACATC	
DNA sequence Toxo-SAG3primers	F	ATGCAGCTGTGGCGGCGCAG	1158bp
	R	TTAGGCAGCCACATGCACAAG	

Table.2. Maxime PCR PreMix Kit

PCR Master mix	Volume
DNA template	5µL
18SrRNA primary Forward primer (10pmol)	1µL
18SrRNA primary Reverse primer (10pmol)	1µL
PCR water	13µL
Total volume	20µL

Table.3. thermocycler system

PCR step	Temp.	Time	repeat
Initial Denaturation	95C	5min	1
Denaturation	95C	30sec.	40 cycle
Annealing	58C	30sec	
Extension	72C	30sec	
Final extension	72C	5min	1
Hold	4C	Forever	-





GhaidaaAbbas Jasim and Rasha Imad Ayyal

Table.4. Secondary PCR master mix

Nested PCR Master mix	Volume
PCR product	2µL
18SrRNA secondary Forward primer (10pmol)	1µL
18SrRNA secondary Reverse primer (10pmol)	1µL
PCR water	16 µL
Total volume	20µL

Table.5. thermocycler system

PCR step	Temp.	Time	repeat
Initial Denaturation	95C	5min	1
Denaturation	95C	30sec.	
Annealing	58C	30sec	40 cycle
Extension	72C	30sec	
Final extension	72C	5min	1
Hold	4C	Forever	-

Table 6. the percentage according to organs suspected of bradyzoites of toxoplasmosis in camel

Organ	No.	(+ve)	%
Liver	9	3	33.33 ^B
Meat	25	12	48 ^B
Uterus	36	33	91.66 ^A
Total	70	48	68.57

Similar litter represent no statistically significant at $p < 0.05$

Different letter represent statistically significant at $p < 0.05$

Table 7. The percentage according to gender suspected to bradyzoites of toxoplasmosis in camel

Sex	NO.	Number(+ve)	%
Male	28	9	32.14 ^B
Female	42	39	92.85 ^A
Total	70	48	68.57

Different letter represent statistically significant at $p < 0.05$

Table 8. Show the percentage according to organs suspected to bradyzoites to toxoplasma in goat

Organ	N0	(+ve)	%
Uterus	15	7	46.66A
Placenta	15	11	73.33B
Fetus	15	11	73.33B
Meat	25	16	64A
Total	70	45	64.28

Similar litter represent no statistically significant at $p < 0.05$

Different letter represent statistically significant at $p < 0.05$





GhaidaaAbbas Jasim and Rasha Imad Ayyal

Table 9. the percentage according to gender suspected to bradyzoites of toxoplasmosis in goat

Sex	N0.	Number(+ve)	%
Male	25	16	64 ^B
Female	45	29	64.44 ^A
Total	70	45	64.28

Different letter represent statistically significant at p < 0.05

Table10. the percentage of toxoplasmosis according to organs suspected to bradyzoites to toxoplasmosis in human

Organ	N0	(+ve)	%
Placenta	60	20	33.33
Fetus	60	20	33.33
Total	60	20	33.3

Table 11 Compression of the result of nPCR according to the different species

Species	nPCR	(+ ve)	%
Camel	32	18	54.54 ^A
Goat	33	17	51.51% ^A
Human	30	18	60% ^A
Total	95	53	55.20%

Similar litter represents no significant difference at p < 0.05

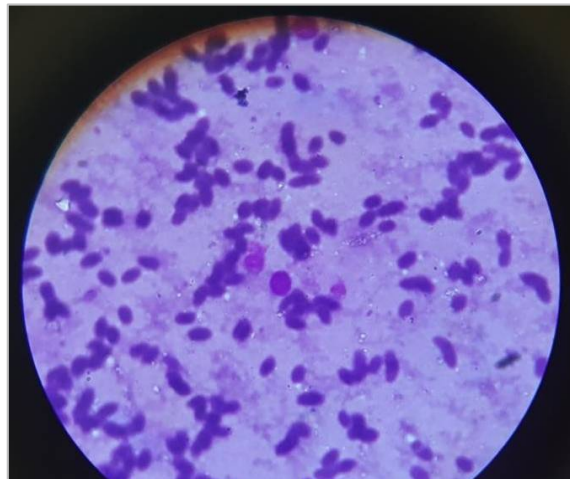


Figure 1.the bradyzoite in camel using Impression method, staining with Gemisa (X100).

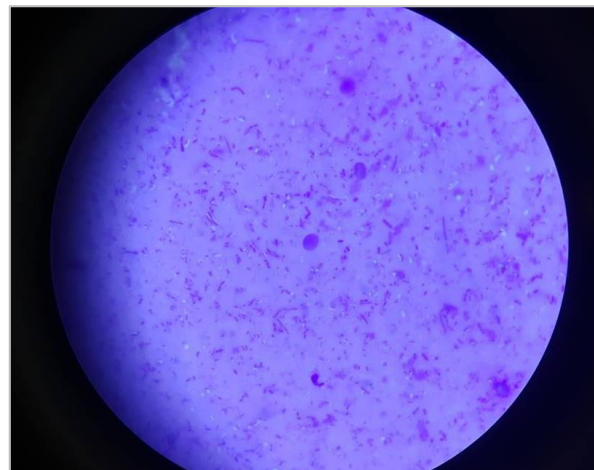


Figure 2. The bradyzoite in goat using impression Method and staining with Gemisa (X100).





GhaidaaAbbas Jasim and Rasha Imad Ayyal

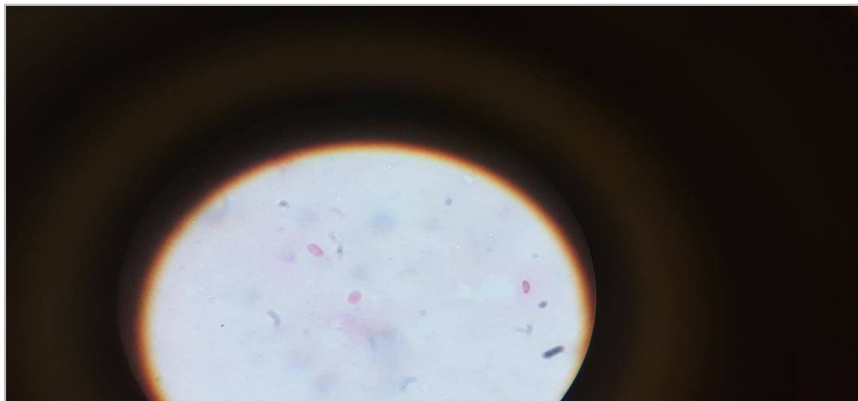


Figure 3. the bradyzoite in human using impression method and staining with Gemisa stain (X100)

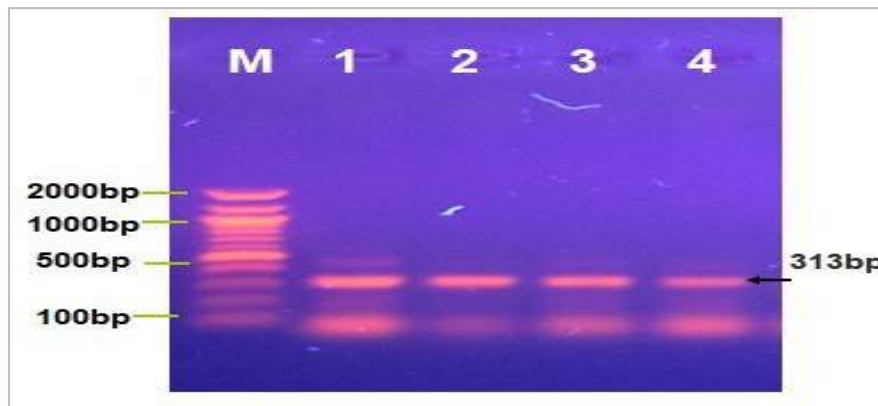


Figure 4. Agarose gel electrophoresis image that show the NestedPCR product analysis of small subunit ribosomal RNA gene in *Toxoplasma gondii*. Where Marker ladder (2000-100bp), (1-4) some positive *Toxoplasma gondii* from camel samples at 313bp PCR product size

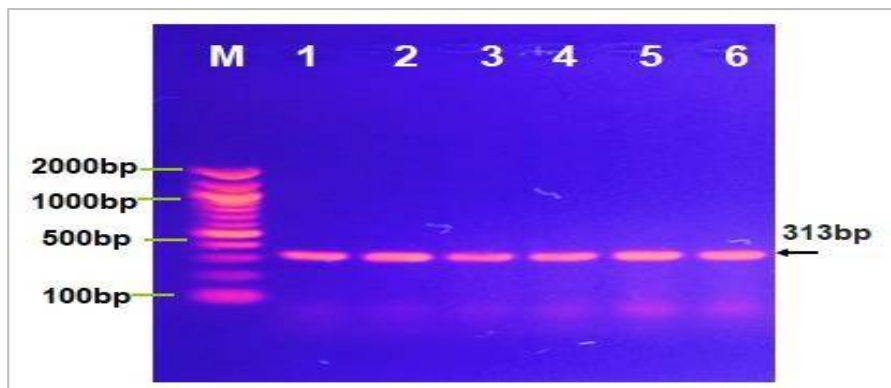


Figure 5. Agarose gel electrophoresis image that show the Nested PCR product analysis of small subunit ribosomal RNA gene in *Toxoplasma gondii*. Where Marker ladder (2000-100bp), (1-6) some positive *Toxoplasma gondii* from goat samples at 313bp PCR product size

